EJA

European Journal of Anatomy

Volume 25 - Number 5 September 2021

Indexed in:

CLARIVATE
- JCR:2020
- Q4 (21/23)
- I.F. J.C.I.: 0.19

DIALNET

EMBASE / Excerpta Medica

SCOPUS
- SJCR: 2020
- Q4 (31/39)
- I.F.: 0.162

Emerging Sources Citation Index

LATINDEX. Catálogo v1.0 (2002-2017)

Official Journal of the Spanish Society of Anatomy

www.eurjanat.com

EJA
European Journal of Anatomy
Volume 25 - Number 5 September 2021

CONTENTS

Effect of naproxen on testicular morphometry and serum gonadotropin level of cadmium intoxication in rats

Oluwatomilayo P. Odum[1], Oluwaseun A. Adeyanju[2], Toluwase S. Olawuyi[3], Ayodele O. Soladoye[4], Oluwole B. Akinola[1]

[1] Department of Anatomy, Faculty of Basic Medical Science, University of Ilorin, Nigeria

[2] Department of Physiology, college of Health Science, Afe Babalola University Ado-Ekiti, Nigeria

[3] Department of Anatomy, Faculty of Basic Medical Science, Federal University of Technology, Akure, Nigeria

[4] Physiology Department, College of Health Science, Bowen University Iwo, Nigeria

SUMMARY

Nonsteroidal anti-inflammatory drugs that are cyclooxygenase (COX) enzyme inhibitors like naproxen (NAP) and prostaglandins play important roles in the regulation of reproductive functions in females. Cadmium (CAD) is a toxicant that poses effects on various organs in humans and experimental animals. The aim of this study is to investigate the ameliorating effect of naproxen (NAP) against cadmium-induced testicular toxicity on adult Wistar rats with the objectives on histology, hormonal and biochemical parameters. The total number of animals used were fifteen (15) and were grouped into three (3) (n=5 per group): control (CON); Cadmium (CAD; 5 mg/kg) and Cadmium + Naproxen (NAP; 20 mg/kg) for the period of thirty days. Twenty-four hours after the last administration, the animals were weighed and sacrificed using chloroform as a sedative. The organs were located, removed and weighed using an electronic sensitive analytical balance (Sartorius). Results: There are significant differences in the lumen of the control and the group exposed to CAD, which shows that CAD has the ability to disrupt the seminiferous tubules. Significant differences were also found in the epithelium thickness of the CAD-treated groups—with or without NAP.

Morphological alterations were not reversed in the rats exposed to CAD treatment with NAP. Hormonal findings shows that Luteinizing hormone (LH), Follicle stimulating hormone (FSH) were markedly significant ($p<0.05$), but biochemical findings were not significant. In conclusion, CAD induced testicular damage as seen by the histological and morphological observation of the testes, and naproxen ameliorated cadmium-induced testicular damage.

Key words: Cadmium – Naproxen – Testis – Morphology – Gonadotropin – Testicular damage – Heavy metals – Non-steroidal anti-inflammatory drug (NSAID)

INTRODUCTION

Cadmium (CAD) is a toxic heavy metal extremely harmful to humans and other mammalian species.

Corresponding author:
Oluwatomilayo Odum. Department of Anatomy, Faculty of Basic Medical Science, University of Ilorin, Nigeria.
E-mail: oluwatomilayopatience@gmail.com

Submitted: July 28, 2020. **Accepted:** March 29, 2021

It is present in air, soil, sediments, water and smoke. After intake, CAD accumulates in multiple organs and tissues (Järup and Akesson, 2009). Exposure to CAD leads to a wide range of health defects (Nemmiche et al., 2007; Donpunha et al., 2011). For this reason, the International Agency for Research on Cancer has categorized CAD as carcinogenic to humans and animals (IARC, 1993). Unfortunately, human exposure to cadmium is on the increase, particularly in developing countries, due to rapidly growing industries with increasing consumption and subsequent release into the environment. Humans are exposed to CAD, mainly through occupational and environmental contamination (Satarug and Moore, 2004). Non-occupational exposure to CAD predominantly results from smoking, air pollution and consumption of CAD-contaminated seafood and water (Järup et al., 2000; Waisberg et al., 2003). Cadmium has an extremely long biological half-life of 15 years that essentially makes it a cumulative toxin in the liver and kidney (Ercal et al., 2001). However, the dose above which CAD causes early health effects is largely unknown (Thijssen et al., 2007). Several underlying mechanisms at cellular or even molecular levels have been proposed for CAD toxicity. There is a growing interest in the plausible manners of protection from adverse effects induced by CAD exposure. Hence, it seems reasonable that special attention should be directed to agents that can prevent or reduce this metal-induced toxicity (Brzoska et al., 2015; de Moura and Ribeiro, 2015).

Naproxen (NAP) is a Nonsteroidal Anti-inflammatory Drug (NSAID) of the propionic acid class and is commonly used for relief in a wide variety of conditions in which there is pain, fever, swelling and stiffness. It is the preferred NSAID for long-term use in people with a high risk of cardiovascular complications (Richy et al., 2004). Naproxen works by reversibly inhibiting both the Cyclooxygenase-1 (COX-1) and Cyclooxygenase -2 (COX-2) enzymes (Duggan et al., 2010; Hinz et al., 2008). Using agents that have not exhibited many side effects for both treatments and protective measures and that have strong anti-inflammatory effects is very important. Therefore, this study aims at investigating the acute effects of naproxen on cadmium-induced testicular damage.

MATERIALS AND METHODS

Breeding of the Animals

The study was conducted in accordance with the National Institute of Health Guide for the Care and Use of Laboratory Animals, approved by the Institutional Review Board of the University of Ilorin with code UERC/BMS/097, and every effort was made to minimize both the number of animals used and their suffering. Male Wistar rats (8-10 weeks old) were obtained from the animal holding of the Department of Anatomy, Ladoke Akintola University of Technology, Ogbomoso (Oyo State, Nigeria). The rats were housed in cages (made from wood, wire gauze and net) under natural light and dark cycles at room temperature. The floor of the cages was made with wood to make it comfortable for the rats, and it was covered with sawdust to provide a soft floor for the rats and to make cleaning of the cage convenient when littered. They were fed with rat pellets purchased from approved stores, and water was given *ad libitum.* They were grouped and left to acclimatize for 2 weeks before the study commenced.

Experimental design

The total numbers of animals used were fifteen. They were grouped into three: one (1) control and two (2) experimental groups with consideration towards size variation. Cadmium was added to drinking water, while naproxen was administered using a feeding tube (orogastric cannula, size-6). The animals were treated for a period of thirty days.

Group 1: (control) (CON): (n = 5): Given rat pellets and distilled water.

Group 2: (n = 5): Given cadmium-exposed (CAD) and pellets.

Group 3: (n = 5): Given cadmium + naproxen – treated rats (CAD+NAP) and pellets.

The CAD-treated rats received 5 mg/kg of cadmium as reported previously (Shagirtha et al., 2011).

Cadmium-exposed rats were treated with Naproxen at 20 mg/kg body weight for 15 days. Naproxen was administered orally through orogastric cannula.

Collection and processing of the samples

Twenty-four hours after the last administration, the animals were weighed and thereafter sacrificed by the use of chloroform as a sedative. Blood was collected by cardiac puncture into EDTA bottles for serum FSH, LH and C-reactive protein (CRP) analysis. The animals' abdominal cavity was opened by a midline abdominal incision and the reproductive organs (Testes) were removed. Testes were fixed in Bouin's fluid. Epididymis were placed in 0.9% normal saline and minced with 0.9% of normal saline for semen analysis. Sperm morphological characteristics were graded as normal or otherwise, according to Saalu et al. (2008).

Biochemical Studies

The level of LH, FSH and CRP were estimated using Accu Bind ELISA Microwell by Mono bind Inc. Lake Forest, CA 92630, USA. Malodialdehyde levels in serum were measured according to the method of Stock and Domandy (1971).

Luteinizing Assay Procedure

LH was quantitatively determined according to the manufacturer instruction based on the method of Wennink et al. (1990). Essentially, biotinylated monoclonal and enzyme-labeled antibodies are directed against LH epitope— the immunologically active site. The reaction between LH antibodies and native LH forms a sandwich complex that binds with the streptavidin coated to the well. Following the completion of the required incubation period, the enzyme-LH antibody bound conjugate is separated from unbound enzyme-LH conjugated by separation and decantation. The activity in the antibody-bound fraction is directly proportional to the native antigen concentration. The activity of the enzyme present on the surface of the well was quantified by reaction with suitable substrate to produce color.

Twenty-five microliters (25 µl) of the standard, the specimens and controls were dispensed into appropriate wells. Twenty-five microliters (25 µl) of enzyme conjugate reagent were pipetted into the wells and thoroughly mixed for 30 seconds, and incubated at a temperature of 36°C for 60 min. The microtiter wells were rinsed and flicked 5 times with 300 µl of washing solution. The wells were struck sharply with absorbent paper to remove all residual water. Hundred microliters (100 µl) of TMB substrate solution were added to each well, and mixed and then incubated at room temperature for 15 min. The reaction was stopped using 100 µl of stopping solution. The samples were gently mixed for 30 seconds until the blue color changed to yellow. Absorbance was read at 450 nm with Rayto: RT-2100C, Microplate Reader within 15 min.

Follicle Stimulating Hormone Assay Procedure

Follicle stimulating hormone was assayed according to Simoni et al. (1997). 25 µl of the standard, the specimens and controls was dispensed into appropriate wells. 50 µl of enzyme conjugate reagent was pipetted into the wells and thoroughly mixed for 30 seconds and incubated at a temperature of 36°C for 60min. The microtiter wells were rinsed and flicked 5 times with 300µl of washing solution. The wells were struck sharply with absorbent paper to remove all residual water. 100µl of TMB substrate solution were added to each well and mixed and then incubated at room temperature for 15 min. The reaction was stopped using 100µl of stopping solution. The samples were gently mixed for 30 seconds until the blue color changed to yellow. Absorbance was read at 450 nm with a microtiter well reader within 15 min C-reactive protein (CRP).

The level of plasma CRP was estimated by using commercially available enzyme-linked immunosorbent assay (ELISA) kit (Accu Bind ELISA Microwell by Monobind Inc. Lake Forest, CA 92630, USA). The test was performed using the previously described method of López-Alcaraz (2014). Briefly, 0.050ml (50 µl) of the appropriate serum reference, control or specimen was pipetted into assigned well. 100 µl of CRP-Enzyme Reagent was added to all wells. The microplate was swirled gently for 20-30 seconds for proper mixing.

The plate was incubated at room temperature for 15 min. The content of the microplate was discarded by decantation (using absorbent paper to blot the plate dry). 350 µl of buffer were added

and decanted (the procedure was done thrice for proper washing of microplate). 100µl of working substrate were added to all wells. The reagents were added in the same order to minimize reaction time differences between wells. The plate was incubated at room temperature for 15 min. 50 µl of stop solution were added to each well and was mixed for 15-20 sec. Finally, each absorbent was read at 450 nm in a microplate reader (using a well referenced wavelength of 620-630 nm to minimize well imperfection).

Determination of Plasma Malondialdehyde

Malondialdehyde levels in plasma were measured according to the protocol outlined by Stocks and Domandy (1971). The reaction mixture contained 100 µl of plasma and 20% trichloroacetic acid (1 ml). The above were mixed and centrifuged at 2000 rpm for 5 min to obtain the supernatant. 0.5 ml of supernatant is mixed with 0.7% thiobarbituric acid (1 ml); the tubes were heated in a water bath at 100^{o}C for 20 min and all tubes were cooled in water. The spectrophotometer was blanked using the reagent blank at 532 nm. Absorbance of tests and standards were read. Malondialdehyde level was calculated in plasma.

Semen Analysis

After sacrifice, the caudal epididymis of rats in each of the experimental group was removed and minced thoroughly in a specimen bottle containing 0.9% normal saline for a few min to allow the sperms to become motile and swim out from the caudal epididymis (Saalu et al., 2008).

Sperm count and motility

After 5 min incubation at 37°C (with 5% CO_2), the semen was then taken with a 1 ml pipette, dropped on a clean slide, and covered with cover slips. The slides were examined under light microscope for sperm motility (Saalu et al., 2008) and with the aid of the improved Neubauer hemocytometer (Deep1/10mm LABART, Germany) counting chamber, as described by Pant and Srivastava (2003); the spermatozoa were counted under the light microscope. The counting was carried out in five thoma chambers.

Sperm morphology

This was done as described by Saalu et al. (2013). The sperm morphology was evaluated with the aid of a light microscope at x400 magnification. The caudal sperm was taken from the original dilution for motility, and diluted 1:20 with 10% neutral buffered formalin (Sigma- Aldrich, Canada). In wet preparations using phase contrast optics, the spermatozoa were categorized. In this study a spermatozoon was considered morphologically normal and abnormal based on:

Well-defined acrosomal region comprising 40-70% of the head area.

No neck, mid-piece or tail defects and no cytoplasm droplet more than one-third the size of normal sperm head.

Histological Procedures

The histology of the testes was done by modifying the method reported by Bancroft and Gamble (2008). The organs were harvested and fixed in Bouin's fluid for 24h, after which it was transferred to 70% alcohol for dehydration. The tissues were washed through 90% and absolute alcohol and xylene for different durations before they were transferred into two changes of molten paraffin wax for 1 hour each in an oven at 65°C for infiltration. They were subsequently embedded, and serial sections were cut using rotary microtome at 5 micrometers.

The tissues were picked up with albumenized slides and left to dry on a hot plate for 2 min. The slides were dewaxed with xylene and washed with absolute alcohol (2 changes); 70% alcohol, 50% alcohol and then water for 5 min. The slides were then stained with Hematoxylin and Eosin. The slides were mounted in DPX. Photomicrographs were taken at x100 magnification.

Statistical analysis

Results obtained from the analysis of andrological parameters as well as testicular body weight ratio of the Wistar rats were analyzed statistically to see the correlation between the results using Sigma plot (SPW v. 12). The results were presented as mean ± SEM with significant level at P-value <0.05 while the histological

examination, Sperm analysis, FSH and LH were carefully studied and analyzed to establish any correlation between the groups.

RESULTS

Naproxen reversed spermatid defects in cadmium-induced testicular damage. Exposure of the rats to cadmium led to significant decrease in the normal concentration of spermatids, which was however reversed in the rats treated with naproxen (Fig. 1A). There was also increase in the percentage of head defects in the cadmium-exposed rats, which was reversed in the naproxen – treated rats (Fig. 1B). There was increased percentage of neck and tail defects respectively in the rats exposed to cadmium. Whereas there was no change in this in the rats treated with naproxen, the defects were not aggravated (Fig. 1 C, D).

Naproxen ameliorated sperm motility defect in cadmium-induced testicular damage. Cadmium exposure led to significant decrease in sperm concentration, motility and motility percentage, which were however reversed in the rats treated with naproxen (Fig. 2 A-C).

Naproxen exacerbated testicular damage in cadmium-exposed rat. Enlargement of interstitial space and disruption of seminiferous tubules were observable in the cadmium-exposed group in contrast to the control group. Treatment with naproxen did not reverse the morphological damage caused by cadmium; rather, more morphological damage was seen, as there was enlargement in space of the lumen of the tubule (Fig. 3). H&E (×100). The arrow shows point of degeneration of basement membrane. IS- Interstitial Space. LT- Lumen of the tubule.

Naproxen reversed reduction in luteinizing hormone caused by exposure of rats to Cadmium. Although there was no significant change in the C-reactive protein (CRP), malondialdehyde (MDA) and follicular stimulating hormone (FSH) in the rats exposed to cadmium, the luteinizing hormone (LH) was significantly reduced. However, the reduction in LH in cadmium exposed rats was reversed with naproxen treatment (Table 1).

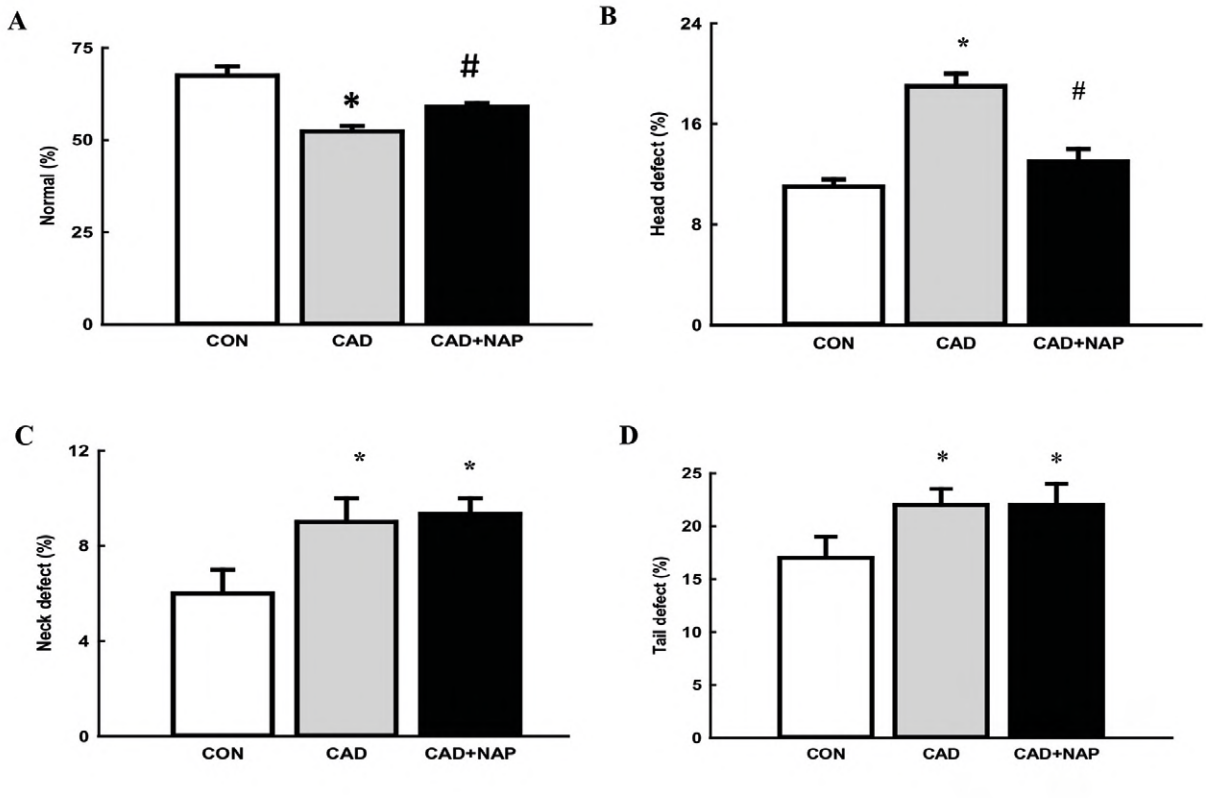

Fig. 1.- Naproxen reversed spermatid defects in cadmium-induced testicular damage. % normal spermatid (A), % head defect (B), % neck defect (C), % tail defect (D). (*p<0.05 vs. control; #p<0.05 vs. CAD).

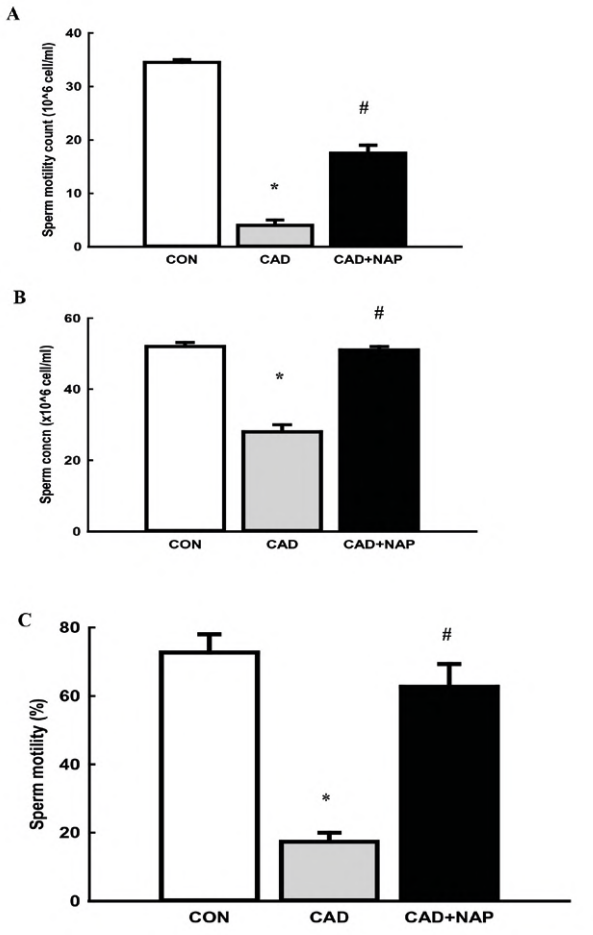

Fig. 2.- Naproxen ameliorated sperm motility defect in cadmium-induced testicular damage. Sperm motility (A), Sperm concentration (B) and % sperm motility (C). (*p<0.05 vs. control; #p<0.05 vs. CAD).

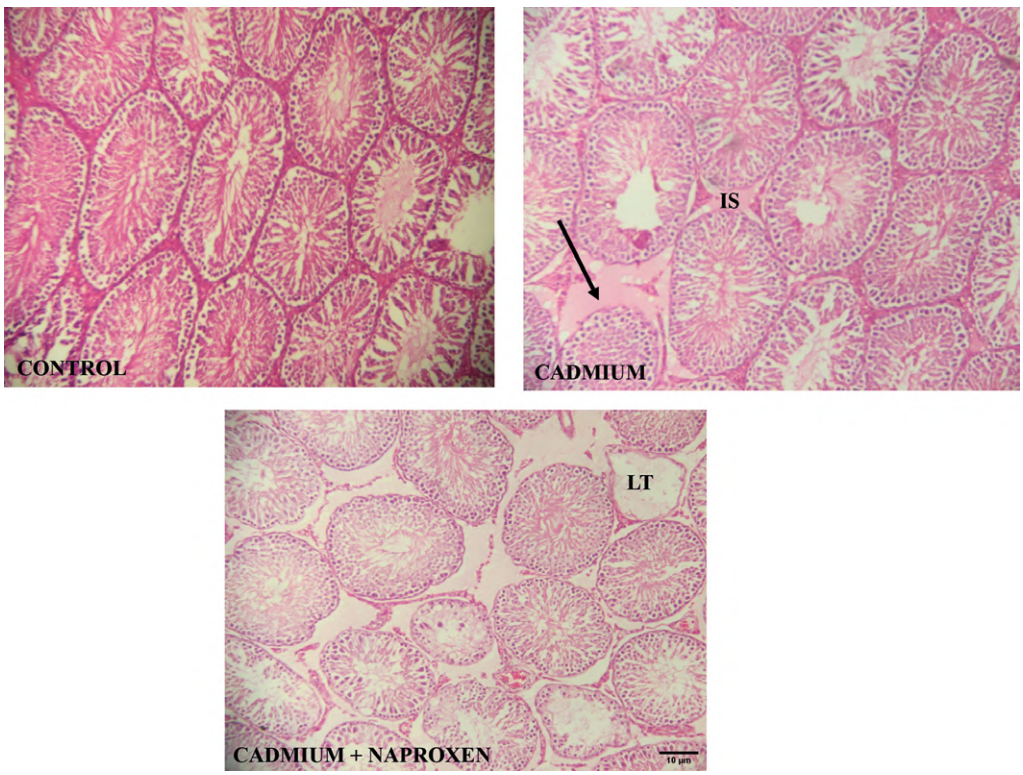

Fig. 3- Naproxen exacerbated testicular damage in cadmium exposed rat. Photomicrographs of testis of the control, cadmium exposed and naproxen treated rat. H&E (100X, scale bar = 10 µm). Arrow shows point of degeneration of basement membrane. IS- Interstitial Space. LT- Lumen of the tubule.

Table 1. Naproxen reversed reduction in luteinizing hormone caused by exposure of rats to Cadmium.

	Con	CAD	CAP+NAP
CRP (mg/dl)	0.1 ± 0.0	0.1 ± 0.0	0.1 ± .0
MDA (mg/dl)	2.7 ± 0.2	2.8 ± 0.1	2.7 ± 0.2
FSH (mg/dl)	3.6 ± 0.6	4.6 ± 0.6	3.3 ± 0.6
LH (mg/dl)	4.9 ± 0.2	2.4 ± 0.2*	3.6 ± 0.3#

CRP- C-reactive protein, MDA- Malondialdehyde, FSH- Follicular stimulating hormone, LH- Luteinizing hormone. * Significant difference from control, # significant difference from CAD.

DISCUSSION

In the last decades, discussion regarding the relationship or development of diseases induced by environmental pollutants is increasing in the scientific literature. Among the numerous toxic substances to which human and other mammalian species are exposed to is cadmium, a heavy metal whose half-life ranges between 10 and 30 years. It promotes extensive damage to several tissues such as liver, kidney, lungs and blood (Nair et al., 2013). Testes and spleen are affected by acute cadmium (CAD) intoxication (Santos et al., 2004; Yiin et al., 2000).

The result of this study showed that CAD caused atrophy and disruption of the seminiferous tubules, increase in interstitial space with reduced Leydig cells, disruption of germinal layers, degeneration and disorganization of cellular layer of the seminiferous tubules, disruption of interstitial tissue, reduced spermatocyte and reduction of mature spermatids. This observation is in agreement with previous studies (Martins et al., 2007; Adamkovicova et al., 2010).

Histopathological damage to the seminiferous tubules may be as a result of unique vasculature and morphological layout of the blood testes barrier (BTB) of the testis (Erica et al., 2009). Treatment of cadmium-exposed rats with NAP does not reverse the morphological alterations.

It was also observed that CAD exposure caused reduction in total sperm count, sperm concentration, sperm motility, and luteinizing hormone. Reduction of follicle stimulating hormone, luteinizing hormone and Leydig cell can probably be the reason for the release of immature sperms into the lumen, reduced sperm count, sperm concentration and sperm motility, which can lead to male infertility. A previous study has reported altered circulation of luteinizing hormone (LH) and follicle stimulating hormone (FSH) in CAD exposure (Lafuente et al., 2004). The endocrine disruption induced by CAD is likely to be multi- factorial mediated via its effects on Leydig cells and/or the hypothalamic-pituitary-testicular axis (Erica et al., 2009). NAP treatment however reversed these defects.

The morphological observations of the testis showed that CAD causes malformation to spermatids. Animals treated with CAD have significantly increased malformed spermatids compared to those of the CON. NAP treatment however reversed this defect. Therefore, it cannot be concluded that naproxen can be teratogenic to spermatogenesis.

Exposure to CAD does not lead to inflammation as found in this experiment. There were no significant differences found in the level of CRP in serum of the control group and both groups exposed to CAD, this is in disagreement with previous reports by Kumas et al. (2016) who recorded increase in serum CRP level of rats treated with CAD (0.5 mg/kg/day) intraperitoneally for 10 days and Ajilore et al. (2016) where treatment of rats with 5 mg/kg of cadmium through oral route for 2 weeks led to significant reduction in hepatoglobin concentration a CRP. Administration of CAD does not increase level of MDA in serum as there were no significant differences found between the CON group and those exposed to CAD. This result did not correlate with another report by Majedah et al. (2010) who observed increase in serum level of MDA leading to oxidative stress after intraperitoneal administration of a single dose of cadmium at 5 mg.

It was discovered in this study that NAP could cause damage to the seminiferous tubules, as there was increased lumen enlargement and reduction of spermatogonium compared to group that was exposed to CAD without treatment. This observation correlates with a previous study (Uzun et al., 2014). The diameters and cross-sectional areas of the seminiferous tubules appeared different, but the differences were not significant. There are significant differences in the lumen of the control and the group exposed to CAD, which shows CAD has the ability to disrupt the seminiferous tubules. There was significant difference in epithelium thickness of the CAD with or without NAP-treated groups. This shows that NAP does not have ameliorative effect on CAD-induced testicular damage.

CONCLUSION

Cadmium exposure led to reduction in the circulating level of Follicle stimulating hormone and Luteinizing hormone. Reduction in the serum level of this hormone will lead to inhibition of spermatogenesis and immaturity of spermatogonia, which can lead to male infertility. It can cause disruption of andrological parameters and the histo-architecture of the testicular histology. Furthermore, naproxen, an anti-inflammatory drug, is able to restore biochemical deficit, but does not restore testicular morphological alterations in cadmium-induced animals.

REFERENCES

ADAMKOVICOVA M, TOMAN R, CABAJ M (2010) Diazinon and cadmium acute testicular toxicity in rats examined by histopathological and morphometrical methods. *Slovak J Anim Sci*, 43(3): 134-140.

AJILORE B, FALOLU I, OLANIYAN O (2016) Effect of pyrus communis (common pear) seeds on selected parameters of liver function in rats treated with cadmium. *ASRJETS*, 23(1): 41-53.

BANCROFT J, GAMBLE M (2008) Theory and practice of histological techniques. 2nd edition. Churchill Livingston, New York, pp 126-127.

BRZÓSKA MM, BOROWSKA S, TOMCZYK M (2015) Antioxidants as a potential preventive and therapeutic strategy for cadmium. *Curr Drug Targets*, 17(12): 1350-1384.

DE MOURA CF, RIBEIRO DA (2015) Are food compounds able to modulate noxious activities induced by cadmium exposure? *Crit Rev Food Sci Nutr*, 57(3): 632-636.

DONPUNHA W, KUKONGVIRIYAPAN U, SOMPAMIT K, PAKDEECHOTE P, KUKONGVIRIYAPAN V, PANNANGPETCH P (2011) Protective effect of ascorbic acid on cadmium-induced hypertension and vascular dysfunction in mice. *Biometals*, 24(1): 105-115.

DUGGAN KC, WALTERS MJ, MUSEE J, HARP JM, KIEFER JR, OATES JA, MARNETT LJ (2010) Molecular basis for cyclooxygenase inhibition by the non-steroidal anti-inflammatory drug naproxen. *J Biol Chem*, 285(45): 34950-34959.

ERCAL N, GURRER-ORHAN H, AYKIN-BURNS N (2001) Toxic metals and oxidative stress. Part I: Mechanisms involved in metal induced oxidative damage. Curr Top Med Chem, 1: 529-539.

ERICA RS, DOLORES DM, CATARINA SP, CHENG CY (2009) Cadmium-induced testicular injury. *Toxicol Appl Pharmacol*, 238(3): 240-249.

FRIBERG L, ELINDER CG, KJELLSTROM T (1992) Cadmium. Environmental health criteria 134, World Health Organization, Geneva, 1992. Available from http://www.inchem.org/documents/ehc/ehc/ehc134.htm

HINZ B, CHEREMINA O, BESZ D, ZLOTNICK S, BRUNE K (2008) Impact of naproxen sodium at over-the-counter doses on cyclooxygenase isoforms in human volunteers. *Int J Clin Pharmacol Ther*, 46(4): 180-186.

IARC (1993) Beryllium, cadmium, mercury, and exposures in the glass manufacturing industry. Working Group views and expert opinions, Lyon, 9-16. *IARC Monogr Eval Carcinog Risks Hum*, 58: 1-415.

JÄRUP L, AKESSON A (2009) Current status of cadmium as an environmental health problem. *Toxicol Appl Pharmacol*, 238(3): 201-208.

JÄRUP L, HELLSTROM L, ALFVEN T, CARLSSON MD, GRUBB A, PERSSON B (2000) Low level exposure to cadmium and earlykidney damage. The OSCAR Study. *Occup Environ Med*, 57: 668-672.

KUMAS M, ESREFOGLU M, BAYINDIR N, IRAZ M, AYHAN S, MEYDAN S (2016) Protective effects of curcumin on cadmium-induced renal injury in young and aged rats. *Bezmialem Science*, 3: 92-98.

LAFUENTE A, GONZALEZ-CARRACEDO A, ROMERO A, CANO P, ESQUIFINO AI (2004) Cadmium exposure differentially modifies the circadian patterns of norepinephrine at the median eminence and plasma LH, FSH and testosterone levels. *Toxicol Lett*, 146: 175-182.

LÓPEZ-ALCARAZ F (2014) Higher levels of C-reactive protein associated with higher adiposity in Mexican schoolchildren. *Nutri Hosp*, 3: 531-536.

MAJEDAH A, FLORENCE E, ELIJAH O, JEROHAM T, MABAYOJE A, ALEXANDER E (2010) Lithium protects against toxic effects of cadmium in the rat testes. *J Assist Reprod Genet*, 27(8): 469-476.

MARTIN LY, HAIYAN C, XIAOYAN L, HOOMAN A, DIANA MOUHAN S, GRACE SANGEUN L, DAVID NH, WENDIE A, KAY C, REX H, ALDONS JL, MICHAEL (2007) FK506, a calcineurin inhibitor, prevents cadmium-induced testicular toxicity in, mice DC. *Toxicol Sci*, 100(2): 474-485.

NAIR AR, DEGHESELLE O, SMEETS K, VAN KERKHOVE E, CUYPERS A (2013) Cadmium-induced pathologies: where is the oxidative balance lost (or not)? *Int J Mol Sci*, 14(3): 6116-6143.

NEMMICHE S, CHABANE-SARI D, GUIRAUD P (2007) Role of alpha-tocopherol in cadmium-induced oxidative stress in Wistar rat's blood, liver and brain. *Chem Biol Interact*, 170(3): 221-230.

PANT N, SRIVASTAVA SP (2003) Testicular and spermatotoxic effects of quinalphos in rats. *J Appl Toxicol*, 23: 271-274.

RICHY F, BRUYERE O, ETHGEN O, RABENDA V, BOUVENOT G, AUDRAN M, HERRERO-BEAUMONT G, MOORE A, ELIAKIM R, HAIM M, REGINSTER JY (2004) Time dependent risk of gastrointestinal complications induced by non-steroidal anti-inflammatory drug use: a consensus statement using a meta-analytic approach. *Ann Rheum Dis*, 63(7): 759-766.

SAALU LC, AKUNNA GG, AJAYI JO (2013) Modulating role of bitter leaf on spermatogenic and steroidogenesis functions of the rats testis. *Am J Biochem Mol Biol*, 3: 314-321.

SAALU LC, UDEH R, OLUYEMI KA, JEWO PI, FADEYIBI LO (2008) The ameliorating effects of grapefruit seed ex-tract on testicular morphology and function of varicocelized rats. *Int J Morphol*, 26: 1059-1064.

SANTOS FW, ORO T, ZENI G, ROCHA BT, DO NASCIMENTO PC, NOGUEIRA CW (2004) Cadmium induced testicular damage and its response to administration of succimer and diphenyl diselenide in mice. *Toxicol Lett*, 152: 255-263.

SATARUG S, MOORE MR (2004) Adverse health effects of chronic exposure to low cadmium in foodstuffs and cigarette smoke. *Environ Health Perspect*, 112: 1099-1103.

SHAGIRTHA K, MUTHUMANI M, PRABU SM (2011) Melatonin abrogates cadmium induced oxidative stress related neurotoxicity in rats. *Eur Rev Med Pharmacol Sci*, 15(9): 1039-1050.

SIMONI M, GROMOLL J, NIESCHLAG E (1997) The follicle stimulating hormone receptor: biochemistry, molecular biology, physiology and pathophysiology. *Endocr Rev*, 18: 739-773.

STOCKS J, DORMANDY TL (1971) The autoxidation of human red cell lipids induced by hydrogen peroxide. *Brit J Haematol*, 20: 95-111.

THIJSSEN S, MARINGWA J, FAES C, LAMBRICHTS I, KERKHOVE EV (2007) Chronic exposure of mice to environmentally relevant, low doses of cadmium leads to early renal damage, not predicted by blood or urine cadmium levels. *Toxicology*, 229: 145-156.

UZUN B, ATLI O, PERK B, BURUKOGLU D, ILGIN S (2014) Evaluation of the reproductive toxicity of naproxen sodium and meloxicam in male rats. *Human Exp Toxicol*, 34: 415-429.

WAISBERG M, JOSEPH P, HALE B, BEYERSMANN D (2003) Molecular mechanisms of cadmium carcinogenesis. *Toxicology*, 192: 117-195.

WENNINK JM, DELEMARRE-VAN DE WAAL HA, SCHOEMAKER R, SCHOEMAKER H, SCHOEMAKER J (1990) Luteinizing hormone and follicle stimulating hormone secretion patterns in girls throughout puberty measured using highly sensitive immunoradiometric assays. *Clin Endocrinol*, 33: 333-344.

YIIN SJ, CHERN CL, SHEU JY, LIN TH (2000) Cadmium-induced liver, heart, and spleen lipid peroxidation in rats and protection by selenium. *Biol Trace Elem Res*, 78: 219-230.

Exogenous melatonin restored the cyto-architectural integrity and biochemical activities of the cerebrum in sodium fluoride induced toxicity

Rukayat A. Ibrahim-Abdulkareem[1], Akeem A. Okesina[2], Fatimo A. Sulaimon[1], Abubakar Imam[1], Emmanuel Yawson[3], Olushola O. Oluyomi[1], Salihu M. Ajao[1]

[1] Department of Anatomy, College of Health Sciences, University of Ilorin, Ilorin, Kwara, Nigeria

[2] Department of Human Anatomy Kampala International University, Faculty of Biomedical Sciences, Uganda

[3] Neurobiology division, Anatomy Department, Redeemer's University, Ede, Osun state

SUMMARY

The cerebrum is responsible for motor, sensory and autonomic activities of the human body, and it is believed that fluoride exposure to the biological system can impede these functions. Therefore, it is imperative to introduce melatonin to limit the extent of fluoride toxicity on the cerebrum and understand the mechanism involved in the aforementioned process. Thirty-two rats were randomly selected into 4 groups (n=8, per group). Groups I-IV received oral administration of 0.2ml of normal saline (NS), 500ppm of sodium fluoride (NaF), concurrent administration of sodium fluoride and melatonin (NaF+MLT), and sodium fluoride before melatonin (NaF-MLT) for fourteen days respectively. At the end of these treatments, the rats were euthanized and cerebral tissues were excised for histological, histochemical and biochemical analyses. Sodium fluoride distorted the shapes and size of the cells and caused constriction of the blood vessels, as well as presence of vacuolations in the cells of the pyramidal layer of the cerebral cortex. However, melatonin was able to restore the cytoarchitecture of cells of the pyramidal layer of the cerebral cortex when administered concurrently and after the administration of sodium fluoride (NaF) respectively. Also, melatonin regulated the activities of Superoxide dismutase, Malondialdehyde and Glutathione peroxidase in the cerebrum. Sodium fluoride causes neurodegeneration in the cerebral cortex, and exogenous melatonin can ameliorate the injury caused by sodium fluoride on the cerebral cortex.

Key words: Cerebrum – Neurodegeneration – Cytoarchitecture – Melatonin – Sodium fluoride

INTRODUCTION

Fluoride, a derivative from the element fluorine, is associated to form insoluble complexes with cations like sodium, magnesium, aluminium or calcium (Whitford et al., 1997). These formed complexes have potential roles in biological and toxicological processes (Bigjay et al., 1987). Sodium

Corresponding author:
Okesina Akeem Ayodeji. Department of Human Anatomy, Kampala International University, Faculty of Biomedical Sciences, Uganda. Phone: +2348033725777. E-mail: akeemokesina@gmail.com

Submitted: January 30, 2021. **Accepted:** April 8, 2021

fluoride is an ionic compound formed from sodium ion (Na^+) and fluoride ion (F^+) (ASTDR, 2003; Wells, 1984). Some of the beneficial role of sodium fluoride is that it can be used as both a dietary supplement and multivitamin (Thomson/Micromedex, 2006; McEvoy, 2006). The toxicity effects of fluoride have been reported in various tissues via cell enzyme inhibition and activation, depending on the type of the enzyme involved (Adamek et al., 2005, Mendoza-Schulz et al., 2009). Excessive exposure to fluoride brings about increase in the production of anion superoxide (O_2–) (Garcia-Montalvo et al., 2009; Hassan and Yousef, 2009) and other hydroxyl radicals that may initiate hazardous effects of fluoride (Urbansky, 2002), ER stress and reactive oxygen species (ROS) production (Hassan and Yousef, 200; Lui et al., 2003; Sireli and Bulbul, 2004). Fluoride is also known to cross the blood-brain barrier (BBB) to cause neuronal degeneration resulting in central nervous system (CNS) dysfunction (Claro et al., 1990). Myelin splitting, vacuolation of mitochondrial, compressed Golgi cisternae, dilatation, and scattering of the rough endoplasmic reticulum of neurons were all affected after treatment with sodium fluoride on the brain (Reddy et al., 2011). Furthermore, the use of sodium fluoride in the treatment of water and as an additive in toothpaste is still frequent, and it is known to cause a deleterious effect (low intellectual coefficient, neurodegeneration) in the brain (Chauhan et al., 2014). The effect of fluoride on the cerebral cortex of both neonatal and adult rats has been established to show loss of cellular layer and major neurodegeneration changes in the motor cortex (Shivaraiashankara et al., 2002; Shashi, 2003).

Melatonin is an indoleamine that is secreted by the pineal gland of the brain to influence the sleep and wake cycle (Choi, 2013), also known as the hormone of darkness (Master-Israilov et al., 2015), and known to have numerous functions such as antioxidant, neuroprotective, anti-inflammatory, anti-apoptotic, or regulatory of energy balance. It is known to freely permeate all morphophysiological barrier of cells in any organ (Shida et al., 1994; Reiter, 1996) and to be concentrated in free-radical generating tissues to prevent potential damage (Reiter, 2000).

Although it has been established that fluoride have the ability to cause deleterious effects ranging from learning and memory deficiency to motor activity impairment (Saad El-Dien et al., 2010; Nasir and Asad, 2013), treatment against this effect has not been established, however. Therefore, it is imperative to understand the possible mechanism of exogenous melatonin against the deleterious effects of fluoride on the cerebrum.

MATERIALS AND METHODS

Chemicals and Drugs

Melatonin: Melatonin in its tablet form was obtained from a local Pharmaceutical Company and produced by Good Neighbour Pharmacy, Broadway industries, United State of America (ABC# 10148547). Melatonin was subsequently dissolved in 0.9 ml of Normal saline (Petri et al., 2011).

Sodium Fluoride: Sodium fluoride salt was obtained from Denis store at Taiwo Road in Ilorin and produced by Guangdong Guanghua Chemical factory co. ltd. Shanton Guangdong, China (#515000). Oxidative stress parameters (MDA), superoxide dismutase (SOD) using SOD assay kit, a product of the Cayman Chemicals, 1180 E. Ellsworth Rd. Ann Arbor, MI. the USA. Item No: 706002, and glutathione GSH using GSH Assay Kit (Colorimetric) Catalog Number KA0797 from Abnova. Sodium fluoride was later administered through drinking water to the animals.

Experimental Design

Forty rats weighing between 150-200g were used for this study with free access to food and water *ad libitum*, and exposed to normal light/dark cycle and normal room temperature/ humidity. Experimental protocols were in strict compliance with the guideline for animal research, as detailed in the NIH Guidelines for the Care and Use of Laboratory Animals (2011) and approved by the ethical committee of the University of Ilorin, Ilorin (UERC/ASN/201/856).

The animals were randomly divided into four groups (I- IV), which received oral administration

of 0.2ml of normal saline (NS), 500ppm of sodium fluoride (Kour and Singh, 1980) (NaF), (MLT), concurrent administration sodium fluoride and melatonin (NaF+MLT), and sodium fluoride before melatonin (NaF-MLT) respectively. Note 10 mg/kg of melatonin was given according to Bustos-Obregón et al., 2013).

Tissue Collection

All antibodies were procured from Dianova (GmbH/Warbugstr. 45/20354 Hamburg. Also, reagents and buffers used in this study were molecular biology grade (99.9% pure) from Sigma-Aldrich. At the end of the various treatments, i.e., twenty-four hours later, the animals were sedated with intramuscular administration of 20 mg/kg of ketamine perfused through the heart (Ajao et al., 2010), and cerebral tissues were excised.

Histological/Histochemical procedures

The excised cerebral tissue was initially fixed in four percent paraformaldehyde overnight after extraction, and later transferred to 30% sucrose solution, before taken for histological and histochemical analyses, which were Hematoxylin and Eosin stain to demonstrate the general cytoarchitecture, and Cresyl Fast Violet stains to demonstrate the presence of Nissl bodies respectively.

Determination of Biochemical Parameters

0.1 g of the cerebrum was extracted from the rest of the brain and homogenized in 0.4 ml of five percent sucrose solution; the tissue was further centrifuged at 3000 rpm for 10 minutes, and the clear supernatant was separated into plain bottles. The supernatant was later taken to determine the level of oxidative stress using Superoxide dismutase, malondialdehyde and Glutathione peroxidase enzymes-linked immunosorbent assay commercial kit (ELISA).

Data Analysis

All data were expressed as mean ± standard error of the mean. Differences among control and the experimental groups were considered with $P<0.05$ as statistically significant, using one-way analysis of variance (ANOVA), followed by Tukey *post hoc* test to determine the differences between the groups. The statistical tests were performed using GraphPad Prism version 5.0.

RESULTS

Qualitative results

Cytological arrangement after exposure to fluoride and melatonin

The control group showed a normal cytoarchitecture pattern with presence of normal granular cells (NGC), and the presence of glial (GC) (Fig. 1), densely stained Nissl substance represented (NC) (Fig. 2). Sodium fluoride (NaF) slide showed presence of damaged cells with shrunken nucleus (Pyknotic cell (PC)), presence of pericellular halos (PH), large-sized granular cells (Fig. 1), and sparsely stained Nissl substance with the presence of vacuolations; pyknotic cells (PC) (Fig. 2). Sodium fluoride and melatonin (NaF+MLT) concurrent group showed cells to have normal cytoarchitecture (NC, NPYC), spindle-shaped pyramidal cell (DPYC), pericellular halos (PH) (Fig. 1) densely stained (NC) and sparsely stained (SC) Nissl substance (Fig. 2); Sodium fluoride-melatonin (NaF-MLT) group showed some normal granular cell (NC, NGC) and shrunken cell (PC) (Fig. 1) and densely stained (NC), sparsely stained (SC) Nissl substance and pyknotic appearance (PC) (Fig. 2).

Quantitative results

The effects of fluoride and melatonin using oxidative stress markers

The activity of SOD in the cerebral cortex of the animals that received sodium fluoride (NaF) group showed a significant decrease compared to the groups that received melatonin as treatment plan; Table 1. In addition, the concentration of the MDA in the cerebral cortex of the control (NS), sodium fluoride+melatonin (NaF+MLT) and sodium fluoride-melatonin (NaF-MLT) animals showed significance decrease as compared to sodium fluoride (NaF) group; Table 1. Also, the activity of glutathione in the cerebral cortex of control (NS), sodium fluoride+melatonin (NaF+MLT), sodium

fluoride-melatonin (NaF-MLT) animals showed statistical significance increase as compared to the sodium fluoride (NaF) group only. Furthermore, there was no statistically significant difference between NaF+MLT, NaF-MLT groups as compared to control (NS) group Table 1.

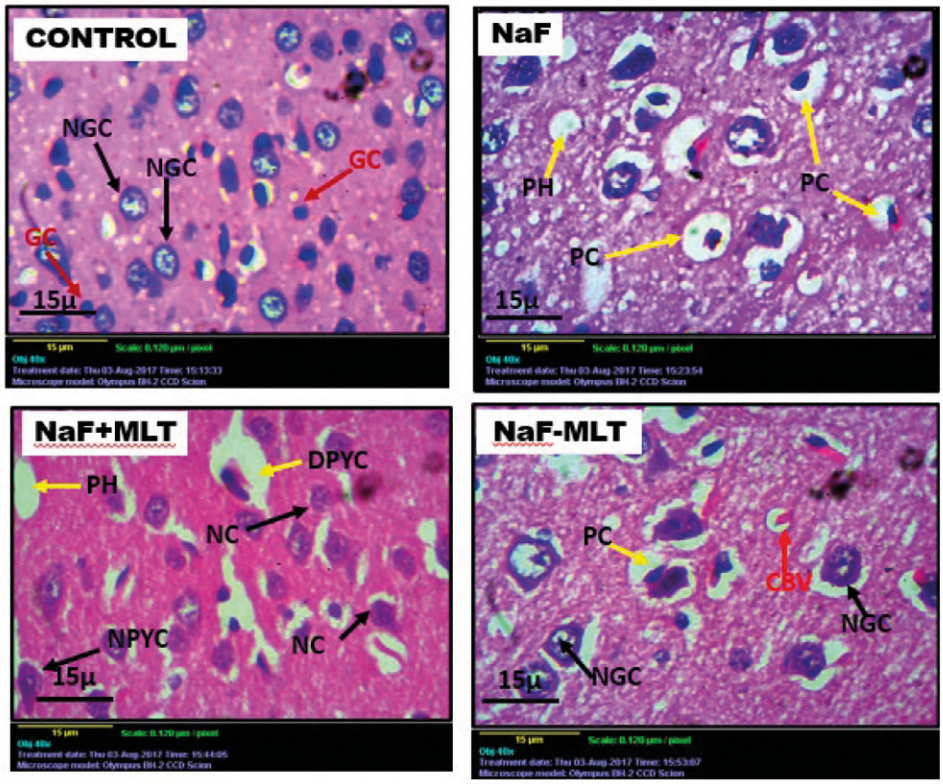

Fig. 1.- Haematoxylin and Eosin stains showing the general cytoarchitecture of the pyramidal layer of the cerebrum of rats. NGC- Normal granular cell; GC- Glia cell; PC- Pyknotic cell; NC- Normal cell; NPYC- Normal pyramidal cell; DPYC- Damaged pyramidal cell; PH- Pericellular halos; PC-CBV- Pyknotic cell with constricted blood vessel; CBV- Constricted blood vessel. Scale bars = 15 µm.

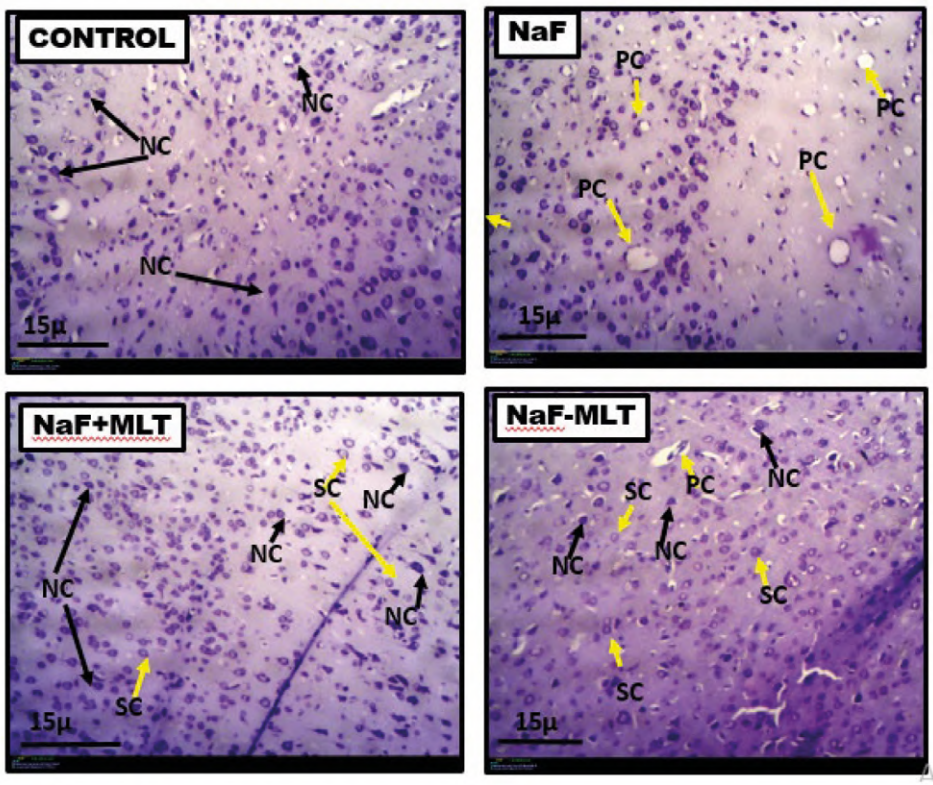

Fig. 2.- Cresyl fast violet stain showing the arrangement of Nissl substance in the pyramidal layer of the cerebrum of rat. NC- Densely stained Nissl substance; PC- Pyknotic cell; SC- Sparsely stained Nissl substance. Scale bars = 15µm.

Table 1. The actions of sodium fluoride and melatonin on oxidative stress markers.

Groups	SOD (U/L) Mean±SEM	MDA (mM) Mean±SEM	GSH (mM) Mean±SEM
NS (control)	2.10±0.10	0.83±0.01	0.14±0.01
NaF	1.19±0.01[a]	0.99±0.01[a]	0.08±0.01[a]
NaF±MLT	1.91±0.01[b]	0.81±0.01[b]	0.11±0.01
NaF-MLT	1.61±0.01[ab]	0.84±0.10[b]	0.13±0.01

[a b] statistically significant difference as compared to normal saline (NS), sodium fluoride (NaF) groups respectively ($p<0.05$).

DISCUSSION

The pyramidal cells in the cerebral cortex showed degenerative changes after administration of sodium, which affected cellular arrangement by inducing the opening of the permeability transition pore and inhibiting the cell membrane potential (Mendoza-Schulz et al., 2009; Chauhan et al., 2014; Anuradha et al., 2001; Geeraerts et al., 1986; Mullenix et al., 1995; Shashi and Kumar, 2016). The ameliorative changes seen were the result of the administration of exogenous melatonin against neural inflammation and apoptotic properties of sodium fluoride neurotoxicity, by acting on some proteins that are involved in the protection of the brain and regulation of its receptors: i.e., melatonin was able to rescue the neural cells through activation of their receptors. (Dun-Xian, 2016; Wang et al., 2009; Tapias et al., 2009; Rao et al., 2010).

The cellular components, the ribosome and endoplasmic reticulum, which are the major sites of protein synthesis in the neuron, were studied by Nissl staining. There was evidence of sparsely stained Nissl bodies due to the loss of the rough endoplasmic reticulum, which is caused by the effect of sodium fluoride. Furthermore, it has been suggested that fluoride degenerates the cell bodies, and this causes the rough endoplasmic reticulum to become scattered (Saad El-Dien et al., 2010; Zhan et al., 2006; Zhang et al., 1999). Also, Reiter suggested that fluoride causes the rough endoplasmic reticulum to become scattered. However, the treatment with melatonin was able to reduce disintegration and dispersal of Nissl bodies, i.e., reducing chromatolysis in these cells by up-regulating the neurotrophic hormone like BDNF, synapsin 1 (Jing et al., 2017).

Sodium fluoride has been established to decrease some enzyme activity in the cells by increasing reactive oxygen species (ROS) in the mitochondria, leading to cellular damage. In this study, the level of superoxide dismutase (SOD) in the group administered sodium fluoride (NaF) and the group which received the treatment before inducing (MLT-NaF) sodium fluoride decreased. However, the treatment with melatonin suggests that melatonin through its antioxidant property was able to increase superoxide dismutase level, which inhibits the production of ROS, thereby inhibiting oxidative stress and cellular damage. These findings also buttress the fact that melatonin increases antioxidant level by mopping/ scavenging of free radicals produced (Reiter, 2000; Zhang et al., 2003; Reiter et al., 2007; Meda et al., 2014; Ajoke et al, 2020).

The level of glutathione was also reduced in the group administered sodium fluoride (NaF), but the administration of melatonin was able to increase the level of glutathione in the cerebral cortex. It can be suggested that melatonin, through its anti-oxidant property by the importation of cystine for the biosynthesis of glutathione through the cystine glutamate antiporter (system Xc) and exportation of glutamate, leads to inhibition of oxidative stress, which means that melatonin establishes the antioxidant activity through the synthesis and transport of cysteine (Gupta et al., 2003; Clarke et al., 2012; Floreani et al., 1997; Ajoke et al, 2020).

Sodium fluoride can induce lipid peroxidation, which attacks membrane phospholipid and reduces fatty acid concentration. There was a significant increase of malondialdehyde (MDA) in the sodium fluoride (NaF) group as a result of the increase in the production of polyunsaturated fatty

acid, similarly to the treatment before induction (MLT-NaF) group in the cerebral cortex of Wistar rats. However, the treatment group that received melatonin showed decrease in lipid peroxidation. This finding suggests that melatonin can regulate the concentration of malondialdehyde in the cerebral cortex of Wistar rats by inhibiting lipid peroxidation cascade/ pathway; which adds to the fact that melatonin is able to restore fatty acid concentration by decreasing lipid peroxidation (Meda et al., 2014; Baydas et al., 2002; Rodriguez et al., 2004).

SUMMARY OF FINDINGS

Melatonin reduced the rate of neural inflammation and also regulated the process of apoptosis in the cells of a damaged cerebrum (Fig. 3). Furthermore, melatonin promoted protein synthesis by reducing chromatolysis in the cells of the cerebrum (Fig. 3). Lastly, melatonin limited the extent of oxidative stress by increasing the levels of superoxide dismutase, increased the importation of cysteine for the biosynthesis of glutathione, and reduced the amount of oxidative degradation of lipids in the cerebrum (Fig. 3).

CONCLUSION

At the end of the study, melatonin was able to limit the extent of sodium fluoride damage by causing reduction in neural inflammation and regulating apoptosis, reduction in the proliferation of chromatolytic cells and reduction in the generation of free radicals. Therefore, melatonin (exogenous) acts as an ameliorative substance on the cyto-architectural and biochemical damage induced by sodium fluoride on the cerebrum of adult Wistar rats.

ACKNOWLEDGEMENTS

We want to express our gratitude to the staff and technicians of histopathology Department, University of Ilorin, for the assistance provided for the histological and histochemical analyses of this work. Also, we appreciate the support of the technical staff of the chemical pathology laboratory, University of Ilorin during the enzyme study of this work. Lastly, we thank both the academic and technical staff of the department of Anatomy, University of Ilorin for both academic and technical input to this study.

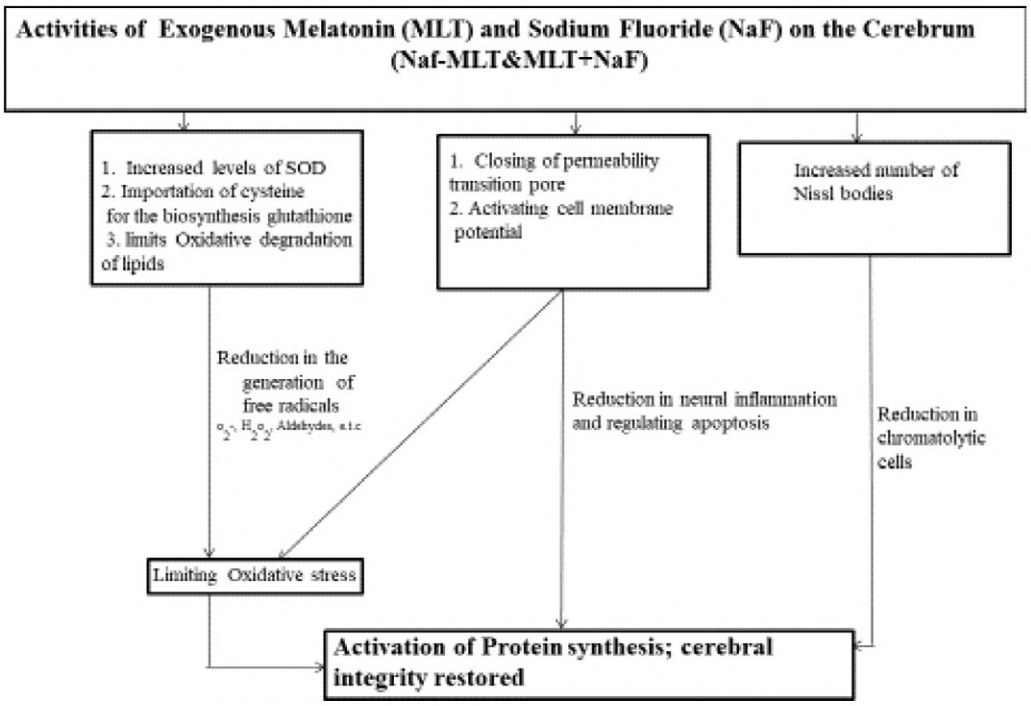

Fig. 3.- Role of exogenous melatonin on sodium fluoride induced cerebellar damage.

REFERENCES

ADAMEK E, PAWŁOWSKA-GÓRAL P, BOBER K (2005) In vitro and in vivo effects of fluoride ions on enzyme activity. *Ann Acad Med Stetin,* 51: 69-85.

AJAO MS, OLALEYE O, IHUNWO AO (2010) Melatonin potentiates cells proliferation in dentate gyrus following ischemic brain injury in adult rats. *J Anim Vet Adv*, 9(11): 1633-1638.

AJOKE SF, AYODEJI OA, LEKEN IA, YETUNDE UR, RUKAYAT IA, AMINU I, YETUNDE AM, MONSUR S, RAHEEM AAI, IYABO AA, SALIHU AM (2020). Exogenous Melatonin Ameliorates Pontine Histoarchitecture and Associated Oxidative Damage in Sodium Fluoride Induced Toxicity. *NJNS*, 17(2):4-10

ANURADHA CD, KANNO S, HIRANO S (2001) Oxidative damage to mitochondria is a preliminary step to caspase-3 activation in fluoride-induced apoptosis in HL-60 cells. *Free Rad Bio Med,* 31: 367-373.

ATSDR (Agency for Toxic Substances and Disease Registry) (2003) Toxicological Profile for Fluorides, Hydrogen Fluoride, and Fluorine, U.S. Department of Health and Human Services, Public Health Service, Atlanta, GA. P.187.

BAYDAS G, GURSU MF, YILMAZ S, CANPOLAT S, YASAR A, CIKIM G, CANATAN H (2002) Daily rhythm of glutathione peroxidase activity, lipid peroxidation and glutathione levels in tissue of pinealectomized rats. *Neurosci Lett*, 323: 195-198.

BIGAY J, DETERRE P, PFISTER C, CHABRE M (1987) Fluoride complexes of aluminium or beryllium act on G-proteins as reversibly bound analogues of the gamma phosphate of GTP. *EMBO J,* 6: 2907-2913.

BUSTOS-OBREGÓN E, POBLETE D, CATRIAO R, FERNANDES FH (2013) Protective role of melatonin in mouse spermatogenesis induced by sodium arsenite. *Int J Morphol,* 31(3): 849-856.

CHAUHAN A, SINGH H, SINGH R (2014) Sodium fluoride toxicity on blood parameter and catalase activity of Indian fresh water iarvicidal fih channa straitus. *Curr World Environ*, 9(3): 952-956.

CHOI J (2013) Melatonin: drug supplement, free radical damage. Huntington's Outreach Project for Education at Standford *HOPES*.

CLARKE M, CROCKETT S, SIMS B (2012) Melatonin induces neuroprotection via system Xc regulation in neural stem cells. *J Stem Cell Res Ther*, 2(2): 120.

CLARO E, WALLACE MA, FAIN JN (1990) Dual effects of fluoride on phosphoinositide metabolism in rat brain cortex. *Biochem J*, 268(3): 733-737.

DUN-XIAN T (2016) Melatonin and Brain. *Curr Neuropharmacol*, 8(3): 161.

FLOREANI M, SKAPER SD, FACCI L, LIPARTITI M, GLUSTI P (1997) Melatonin maintains glutathione homeostasis in kainic-exposed rat brain tissues. *FASEB J,* 11: 1309-1315.

GARCIA-MONTALVO EA, REYES-PEREZ H, DEL RAZO LM (2009) Fluoride exposure impairs glucose tolerance via decreased insulin expression and oxidative stress. *Toxicology*, 263: 75-83.

GEERAERTS F, GIJS G, FINNE E, CROKAERT R (1986) Kinetics of fluoride penetration in liver and brain. *Fluoride*, 19: 108-112.

GUIDE FOR THE CARE AND USE OF LABORATORY ANIMALS (2011) 8th ed. Retrieved from http://www.google.com.ng/?gfe_rd=cr&ei=KWkSVvy7MtPH8gehuLvQDg#q=nih+guidelines+animal+care. [Accessed: October 05, 2015].

GUPTA YK, GUPTA M, KOHLI K (2003) Neuroprotective role of melatonin in oxidative stress vulnearable brain. *Indian J Physiol Pharmacol*, 47: 373-386.

HASSAN HA, YOUSEF MI (2009) Mitigating effects of antioxidant properties of black berry juice on sodium fluoride induced hepatotoxicity and oxidative stress in rats. *Food Chem Toxicol*, 47: 2332-2337.

KOUR K, SINGH J (1980) Histological finding of mice testes following fluoride ingestion. *Fluoride,* 13: 160-162.

LIU G, CHAI C, CUI L (2003) Fluoride causing abnormally elevated serum nitric oxide levels in chicks. *Environ Toxicol Pharmacol*, 13: 199-204.

MASTERS-ISRAILOV A, PANDI-PERUMAL SR, SEIXAS A, JEAN-LOUIS G, MCFARLANE SI (2015) Melatonin, the hormone of darkness: from sleep promotion to Ebola treatment. *Brain Disord Ther*, 4: 151.

MCEVOY GK (2006) American Hospital Formulary Service. AHFS Drug Information. American Society of Health-System Pharmacists, Bethesda, MD.

MEDA R, BHATT RN, VYAS DD, RAO MV (2014) Melatonin protection on fluoride induced neurotoxicity in the male rat. *Indian J Applied Res*, 4(1): 551-553.

MENDOZA-SCHULZ A, SOLANO-AGAMA C, ARREOLA-MENDOZA L, REYES-MARQUEZ B, BARBIER O, DEL RAZO LM, MENDOZA-GARRIDO ME (2009) The effects of fluoride on cell migration, cell proliferation, and cell metabolism in GH4C1 pituitary tumour cells. *Toxicol Lett*, 190: 179-186.

MULLENIX PJ, DENBESTEN PK, SCHUNIOR A, KERNAN WJ (1995) Neurotoxicity of NaF in rats. *Neurotoxicol Teratol,* 17: 169-177.

NASIR N, ASAD R (2013) Effects of flouride on CA3 region of hippocampus in adult albino rats. *J Asian Sci Res*, 3(7): 729-733.

PETRI ES, AJAO MS, OLALEYE O, IHUNWO AO (2011) Effect of melatonin on neuronal nitric oxide synthase expressing cells following global cerebral ischemia. *J Anim Vet Adv,* 10(4): 395-400.

RAO MV, PUROHIT A, PATEL T (2010) Melatonin protection on mercury exerted brain toxicity in rat. *Drug Chemic Toxicol,* 33(2): 209-216.

REDDY YP, REDDY KP, KUMAR KP (2011) Neurodegenerative changes in different regions of brain, spinal cord and sciatic nerve of rats treated with sodium fluoride. *J Med Allied Sci,* 1(1): 30-35.

REITER J (2000) Melatonin; lowering the high price of free radicals. *News Phy Sci*, 15: 246-250.

REITER RJ, TAN DX, TERRON PM, FLORES LJ, CZARNOCKI Z (2007) Melatonin and its metabolites: new findings regarding their production and their radical scavenging actions. *Acta Biochim Pol*, 54(1): 1-9.

REITER RJ (1996) Functional diversity of the pineal hormone melatonin: Its role as an antioxidant. *Exp Clin Endocrinol Diabetes,* 104: 10-16.

RODRIGUEZ C, MAYO JC, SAINZ RM, ANTOLIN I, HERRERA F, MARTIN V, REITER RJ (2004) Regulation of antioxidant enzymes: a significant role for melatonin. *J Pineal Res*, 36: 1-9.

SAAD EL-DIEN HM, EL GAMAL DA, MUBARAK HA, SALEH SM (2010) Effect of fluoride on rat cerebellar cortex: light and electron microscopic studies. *Egyptian J Histol*, 33: 245-256.

SHASHI A, KUMAR J (2016) Neurotoxicity induced by fluoride in rat cerebral cortex. *Int J Curr Microbiol App Sci*, 5(10): 938-951.

SHASHI A (2003) Histopathological investigation of fluoride-induced neurotoxicity in rabbits. *Fluoride*, 36(2): 95-105.

SHIDA CS, CASTRUCCI AML, LAMY-FREUND MT (1994) High melatonin solubility in aqueous medium. *J Pineal Res,* 16: 198-201.

SHIVARAIASHANKARA YM, SHIVASHANKARA A, GOPALAKRISHNA PB, MUDDANNA SR, HANUMANTH SR (2002) Histological changes in the brain of young fluoride intoxicated rats. *Fluoride*, 35: 12-21.

SIRELI M, BULBUL A (2004) The effect of acute fluoride poisoning on nitric oxide and methaemoglobin formation in the Guinea pig. *Turk J Vet Anim Sci*, 28: 591-595.

TAPIAS V, ESCAMES G, LOPEZ LC (2009) Melatonin and its brain metabolite N(1)-acetyl-5-methoxykynuramine prevent mitochondrial nitric oxide synthase induction in parkinsonian mice. *J Neurosci Res*, 87: 3002-3010.

THOMSON/MICROMEDEX (2006) Drug information for the health care professional. Volume 1, Greenwood Village, CO. p 2711.

URBANSKY ET (2002) Fate of fluorosilicate drinking water additives. *Chem Rev*, 102: 2837-2854.

WANG X, FIGUEROA BE, STAVROVSKAYA IG, ZHANG Y, SIRIANNI AC, ZHU S, DAY AL, KRISTAL BS, FRIEDLANDER RM (2009) Methazolamide and melatonin inhibit mitochondrial cytochrome c release and are neuroprotective in experimental models of ischemic injury. *Stroke*, 40: 1-10.

WELLS AF (1984) Structural inorganic chemistry. Clarendon Press, Oxford.

WHITFORD GM, PASHLEY DH, GARMAN RH (1997) Effects of fluoride on structure and function of canine gastric mucosa. *Dig Dis Sci,* 42: 2146-2155.

ZHAN XA, WANG M, XU ZR, LI JX (2006) Toxic effects of fluoride on kidney function and histological structure in young pigs. *Fluoride*, 39(1): 22-26.

ZHANG WH, WANG X, NARAYANAN M, ZHANG Y, HUO C, REED JC, FRIEDLANDER RM (2003) Fundamental role of the rip2/caspase-1 pathway in hypoxia and ischemia-induced neuronal cell death. *Proc Natl Acad Sci USA*, 100: 16012-16017.

ZHANG Z, XU X, SHEN X, XU X (1999) Effect of fluoride exposure on synaptic structure of brain area related to learning memory in mice. *Wei Sheng Yan Jiu*, 28(4): 210-212.

Evaluation of mesenchymal stem cell therapy on diabetic rats' thyroid function (Histological and Biochemical study)

Shaimaa M. Hassan[1], Maha M. Anani[2], Ahmed S. Salman[4,5], Abdullah A. Almilaibary[6], Seham A. Abdel Aziz[3],

[1] Histology and Cell Biology, Faculty of Medicine, Menoufia University, Menoufia, Egypt

[2] Department of Clinical Pathology, Faculty of Medicine, Suez Canal University, Ismailia, Egypt

[3] Histology and Cell Biology, Faculty of Medicine, Menoufia University, Menoufia, Egypt

[4] Department of Anatomy, Faculty of Medicine, Menoufia University, Egypt

[5] Department of Anatomy and Histology, Faculty of Medicine, The University of Jordan, Amman, Jordan

[6] Department of Family and Community medicine , Faculty of Medicine ,Albaha University , Saudi Arabia

SUMMARY

Thyroid hormones play a crucial role in the body's metabolism, and in patients with diabetes thyroid dysfunction diseases are common. Type 1 diabetes mellitus can be treated with daily insulin injections, but this treatment is often accompanied by multiple complications.

Studies have shown, however, that mesenchymal stem cells (MSCs), having produced remarkable improvement in diabetic rat models, can differentiate into insulin-producing cells that could be used for treatment of diabetes mellitus. To evaluate effects of bone-marrow-derived stem cell transplantation on rats with induced diabetes mellitus by assessing their thyroid hormones, thyroid autoantibodies, and structural changes in thyroid gland sections before and after MSC transplantation, this study used 40 adult male albino rats: 10 for MSC isolation; 30 randomly divided into control, diabetic, and MSC-treated groups. In 20, diabetes mellitus was induced by streptozotocin injection. Of the diabetic group, 10 were treated with bone-marrow-derived stem cells. Histological studies (light, electron microscopy) of thyroid sections were observed; thyroid hormones, thyroid peroxidase, and thyroglobulin antibodies were measured in the serum.

Diabetic rats' thyroid glands showed distorted histological structure, a drop in thyroid stimulating hormone (TSH), and elevation of thyroid hormone level. Microscopically, the thyroid gland of bone-marrow-derived stem cell-treated rats yielded significantly ameliorated histological appearance and significantly increased TSH levels, along with thyroid hormones decreased toward normal levels. Diabetes induces thyroid dysfunction and thyroid tissue injury. Bone-marrow-derived stem-cell therapy protects against thyroid gland diabetes-induced tissue injury.

Key words: Diabetes mellitus – Autoimmune thyroiditis – Mesenchymal stem cell – Histopathology – Streptozotocin

Corresponding author:
Dr. Ahmed Salman. Faculty of Medicine, The Jordan University Queen Rania Street, Amman, Jordan. Phone: +962790627433. E-mail: Ahmedsalman1971@gmail.com

Submitted: February 1, 2021. **Accepted:** May 23, 2021

INTRODUCTION

In clinical practice, diabetes mellitus (DM) and thyroid dysfunction are the most prevalently encountered endocrine diseases. In fact, incidence of thyroid disorders in diabetic patients is greater than in the normal population and is affected by autoimmune diseases, age, and gender (Kadiyala et al., 2010). Thyroid hormones participate in controlling functions of pancreases and carbohydrate metabolism. Moreover, diabetes influences thyroid function laboratory results (Leong et al., 1999). Patients with hypothyroid and type 1 diabetes mellitus (T1 DM) experience more hypoglycemic attacks than diabetic patients with normal thyroid function, and studies have reported hypothyroidism common in diabetic patients with insulin resistance (Maratou et al., 2009). Disturbance of thyroid hormones' levels has been reported in diabetic patients, particularly in those with non-controlled diabetes, who reveal depressed nocturnal thyroid stimulating hormone (TSH) peak and reduction of response to thyrotropin-releasing hormone (TRH) (Nilgün Gürsoy, 1999).

In addition, untreated thyroid dysfunction disease may augment existing cardiovascular disease and deteriorate diabetic patients' metabolic control (Mohn et al., 2002). Furthermore, autoimmune thyroid disease (ATD) includes Hashimoto's thyroiditis, Graves' disease, and postpartum thyroiditis. ATD and T1 DM have common predisposition genes in that both diseases can be associated with other autoimmune syndromes such as Addison's and coeliac diseases (Barker, 2006; Pilia et al., 2011). Besides that, ATD and T1 DM share in polyglandular autoimmune syndromes (Dittmar and Kahaly, 2003). ATD shows elevation of serum level thyroid peroxidase (TPO Ab) and thyroglobulin (TG Ab) antibodies (Weetman and McGregor, 1994), which are also detected in T1 DM patients (Hanukoglu et al., 2003); the existence of these antibodies predicts incidence of thyroid diseases (González et al., 2007).

Autoimmune demolition of pancreatic beta cells results in T1 DM with expression of insulin autoantibodies. TI insulin-dependent DM is a metabolic disease that causes beta cell autoimmune destruction requiring insulin replacement (Dave et al., 2015). In rat-model DM, streptozotocin is used to induce T1 DM by destruction of pancreatic beta cells, in turn leading to reduction of insulin and, consequently, significant hyperglycemia. Long-lasting hyperglycemia results in irreversible tissue damage and dysfunction of various organs (El Barky et al., 2017).

The main treatment for T1 DM is insulin injection, but, unfortunately, many complications occur in DM, even with long-term insulin therapy (Chen et al., 2004). Therefore, a new approach for treating DM and its complications has become a priority. Extracted from bone marrow and used in body-tissue repair and rebuilding, mesenchymal stem cells (MSCs) offer advanced DM therapy (Boháčová et al., 2018) because MSCs can differentiate into cells of all three germ layers; they also have high proliferative potential ex vivo, so they are considered for use in tissue engineering and cell transplantation (Das et al., 2013). In addition, the two endocrine disorders of DM and thyroid dysfunction are greatly associated in animals and humans (Duntas et al., 2011). Indeed, in animal models of diabetes, MSC transplantation has shown increased metabolism and is considered a new therapeutic choice for insulin-dependent DM (Dave et al., 2015).

Many studies have been conducted on MSC treatment's effect on various organs affected by diabetes, but few have examined its efficacy in the thyroid gland. Therefore, this study evaluated MSC's transplantation effects on diabetic rats' thyroid glands by assessing alterations of their thyroid hormone level, thyroid autoantibodies, and structural and ultrastructural changes.

MATERIALS AND METHODS

Animals

After the Medical Research Ethical Committee, Faculty of Medicine at Suez Canal University approved this study's protocol, forty 180-200 g adult male albino rats were allowed a laboratory-rat chow diet and water ad libitum. Care and hygiene were undertaken to maintain a constantly healthy location and atmosphere for the rats, housed under standard conditions of temperature and lighting (12-h light/dark cycles). All rats received care in accordance with the rules and regulations of the Medical Research Ethical

Committee, Faculty of Medicine, Suez Canal University.

Mesenchymal stem cells isolation

Ten rats were sacrificed to obtain MSCs from their bone marrow, which was harvested by flushing the tibiae and femurs of 2-4 week-old white rats with DMEM supplemented with 10% FBS. Nucleated cells were isolated with a density gradient (Ficoll) and resuspended in medium supplemented with 1% penicillin-streptomycin (Anani et al., 2014). Cells were plated and incubated at 37° C in 5% humidified CO_2 within a medium changed every 3-4 days. Typically, cells were maintained for 12-14 days as primary culture or upon formation of big colonies. Cultures were washed twice with phosphate buffer saline (PBS). Cells were then trypsinized (0.25%) in 1-mM EDTA for 5 min at 37° C. After centrifugation, cells were suspended with a serum-supplemented medium and incubated in a 50 cm^2 culture flask (Falcon). First-passage MSC cultures were characterized by their stickiness and fusiform shape (Rochefort et al., 2005), and 6 x 10^6 of cells were injected and adjusted for dosing in a 1-ml PBS solution (Alhadlaq and Mao, 2004). Streptavidin-biotin immunoperoxidase was used to detect CD29 (integrin beta-1) and CD44 (receptor for hyaluronate and osteopontin) (purchased from Labvision, New York, USA) as a marker of MSCs (Abdel Aziz et al., 2007).

Experimental groups

Thirty rats were divided into three experimental groups of 10: Group I (Control); Group II, diabetic group (DM); and Group III, diabetic group treated with mesenchymal stem cells (DM+MSC).

Group I (Control): Healthy rats received no medications during the experiments. Their fasting blood glucose was approximately 105 mg/dl.

Group II (DM) and Group III (DM+MSC): Diabetes mellitus was induced in these rats by a single intraperitoneal injection of streptozotocin (STZ) (Sigma-Aldrich, St. Louis, MO), 45 mg/kg body weight, freshly dissolved in 50 mM of sodium citrate buffer (pH 4.5). Two days after STZ administration, rats with 12-hour fasting blood glucose values exceeding 250 mg/dl were considered diabetic (Santos et al., 2013). Blood glucose was tested using a glucose monitor (Accu-Chek Active, Roche, Mannheim, Germany), and blood samples were taken from the rats' tail veins.

Four weeks after diabetes induction, diabetic rats were randomly divided. Half received mesenchymal cells (1×10^5 cells/rat), injected via tail veins (Antunes et al., 2014), while the other groups received the same amount of the vehicle. Thyroid stimulating hormone (TSH), triiodothyronine (T3), thyroxine (T4) levels, free T4, T3, and thyroid autoantibodies (TPO Ab, TG Ab) were measured for all groups; venous blood samples were collected from retro-orbital plexuses. Serum TSH, T3, T4, and free T4 and T3 concentrations were measured by Enzyme Linked Fluorescent Assay (ELFA) (Biomerieux Mini VIDAS Automated Immunoassay System, France). TPO Ab and TG Ab were measured by immunoradiometric assays (Abbott Laboratories, Abbott Park, IL, USA).

After 6 weeks of mesenchymal cell injection, all rats were sacrificed. Neck skin was incised, and the trachea was exposed and dissected. The thyroid gland was removed, one lobe then used for light microscope examination and the other for electron microscope examination.

Light microscopic (LM) study

After thyroid removal, portions of the thyroid gland were fixed in 10% buffered formaldehyde for 2 days and processed for paraffin sections. Sections 5 µm thick were cut and stained with hematoxylin and eosin (H & E) (Kiernan, 2015).

Electron microscopy (EM) study

Gluatraldehyde 3% buffer at pH 7.4 was used to fix thyroid gland specimens. Tissues were removed and fixed again in 1.3% osmium tetroxide in phosphate buffer (pH 7.4) for 1h, then inserted in an epoxy resin mixture and processed and embedded in Epon capsules. Semi-thin sections, i.e., one µm of Epon capsule, were cut using LKB ultra-microtome and then stained with toluidine blue. Ultrathin sections (70-90 nm) were prepared and stained with uranyl acetate and lead citrate (Bozzola and Russell, 1999). Stained grids were then examined by a (JEOL) EM 1010 at the Egyptian National Cancer Institute of Cairo.

Morphometric study

Hematoxylin and eosin slides were examined under a standard microscope. With an X40 lens, five fields of each slide were photographed using a Nikon E400 digital microphotography system (N150, Nikon Co., Tokyo, Japan). Follicular epithelial height was measured using Digimizer software program version 4.6.1.

Quantitative assessment and statistics

All data were analyzed statistically using Graph Pad prism version 4. Data were expressed as mean ± SD and analyzed using one-way analysis of variance (ANOVA) and the Kruskall-Wallis test, followed by Dunn's multiple comparison post-hoc test for comparison among all groups. Differences were significant at p-values of <0.05.

RESULTS

Light Microscopic results

Haematoxylin and eosin (H & E) staining:

Group I (control): Thyroid sections' histological examination revealed many thyroid follicles of variable size surrounded by a connective tissue capsule, and their cavities contained an acidophilic colloid. Each follicle was lined by a single layer of cuboidal follicular cells with round vesicular nuclei and parafollicular cells with flattened nuclei. Interfollicular cells and minute blood capillaries were found between follicles (Figs. 1a, 2a).

Group II (DM): In the diabetic group, the thyroid gland H & E-stained sections showed variable morphological changes: Thin capsule (Fig. 1b) and the parenchyma showed congested blood vessels (Figs. 1c, d, e, 2d). The tyroid follicles' size varied, some large and dilated (Figs. 1c, d), others shrunken and atrophied (Figs. 1d, 2d, e), and some follicles were fused (Fig. 1e).

Follicles were lined by flattened epithelium (Figs. 2b, e), with some lined by multilayers of follicular cells (Figs. 1b, 2b, c), while others had lost their epithelial lining (Fig. 2b), showing hyperemia between follicular cells (Figs. 1b, 2b, c). Several lining epithelial cells showed dark stained pyknotic nuclei (Fig. 2e). The follicles' lumen contained a vacuolated colloid or were completely devoid of colloid (Figs. 1b, c, d, 2d).

Group III (DM + MSC): For diabetic rats, thyroid gland H & E-stained sections treated with mesenchymal stem cells revealed marked improvement and restored normal thyroid histological architecture. Follicles were lined with one layer of cuboidal cells with rounded euchromatic nuclei. Interfollicular cells were present between follicles. Most follicles' lumen was filled with colloid, but some showed vacuolated colloid (Figs. 1f, 2f).

Electron microscopic results

Group I (Control): Electron microscopic examination of the control group's thyroid glands revealed that follicular cells contained euchromatic nuclei with prominent nucleoli and well- defined nuclear membranes. Their cytoplasm had rough endoplasmic reticulum, normal mitochondria, and, occasionally, small dense granules (lysosomes). Their apical surfaces showed apical abundant microvilli protruding into follicular lumen filled with colloid (Figs. 3a, 4a).

Group II (DM): In the diabetic group, electron microscopic sections of the thyroid glands showed follicular cells with irregular electron-dense nuclei with clumped peripheral heterochromatin. Their cytoplasm showed dilated rough endoplasmic reticulum (Figs. 3b, 4c, d), swollen degenerated mitochondria, few electron-dense granules (lysosomes), and many collagen fibers (Figs. 3b, e, 4b); other cells had marked shrunken nuclei and complete loss of cytoplasmic organelles (Fig. 3d). Moreover, some cells had flattened nuclei (Fig. 3e) or fragmented nuclei (Fig. 4b). Some follicles were lined by more than one layer of follicular cells with irregular shrunken dark nuclei with vacuolated cytoplasm (Figs. 5a, b, c). Follicular cells showed dome-shaped apical borders, and microvilli protruded into their follicular lumen (Figs. 5b, c). Dilated blood vessels were observed between follicular cells (Fig. 4e). Follicular cell division in the form of prophase, metaphase, and anaphase was also observed (Figs. 5d, e, f).

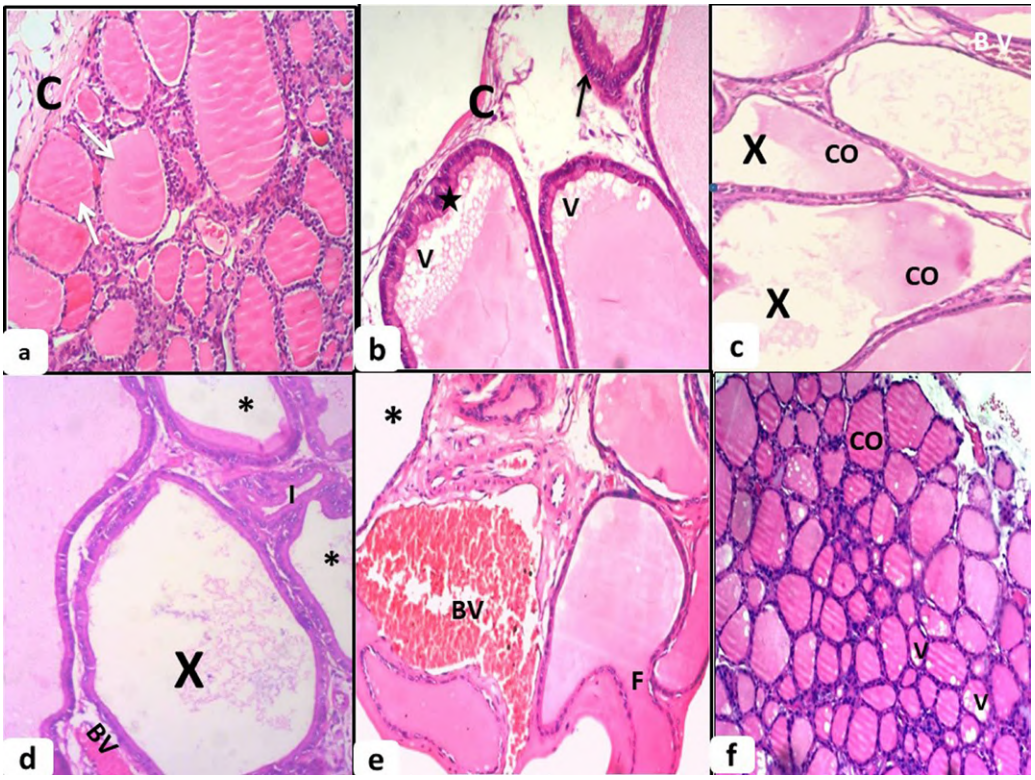

Fig. 1.- Photomicrographs of thyroid gland sections. **(a)** Control group (I) showing a thyroid gland surrounded by a connective tissue capsule (C). The parenchyma is composed of multiple relatively moderate-size rounded follicles (white arrows), and some larger follicles appear at the periphery. **(b-e)** Diabetic group (II) showing thin capsule (C). Some thyroid follicles are lined with multiple layers of follicular cells (stars), others show hyperemia between follicular epithelium (black arrows), and yet others have large dilated thyroid follicles (X) with decreased colloid (Co) and vacuolated colloid (V). Note: There are fused thyroid follicles (F), empty follicles (*), involuted follicles (I), and dilated congested blood vessels (BV). **(f)** The MSC-treated group (III) showing nearly normal thyroid follicles with colloid in their lumina (Co) but still with colloidal vacuoles (V). (H&E, x100).

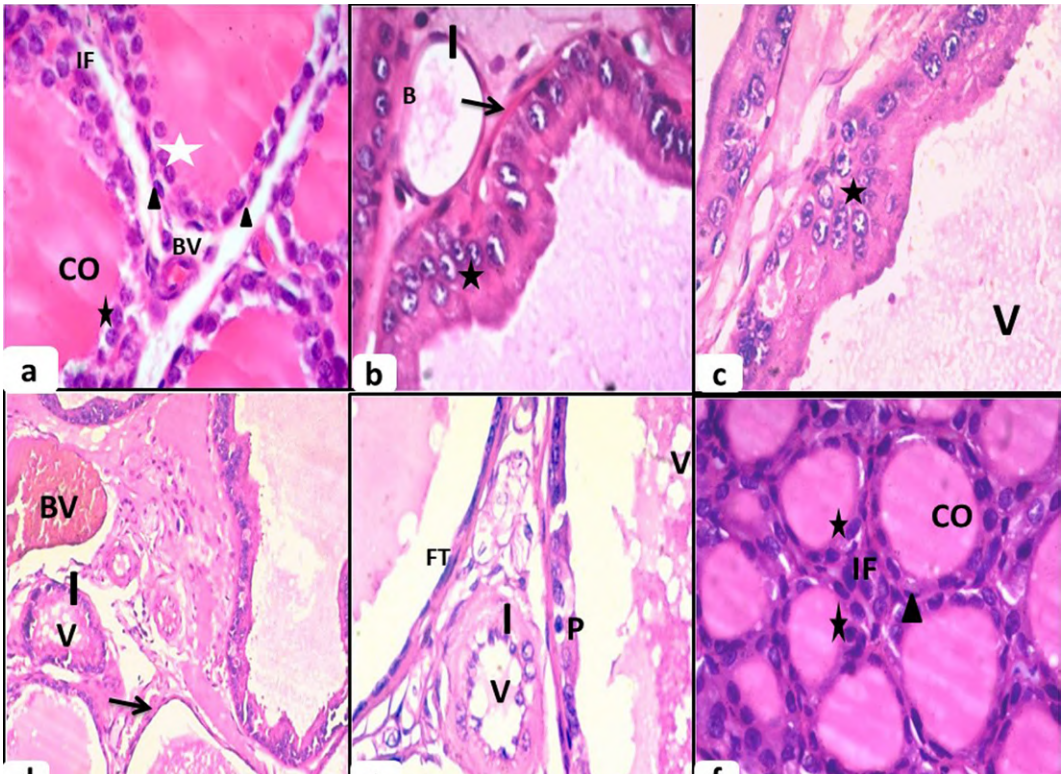

Fig. 2.- Photomicrographs of thyroid gland sections. **(a)** Control group (I) showing normal thyroid architecture with variable follicles lined with cuboidal follicular cells with rounded nuclei (white stars) and parafollicular cells with flattened nuclei (arrow heads). Follicular lumen is filled with homogenous acidophilic colloid (Co). Interfollicular cells (IF) and blood capillaries (BV) appear in connective tissue between follicles. **(b-e)** Diabetic group (II) showing part of thyroid follicles lined with multiple layers of follicular cells (black stars) and hyperemia between follicular epithelium lining (arrow). Additionally, microfollicles or involuted follicles (I) lined with flattened epithelium (FT) with areas of lost epithelium (B) and others with dark pyknotic nuclei (P) containing scanty vacuolated colloid (V). **(f)** MSC-treated group (III) showing improvement of thyroid gland's normal architecture, cuboidal follicular cells (stars) and parafollicular cells (arrow head); homogenous acidophilic colloid **(CO)** filling lumen and interfollicular cells (IF) are noted (H&E, x400).

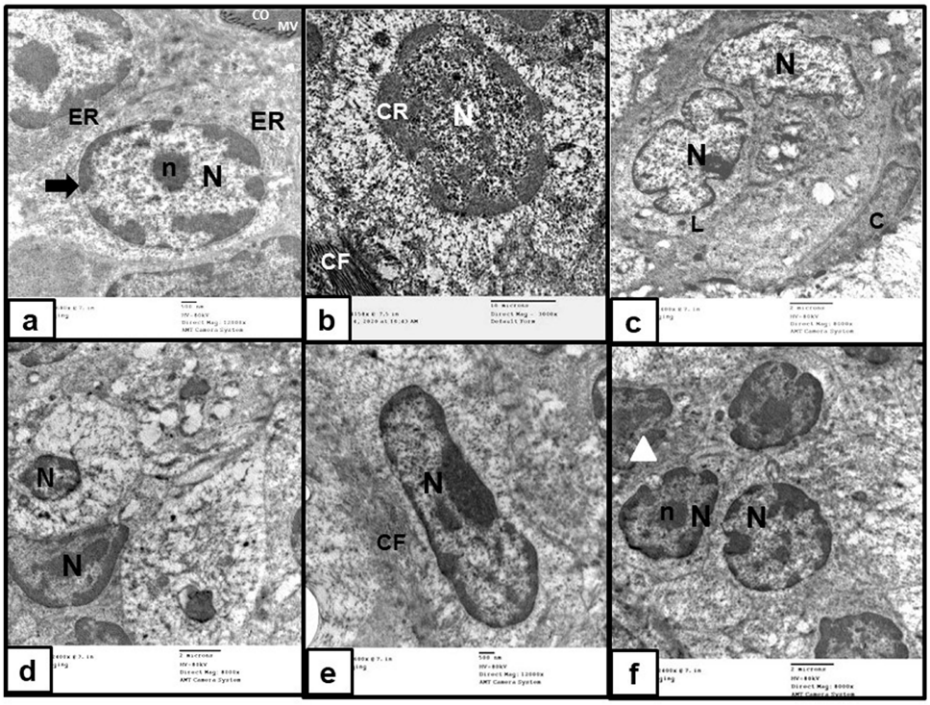

Fig. 3.- Electron micrograph of thyroid follicles of group: **(a)** Control group (I) showing cuboidal follicular cells with rounded euchromatic nuclei (N), prominent nucleoli (n), and well-defined nuclear membranes (white arrow). Their cytoplasm shows cisternae of rough endoplasmic reticulum (ER). Apical surfaces show apical abundant microvilli (MV) protruding into follicular lumen that contains colloid (CO) (x12000). **(b)** Diabetic group (II) showing follicular cell with irregular nucleus (N) with clumped peripheral heterochromatin (CR); many collagen fibers (CF) occupy its cytoplasm (x3000). **(c)** Others with irregular indented nuclei (N), cytoplasm containing lysosomes (L), surrounded by parafollicular C cell (C) (x8000). **(d)** Others with marked shrunken nuclei (N) and complete loss of cytoplasmic organelles (x8000). **(e)** Other cells with flattened nuclei (N) surrounded by many collagen fibers (CF) (x12000). **(f)** Stem cell treated group (III) showing marked amelioration of ultrastructure compared to Group II. Most follicular cells have nearly normal euchromatic nuclei (N) and prominent nucleoli (n). Their cytoplasm has nearly normal organelles, but some cells still show small irregular electron-dense nuclei (arrow heads) (x8000).

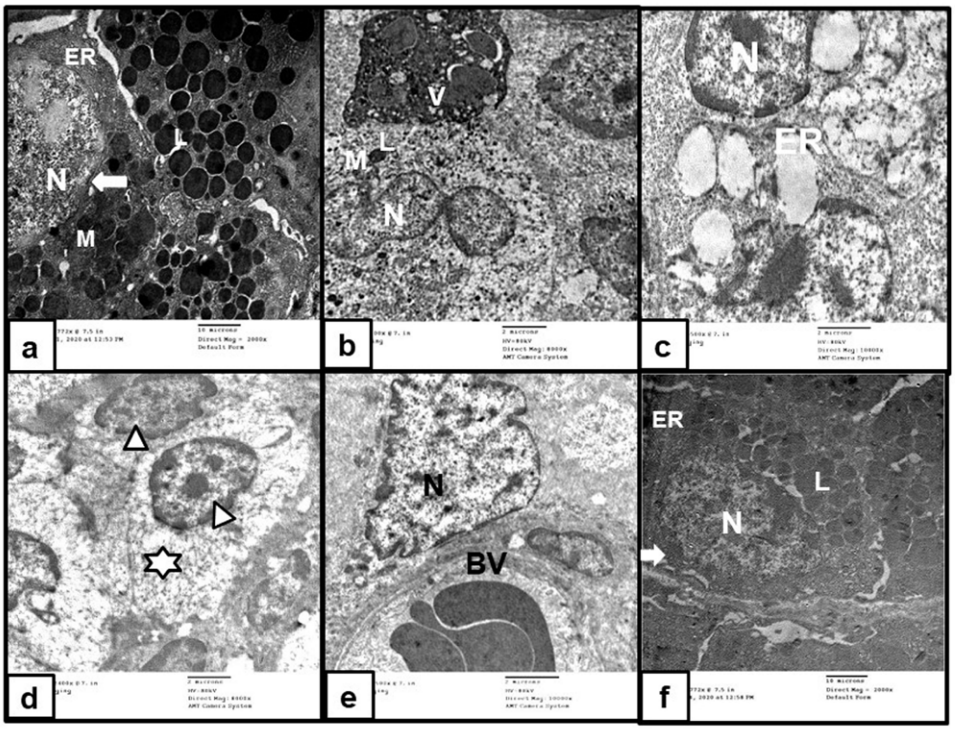

Fig. 4.- Electron micrograph of thyroid follicles: **(a)** Control group (I) showing cuboidal cells with euchromatic nuclei (N) and well-defined nuclear membranes (arrow). Their cytoplasm contains cisternae of rough endoplasmic reticulum (ER), mitochondria (M), and many lysosomes (L) (x2000). **(b-e)** Diabetic group (II) (b) showing follicular cells with fragmented nuclei (N), their cytoplasm containing degenerated mitochondria (M) and lysosomes (L). Vacuolated colloid are also noted (V) (x8000). (c) Others with dark nuclei (N) and large cytoplasmic areas occupied by dilated profiles of rough endoplasmic reticulum (ER) (x10000). (d) Irregular shrunken dark nuclei (arrow heads) surrounded by empty zones devoid of organelles (star) (x8000). (e) Dilated congested blood vessel are also observed (BV). **(f)** MSC-treated group (III) showing follicular cell with oval-to-rounded euchromatic nuclei (N) and well-defined nuclear membranes (arrow). Their cytoplasm shows cisternae of rough endoplasmic reticulum (R) and multiple lysosomes (L) (x2000).

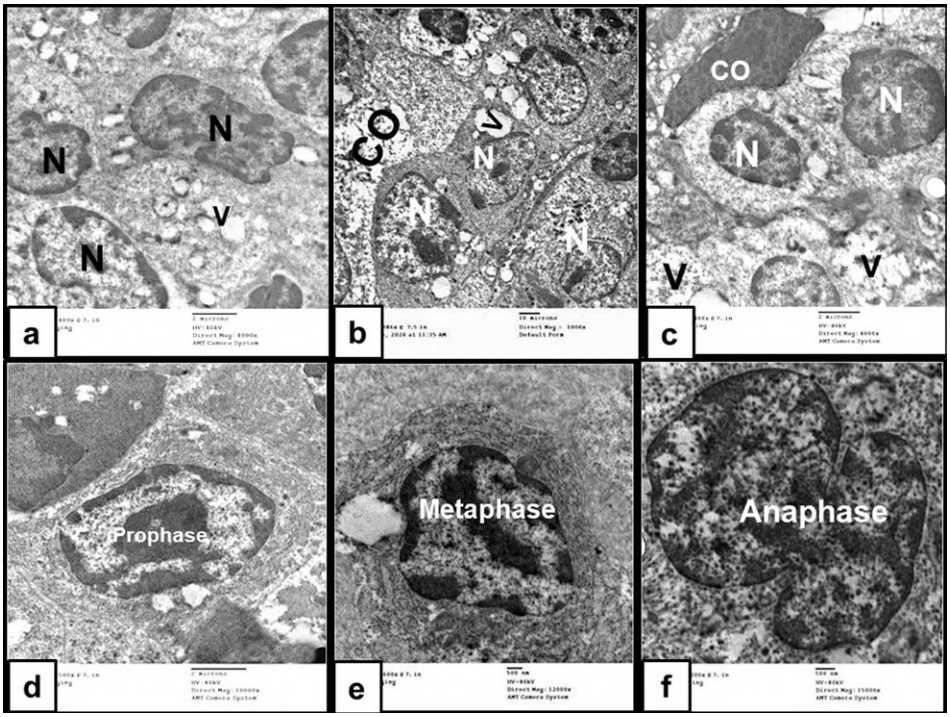

Fig. 5.- Electron micrograph of thyroid follicles of diabetic group (II): **(a-c)** Showing severely affected follicle lined by more than one layer of cells with irregular shrunken dark nuclei (N). The cells exhibit many empty zones devoid of organelles and multiple vacuoles (V). (b & c) Showing columnar follicular cells with dome-shaped apical border, with dark nuclei (N) and lost apical microvilli; the follicular lumen contains colloid (CO). **(d-f)** Showing follicular cell division in forms of prophase, metaphase, and anaphase. (a) (x8000); (b) (x1000); (c) (x8000); (d) (x10000); (e) (x12000); (f) (x15000).

Group III (DM + MSC): Electron microscopic sections of thyroid glands belonging to diabetic rats treated with mesenchymal stem cells revealed marked amelioration of ultrastructure compared to the diabetic group. Most follicular cells had nearly normal euchromatic nuclei with prominent nucleoli with well-defined nuclear membranes. Their cytoplasm had nearly normal organelles, that is, rough endoplasmic reticulum and lysosomes. However, some cells still showed small irregular electron-dense nuclei (Figs. 3f, 4f).

Biochemical results

Diabetic rats showed increased serum TSH concentration, along with reduced serum total T3, total T4, free T3, and free T4 concentrations (Table 1). In the MSC group, these thyroid hormones' serum concentrations were nearly the same as those of the control group (Table 1). However, compared with control rats, diabetic animals showed elevated sera TPO and TG antibodies that returned to normal in mesenchymal-treated rats (Table 1).

Morphometric results

Compared to the control group, the diabetic group had significantly higher follicular cell height. In the MSC-treated group, on the other hand, follicular height decreased markedly (Table 1).

DISCUSSION

Globally, DM is a remarkably common endocrine disease affecting various organs, but it is especially associated with thyroid dysfunction (Chen et al., 2004). In this study, however, serum TSH was elevated, whereas in diabetic rats, T3 and T4 levels decreased so that these biochemical markers improved toward normal in mesenchymal cell-treated rats. These results correspond to those of Da Silva et al. (2018), who reported reduction of T3 and T4 levels with an elevated TSH level in diabetic rats' thyroid function. Indeed, in many experimental studies of diabetic rats, researchers have reported that long-lasting diabetes affects thyroid function because significant hyperglycemia leads to depression of the hypothalamus pituitary-thyroid hormonal axis, in turn leading to reduction of thyrotropin-

releasing hormone (TRH) (Rondeel et al., 1992) and to decline of TSH secretion. Moreover, the thyroid response to TSH is diminished in diabetic rats (Bagchi et al., 1981). Furthermore, T3 and T4 synthesis and thyroperoxidase activity decrease (Moura et al., 1986), and deiodination of T4 to T3 in tissues diminishes (Schröder et al., 1992).

Decline in TSH could be due to augmentation of thyroid DUOX activity, crucial for thyroperoxidase and thyroid hormone synthesis (Fortunato et al., 2010), and otherwise to increased NOX4 activity in diabetic rats' thyroid glands, which participates in raising reactive oxygen species (ROS) synthesis. Accumulated ROS causes thyroid oxidative damage, thus exposing diabetic patients to thyroid hormones' disruption (Santos et al., 2013).

Increased serum TPO and TG antibodies in diabetic animals in our study has also been reported by López Medina et al., (2004), Ridha and Zubaidi (2019) and Sharifi et al. (2008). Type 1 diabetes is greatly associated with thyroid antibodies: thyroid peroxidase and thyroglobulin antibodies are predominant in type 1 DM patients and in their first-degree kin (Hanukoglu et al., 2003). These antibodies are common in uncontrolled diabetic patients and may cause elevated TSH and thus hypothyroidism by segregate thyroid hormone (Ridha and Al Zubaidi, 2019).

In this study, diabetic rats showed distorted thyroid histology with hyperemia and cellular infiltration. This finding accorded with that of Yetim et al. (2015), who reported that diabetic rats' thyroids showed large thyroid follicles with flat squamous or cuboidal lining epithelium and wide lumen. Follicles were distorted, diminishing colloid contents (Yetim et al., 2015). In another study of diabetes' effect on the thyroid, researchers found inflammation of thyroid tissue and its follicles with lymphocyte infiltration (Wright et al., 1983). This could be explained as hyperglycemia resulting from insulin deficiency causing Advanced Glycation End-Products (AGE). As reported by Hasegawa et al. (2011), these products connect receptors with cytokine release, causing inflammation, increased endothelial permeability, fibroblast proliferation, and increased extracellular matrix.

Table 1. Serum thyroid stimulating hormone (TSH), triiodothyronine (T3), thyroxine (T4) levels, free T4, T3, thyroid peroxidase antibodies (TPO Ab), thyroglobulin antibodies (TG Ab) and height of follicular cells (µm) in the studied groups. Data presented as Mean ± SD.

	Normal reference ranges	Group I (control) Mean ± SD (n=10)	Group II (DM) Mean ± SD (n=10)	Group III (DM + MSC) Mean ± SD (n=10)
TSH	0.4-4.5 uUl/ml	1.63 ± 0.74	5.8 ±0.85 ***	1.62 ± 0.98 ###
T3	65.0-205 ng/ dl	114.1 ± 41.66	48.6 ± 7.73 ***	114.5 ± 40.09 ###
T4	3.9-14 ug/dl	9.2 ± 3.259	2.63 ± 0.61 ***	9.20 ± 3.55 ###
Free T3	2-4.4 pmol/l	2.7 ±0.48	1.65 ± 0.29 ***	2.84 ± 0.64 ###
Free T4	0.9-1.7 ng/dL	1.3 ± 0.22	0.95 ± 0.26 *	1.3 ± 0.22 #
TPO Ab	0.0-0.6 IU/ml	1.28 ± 0.22	11.5 ± 3.89 ***	1.37 ± 0.23 ##
TG Ab	0.0-60 IU/ml	3.7 ± 1.7	59.6 ± 21.94 ***	26.5 ± 12.48 *
Height of follicular cells (µm)		10.4 ± 2.98	20.24 ± 7.57 *	7.9 ± 3.47 ###

*, ** or *** Denotes significant difference between DM or DM +MSC vs control, $p<0.05$, $p<0.01$ or $p<0.001$, respectively. #, ## or ### Denotes significant difference between DM and DM + MSC groups, $p<0.05$, $p<0.01$ or $p<0.001$, respectively.

Our study revealed diabetic rats' increased follicular cell height: TSH synthesized and secreted from pituitary thyrotrophs positively regulates thyroid gland activity, which is controlled by the hypothalamic TSH-releasing hormone. TSH acts on specific membrane receptors of follicular cells and stimulates activity of the sodium-iodine symporter of intracellular enzymes involved in thyroid hormones' synthesis. Therefore, when the level of serum thyroid hormones decreases, TSH feedback inhibition is attenuated, and more TSH is secreted; this supports hyperplasia and hypertrophy of thyroid cells and disturbs the thyroid gland's function (Boelaert et al., 2009; Chiamolera and Wondisford, 2009).

The present study's electron microscopic examination of diabetic rats' thyroid follicular cells showed marked dilatation of rough endoplasmic reticulum; swollen degenerated mitochondria; some, or complete, loss of cytoplasmic organelles; and irregular, shrunken, or fragmented nuclei—as also reported by (Bestetti et al., 1987). Denham et al. (1997) confirmed that mitochondrial damage was due to increased proinflammatory cytokines such as TNF-α.

Dilatation of rough endoplasmic reticulum was attributed to formation of oxygen-derived free radicals that induce lipid peroxidation and cause damage to mitochondria and cytoplasmic organelle membrane structures. Accordingly, membranes' stability and integrity are disrupted, leading to osmolality changes and hydropic cell degeneration (Guo et al., 2013). Lipid peroxidation triggers endonuclease enzymes, thus leading to nuclear degeneration (Zhang et al., 2012).

In our work, mesenchymal stem cells (MSC) improved thyroid hormone levels and ameliorated thyroid structure and ultrastructure. This result accords with an examination of MSCs' influence on thyroid function and ROS generation in type I diabetes; previous research found that MSC therapy controlled thyroid ROS generation, thyroid hormones levels remained low, and serum TSH concentrations increased. TPO activity decreased in diabetes, and MSC treatment did not normalize TPO. In our study, MSC treatment decreased serum TSH levels compared to the diabetic group, but TPO levels were normalized in the MSC-treated group, contrary to this study (da Silva et al., 2018).

Many experiments have tested MSC's efficacy for treatment of type 1 DM. Transplantation of 1×10^6 bone marrow MSCs with pancreatic islet cells to type 1 diabetic rats effectively reduced blood glucose levels to under 200 mg/dl after 15 days (Figliuzzi et al., 2009). In many additional experiments, MSC treatment has reduced blood glucose levels in the rat model of diabetes (Lin et al., 2009; Si et al., 2012). In clinical trials, MSC plays an effective role in controlling type 1 diabetes (Carlsson et al., 2015; Jiang et al., 2011). In in vivo studies, MSC is trans-differentiated into insulin-producing cells. Moreover, streptozotocin-induced diabetic rats have shown noticeable elevation of blood insulin levels (Lin et al., 2009).

MSCs' role in controlling blood glucose level can be explained by its secretion of a variety of cytokines and growth factors that help protect damaged cells from apoptosis and enable proliferation of intrinsic pancreatic progenitor cells. This paracrine effect correlates with angiogenesis, anti-inflammatory activities, cell protection, apoptosis resistance, and promotion of mitosis (El Barky et al., 2018). Moreover, MSCs can trans-differentiate into insulin-producing cells and prolong islet cells' viability and function with subsequent formation of pancreatic tissue having the capability of maintaining beta cell function. This leads to decreased blood glucose levels and increased serum insulin in both humans and animals (Dave et al., 2015; Timper et al., 2006). Thus, stem cells can replace the need for islet cell transplantation with semi- analogous effects. However, MSC transplantation is restricted due to the need for much equipment and cell viability (Luo, 2012). More studies are necessary for better understanding of MSCs' mode of action derived from bone marrow and its special effects on damaged tissues.

Further research is also required to understand more about the amount of transported MSCs and transplantation's proper timing so as to employ cells efficiently in regenerative medical applications.

CONCLUSION

Diabetes induces thyroid dysfunction and thyroid tissue injury, but MSCs can help protect against diabetes-induced tissue injury of the thyroid gland. Future studies are required to fully appraise the leverage of stem cell therapy in treatment of DM and its complications.

REFERENCES

ABDEL AZIZ MT, ATTA HM, MAHFOUZ S, FOUAD HH, ROSHDY NK, AHMED HH, RASHED LA, SABRY D, HASSOUNA AA, HASAN NM (2007) Therapeutic potential of bone marrow-derived mesenchymal stem cells on experimental liver fibrosis. *Clin Biochem*, 40(12): 893-899.

ALHADLAQ A, MAO JJ (2004) Mesenchymal stem cells: isolation and therapeutics. *Stem Cells Develop*, 13(4): 436-448.

ANANI M, NOBUHISA I, OSAWA M, IWAMA A, HARADA K, SAITO K, TAGA T (2014) Sox17 as a candidate regulator of myeloid restricted differentiation potential. *Dev Growth Differ*, 56(6): 469-479.

ANTUNES MA, ABREU SC, CRUZ FF, TEIXEIRA AC, LOPES-PACHECO M, BANDEIRA E, OLSEN PC, DIAZ BL, TAKYIA CM, FREITAS IPRG, ROCHA NN, CAPELOZZI VL, XISTO DG, WEISS DJ, MORALES MM, ROCCO PRM (2014) Effects of different mesenchymal stromal cell sources and delivery routes in experimental emphysema. *Respir Res*, 15(1): 118-118.

BAGCHI N, BROWN TR, SHIVERS B, LUCAS S, MACK RE (1981) Decreased thyroidal response to thyrotropin in diabetic mice. *Endocrinology*, 109(5): 1428- 1432.

BARKER JM (2006) Type 1 diabetes-associated autoimmunity: natural history, genetic associations, and screening. *J Clin Endocrinol Metab*, 91(4): 1210-1217.

BESTETTI GE, REYMOND MJ, PERRIN IV, KNIEL PC, LEMARCHAND-BÉRAUD T, ROSSI GL (1987) Thyroid and pituitary secretory disorders in streptozotocin-diabetic rats are associated with severe structural changes of these glands. *Virchows Archiv B*, 53(1): 69.

BOELAERT K, SYED AA, MANJI N, SHEPPARD MC, HOLDER RL, GOUGH SC, FRANKLYN JA (2009) Prediction of cure and risk of hypothyroidism in patients receiving 131I for hyperthyroidism. *Clin Endocrinol (Oxf)*, 70(1): 129-138.

BOHÁČOVÁ P, FAU-HOLÁŇ V, HOLÁŇ V (2018) Mesenchymal stem cells and type 1 diabetes treatment. [Mezenchymální kmenové buňky a léčba diabetu 1. typu.]. *Vnitr Lek*, 64(7-8): 725-728.

BOZZOLA JJ, RUSSELL LD (1999) Electron Microscopy: Principles and Techniques for Biologists (2nd ed.). London: Jones and Bartlett.

CARLSSON P-O, SCHWARCZ E, KORSGREN O, LE BLANC K (2015) Preserved □-cell function in type 1 diabetes by mesenchymal stromal cells. *Diabetes*, 64(2): 587-592.

CHEN L-B, JIANG X-B, YANG L (2004) Differentiation of rat marrow mesenchymal stem cells into pancreatic islet beta-cells. *World J Gastroenterol*, 10: 3016-3020.

CHIAMOLERA MI, WONDISFORD FE (2009) Thyrotropin-releasing hormone and the thyroid hormone feedback mechanism. *Endocrinology*, 150(3): 1091-1096.

DA SILVA DLSG, DE FREITAS ML, CAHIL GM, DE SÃO JOSÉ VS, NETO FM, CARDOSO RC, DA COSTA VMC, FORTUNATO RS, DE CARVALHO DP, MEDEI EH, FERREIRA ACF (2018) Influence of stem cell therapy on thyroid function and reactive oxygen species production in diabetic rats. *Horm Metab Res*, 50(04): 331-339.

DAS M, SUNDELL IB, KOKA PS (2013) Adult mesenchymal stem cells and their potency in the cell-based therapy. *J Stem Cells*, 8(1): 1-16.

DAVE SD, VANIKAR AV, TRIVEDI HL, THAKKAR UG, GOPAL SC, CHANDRA T (2015) Novel therapy for insulin-dependent diabetes mellitus: infusion of in vitro-generated insulin-secreting cells. *Clin Exp Med*, 15(1): 41-45.

DITTMAR M, KAHALY GJ (2003) Polyglandular autoimmune syndromes: immunogenetics and long-term follow-up. *J Clin Endocrinol Metab*, 88(7): 2983-2992.

DUNTAS LH, ORGIAZZI J, BRABANT G (2011) The interface between thyroid and diabetes mellitus. *Clin Endocrinol (Oxf)*, 75(1): 1-9.

EL BARKY A, HUSSEIN S, ALM-ELDEEN A-E, HAFEZ A, MOHAMED TM (2017) Saponins and their potential role in diabetes mellitus. *Diabetes Manag*, 7: 148-158.

EL BARKY AR, EZZ AAH, ALM-ELDEEN A-E, HUSSEIN SA, HAFEZ YA, MOHAMED TM (2018) Can stem cells ameliorate the pancreatic damage induced by streptozotocin in rats? *Canad J Diabetes*, 42(1): 61-70.

FIGLIUZZI M, CORNOLTI R, PERICO N, ROTA C, MORIGI M, REMUZZI G, REMUZZI A, BENIGNI A (2009) Bone marrow–derived mesenchymal stem cells improve islet graft function in diabetic rats. *Transplant Proc*, 41(5): 1797-1800.

FORTUNATO RS, LIMA DE SOUZA EC, HASSANI RA-E, BOUFRAQECH M, WEYEMI U, TALBOT M, LAGENTE-CHEVALLIER O, DE CARVALHO DP, BIDART J-M, SCHLUMBERGER M, DUPUY C (2010) Functional consequences of dual oxidase-thyroperoxidase interaction at the plasma membrane. *J Clin Endocrinol Metab*, 95(12): 5403-5411.

GONZÁLEZ GC, CAPEL I, RODRÍGUEZ-ESPINOSA J, MAURICIO D, DE LEIVA A, PÉREZ A (2007) Thyroid autoimmunity at onset of type 1 diabetes as a predictor of thyroid dysfunction. *Diabetes Care*, 30(6): 1611-1612.

GUO C, SUN L, CHEN X, ZHANG D (2013) Oxidative stress, mitochondrial damage and neurodegenerative diseases. *Neural Regen Res*, 8(21): 2003-2014.

HANUKOGLU A, MIZRACHI A, DALAL I, ADMONI O, RAKOVER Y, BISTRITZER Z, LEVINE A, SOMEKH E, LEHMANN D, TUVAL M, BOAZ M, GOLANDER A (2003) Extrapancreatic autoimmune manifestations in type 1 diabetes patients and their first-degree relatives. *Diabetes Care*, 26(4): 1235-1240.

JIANG R, HAN Z, ZHUO G, QU X, LI X, WANG X, SHAO Y, YANG S, HAN ZC (2011) Transplantation of placenta-derived mesenchymal stem cells in type 2 diabetes: a pilot study. *Front Med*, 5(1): 94-100.

KADIYALA R, PETER R, OKOSIEME OE (2010) Thyroid dysfunction in patients with diabetes: clinical implications and screening strategies. *Int J Clin Pract*, 64(8): 1130-1139.

KIERNAN JA (2015) Histological and Histochemical Methods: Theory and Practice (5th ed.). Scion Publishing Ltd., London.

LEONG KS, WALLYMAHMED M, WILDING J, MACFARLANE I (1999) Clinical presentation of thyroid dysfunction and Addison's disease in young adults with type 1 diabetes. *Postgrad Med J*, 75(886): 467-470.

LIN P, CHEN L, YANG N, SUN Y, XU YX (2009) Evaluation of stem cell differentiation in diabetic rats transplanted with bone marrow mesenchymal stem cells. *Transplant Proc*, 41(5): 1891-1893.

LÓPEZ MEDINA JA, LÓPEZ-JURADO ROMERO DE LA CRUZ R, DELGADO GARCÍA A, ESPIGARES MARTÍN R, BARRIONUEVO PORRAS JL, ORTEGA MARTOS L (2004) Beta-cell, thyroid and celiac autoimmunity in children with type 1 diabetes. [Autoinmunidad pancreática, tiroidea y relacionada con la celiaquía en niños con diabetes mellitus tipo 1]. *An Pediatr (Barc)*, 61(4): 320-325.

LUO L-G (2012) Islet transplantation challenge–human islet longevity: A potential solution from bone marrow cells. *J Bioanal Biomed*, 4(4): 1-5.

MARATOU E, HADJIDAKIS DJ, KOLLIAS A, TSEGKA K, PEPPA M, ALEVIZAKI M, MITROU P, LAMBADIARI V, BOUTATI E, NIKZAS D, TOUNTAS N, ECONOMOPOULOS T, RAPTIS SA, DIMITRIADIS G (2009) Studies of insulin resistance in patients with clinical and subclinical hypothyroidism. *Eur J Endocrinol*, 160(5): 785-790.

MOHN A, DI MICHELE S, DI LUZIO R, TUMINI S, CHIARELLI F (2002) The effect of subclinical hypothyroidism on metabolic control in children and adolescents with Type 1 diabetes mellitus. *Diabet Med*, 19(1): 70-73.

MOURA EG, PAZOS CC, ROSENTHAL D (1986) Insulin deficiency impairs thyroid peroxidase activity: a study in experimental diabetes mellitus. In: Medeiros-Neto G, Gaitan E (eds.). *Frontiers in Thyroidology*, Vol 1 (pp 627-630). Springer US, Boston, MA.

NILGÜN GÜRSOY ET, ERDINÇ E, ŞAZI İ, AYHAN ARıNıK (1999) The relationship between the glycemic control and the hypothalamus-pituitary-thyroid axis in diabetic patients. *Turkish J Endocrinol Metab*, 4: 163-168.

PILIA S, CASINI MR, CAMBULI VM, IBBAA, CIVOLANI P, ZAVATTARI P, INCANI M, MOSSA P, BARONI MG, MARIOTTI S, LOCHE S (2011) Prevalence of Type 1 diabetes autoantibodies (GAD and IA2) in Sardinian children and adolescents with autoimmune thyroiditis. *Diabet Med*, 28(8): 896-899.

RIDHA M, AL ZUBAIDI M (2019) Thyroid auto immune antibodies in children with Type-I Diabetes mellitus in relation to diabetes control. *Pak J Med Sci*, 35(4): 969-973.

ROCHEFORT GY, VAUDIN P, BONNET N, PAGES J-C, DOMENECH J, CHARBORD P, EDER V (2005) Influence of hypoxia on the domiciliation of mesenchymal stem cells after infusion into rats: possibilities of targeting pulmonary artery remodeling via cells therapies? *Respir Res*, 6(1): 125.

RONDEEL JM, DE GREEF WJ, HEIDE R, VISSER TJ (1992) Hypothalamo-hypophysial-thyroid axis in streptozotocin-induced diabetes. *Endocrinology*, 130(1): 216- 220.

SANTOS MCS, LOUZADA RAN, SOUZA ECL, FORTUNATO RS, VASCONCELOS AL, SOUZA KLA, CASTRO JPSW, CARVALHO DP, FERREIRA ACF (2013) Diabetes mellitus increases reactive oxygen species production in the thyroid of male rats. *Endocrinology*, 154(3): 1361-1372.

SCHRÖDER-VAN DER ELST JP, VAN DER HEIDE D (1992) Effects of streptozocin-induced diabetes and food restriction on quantities and source of T4 and T3 in rat tissues. *Diabetes*, 41(2): 147.

SHARIFI F, GHASEMI L, MOUSAVINASAB N (2008) Thyroid function and anti-thyroid antibodies in Iranian patients with type 1 diabetes mellitus: influences of age and sex. *Iran J Allergy Asthma Immunol*, 7(1): 31-36.

SI Y, ZHAO Y, HAO H, LIU J, GUO Y, MU Y. SHEN J, CHENG Y, FU X, HANW (2012) Infusion of mesenchymal stem cells ameliorates hyperglycemia in type 2 diabetic rats: identification of a novel role in improving insulin sensitivity. *Diabetes*, 61(6): 1616-1625.

TIMPER K, SEBOEK D, EBERHARDT M, LINSCHEID P, CHRIST-CRAIN M, KELLER U, MÜLLER B, ZULEWSKI H (2006) Human adipose tissue-derived mesenchymal stem cells differentiate into insulin, somatostatin, and glucagon expressing cells. *Biochem Biophys Res Commun*, 341(4): 1135-1140.

WEETMAN AP, MCGREGOR AM (1994) Autoimmune thyroid disease: further developments in our understanding. *Endocr Rev*, 15(6): 788-830.

WRIGHT JR, SENHAUSER DA, YATES AJ, SHARMA HM, THIBERT P (1983) Spontaneous thyroiditis in BB Wistar diabetic rats. *Vet Pathol*, 20(5): 522-530.

YETIM Z, UNAL D, KARAMESE S, MERCANTEPE T, SELLI J, POLAT E, BÜYÜK B (2015) Effects of menopause and diabetes on the rat thyroid gland: a histopathological and stereological examining. *J Interdiscip Histopathol*, 3.

ZHANG Y, CHEN Y, SUN L, LIANG J, GUO Z, XU L (2012) Protein phosphatases 2A as well as reactive oxygen species involved in tributyltin-induced apoptosis in mouse livers. *Environ Toxicol*, 29(2): 234-242.

Radiological anatomy of the suboccipital segment of the vertebral artery in a select South African population

Bukola R. Omotoso[1], Rohen Harrichandparsad[2], Kapil S. Satyapal[1], Lelika Lazarus[1]

[1] Discipline of Clinical Anatomy, School of Laboratory Medicine and Medical Sciences, College of Health Sciences, University of KwaZulu-Natal, Westville Campus, Durban, South Africa

[2] Department of Neurosurgery, School of Clinical Medicine, College of Health Sciences, Nelson R Mandela School of Medicine, University of KwaZulu-Natal, Durban, South Africa

SUMMARY

Vertebral artery (VA) injuries remain one of the most encountered complications during surgical intervention at the craniovertebral junction (CVJ). Anatomically, the suboccipital segment is the most complicated segment of the VA. The artery undergoes a series of bends to form proximal and distal loops. In addition to this standard anatomical description, previously reported variant anatomies such as fenestration, persistent first intersegmental artery (FIA), hypoplasia, and extradural origin of the posterior inferior cerebellar artery (PICA) also contribute to the complexity of this segment. We evaluated the anatomical features of the V3 component of the VA in a South African population to provide useful data on the prevalence of variation and morphometry of the VA. The study is an observational, retrospective chart review of 554 consecutive South African patients (Black, Indian, and White) who had undergone computed tomography angiography (CTA) at Lenmed Ethekwini Hospital and Heart Centre, Durban, South Africa, from January 2009 to September 2019. Various morphological variations were registered in the course of the VA: (1) Hypoplasia; (2) Extradural (V3) origin of PICA; (3) persistent FIA; and (4) VA fenestration. Hypoplasia was observed in 5.6% of cases. The overall prevalence of the last three variations was 4.2% of the total patients. Codominance was observed in 42.6% of patients, left dominance in 34.3%, and right dominance in 23.1% of patients. Since failure to identify these morphological variations can result in inadvertent injury to the VA with serious neurological consequences, it is therefore imperative to recognize these variations preoperatively. Knowledge of these variations will also assist in the interpretation of radiographs.

Key words: Suboccipital segment of the vertebral artery – Vertebral artery hypoplasia – Fenestration – Vertebral artery dominance – Posterior inferior cerebellar artery – Persistent first intersegmental artery

INTRODUCTION

Vertebral artery (VA) injuries remain the most common type of injury during cervical spine

Corresponding author:
Lelika Lazarus. University of KwaZulu-Natal, Discipline of Clinical Anatomy, School of Laboratory Medicine and Medical Sciences, College of Health Sciences, University of KwaZulu-Natal, Westville Campus, 4000 Durban, South Africa. E-mail: ramsaroopl@ukzn.ac.za

Submitted: January 25, 2021. **Accepted:** May 31, 2021

surgery (DeCarvalho et al., 2019). The risk of injury as a complication of surgery is a major problem, especially at the craniovertebral junction (CVJ) due to the variable course of the artery (Yamazaki et al., 2012). The VA is classically divided into four segments. The first segment (V1) extends from the origin at the subclavian artery to the C6 transverse process. The second segment (V2) extends from C6 to axis vertebra (C2) transverse processes. The third segment (V3) extends from the transverse foramen of the C2 to the point of penetration of the dura mater at the foramen magnum. The intracranial segment (V4) extends from the foramen magnum dura to the vertebrobasilar junction. The V3 part is the segment of the artery at the CVJ, also known as the suboccipital segment (Campero et al., 2011). The V3 is the most anatomically complicated segment of the VA. The artery undergoes a series of bends to form a proximal and a distal loop while passing through the transverse foramen of the axis and atlas vertebrae. Although arterial tortuosity is a morphological variation in the course of the VA frequently reported in the V1 and V2 segments, natural loop formation distinguishes the V3 from other segments of the artery.

The V3 segment of the VA is subdivided into three portions: the vertical part (V3v) ascends through the transverse foramen of C2 and atlas (C1); the horizontal part (V3h) extends from the transverse foramen of C1 and courses in the VA groove on the upper surface of the posterior arch of the atlas; and an oblique part (V3o) extends from the groove to the point of penetration of the posterior atlantooccipital membrane (George and Cornelius, 2001, Ulm et al., 2010). Apart from this standard anatomical description, anatomical variants such as fenestration, persistent first intersegmental artery (FIA), posterior inferior cerebellar artery (PICA) arising from the V3 segment, and hypoplasia have been reported at this segment (Uchino et al., 2012; Fortuniak et al., 2016). Failure to identify these morphological variations preoperatively may compromise collateral circulation resulting in brainstem infarction (Fortuniak et al., 2016). In FIA, the VA courses below the C1 arch to enter the spinal canal after leaving the transverse foramen of C2 without passing through the transverse foramen of C1. Fenestration was registered when the VA split into two vessels along the V3 segment, which rejoined distally before entering the dura mater. The origin of the PICA from the V3 segment was recognized as the extradural origin of PICA.

The prevalence of fenestration, persistent FIA, and PICA arising from the V3 segment have been observed in the normal population without CVJ anomalies. Most of the reports are from the Asian continent (Uchino et al., 2012; Wakao et al., 2014; Kim, 2016, Arslan et al., 2019), with few reports from Europe and the United States (O'Donnell et al., 2014; Fortuniak et al., 2016). Reports from the African continent are scarce. There is no report on the prevalence of morphological variation at the V3 segment in the South African population to the best of our knowledge. Genetic and environmental factors, including local hemodynamic influences, have been suggested to play a specific role in the endmost structure of the VA (Sikka and Jain, 2012). Therefore, racial differences in the Asian and Western populations could account for the disparity in the published reports (Arslan et al., 2019). As a result, it was considered crucial to describe the prevalence of these morphologic variations in a South African population. According to a textbook of complications in neurosurgery by DeCarvalho and co-authors, the incidence of anatomical variation increases the likelihood of injury, especially if it is not identified preoperatively (DeCarvalho et al., 2019). Therefore, the overall knowledge of the course of the V3 segment of the VA and prevalence of possible variation is essential to reduce the risk of catastrophic complications associated with vascular injury during a surgical intervention at the skull base (Hsu et al., 2017).

We evaluated the anatomical features of the V3 segment of the VA in a South African population using 3D computed tomography angiography (CTA) to provide valuable data on the prevalence of variation and morphometry of the VA. The reports from this study will also contribute to the knowledge of evidence-based anatomy in teaching anatomy and clinical practice.

MATERIALS AND METHODS

Patient Population

We reviewed the records of 554 South African patients who underwent multidetector CTA at Lenmed Ethekwini Hospital and Heart Centre, Durban, South Africa, from January 2009 to September 2019. The patient population represents the KwaZulu-Natal region. The design was approved by the Institutional Review Board/ Ethics Committee (Biomedical Research Ethics Committee of the University of KwaZulu-Natal with ethical No: BE 148/19). The angiographies were from 307 males (55.4%) and 247 females (44.6%). The average age of the patients is reported as median (interquartile range): 62 (23) (range: 10-99) years; 62 (25) for female patients and 61 (23) for male patients. Race was defined according to the guidelines outlined in the modern systems of racial classification in the Republic of South Africa (Khalfani and Zuberi, 2001). The South African population is divided into four main racial groups: White, Black, Indian, and Colored. Three population groups were included in the present study: Indian 176 (31.8%), White 287 (51.8%), and Black (16.4%). Images were analyzed using a Picture Archiving Communication System (PACS) Tools. The MDCTA images were examined for vascular variations by a neurosurgeon, a neuroradiologist, and an anatomist using the coronal and sagittal view. Patients with congenital abnormalities at the CVJ such as atlantoaxial dislocation, Down syndrome, Klippel-Feil syndrome, or osseous anomalies were excluded from the study to obtain data from the normal population.

Imaging Technique

The imaging examination was performed on a 64-detector row computed tomography (CT) scanner (Lightspeed CT, GE Healthcare Medical Systems, Milwaukee, WI, USA) with the following scanning protocol: 120 kVp, 697 mAs, beam collimation 64 × 0.625 mm, gantry rotation time 0.4 s, section thickness 0.625 mm, pitch 0.969:1 and reconstruction interval of 0.625 mm. During the procedure, 80 mL of non-ionic iodinated contrast followed by 40 mL saline was infused via a double power injector (Medex flowSens, Guerbet USA) into the patient's antecubital vein (4 mL/s).

Dimensions of the V3 Segment

The course of the V3 segment and tortuosity (proximal and distal loop) were analyzed. The diameters, lengths, and angles of arteries were measured with the Picture Archiving Communication System (PACS) Tools. The measurement of each part of the V3 was taken on the coronal view of the CTA images (Fig.1). The diameter of the vertical portion was measured before the VA entered the transverse foramen of the atlas vertebra, while the horizontal diameter was measured above the transverse foramen of the atlas. A diameter of ≤ 2.5 mm was described as hypoplasia according to the method provided by Chen and co- authors (Chen et al., 2010). We classified the VA as dominant if the diameter was larger than that of the contralateral side by a difference of ≥ 0.3 mm according to the method described by Zhang et al. (2014). When the bilateral VAs had a similar diameter or the difference between the VAs was less than 0.3 mm, we referred to them as being "equal" or "codominant." We measured the angles between the proximal and distal loops to evaluate the degree of tortuosity. The proximal loop of the V3 is formed as the VA bends to enter the transverse foramen of the C2 vertebra. The distal loop is present at the transition from the vertical to the horizontal portion at the transverse foramen of the C1 vertebra (Fig. 1).

Statistical Analysis

Categorical and continuous variables were analyzed using SPSS version 27 (SPSS Inc., Chicago, IL, USA). Categorical variables were analyzed using the chi-square test. Because the continuous variables are not normally distributed, the Kruskal-Wallis test followed by the Wilcoxon Signed-Rank test was used to detect significant differences in the obtained values for continuous variables. All tests were performed at 95% confidence with a p-value of < 0.05.

RESULTS

Continuous variables are presented as median, interquartile range (IQR), and Range. Categorical variables are presented by a number (N) and percentage. The interclass coefficient correlation

for intra-observer reliability testing was 99 % for the V3v length; 97 % for V3v diameter; 99 % for V3h length and diameter; 99 % for V3o length, proximal and distal loop.

For inter-observer reliability testing, the intraclass correlation ranges between 72% to 96% for all the parameters.

Vascular Variation

We registered four types of variation at the V3 segment: (1) hypoplasia; (2) extradural (V3) origin of PICA; (3) persistent FIA; and (4) VA fenestration. The most frequently observed variation was hypoplasia, found in 5.6% of cases (62/1108). Incidence of bilateral hypoplasia was registered in 0.9% (5/554) of patients. The prevalence of the last three, excluding hypoplasia, was diagnosed in 4.2% (23) of the total patients (23 cases/554). There was no significant racial or gender difference in the incidence of variation. The results are summarized in Table 1.

Morphometric Analysis of the Vertebral Artery Diameter

We observed that the average diameter of the VA increases from the vertical (median (IQR)) (Left- 3.43 (0.61) mm; Right- 3.25 (0.70) mm) to the horizontal part (Left- 3.69 (0.89) mm; Right- 3.60 (0.71) mm) and oblique part (Left- 3.55 (0.79) mm; Right- 3.48 (0.83) mm). The average diameter is significantly larger on the left (vertical portion p=0.000, horizontal portion p=0.001, and oblique portion p=0.006) than on the right side. Most of the VAs had similar diameters (42.6%) with differences of ≤ 0.3 mm between the two sides. We observed a left pattern of dominance in 190 patients (34.3%) and right dominance in 128 patients (23.1%). Concerning the racial groups, the diameter of the left V3v was significantly different across the racial groups (p=0.002; specifically, between Black and Indian p=0.001; between White and Indian p=0.014). On the right V3v, there was no significant difference across the racial groups (p=0.368). The diameter of the left V3h showed a significant difference across the

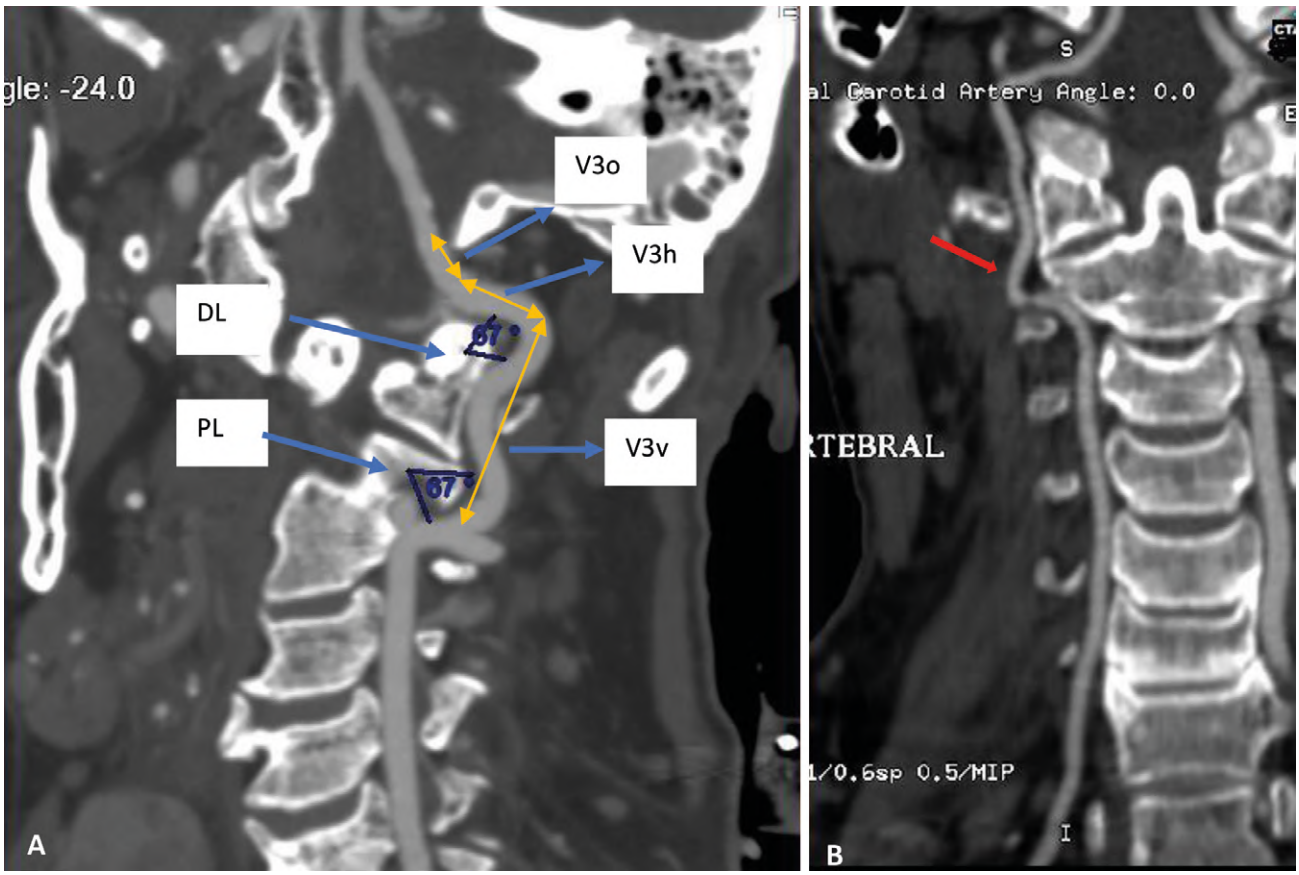

Fig. 1.- Oblique (**A**) and Coronal (**B**) view of CTA image. **A)** V3 segment of the left VA. V3v – vertical segment of the VA; V3h – horizontal segment of the VA; V3o oblique segment of the VA; PL – proximal loop of V3; DL – distal loop of V3. **B)** The red arrow illustrated right VA hypoplasia.

racial groups (p=0.002; specifically, between Black and White p=0.03; Black and Indian p=0.001). On the right V3h, there was no significant difference across the racial groups (p=0.286). The diameter of the left V3o also showed a significant difference across the racial groups (p=0.014; specifically, between White and Black p=0.005; Indian and Black p=0.01).

On the right V3o, there was no significant difference across the racial groups (p=0.315). The average diameter is summarized in Table 2. For gender, the average diameter of the V3o is significantly larger in females on the left (p=0.000). There were no significant gender differences on the right (p=0.063). The average diameter is summarized in Table 3.

Table 1. Incidence of Anatomical Variations at the suboccipital segment of the VA diagnosed by CTA FIA- Persistent first intersegmental artery, FEN- fenestration, PICA- posterior inferior cerebellar artery.

Type of Variation	Total number of cases (incidence %)	Male/Female	Left/Right	Simultaneous Variation
Hypoplasia	62 (5.6)	36/21	25/37	-
Extradural PICA Origin	16 (1.44)	11/5	8/8	-
Persistent FIA	5 (0.45)	1/4	1/4	-
FEN	2 (0.18)	0/2	1/1	2 with FIA

Table 2. Diameter and length of the vertebral artery V3 segment grouped according to race and laterality in South African patients. Results are in mm. Median and (IQR). Range in mm.

Racial Group	Parameters	V3v		V3h		V3o	
		Left	Right	Left	Right	Left	Right
Black	**Diameter**	3.25(0.77) (2.02-6.25)	3.16(0.66) (1.93-5.28)	3.52(0.64) (2.11-6.25)	3.52(0.71) (1.94-5.63)	3.69(1.14) (2.46-6.95)	3.45(0.97) (2.33-6.42)
	Length	24.89(10.3) (6.21-84.7)	23.26(8.46) (10.6-48.3)	7.17(3.22) (3.55-15.0)	7.03(2.72) (3.21-13.5)	4.32(1.9) (1.89-18.74)	4.01(1.78) (1.86-6.39)
Indian	**Diameter**	3.52(0.75) (2.11-7.04)	3.44(0.79) (0.79-5.98)	3.87(0.88) (2.11-7.92)	3.60(0.71) (0.79-6.07)	3.61(0.79) (2.02-6.42)	3.52(0.79) (2.33-5.46)
	Length	24.72(12.63) (11.8-48.7)	23.10(9.44) (11.7-39.7)	7.55(3.03) 3.69(0.82)	7.26(2.8) (2.95-11.8)	4.75(1.98) (2.47-8.25)	4.42(1.94) (1.89-7.44)
White	**Diameter**	3.43(0.53) (0.79-6.95)	3.25(0.64) (1.85-5.72)	3.69(0.82) (0.79-6.42)	3.60(0.80) (1.85-5.54)	3.52(0.8) (0.79-5.9)	3.43(0.7) (0.79-5.72)
	Length	21.94(11.82) (10.6-45.6)	20.60(11.74) (8.71-46.6)	6.19(2.88) (2.67-16.5)	6.08(3.15) (2.6-13.9)	3.50(1.85) (1.05-9.7)	3.36(1.83) (1.32-7.56)

Table 3. Diameter and length of the vertebral artery V3 segment grouped according to gender and laterality differences in South African patients. Results are in mm. Median and (IQR). Range in mm.

		V3v		V3h		V3o	
		Left	Right	Left	Right	Left	Right
Male	**Diameter**	3.43(0.53) (2.02-6.95)	3.25(0.64) (0.79-5.98)	3.69(0.97) (2.11-6.42)	3.52(0.71) (0.79-5.54)	3.45(0.79) (0.79-6.42)	3.52(0.7) (0.79-5.72)
	Length	24.40(11.76) (6.22-46.3)	22.30(9.95) (10.6-43.6)	6.95(2.98) (2.84-16.5)	6.93(3.0) (2.60-13.5)	4.08(1.89) (1.32-7.45)	3.89(1.91) (1.89-8.25)
Female	**Diameter**	3.43(0.70) (0.79-7.04)	3.25(0.70) (1.85-5.72)	3.69(0.88) (0.79-7.92)	3.69(0.71) (1.85-6.07)	3.77(0.72) (2.02-6.95)	3.61(0.79) (2.2-6.42)
	Length	22.10(11.16) (8.71-48.7)	21.57(10.9) (10.6-48.3)	6.45(3.22) (2.67-15.3)	6.44(3.0) (2.95-13.9)	3.96(0.88) (1.05-18.7)	3.76(1.98) (1.87-7.56)

Length

The length of the V3 was significantly greater on the left than the right side in all parts of the artery (median (IQR)). V3v (23.19 (11.72) mm, 21.80 (10.34) mm) p=0.000; V3h (6.75 (3.17) mm, 6.67 (3.01) mm) p=0.000; V3o (4.03 (1.96) mm, 3.82 (1.93)) mm p=0.000. Within the racial groups, the length of the left and the right V3v showed a significant difference across the racial groups (Left p=0.011, but there was no specific difference between the racial groups; Right p=0.005; specifically, between White and Black p=0.035; White and Indian p=0.003). The average length of the horizontal portion (V3h) showed a significant difference across the racial groups (Left p=0.000; specifically, between White and Black p=0.008; White and Indian p=0.000; Right p=0.000; specifically, between White and Black p=0.011; White and Indian p=0.000). The average length of the oblique portion also showed a significant difference across the racial groups (Left p=0.000; between White and Black p=0.015; White and Indian p=0.000; Black and Indian p=0.025; Right p=0.000; specifically, between White and Black p=0.001; White and Indian p=0.000). The average length across the racial groups and laterality are summarized in Table 2. There were no significant gender differences in the VA length on both sides. The results are summarized in Table 3.

Proximal and Distal Loop Angle

The average angle of the proximal loop was significantly larger on the left (median (IQR)) (67° (24°)) compared to the right (65.66° (25.33°)) side (p=0.001). There was no significant difference in the angle of the distal loop on the right and left sides (Right- 67° (14°), Left- 66° (15°)). We did not observe any significant differences across gender and racial groups. The results are summarized in Table 4.

DISCUSSION

Iatrogenic injury to the VA during procedures around C1/2 constitutes a potentially catastrophic complication that may result in permanent neurological deficits or even death (Vergara et al., 2012; Akinduro et al., 2016). Studies have reported rates ranging from 1.7% - 9.0% (Vergara et al., 2012; Elliott et al., 2014; Liang et al., 2004). Adequate information about anatomical variation can influence the choice of surgical procedure at the CVJ. Apart from the risk of injury, morphological variation at the V3 segment of the VA may result in complications such as brainstem infarction if not recognized during preoperative planning (Fortuniak et al., 2016).

Hypoplasia of the VA has been previously described by different criteria in the literature. Using a measure of diameter ≤ 2.5mm according to the method provided by Chen et al. (2010), we observed a 5.6% (62 cases/1108 VAs) incidence of hypoplastic VA (Fig. 1B). Our results agreed with the findings of O'Donnell and co-authors (6.26%) in the US population, although hypoplasia was defined by different criteria (O'Donnell et al., 2014). By contrast, a similar study in the Asian population reported an incidence of 10% (Arslan et al., 2019), while another study in the European

Table 4. Characteristics of proximal and distal loops of the vertebral artery V3 segment grouped according to gender and racial group in South African patients. Results are in degrees. Median and (IQR). Range in degrees.

	Proximal Loop		Distal Loop	
	Left	Right	Left	Right
Male	67.33(22.83) (42.7-118.7)	65.66(25.17) (39-116.7)	66.66(14.67) (42.7-114.7)	67(16) (37.3-110.7)
Female	68.16(25.17) (36.3-120)	65.33(26.17) (36.3-111.7)	66(16) (41.7-115.3)	66.66(14.16) (43.4-97.3)
Black	66(23) (36.3-118.6)	68(32) (42-109.6)	65.50(18.92) (41.7-107.6)	69.66(17.17) (43-105.3)
Indian	68.16(29.17) (42.7-120)	63.33(24.67) (39.7-111.7)	66(19) (39.7-115.3)	65.33(16.67) (39.7-110.7)
White	67.50(22.83) (43.3-116.7)	66(22.16) (36.3-116.7)	67.16(13.25) (37.4-114.7)	67.33(13.83) (37.4-114.7)

population reported an incidence of 20% (Fortuniak et al., 2016). In the studies mentioned above, a VA was considered hypoplastic if it was half or less than half of the diameter of its counterpart. We suggest that the disparity in the above studies and the present study may have resulted from the differences in the average diameter of the population studied. Going by the criteria described by Fortunaik et al. (2016) and O'Donnell et al. (2014), it may be practically impossible to report the occurrence of bilateral hypoplasia. Five (out of a total of 57) patients had bilateral hypoplasia in the present study. Because of the compromised blood flow in the VA with a reduced diameter (Chen et al., 2010), surgeons need to be aware of its possibility, which may require special attention during surgical intervention.

PICA is the principal branch of the VA, and it typically originates from the intracranial part of the vertebral artery (4th segment). However, due to numerous embryonic vessels forming the VA and its branches, PICA sometimes emerges from the V3 part. An abnormal course of the VA or its PICA branch below the C1 arch may predispose the arteries to iatrogenic injuries during drilling, tapping and insertion of lateral mass screws (Arslan et al., 2019). Previous studies have reported the incidence of extracranial origin of PICA between 0.4% to 2.9% (Table 5). The prevalence in the present study is similar to previous reports (Table 5). It is important to note that no perforating arteries emerge from the PICA of extradural origin. Instead, the perforators originate from the intracranial VAs (Mercier et al., 2008). The incidence of PICA arising from the V3 was observed at the oblique part in all the cases. This site of origin is also described as the C1 origin of the PICA. This information is clinically significant to prevent iatrogenic injury to PICA during surgical interventions at the upper cervical spine and posterior approaches to the lower brainstem (Miao et al., 2020).

The prevalence of FIA ranges between 0.01% to 3.2% (Table 5), similar to the prevalence in our series (0.45%; 5 cases/1108 VAs). We observed bilateral persistent FIAs in one of the patients (Fig. 2B). The simultaneous persistence of the FIA and the typical branch of the VA results in fenestration at the V3 segment (Uchino et al., 2012), as shown in Fig. 3. Both unilateral and bilateral persistent FIA can be easily overlooked (Uchino et al., 2012). An awareness of this variant anatomy and careful review of images will assist in proper identification to prevent VA injury.

Fenestration extended between the vertical and horizontal portion of the V3 segment in the two cases observed in the present study (Fig. 3). The two limbs of the fenestrated segment had a similar diameter. The prevalence of fenestration registered in the present study (0.18%; 2

Table 5. Prevalence of anatomical variations at the V3 segment of the VA in different population groups.

Author (year)	Population	Type of study	Sample Size	Anatomical Variations (Patients %)			
				Hypoplasia	Extradural PICA Origin	FEN	Persistent FIA
Uchino et al., 2012	Japan	MRA	2739	0	30(1.1)	25(0.9)	87(3.2)
O'Donnell et al., 2014	US	CTA	975	61(6.26)	4(0.4)	1(0.01)	1(0.01)
Wakao et al., 2014	Japan	CTA	480	0	5(1.3)	5(1.3)	7(1.8)
Fortuniak et al., 2016	Poland	CTA	1800	360(20)	11(0.61)	3(0.16)	0
Kim et al., 2016	South Korea	CTA	546 314	0 0	11(2.0) 9(2.9)	2(0.4) 2(0.6)	7(1.3) 8(2.5)
Arslan et al., 2019	Turkey	CTA	200	10	2(1)	0	1(0.5)
Present study	**South Africa**	**CTA**	**554**	**57(10.3)**	**16(2.9)**	**2(0.4)**	**5(1.0)**

cases/1108 VA arteries) agrees with the reports from Western countries (Fortuniak et al., 2016), (O'Donnell et al., 2014), and is lesser than the report from a large series study of the Asian population (Uchino et al., 2012) (Table 5). There is a possibility of compromised blood flow at the proximal and distal end of the fenestrated segment of the VA, which may result in transient ischemic attacks (Omotoso et al., 2021). In addition, the passage of the catheter through the normal contralateral VA in patients with this unilateral vascular variation can expose the hindbrain to the risk of ischemia during neuroendovascular procedures (Fortuniak et al., 2016).

In the present study, most patients had equal VA diameters (codominance) (42.6%), the left side was dominant in 34.3%, and right-sided dominance was registered in 23.1%. Our study's pattern of dominance concurs with a previous report in the Asian population (49% equal dominance, 30% left dominance) (Arslan et al., 2019). It is imperative to identify and protect the dominant VA during a surgical intervention at the CVJ. Furthermore, the dominant VA must not be ligated when repairing VA injury, as it can result in permanent neurologic deficit (DeCarvalho et al., 2019).

The race, gender and side differences in the diameter and length of the V3 segment have been previously reported in the American, South African, and Asian populations (Alfaouri-Kornieieva and Al-Hadidi, 2014; Lang and Kessler, 1991; Mitchell, 2004). According to Mitchell's reports, there were no significant gender or laterality differences based on detailed histological analysis of South African adult cadavers (Witwatersrand region). The average diameter of the horizontal portion in our results is less than, but close to, the average value of the above histological reports (3.75±0.72 mm) (Mitchell, 2004) and MRA reports on the Asian population (3.8±0.51 mm) (Alfaouri-Kornieieva and Al-Hadidi, 2014). Noticeably, the average diameter of the vertical portion was smaller than that of the horizontal and oblique portion in our results. On the contrary, Alfaouri-Kornieieva and co-author (2014) reported a gradual decrease

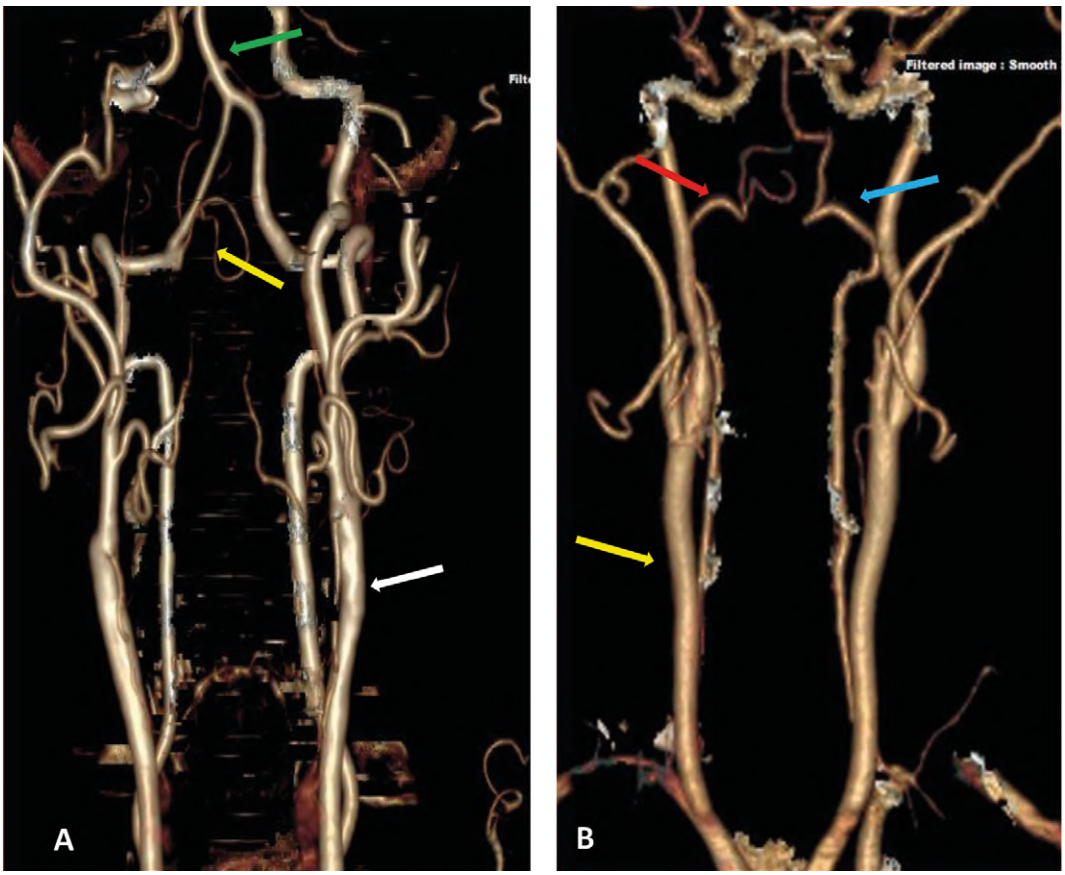

Fig. 2.- Anterior view of 3D-CTA reconstructed images showing the vertebral, basilar, and carotid arteries. **A)** PICA (yellow arrow) originates from the oblique part of V3 of the left VA. The green arrow illustrated the basilar artery. The white arrow illustrated the right common carotid artery **B)** The red and blue arrow illustrated bilateral persistent FIA. The yellow arrow illustrated the left common carotid artery.

from the vertical part to the oblique part in their MRA study. The entire length of the V2 and part of the V3 segment (excluding the horizontal and oblique part) of the VA is restricted within the transverse foramen of the cervical vertebrae, as shown in our CTA series (Fig. 1). We hypothesize that the artery could expand after its exits from the transverse foramen of the atlas (C1) vertebra, which may be a possible explanation for the differences. In agreement with the previous reports by Alfaouri-Kornieieva and co-author (2014) and Arslan et al. (2019), we registered a significantly larger left VA in all parts of the V3 segment (Alfaouri-Kornieieva and Al-Hadidi, 2014; Arslan et al., 2019). The total length of the vertical, the horizontal, and the oblique part in the present study agreed with a previous American study, which reported an average length of 38.91±5.53 (Lang and Kessler, 1991). In our study, the average length of the vertical part was similar, but the average length of the horizontal and the oblique part was shorter than in the Asian population (23.22±2.7 mm, 17.2±2.85 mm, and 12.31±1.8 mm, respectively) (Alfaouri-Kornieieva and Al-Hadidi, 2014). Generally, the disparity noted in the morphometry between the present study and the reports mentioned above may be due to differences in the modality of the studies. In the present study, we observed that the average length showed a significant difference across the racial groups. This dissimilarity may be due to some genetic factors. However, more studies may be required from other regions of South Africa to corroborate this theory.

ACKNOWLEDGEMENTS

Institution responsible for research support: College of Health Sciences (CHS funding), University of KwaZulu-Natal, Durban, South Africa.

REFERENCES

AKINDURO OO, BAUM GR, HOWARD BM, PRADILLA G, GROSSBERG JA, RODTS Jr GE, AHMAD FU (2016) Neurological outcomes following iatrogenic vascular injury during posterior atlanto-axial instrumentation. *Clin Neurol Neurosurg*, 150: 110-116.

ALFAOURI-KORNIEIEVA M, AL-HADIDI AM (2014) Morphology of the vertebral artery in Asian population. *Asian J Med Sci*, 5(4): 84-88.

Fig. 3.- 3D-CTA reconstructed images showing the vertebral, basilar, and carotid arteries. Anteroposterior view, fenestration, and persistent FIA at the V3 segment of the left VA (yellow arrow). The white arrow illustrated the left internal carotid artery.

ARSLAN D, OZER MA, GOVSA F, KITIS O (2019) Surgicoanatomical aspect in vascular variations of the V3 segment of vertebral artery as a risk factor for C1 instrumentation. *J Clin Neurosci*, 68: 243-249.

CAMPERO A, RUBINO PA, RHOTON AL (2011) Anatomy of the vertebral artery. In: *Pathology and surgery around the vertebral artery*. Springer Paris, pp 29-40.

CHEN Y-Y, CHAO A-C, HSU H-Y, CHUNG C-P, HU H-H (2010) Vertebral artery hypoplasia is associated with a decrease in net vertebral flow volume. *Ultrasound Med Biol*, 36(1): 38-43.

DECARVALHO SA, ABD-EL-BARR MM, GROFF MW (2019) Vascular complications in cervical spine surgery (anterior and posterior approach). In: *Complications in Neurosurgery*. Elsevier, pp 314-319.

ELLIOTT RE, TANWEER O, BOAH A, MORSI A, MA T, FREMPONG-BOADU A, SMITH ML (2014) Comparison of screw malposition and vertebral artery injury of C2 pedicle and transarticular screws: meta-analysis and review of the literature. *Clin Spine Surg*, 27(6): 305-315.

FORTUNIAK J, BOBEFF E, POLGUJ M, KOŚLA K, STEFAŃCZYK L, JASKÓLSKI DJ (2016) Anatomical anomalies of the V3 segment of the vertebral artery in the Polish population. *Eur Spine J*, 25(12): 4164-4170.

GEORGE B, CORNELIUS J (2001) Vertebral artery: surgical anatomy. Operative techniques in *Neurosurgery*, 4(4): 168-181.

HSU WK, KANNAN A, MAI HT, FEHLINGS MG, SMITH ZA, TRAYNELIS VC, GOKASLAN ZL, HILIBRAND AS, NASSR A, ARNOLD PM (2017) Epidemiology and outcomes of vertebral artery injury in 16582 cervical spine surgery patients: an AO Spine North America Multicenter Study. *Global Spine J*, 7 suppl 1: 21S-27S.

KHALFANI AK, ZUBERI T (2001) Racial classification and the modern census in South Africa, 1911-1996. *Race and Society*, 4(2): 161-176.

KIM MS (2016) Developmental anomalies of the distal vertebral artery and posterior inferior cerebellar artery: diagnosis by CT angiography and literature review. *Surg Radiol Anat*, 38(9): 997-1006.

LANG J, KESSLER B (1991) About the suboccipital part of the vertebral artery and the neighboring bone-joint and nerve relationships. *Skull Base Surg*, 1(1): 64.

LIANG M-L, HUANG M-C, CHENG H, HUANG W-C, YEN Y-S, SHAO K-N, HUANG C-I, SHIH Y-H, LEE L-S (2004) Posterior transarticular screw fixation for chronic atlanto-axial instability. *J Clin Neurosci*, 11(4): 368-372.

MERCIER P, BRASSIER G, FOURNIER H, PICQUET J, PAPON X, LASJAUNIAS P (2008) Vascular microanatomy of the pontomedullary junction, posterior inferior cerebellar arteries, and the lateral spinal arteries. *Interv Neuroradiol*, 14: 49-58.

MIAO H-L, ZHANG D-Y, WANG T, JIAO X-T, JIAO L-Q (2020) Clinical importance of the posterior inferior cerebellar artery: a review of the literature. *Int J Med Sci*, 17(18): 3005-3019.

MITCHELL J (2004) Differences between left and right suboccipital and intracranial vertebral artery dimensions: an influence on blood flow to the hindbrain? *Physiother Res Int*, 9(2): 85-95.

O'DONNELL CM, CHILD ZA, NGUYEN Q, ANDERSON PA, LEE MJ (2014) Vertebral artery anomalies at the craniovertebral junction in the US population. *Spine, (Phila Pa 1976)* 39(18): E1053-E1057.

OMOTOSO BR, HARRICHANDPARSAD R, MOODLEY IG, SATYAPAL KS, LAZARUS L (2021) Fenestration of the vertebrobasilar junction detected with multidetector computed tomography angiography. *Folia Morphol*, doi: 10.5603/FM.a2021.0028.

SIKKA A, JAIN AJARI (2012) Bilateral variation in the origin and course of the vertebral artery. *Anat Res Int*, 2012: 580765.

UCHINO A, SAITO N, WATADANI T, OKADA Y, KOZAWA E, NISHI N, MIZUKOSHI W, INOUE K, NAKAJIMA R, TAKAHASHI M (2012) Vertebral artery variations at the C1-C2 level diagnosed by magnetic resonance angiography. *Neuroradiology*, 54(1): 19-23.

ULM AJ, QUIROGA M, RUSSO A, RUSSO VM, GRAZIANO F, VELASQUEZ A, ALBANESE E (2010) Normal anatomical variations of the V3 segment of the vertebral artery: surgical implications. *J Neurosurg Spine*, 13(4): 451-460.

VERGARA P, BAL JS, HICKMAN CASEY AT, CROCKARD HA, CHOI D (2012) C1-C2 posterior fixation: are 4 screws better than 2? *Oper Neurosurg*, 71 supl 1: ons86-ons95.

WAKAO N, TAKEUCHI M, NISHIMURA M, RIEW KD, KAMIYA M, HIRASAWA A, KAWANAMI K, IMAGAMA S, SATO K, TAKAYASU M (2014) Vertebral artery variations and osseous anomaly at the C1-C2 level diagnosed by 3D CT angiography in normal subjects. *Neuroradiology*, 56(10): 843-849.

ZHANG D-P, ZHANG S-L, ZHANG J-W, ZHANG H-T, FU S-Q, YU M, REN Y-F, JI P (2014) Basilar artery bending length, vascular risk factors, and pontine infarction. *J Neurol Sci*, 338(1-2): 142-147.

Macroscopic and digital anthropometry of the human scaphoid: a comparative study

Patricia Gómez Barbero[1], Pau Rey Vidal[2], Daniel Montaner Alonso[1], José L. Rodrigo Pérez[1]

[1] Doctor Peset University Hospital, Valencia, Spain

[2] LLuis Alcanys Hospital, Xàtiva, Spain

SUMMARY

The purpose of this study was to establish an appropriate measurement system to accurately determine scaphoid anthropometry. It has been found that, following a scaphoid fracture, it is as important to achieve healing as it is to restore the bone's natural anatomy. To that end we performed an analysis comparing macroscopic caliper-based measurements with digital CT-based measurements of a 3D reconstructed scaphoid. A caliper was used to macroscopically measure twenty-six scaphoid specimens, evaluating length and thickness, both at the level of the waist and of the poles. Subsequently, a CT-scan was performed of all scaphoid specimens making the measurements once again with the same bone landmarks, but using the 3D CT reconstruction. Lastly, a comparative study was performed between the results of the two measuring systems employed.

A statistically significant mean difference was found ($p<0.05$) between the macroscopic and the digital measurements, both in terms of the length [0.51 mm (SD=0.79)] and the thickness of the waist [0.57 mm (SD= 0.76)]. This means that significant differences do exist between measuring the length and the thickness of the scaphoid waist digitally or with a caliper. Lastly, a comparison was made between the samples from the proximal pole with those from the distal pole. Although no significant differences were observed between one measuring system and the other with respect to the proximal pole, statistically significant differences were found regarding the distal pole measurements ($p=0.003$). Digital measurements were seen to be superior to macroscopic measurements, as they provided more reliable and accurate results. To minimize errors when making digital measurements it is essential to perform a CT-scan where slice interval is smaller than slice thickness. Moreover, female scaphoids have shown themselves to be morphometrically smaller than male scaphoids.

Keywords: Scaphoid bone – Anatomy – Fracture – Macroscopic measurement – Digital measurement

INTRODUCTION

Scaphoid fractures account for 11% of all hand fractures and 80% of carpal fractures (Arsalan-Werner et al., 2016). Depending on how stable the fracture may be, treatment may be conservative (in fractures with displacements <1 mm, a scapholunate angle <60º and a capito-lunate angle <15º); or surgical (rest of cases).

Corresponding author:
Dr. Patricia Gómez Barbero. Av. Gaspar Aguilar, 90-6º (Department of Traumatology), 46017 Valencia, Spain. E-mail: Gomez.barbero.patricia@gmail.com ORCID: 0000-0002-2408-0020

Submitted: April 5, 2021. **Accepted:** June 6, 2021

The 70% of scaphoid fractures are stable fractures that affect the middle third where splinting treatment allows consolidation. However, it is subject to a long immobilization time and is not exempt from complications such as post-immobilization stiffness, consolidation in poor position with scaphoid flexion, which would lead to a SMAC wrist (Scaphoid Malunion Advanced Collapse), or nonunion. In the last 20 years, the advent of cannulated implants and the availability of more versatile instrumentation have turned percutaneous internal fixation into the primary treatment for acute scaphoid fractures, both in stable and unstable injuries, with healing rates of 95% (Letta et al., 2014).

The goal of surgical treatment is to achieve bone healing and restore scaphoid anatomy. To be successful, it is essential to have a good understanding of the bone's three-dimensional anatomy, its spatial orientation within the carpus, and its morphologic and morphometric variability. Several authors have examined the gender-related variations in scaphoid anthropometry or compared the variables associated to the macroscopic and digital measurements of the bone (Ceri et al., 2004; Crisco et al., 2005; Guo and Tian, 2011). Nevertheless, no studies have so far been performed comparing those two measurement systems and showing the superiority of one over the other. Within clinical practice, it is common to resort to macroscopic measurement of a piece intraoperatively to select implant sizing. However, correct preoperative planning is required, where 3-dimensional imaging tests provide complete information on the injury. In addition, in recent years much progress has been made in custom implants based on digital imaging tests.

The purpose of this study is to analyze how measurements may vary as a function of the measurement system employed. Our hypothesis is that no significant differences are obtained in scaphoid length and thickness when making the measurement macroscopically with a caliper on the anatomic specimen as compared to making it digitally from a computed tomography (CT) with 3D reconstruction. The study also included a gender-based comparison.

MATERIALS AND METHODS

The study was performed with 30 formaldehyde- and cryopreserved scaphoid specimens. In order to obtain the largest possible sample, different conservation methods have been used since they do not influence the morphometric and morphological study. The samples were in all cases extracted through a dorsal approach, sectioning the ligamentous attachments to the periscaphoid carpal bones, always sparing the cartilaginous cover of the joint surfaces.

Before starting the analysis, all the specimens were macroscopically examined. Four were excluded, because they presented with degenerative changes secondary to a previous condition, which could lead to a misleading result and distort our findings. Finally, the total number of scaphoid specimens included was 26 (15 females and 11 males), with a mean age of 70.3 years (range: 53-89 years). Of them, 14 were left (53.85%) and 12 were right (46.15%) scaphoids. Four of the anatomic specimens were obtained from independent cadavers, while the other 22 came from scaphoids on both sides of the same cadaver and between the two sides in the same individual.

Macroscopic measurement

The 26 scaphoid specimens selected were measured macroscopically with reference to different bone landmarks. The macroscopic measurement protocol required the use of a manual caliper graduated in 0.05 mm increments, and included an evaluation of both the longitudinal axis and the thickness of the transverse axis. For the measurement of length, one arm of the caliper was placed at the most prominent point of the proximal pole, and the other tangentially to the overhanging distal pole. In addition to the length measurement, using the above-mentioned line as a reference, the thickness of the scaphoid was measured in three areas: scaphoid waist, proximal pole, and distal pole. The waist thickness was measured at the narrowest part of the articulating surface with the capitate, perpendicularly to the longitudinal axis (Fig. 1). The thickness of both poles was also calculated perpendicularly to the longitudinal axis, but placing the caliper 2 mm

from the apex of the proximal and distal joint surfaces, respectively (Heinzelmann et al., 2007).

Digital measurement

The 26 specimens were subjected to a second examination, but on this occasion using imaging techniques. A 64-detector row helical CT scanner (General Electric®, Milwaukee, WI, USA) was used to obtain continuous 0.625 mm-thick slices, ensuring that the slice interval was smaller than the slice thickness to reduce partial volume effects. Images were obtained at 120 kV and the beam pipe current was 335 mA. Results were transferred to a workstation (General Electric® Milwaukee, WI, USA) that was used as a basis to carry out the three-dimensional (3D) reconstruction from the different slices.

The length of the scaphoid was quantified using the 3D reconstructions of the bones with a measurement software that had a built-in micrometer. In all cases, length was determined by the same investigator, measuring the distance between the most prominent point of the proximal and the distal poles. Using this basic line and the sagittal aspect of the scaphoid as a reference, the central thickness of the scaphoid waist was calculated, at 2 mm from the proximal pole and 2 mm from the distal pole (Fig. 2).

Statistical analysis

The differences between both groups were statistically evaluated using the SPSS statistical package (SPSS for Windows 10.0, SPSS Inc, Chicago, IL.). The Kolmogorov- Smirnov test was used to evaluate the normality or goodness of fit of the sample; the mean and standard deviation (SD) of the data with normal distribution were calculated. Either student's T test or the Wilcoxon signed-rank test were applied to study the difference between the measurement systems, depending on the normality of the sample. Statistical significance was set at a p value <0.05.

RESULTS

The first analysis provided the mean values from the macroscopic measurements performed

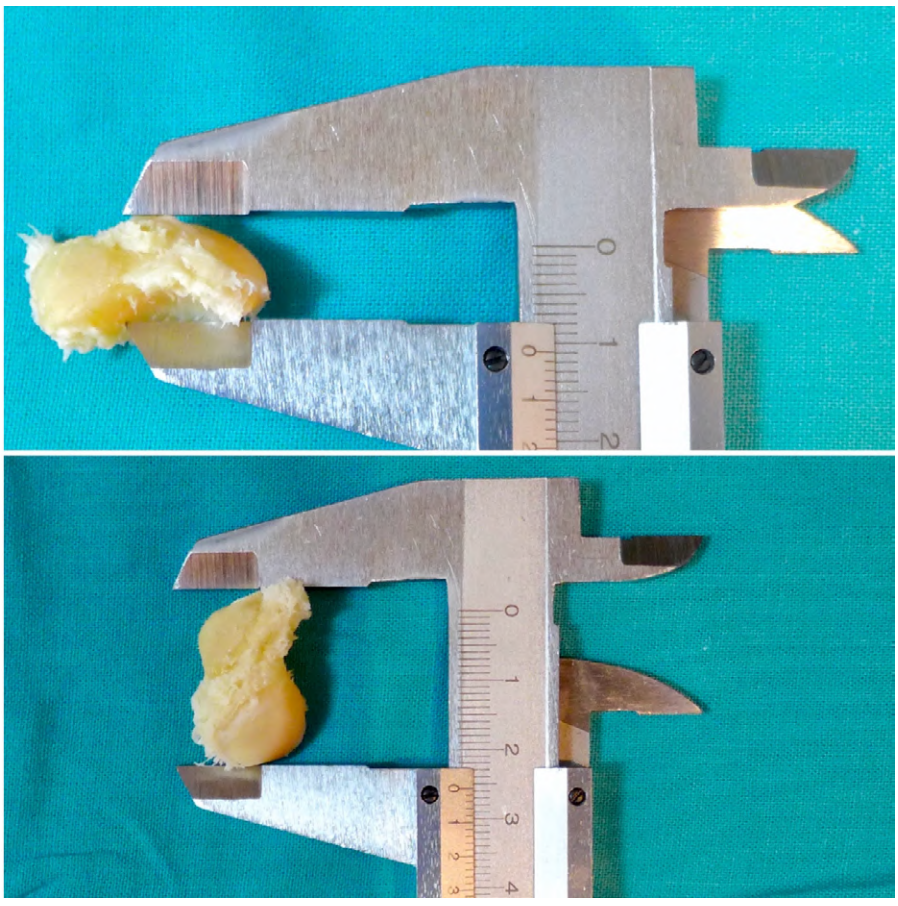

Fig. 1.- Macroscopic measurement with a manual caliper showing how thickness and scaphoid length are measured.

with the caliper. Measurements included the mean length of the scaphoid and mean scaphoid thickness at the level of the waist, the proximal pole, and the distal pole. Table 1 shows the overall mean values, as well as the mean values for males and females (columns 2 and 3). The mean values for the longitudinal axis and thickness across all magnitudes measured macroscopically were higher for males than for females.

This same table also shows the same length and thickness parameters but measured using the digital 3D CT-based technique using the General Electric® scanner, which incorporates a specific calculation software based on 3D CT reconstructions. Again, the values for the male specimens were higher than those for the female ones.

Once the macroscopic and digital measurements (all made by the same investigator) were completed, the results of both exercises were compared considering the sites described above. The purpose was to determine whether one measurement system was superior to the other, as this information would be extremely useful during preoperative planning to ensure a correct anatomic restoration. A student's test was carried out on paired simples following normality. Table 2 shows that a statistically significant mean difference was found between macroscopic and digital measurements both regarding length [0.51 mm (SD=0.79)] and thickness [0.57 mm (SD= 0.76)] of the scaphoid waist. Therefore, statistically significant differences do exist between measuring the length and thickness of the scaphoid wait macroscopically or digitally.

Lastly, a comparison was made between the proximal and the distal pole samples, using the Wilcoxon test. While no statistically significant differences were observed between the two measurement techniques at the proximal pole (p=0.071), such differences were found at the level of the distal pole (p=0.003).

There was no considerable difference between proximal pole, distal pole, waist or length measurement between the right and left sides in the same donor. Always finding minor differences with the macroscopic measurement.

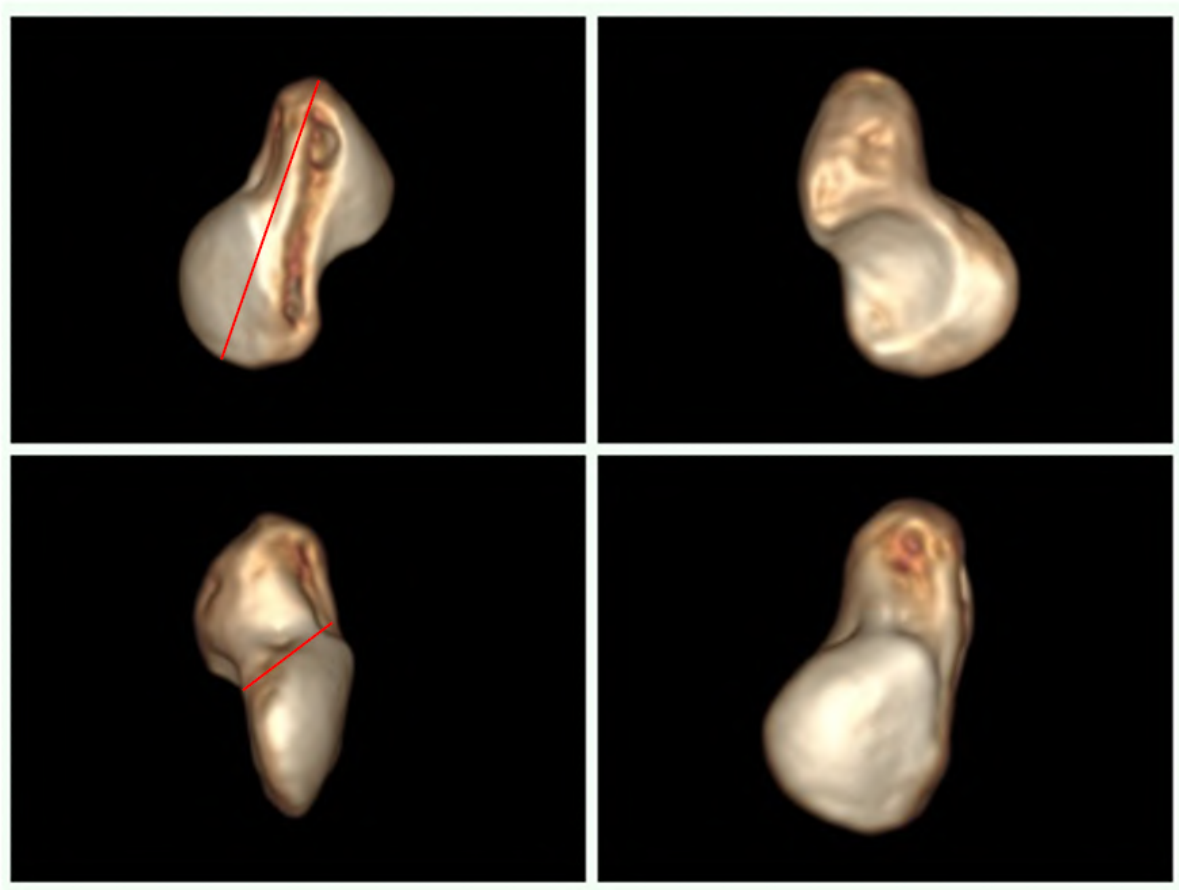

Fig. 2.- Three-dimensional CT reconstruction image for digital measurement.

DISCUSSION

Compson was one of the first authors to write on the importance of understanding the three-dimensional morphology of the scaphoid bone in clinical and surgical practice (Compson et al., 1994). Since then, different methods have been employed to make the relevant measurements, ranging from the use of calipers to the performance of bidimensional imaging tests or even magnetic resonance imaging (MRi) tests and 3D CT scans. Modern image processing techniques provide a better indication of the length, volume, and surface geometry of carpal bones as a whole, although few studies evaluate each of the bones individually (Fukuda et al., 2003).

The longitudinal axis, extending from the most prominent proximal and distal points of the scaphoid, represents the maximum length of the bone and is the reference for all other measurements used to calculate the bone´s thickness. In the first few studies published on the subject, this measurement was made macroscopically, but at present recourse is made to sophisticated imaging techniques such as CT or MRi, with or without 3D reconstruction, which provide more accurate findings and result in fewer errors (Compson et al., 1994; Ceri et al., 2004; Crisco et al., 2005; Guo and Tian, 2011; Heinzelmann et al., 2007).

Macroscopic measurement

The samples presented in this study had a mean length of 26.24 mm according to macroscopic caliper-based measurement (25.28 mm in females and 27.54 mm in males). A comparison with the results of other studies that use this measurement system shows that Heinzelmann, working on a sample of 30 pairs of cadaveric scaphoid specimens, obtained higher values than us, with a mean length of 27 mm in females and of 31 mm in males. Like us, he found that female

Table 1. Mean values obtained with the caliper-based measurement technique and with the digital 3D CT-based measurement technique.

	Macroscopic measurement with caliper			Digital measurement by 3D CT		
	Total Nr=26 Mean (range)	**Female Nr= 15 Mean (range)**	**Male Nr= 11 Mean (range)**	**Total Nr=26 Mean (range)**	**Female Nr= 15 Mean (range)**	**Male Nr= 11 Mean (range)**
Mean length (mm)	26.24 (23-31)	25.28 (23-28.5)	27.54 (23.5-31)	25.72 (22.7-29.5)	25.09 (22.7-28.5)	26.58 (24.1-29.5)
Mean waist thickness (mm)	9.66 (8-11.9)	9.40 (8.1-11.5)	10.01 (8-11.9)	9.08 (7.52-11)	8.78 (7.52-9.92)	9.49 (8-11)
Mean proximal pole thickness (mm)	5.14 (4-7)	5.06 (4-6)	5.42 (4.5-7)	4.96 (4.09-6.1)	4.79 (4.09-6.1)	5.19 (4.5-6)
Mean distal pole thickness (mm)	6.39 (5-9)	6.08 (5-7)	6.8 (5.5-9)	6.91 (5.7-8)	6.71 (5.77-7.7)	7.17 (5.7-8)

Table 2. Results of Student´s t test for paired samples.

	Paired differences					Sig. (bilateral)
	Mean	**SD**	**Standard error of the mean**	**95% CI of the difference**		
				Inferior	**Superior**	
Macrosc. length-CT Length (mm)	0.51	0.79	0.15	0.19	0.84	0.003
Macrosc. waist – CT Waist (mm)	0.57	0.76	0.15	0.26	0.88	0.001

scaphoids are always morphometrically smaller (Heinzelmann et al., 2007). One limitation of this study, however, is that it ignores the donors' racial background, which means that potential race-related size differences were not considered. Our sample is conversely solely made up of specimens from Mediterranean Caucasians. Another author using macroscopic measurements is Kong, who studied 84 scaphoids from a Chinese cohort where the mean length was much smaller than ours, ranging from 18 to 25 mm, indicating that scaphoid size in the Chinese population is smaller than among Caucasians (Kong et al., 2009). Ceri et al. (2004) also conducted a macroscopic evaluation of scaphoids and found a mean length of 25.8 mm, although, like Heinzelmann, he does not provide demographic or gender-related data on his sample.

With respect to the other morphometric parameters measured using a caliper, our study obtained a mean thickness of 9.66 mm at the level of the waist, which ranged between 10.01 mm (males) and 9.40 mm (females). Ceri reports values of 10.9 mm for the waist whereas Heinzelmann obtained 13.6 mm in males and 11.1 mm in females (Ceri et al., 2004; Heinzelmann et al., 2007). At the level of the distal tubercle, our mean thickness value was 6.39 mm, which is in line with the value obtained by Heinzelmann (7.2 mm), the only author who evaluated the thickness of the poles with the same method used in this study. At the proximal tubercle, Heinzelmann's values range between 3.7 and 4.5 mm depending on sex (Heinzelmann et al., 2007). In our study, the variation was between 5.06 mm in women and 5.42 mm in men.

Digital measurement

The same measurements were performed again on every specimen on the basis of a 3D CT reconstruction using a computer measurement software that allows ranges to be manually selected. This calculation system has been used by multiple authors like Fukuda et al. (2003), Ring et al. (2005), Letta et al. (2014), Crisco et al. (2005), Smith and Maj (1993) and Pichler et al. (2010). Table 3 shows the mean length results of our study, and is compared with the rest of the publications that use the same measurement system, although each one uses different samples that range from 26 to 100 scaphoids (Table 3). It should be noted that Guo, to avoid manual errors, used a software that avoids intra- and interobserver variability in the setting of boundary values (Guo and Tian, 2011).

As in other studies, scaphoid length in our study was shorter in females. To date, Crisco has been the only author to quantify this size difference in an attempt to determine the role played by gender. He found shorter lengths not only in the scaphoid (24.8 mm vs 29.3 mm for males) but also in the rest of female carpal bones (Crisco et al., 2005).

In short, the values obtained in our study are similar to those reported in the literature, with differences ranging between 1 and 1.5 mm. Only Smith obtained (considerably) lower values; other authors found anthropometrically higher values (Smith and Maj, 1993). As regards measurements

Table 3. Bibliographic results of mean scaphoid length after digital measurement.

	Sample (N)	Mean length Total (mm)	Mean length Male (mm)	Mean length Female (mm)
Gómez-Barbero	26	25.72	26.58	25.09
Smith	100	24.5	26	22
Fukuda	51	27.8	29.2	25.9
Patterson	35	27.35	29.2	25.5
Letta	52	26.8	28	25.1
Pichler	30	26	27.8	24.5
Guo	30	28	29	27
Crisco	28	27	29.3	24.8

other than those of scaphoid length, our literature search has not found any article that makes a digital evaluation scaphoid thickness at the level of the wait or the poles.

Comparison between macroscopic and digital measurements

The main goal of the present study was to compare the mean values obtained following a macroscopic caliper-based measurement with the values obtained from a digital measurement based on 3D CT reconstruction. Our analysis found statistically significant differences between the two measurement techniques in terms of mean length, waist thickness and proximal pole thickness. Such differences were not found at the level of the proximal pole. It does seem, therefore, that using one method rather than the other could yield different results.

Most articles in the literature mention the superiority of imaging techniques with 3D reconstruction when it comes to planning a surgical procedure, especially for reconstructing the hand following complex fractures (Letta et al., 2014). However, no study provides a comparison between the two measurement techniques.

It is a known fact that macroscopic caliper-based measurements are less precise because of errors typically inherent in manual calculations and due to the device's geometrical tolerance. Although a 3D CT system allows magnification of many details, this technique is not exempt from measurement errors, owing to the interval that exists between the CT slices (0.5 mm) and the accuracy of the CT scanner and of the image reconstruction and processing procedures. In our case, slice intervals were adjusted to be smaller than the thickness of the slices to reduce partial volume effects and allow a precise resection. Moreover, in cases where digital measurements are made, it is typically the investigators themselves that manually determine the measurement points (Fukuda et al., 2003). This limitation can be overcome by recourse to measurement systems such as the one proposed by Guo, which generates measurements on the basis of a computer software (Guo and Tian, 2011).

Our study is the first of its kind to compare the two most common measurement systems. All the measurements made using CT-scans met the normality criterion ($p > 0.05$), while the macroscopic measurements at the level of the poles showed more dissimilar values. For those reasons, we believe that digital measurements based on 3D reconstruction are more accurate and, therefore, more reliable and preferable for a proper anatomic study of the scaphoid, thus ruling out our null hypothesis. In addition, in clinical practice the use of digital measurement shows a double advantage, since it allows us to know the morphology of the lesion in the damaged scaphoid and to plan the definitive treatment; but also to study, from the healthy contralateral scaphoid that is symmetrical, its original anatomy and even manufacture an implant as it reconstructs the damaged bone part (Ten Berg et al., 2015).

Finally, we did not find differences between the left and right scaphoid measurements within the same individual, regardless of the measurement system used. As we have said before, the fact of not finding significant differences has a marked clinical relevance, since in the case of a fracture or pseudoarthrosis, the X-ray of the healthy hand can be taken as a template to plan the reconstruction. This idea has been estimated and proposed by other authors with Heinzelmann et al. (2007), Guo and Tian (2011), Fukuda et al., 2003) or Letta et al. (2014). Only Ceri observed a greater development of the scaphoids as a function of the patient's dominant hand based on Wolff's law (Ceri et al., 2004).

One of the strengths of this study is that it included a large enough sample to produce significant results on a series of scaphoid specimens with no previous history of degenerative changes. However, it must be considered that, as the specimens were obtained through donations, their bone age was usually rather advanced.

REFERENCES

ARSALAN-WERNER A, SAUERBIER M, MEHLING IM (2016) Current concepts for the treatment of acute scaphoid fractures. Eur J Trauma Emerg Surg, 42(1): 3-10.

CERI N, KORMAN E, GUNAL I, TETIK S (2004) The morphological and morphometric features of the scaphoid. J Hand Surg Br, 29(4): 393-398.

COMPSON JP, WATERMAN JK, HEATLEY FW (1994) The radiological anatomy of the scaphoid. Part 1: Osteology. J Hand Surg Br, 19(2): 183-187.

CRISCO JJ, COBURN JC, MOORE DC, UPAL MA (2005) Carpal bone size and scaling in men versus in women. J Hand Surg Am. 30(1): 35-42.

FUKUDA S, ISHIDA O, KIDO M, SUZUMURA F, IKUTA Y (2003) A morphological study of the scaphoid using a mathematical technique and comparative study of the three-dimensional measurements of the scaphoid. Hand Surg, 8(2): 157-161.

GUO Y, TIAN GL (2011) The length and position of the long axis of the scaphoid measured by analysis of three-dimensional reconstructions of computed tomography images. J Hand Surg Eur Vol, 36(2): 98-101.

HEINZELMANN AD, ARCHER G, BINDRA RR (2007) Anthropometry of the human scaphoid. J Hand Surg Am, 32(7): 1005-1008.

KONG W, XU Y, WANG Y, CHEN S, LIU Z, LI X (2009) Anatomic measurement of wrist scaphoid and its clinical significance. Chinese J Traumatol English Ed. 12(1): 41-44.

LETTA C, SCHWEIZER A, FÜRNSTAHL P (2014) Quantification of contralateral differences of the scaphoid: a comparison of bone geometry in three dimensions. Anat Res Int, 2014: 904275.

PICHLER W, WINDISCH G, SCHAFFLER G, HEIDARI N, DORR K, GRECHENIG W (2010) Computer-assisted 3-dimensional anthropometry of the scaphoid. Orthopedics, 33(2): 85-88.

RING D, PATTERSON JD, LEVITZ S, WANG C, JUPITER JB (2005) Both scanning plane and observer affect measurements of scaphoid deformity. 2005:696-701.

SMITH D, MAJ U (1993) Anatomic features of the carpal scaphoid: Validation of biometric measurements and symmetry with three-dimensional MR imaging. Radiology, 187: 187-191.

TEN BERG P, DOBBE JG, STRACKEE SD, STREEKSTRA GJ (2015) Three- dimensional assessment of bilateral symmetry of the scaphoid: An anatomic study. Biomed Res Int, 2015: 547250.

Pituitary gland size in temporal lobe epilepsy

Kaan Yücel [1], Bahattin Hakyemez [2], İbrahim Bora [3]

[1] Department of Anatomy, Medical School of İzmir Democracy University, İzmir, Turkey
[2] Department of Radiology, Department of Radiology, Medical School of Uludag University, Bursa
[3] Department of Neurology, Department of Neurology, Medical School of Uludag University, Bursa

SUMMARY

Reproductive functional disorders and endocrine disorders are common in epileptic patients, particularly in patients with temporal lobe epilepsy (TLE). Pituitary size has been measured in patient populations with several diseases, but not in those with TLE so far. We compared the pituitary gland height and the morphology of its superior margin between patients with TLE and age- and sex- matched controls on magnetic resonance imaging (MRI). We found a smaller pituitary gland in patients with TLE compared to controls without any change of the morphology of its superior margin. The pituitary gland seems to be a site to check on MRI when evaluating a patient with TLE. The implications of this finding related to etiopathogenesis and clinical practice have been discussed.

Key words: Pituitary gland – Magnetic resonance imaging – Height – Temporal lobe epilepsy

INTRODUCTION

Epilepsy has been known since ancient times. It has been proposed that the word either was originated from a Greek word meaning “to seize” (Blair, 2012) or from Latin meaning “to take possession of” (Bromfield et al., 2006). Epilepsy is a heterogeneous common disorder of the central nervous system with recurrent seizures and accompanying different kinds of symptoms (Blair, 2012). The overall prevalence of epilepsy is approximately 6 per 1000 (Bromfield et al., 2006). Following the development of epileptogenesis, a normal network changes into a hyperexcitable network (Bromfield et al., 2006). Epilepsy has two main categories: partial and generalized, depending on the site of origin for the developing seizures. Temporal lobe epilepsy (TLE) is the most common type of partial type epilepsy (Bromfield et al., 2006).

Reproductive functional disorders and endocrine disorders are common in epileptic patients, particularly in patients with TLE in both genders (Herzog, 1989; Morris AND Vanderkolk, 2005; Fawley et al., 2006).

It has been reported that 14-20% of women with TLE had amenorrhea and that more than 50% overall have some form of menstrual dysfunction, and more than half of the men who have TLE suffer from diminished potency or altered sexual interest (Herzog, 1989).

The most common reproductive disorders in women with TLE are as follows: premature ovarian failure, functional hyperprolactinemia, polycystic ovary syndrome, and hypogonadotropic hypogonadism (Fawley et al., 2006). Although different mechanisms have been proposed for the co-morbidity of reproductive disorders and

Corresponding author:
Kaan Yücel, MD, PhD. Department of Anatomy, Medical School of İzmir Democracy University, İzmir, Turkey. E-mail: kaanyucel2014@gmail.com

Submitted: February 17, 2021. **Accepted:** June 30, 2021

TLE, the exact mechanisms are unknown. It is, however, a fact that reproductive function is common in this patient population.

Pituitary gland height (PGH) has been investigated in several diseases out of distinct medical disciplines such as eating disorders (Doraiswamy et al., 1990), thalassemia major (Isik et al., 2014), growth hormone deficiency (Alba et al., 2004; Dumrongpisutikul et al., 2018), Chiari II malformation (Patel et al., 2020), idiopathic intracranial hypertension (Batur Caglayan et al., 2019), multiple sclerosis (Saba et al., 2017), hypopituitarism (Uday et al., 2017) and primary hypothyroidism (Zhang et al., 2012) on Magnetic Resonance Imaging (MRI). PGH represents a good single measure for the assessment of the size of the gland (Lurie et al., 1990), and has been used to evaluate its function (Argyropoulou et al., 2005). Pituitary size, however, has not been measured in patients with TLE so far. We compared the PGH and the morphology of its superior margin between patients with TLE and age- and sex- matched control group, hypothesizing that this gland can be abnormal, probably smaller, compared to the control group given that neuroendocrine symptomatology is common in this group of patients.

MATERIALS AND METHODS

We used a TLE patient group of 42 subjects (19 females; mean age=30.69, SD=13.34) and age-and-sex- matched control group of 42 subjects (mean age=31.09, SD 12.06). The control subjects of the study did not have any neurological or psychiatric disorders, and were not under any drugs, chemical substances (i.e. oral contraceptives for female subjects, cortisone etc.) affecting the morphology of the brain. None was using alcohol. PGH was measured on 1.5 T MRI unit (Magnetom Vision Plus, Siemens, Erlangen, Germany) at the midsagittal plane using T1 weighted spin echo (SE) sequence. PGH was assessed as the maximum distance between the upper margin and base of adenohypophysis perpendicular to the base of sella turcica (Elster et al, 1991). Measurements were performed with the sensitivity of 0.01 cm. In addition to PGH, we also rated the morphology of the superior margin of the gland from 0 through 5. (Elster et al, 1991); 1- concave superior margin; 2-mild concavity of the superior margin (below 2 mm); 3-a plain superior margin; 4-mild convexity of the superior margin (below 2 mm); 5-convex superior margin (Figs. 1, 2). These measurements were made by a neuroradiologist (B.H) and an anatomist (K.Y.) and

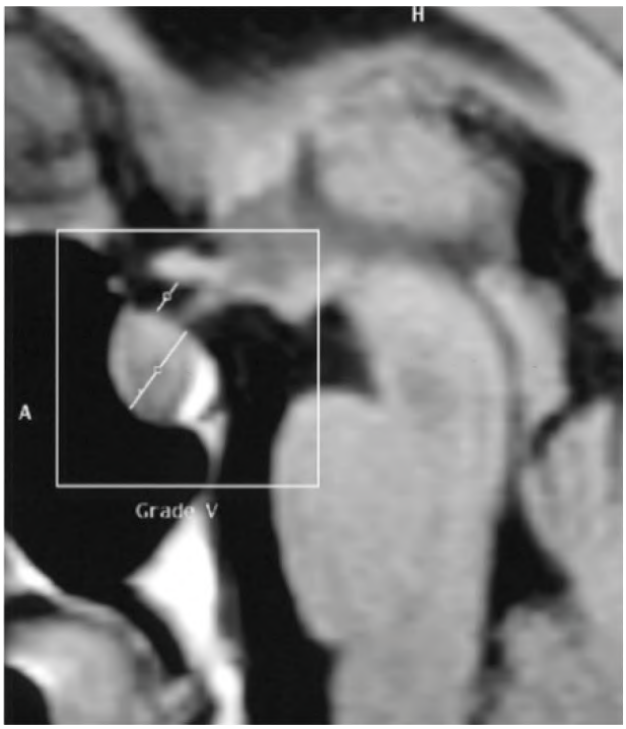

Fig. 1.- Pituitary gland - Grade V and measurement of PGH. The vertical line below in the figure refers to PGH measurement.

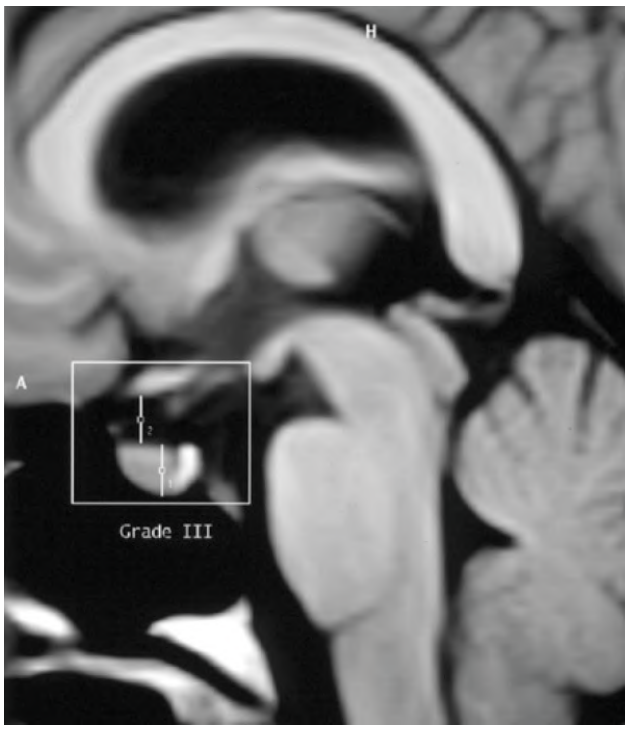

Fig. 2.- Pituitary gland - Grade III and measurement of PGH. The vertical line below in the figure refers to PGH measurement.

the consensus value was taken into consideration. For the statistical analysis Student's t- test, Pearson's correlation coefficient, Mann-Whitney test.

RESULTS

The mean duration of the illness was 14. 65 years (2-65 years), and the mean of the estimated number of the seizures per month was 5.44 seizures. The mean age of onset of epilepsy was 14.39 years (1- 62). There was no difference between male and female patients in terms of age at onset (mean=11.78, SD=14.08, for men and mean=17.5, SD=11.88 for women) and illness duration (mean=15.95, SD=12.40 for men, and mean=11.39, SD=7.2 for women) (ps=0.16). As a whole, TLE subjects had smaller PGH than their age-and-sex-matched controls (p=0.002) (Table 1). While male TLE subjects had a smaller pituitary gland than male control subjects (p<0.001), the size of pituitary glands of female TLE subjects did not differ from those of the female control subjects (p=0.41). There was no difference in PGH for the controls between two genders (p>0.05).

TLE and control groups had the similar means of ratings for the superior margin (p>0.05) (Table 1). When sexes were compared separately, both sexes in each group had the similar means of ratings for the superior margin (p>0.05). When patients with illness duration of more than 10 years (n=24) only were compared to controls, PGH was still smaller (p=0.001). When patients with illness duration equal to or less than 10 years (n=18) were compared to controls, the finding remained still significant (p=0.025).

There was no difference in the PGH between patients taking monotherapy (n=19) and polytherapy (n=23) (p>0.05).

DISCUSSION

In our preliminary study, we found a smaller pituitary gland in patients with TLE compared to age-and-sex-matched controls. The smaller PGH in epileptic patients was refined to male patients only, with no difference between female patients and female controls. Patients on monotherapy did not differ from patients on polytherapy for PGH measurements. We could not find a difference between patients and controls for ratings of the superior margin of the gland.

The association between epilepsy and reproductive disorders is unknown (Fawley et al., 2006). There are, however, several theories suggested so far, trying to explain the higher rate of endocrine disorders in patients with TLE. According to one of these theories, epileptic discharges in the limbic structures such as hippocampus might affect the pulsatile secretion of GnRH (gonadotropin releasing hormone) (Edwards et al., 2000). Hippocampus and cells related to reproductive function in the hypothalamus are highly connected. Therefore, the relation between epileptic discharges arising from hippocampus and hypothalamus seem to be mutual. Accordingly, reproductive disorders have been shown to effect the epileptic charges as well (Herzog, 1989).

The studies with animal models of epilepsy demonstrated hormonal fluctuations and change in the oestrus cycle following seizures (Amado and Cavalheiro, 1998).

Another theory that explained the relation between epilepsy and reproductive disorders was based on the effects of anti-epileptic drugs (particularly carbamezapine, barbiturates, and fenitoin) (Herzog,1989). Changes in testosterone (T)/luteinizing hormone (LH) ratio were reported in men with TLE compared to men with

Table 1. The comparison of the means of PGH (Pituitary gland height) and ratings of the superior margin in both groups.

Variable	TLE (n= 42)	Controls (n=42)	P value
PGH	0. 55 cm	0.66 cm	0.002
Rating of the superior margin	2.88	3.10	>0.05

extratemporal epilepsy as a result of antiepileptic drugs (Bauer et al., 2011). Serum estradiol and dehydroepiandrosterone sulfate (DHEAS) levels were found smaller in women with TLE when compared to those of the controls (Herzog et al., 2003). An inhibition on the pulsatile secretion of luteinizing hormone was considered as the effect of chronic epilepsy and the acute effects of seizures (Luef, 2010).

Antiepileptic drugs might cause imbalances in the endocrine system directly by affecting the serum levels of the hormones or indirectly affecting the neurotransmitter systems affecting the HPA axis such as GABA, glutamate. A common genetic background for TLE and endocrine disorders has also been suggested as a factor. According to this theory, TLE and associated reproductive endocrine disorders may represent the parallel effects of prenatal factors which are common to the development of both the brain and the reproductive system. A common neurotransmitter defect in both disorders has also been suggested to explain the higher rates of endocrine disorders seen in epileptic patients (Herzog, 1989).

Although our study design is cross-sectional, which can also be considered as a limitation, we found abnormal size of pituitary gland in TLE. As far as we know, this is the first study in the literature so far, in which pituitary gland size has been examined in this patient population.

In our structural MRI study, we were not able to find the reason(s) underlying this abnormality. Patients, however, receiving monotherapy and polytherapy at the time of the scan did not differ in PGH (data not shown). This might lead us to suggest that treatment with antiepileptic drugs contributed to a smaller pituitary gland. We, however, are aware that medication history of patients will be more critical at that point, rather than their current treatment, which we could not control in our cross-sectional study. A study in which pituitary gland size compared between those of patients with TLE who have been diagnosed recently and never treated before with those of age- and-gender-matched healthy controls would help answer the question of the effect of antiepileptic drugs on pituitary gland size in a better way.

We could not find a relation between illness duration and PGH. The pituitary gland might be smaller at the beginning of the disease process, or, alternatively, the reduction in the gland might occur in the first years of the disease following a plateau later. These suggestions are parallel to the theories of common genetic defect and effects of epileptic discharges, respectively.

We found smaller PGH in male epileptic patients only, but not in female patients. This might be due to a Type II error, as our female epileptic patient might not be representing the general population with common reproductive disorders. Alternatively, it might be the fact that the males be more vulnerable to the brain damage associated with epilepsy (Briellmann et al., 2000).

The most important limitation of the study is that we could not gather data on the profiles of the TLE patients on the existence of any reproductive disorder as they were undiagnosed for such a disorder. Although the reproductive disorders seem an important aspect of patients with TLE, it seems to be underdiagnosed and overlooked. New neuroimaging studies with TLE patients with and without reproductive disorders will better give us an idea about the pathogenesis of the comorbidity of these disorders, particularly considering the effects of treatment (untreated patients at the beginning of TLE vs. treated chronic patients).

As a conclusion, apart from changes in the volumes of hippocampus (Moghaddam et al., 2021; Riederer et al., 2020;Wu et al., 2020), amygdala (Sone et al., 2018; Na et al., 2020), thalamus (Wu et al., 2020), cerebellar vermis (Marcián et al., 2018), prefrontal cortex (Zhang et al., 2017), etc., change in the size of the pituitary gland should be added to the list of structures with morphometric changes seen in TLE patients as a result of epilepsy itself and treatment without any morphological changes of the superior margin of the gland. The pituiraty gland seems to be a site to check on MRI when evaluating a patient with TLE.

ACKNOWLEDGEMENTS

We are grateful to the MRI technicians at the Department of Radiology of Medical School of Uludag University for their time.

REFERENCES

ALBA M, HALL CM, WHATMORE AJ, CLAYTON PE, PRICE DA, SALVATORI R (2004) Variability in anterior pituitary size within members of a family with GH deficiency due to a new splice mutation in the GHRH receptor gene. *Clin Endocrinol (Oxf),* 60(4): 470-475.

AMADO D, CAVALHEIRO EA (1998) Hormonal and gestational parameters in female rats submitted to the pilocarpine model of epilepsy. *Epilepsy Res,* 32(1-2): 266-274.

ARGYROPOULOU MI, KIORTSIS DN (2005) MRI of the hypothalamic-pituitary axis in children. *Pediatr Radiol,* 35(11): 1045-1055.

BATUR CAGLAYAN HZ, UCAR M, HASANREISOGLU M, NAZLIEL B, TOKGOZ N (2019) Magnetic resonance imaging of idiopathic intracranial hypertension: before and after treatment. *J Neuroophthalmol,* 39(3): 324-329.

BAUER J, DIERKES H, BURR W, REUBER M, STOFFEL-WAGNER B (2011) Disease- and treatment-related effects on the pituitary-gonadal functional axis: a study in men with epilepsy. *J Neurol,* 258(6): 1080-1084.

BLAIR RD (2012) Temporal lobe epilepsy semiology. *Epilepsy Res Treat,* 2012: 751510. BRIELLMANN RS, BERKOVIC SF, JACKSON GD (2000) Men may be more vulnerable to seizure- associated brain damage. *Neurology,* 55(10): 1479-1485.

BROMFIELD EB, CAVAZOS JE, SIRVEN JI, editors (2006) An Introduction to Epilepsy. West Hartford (CT): American Epilepsy Society.

DORAISWAMY PM, KRISHNAN KR, FIGIEL GS, HUSAIN MM, BOYKO OB, ROCKWELL WJ, ELLINWOOD EH JR (1990) A brain magnetic resonance imaging study of pituitary gland morphology in anorexia nervosa and bulimia. *Biol Psychiatry,* 28(2): 110-116.

DUMRONGPISUTIKUL N, CHUAJAK A, LERDLUM S (2018) Pituitary height at magnetic resonance imaging in pediatric isolated growth hormone deficiency. *Pediatr Radiol,* 248(5): 694-700.

EDWARDS HE, MACLUSKY NJ, BURNHAM WM (2000) The effect of seizures and kindling on reproductive hormones in the rat. *Neurosci Biobehav Rev,* 24(7): 753-762.

ELSTER AD, SANDERS TG, VINES FS, CHEN MY (1991) Size and shape of the pituitary gland during pregnancy and post partum: measurement with MR imaging. *Radiology,* 181(2): 531-535.

FAWLEY JA, POULIOT WA, DUDEK FE (2006) Epilepsy and reproductive disorders: the role of the gonadotropin-releasing hormone network. *Epilepsy Behav,* 8(3): 477-482.

HERZOG AG, COLEMAN AE, JACOBS AR, KLEIN P, FRIEDMAN MN, DRISLANE FW, RANSIL BJ, SCHOMER DL (2003) Interictal EEG discharges, reproductive hormones, and menstrual disorders in epilepsy. *Ann Neurol,* 54(5): 625-637.

HERZOG AG (1989) A hypothesis to integrate partial seizures of temporal lobe origin and reproductive endocrine disorders. *Epilepsy Res,* 3(2): 151-159.

ISIK P, YARALI N, TAVIL B, DEMIREL F, KARACAM GB, SAC RU, FETTAH A, OZKASAP S, KARA A, TUNC B (2014) Endocrinopathies in Turkish children with Beta thalassemia major: results from a single center study. *Pediatr Hematol Oncol,*31(7): 607-615.

LUEF G (2010) Hormonal alterations following seizures. *Epilepsy Behav,* 19(2): 131-133.

LURIE SN, DORAISWAMY PM, HUSAIN MM, BOYKO OB, ELLINWOOD EH JR, FIGIEL GS, KRISHNAN KR (1990) In vivo assessment of pituitary gland volume with magnetic resonance imaging: the effect of age. *J Clin Endocrinol Metab,* 71(2): 505-508.

MARCIÁN V, MAREČEK R, KORIŤÁKOVÁ E, PAIL M, BAREŠ M, BRÁZDIL M (2018) Morphological changes of cerebellar substructures in temporal lobe epilepsy: A complex phenomenon, not mere atrophy. *Seizure,* 54: 51-57.

MOGHADDAM HS, AARABI MH, MEHVARI-HABIBABADI J, SHARIFPOUR R, MOHAJER B, MOHAMMADI-MOBARAKEH N, HASHEMI-FESHARAKI SS, ELISEVICH K, NAZEM-ZADEH MR (2021) Distinct patterns of hippocampal subfield volume loss in left and right mesial temporal lobe epilepsy. *Neurol Sci,* 42(4): 1411-1421.

MORRIS GL 3RD, VANDERKOLK C (2005) Human sexuality, sex hormones, and epilepsy. *Epilepsy Behav,* 7 Suppl 2: S22-S28.

NA HK, LEE HJ, HONG SJ, LEE DH, KIM KM, LEE HW, HEO K, CHO KH (2020) Volume change in amygdala enlargement as a prognostic factor in patients with temporal lobe epilepsy: A longitudinal study. *Epilepsia,* 61(1): 70-80.

PATEL D, SAINDANE A, OYESIKU N, HU R (2020) Variant sella morphology and pituitary gland height in adult patients with Chiari II malformation: potential pitfall in MRI evaluation. *Clin Imaging,* 64: 24-28.

RIEDERER F, SEIGER R, LANZENBERGER R, PATARAIA E, KASPRIAN G, MICHELS L, BEIERSDORF J, KOLLIAS S, CZECH T, HAINFELLNER J, BAUMGARTNER C (2020) Voxel-based morphometry-from hype to hope. a study on hippocampal atrophy in mesial temporal lobe epilepsy. *AJNR Am J Neuroradiol,* 41(6): 987-993.

SABA M, EBRAHIMI HA, AHMADI-POUR H, KHODADOUST M (2017) Height, shape and anterior-posterior diameter of pituitary gland on magnetic resonance imaging among patients with multiple sclerosis compared to normal individuals. *Iran J Neurol,* 16(4): 218-220.

SONE D, SATO N, KIMURA Y, WATANABE Y, OKAZAKI M, MATSUDA H (2018) Brain morphological and microstructural features in cryptogenic late-onset temporal lobe epilepsy: a structural and diffusion MRI study. *Neuroradiology,* 60(6): 635-641.

UDAY S, SHAW N, KRONE R, KIRK J (2017) Hypopituitarism in children with cerebral palsy. *Arch Dis Child,* 102(6): 559-561.

WU D, CHANG F, PENG D, XIE S, LI X, ZHENG W (2020) The morphological characteristics of hippocampus and thalamus in mesial temporal lobe epilepsy. *BMC Neurol,* 20(1): 235.

ZHANG WH, ZHU HJ, ZHANG XW, LIAN XL, DAI WX, FENG F, XING XP, JIN ZY (2012) Magnetic resonance imaging findings of pituitary hyperplasia due to primary hypothyroidism. *Zhongguo Yi Xue Ke Xue Yuan Xue Bao,* 34(5): 468-473.

ZHANG Z, LIAO W, XU Q, WEI W, ZHOU HJ, SUN K, YANG F, MANTINI D, JI X, LU G (2017) Hippocampus-associated causal network of structural covariance measuring structural damage progression in temporal lobe epilepsy. *Hum Brain Mapp,* 38(2): 753-766.

Diabetes mellitus induced impairment of sperm parameters in mice: A stereological method

Sara Dadras[1,2], Mohammad Bayat[2], Marefat G. Novin[1,2], Hamid Nazarian[1], Amir Raoofi[3,4], Shabnam Abdi[5], Sina Sadeghzadeh[6], Faezeh Tajari[7], Mohammad-Amin Abdollahifar[1,2]

[1] Infertility and Reproductive Health Research Center, Shahid Beheshti University of Medical Sciences, Tehran, Iran

[2] Department of Biology and Anatomical Sciences, School of Medicine, Shahid Beheshti University of Medical Sciences, Tehran, Iran

[3] Department of Anatomical Sciences, School of Medicine, Sabzevar University of Medical Sciences, Sabzevar, Iran

[4] Leishmaniasis Research Center, Department of Anatomy, Sabzevar University of Medical Sciences, Sabzevar, Iran

[5] Department of Anatomical Sciences & Cognitive Neuroscience, Faculty of Medicine, Tehran Medical Sciences, Islamic Azad University, Tehran, Iran

[6] Bachelor's degree, Cognitive Neuroscience and Evolutionary Psychology, Harvard University, Cambridge, Massachusetts, USA

[7] Student Research Committee, School of Medical Sciences, Shahid Beheshti University of Medical Sciences, Tehran, Iran

SUMMARY

In this study, the effects of diabetes mellitus on stereological changes of sperm parameters in mice were investigated. Mice under standard housing conditions were assigned into two experimental groups: (I) control (II) diabetic (N = 6 mice per group). The sperm samples were collected from the right cauda epididymis of the mice for measuring the sperm and sperm count. The volume of the sperms' heads was estimated using the nucleator method. The length of the sperms flagellum and mid-piece was estimated by counting the number of intersections of the tails and Merz grid test line in an unbiased counting frame, superimposed on live images of sperms. The results showed that the total sperm count and sperm motility in Streptozotocin (STZ)-induced animals was decreased, in comparison with the control groups. Our results showed a significant difference in the volume and surface area of the head and the length of the flagellum between the sperms in the control and diabetic groups. In conclusion, our results indicated that type 1 diabetes induced impairment in sperm parameters.

Key words: Diabetes mellitus – Mice – Morphology – Sperm – Stereology

INTRODUCTION

A chronic illness, diabetes mellitus is caused by chronic elevations in blood sugar levels due to the inability of the pancreas for producing insulin as a result of the destruction of the pancreatic beta cells (Scarano et al., 2006). Diabetes mellitus is associated with abnormalities in carbohydrate, fat, and protein metabolism in target tissues. The

Corresponding author:
Mohammad-Amin Abdollahifar. Infertility and Reproductive Health Research Center, Shahid Beheshti University of Medical Sciences, Tehran, Iran. Department of Biology and Anatomical Sciences, School of Medicine, Shahid Beheshti University of Medical Sciences, Tehran, Iran. E-mail: m_amin58@yahoo.com / abdollahima@sbmu.ac.ir

Submitted: February 21, 2021. **Accepted:** July 11, 2021

Not final proof's revision by the authors

chronic hyperglycemia of diabetes also causes such complications and other dysfunctions in various organs, particularly the eyes, kidneys, heart, blood vessels and reproductive organs (Ning et al., 2009; Ghanbari et al., 2012). Previous studies show that diabetes can affect the neuroendocrine reproductive tract axis and cause sexual dysfunctions. It has been also reported that hyperglycemia can negatively affect sperm quantity and quality in rats (Arikawe et al., 2006; Navarro-Casado et al., 2010). Previous studies reported the adverse effects of diabetes mellitus on the functions of reproductive organs, particularly ejaculation and spermatogenesis; moreover, by dropping testosterone levels, the disease can cause harm to the tissues and the reduction the capacity of testis (Mosher, 1988).

Morphology sperm plays a most important role to determine sperm quality and successful fertilization (Rønn et al., 2000; Noorafshan and Karbalay-Doust, 2010; Kuster et al., 2004; Panahi et al., 2017). Although the World Health Organization (WHO) recommends the investigation of different parts of sperm morphology, little research has been conducted on the volume of the sperms' heads and the mid-piece and tail sperm length, despite the essential role they play in sperm motility (Mossman et al., 2012; de Paz et al., 2011). In other words, most studies have focused on a narrow range of parameters such as analyzing the sperm length and head (Maroto-Morales et al., 2010; Noorafshan and Karbalay-Doust, 2010). This study was conducted through the unbiased application of stereological tools. Regarding the subject mentioned above, this study was conducted in order to explore the effects of diabetes on the sperm head volume of and length of their mid-piece by using stereological methods.

MATERIALS AND METHODS

Animals

This study was conducted on 12 adult mice (28-30 g) that were purchased from the animal center laboratory of the Pasteur Institute in Tehran, Iran. This study was conducted according to the standard directive recommended and approved by the research authorities of Shahid Beheshti University of Medical Sciences, Tehran, Iran (IR. SBMU. RETECH.REC.1395.440). The mice were divided into two groups: (I) Control; (II) Diabetic (40mg/kg STZ). Each group included 6 mice that were housed in standard rat cages and room temperature 22-24°C, 12:12 h light-dark schedule, and were provided with water ad libitum.

Induction of diabetes mellitus

A single dose (55 mg/kg body weight) of intraperitoneal streptozotocin (STZ) injection can cause type 1 diabetes in mice (Zanosar Pharmacia and Upjohn Co, Kalamazoo, MI, USA). One week following the STZ injection, blood samples were taken from the veins of mice's tail in order to analyze the blood glucose levels (Biomine, Rightesttm GM300, Biomine Corporation, Switzerland). Mice with blood glucose level greater than 250 mg/dL were considered to be type 1 diabetic. In our study, the mice's body weight and blood glucose levels were recorded every 2 weeks until the end of the research. Sperm morphology examinations were conducted 30 days after the STZ injection.

Sperm Collection

Sperm samples were collected from the right cauda epididymis of the mice. The sperm sample incubation at 37 °C for 20 minutes, 10 µl of the sample were placed on a slide and sperm motility was observed. The sperm count was measured by counting chamber. Then the sperm smear was prepared for analysis, placed on a slide, air-dried at room temperature, and fixed in methyl alcohol. Then, the sample was stained with Diff-Quik (Seed et al., 1996).

Stereological study

Length of sperms' mid-piece and flagellum estimation

The length of sperms' mid-piece and flagella estimation under the microscope is an application of length estimation in two-dimensional planes (Panahi et al., 2017). The mean length of the sperms' mid-piece and flagella was estimated using the following formulae (Fig. 1):

$$\sum L = \left(\frac{\pi}{2}\right) \cdot \left(\frac{a}{l}\right) \cdot \left(\frac{1}{asf}\right) \cdot \sum I, \quad L = \frac{\sum L}{\sum N}$$

In this formula a/l is the Merz grid constant which was obtained as follows: the area of each basic tile of the grid was X multiplied by Y. Within this tile, there were two semicircles of length of π.d (perimeter of a circle), In this formula d is the diameter of the semicircle. Thus the Merz grid constant a/l was (X_Y) π.d. In this formula asf is the area of the basic tile divided by the area of the counting frame. In this formula ΣI is the summation of the intersection of the tails with the semicircles. In this formula ΣN is the total number of the counted sperms in the unbiased counting frame.

Mean volume estimation of sperm heads

The sperms' volume of head was estimated using the nucleator method (Karlsson and Cruz-Orive, 1997). In this method for each sampled nucleus, two horizontal directions (intercept, Ln) were considered from the central point within the nucleus to the cell borders (Figure 1). The sperm head volume in the number weighted distribution was estimated using the following formula:

$$V_N = \frac{4\pi}{3} \times \overline{l_n^3}$$

Statistical analysis

The data were analyzed using the non-parametric tests (Kruskal-Wallis). Differences were regarded as statistically significant if $P \leq 0.05$.

RESULTS

Total sperm count, motility and sperm mid-piece and tail defect

Our data showed that the total sperm count in STZ-induced animals was decreased, in comparison with the control groups ($P < 0.05$). the

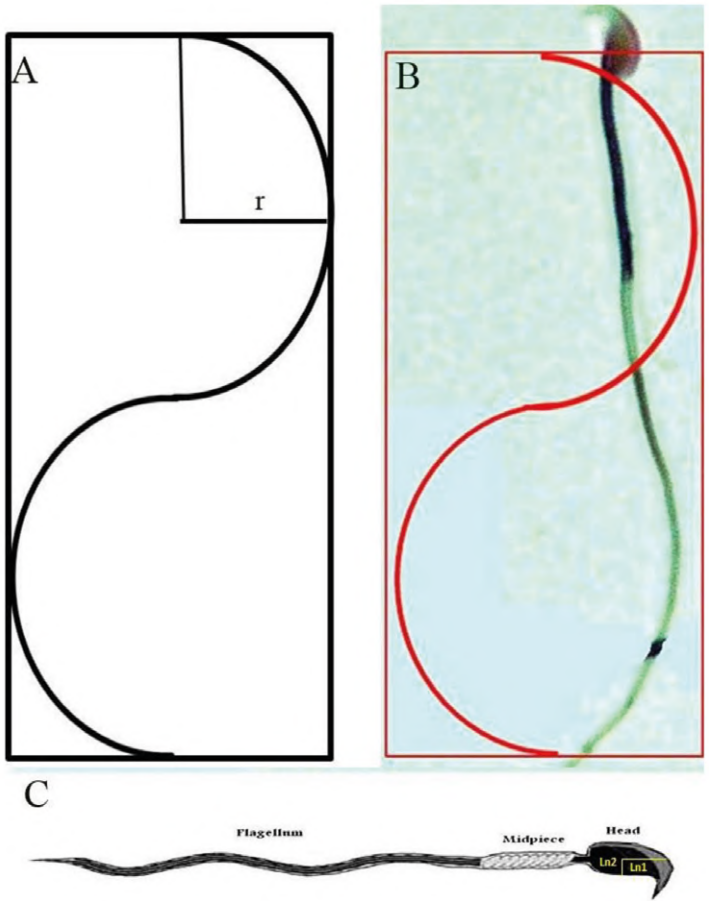

Fig. 1.- Estimation of the sperms mid-piece and flagellum length. (**A**) Two semicircles were located at a rectangle. The length of each semicircle was equal to twice the length of its minor axis (r). The area associated with the semicircle was calculated by multiplying the X by Y and divided by the length of the two semicircles to achieve the area per length. (**B**) The total number of the intersections between the sperms mid-piece and flagellum axes and the cycloid were counted. The semicircle was positioned parallel to the vertical axis. (**C**) For nucleator methods, two horizontal directions (intercept, Ln1 and Ln2) were considered from the central point within the sperm head to the plasma membrane.

results also showed that the sperm motility also decreased in the diabetic groups in comparison to the control groups (P<0.05) (Fig. 2).

Sperm mid-piece length

The results for length of the sperms' mid-piece revealed no significant differences between the control and diabetic groups. Therefore, sperm mid-piece length was not correlated with abnormal sperm morphology in diabetic groups (Fig. 3).

Sperm flagellum length

Our result indicated that the length of the flagellum was decreased in the diabetic groups in comparison to the control rats ($p < 0.05$) (Fig. 3).

Sperm head Volume

The results showed that there was a significant difference in the volume of the sperm heads between the control and diabetic groups ($p<0.05$). Therefore, sperm head volume was associated with abnormal sperm morphology (Fig. 3).

DISCUSSION

In this study investigated the morphological changes of the sperms in STZ-induced diabetic mice using stereological techniques. Our finding showed that the reduction in the sperm count and sperm motility in the diabetic groups in comparison with the control groups. Our results also showed that the reduction in the sperm heads volume and the length of sperm flagellum in the diabetic groups in comparison with the control groups. These sperm structure changes have proven to be detrimental to the chance of success pregnancy (Guneli et al., 2008). Diabetes increased blood glucose levels and created histological changes in mice's testis by reducing spermatogenic cells, cell apoptosis, and other histological changes in the seminiferous tubules. These changes were associated with morphological abnormalities in spermatogenesis (Guneli et al., 2008). Previous

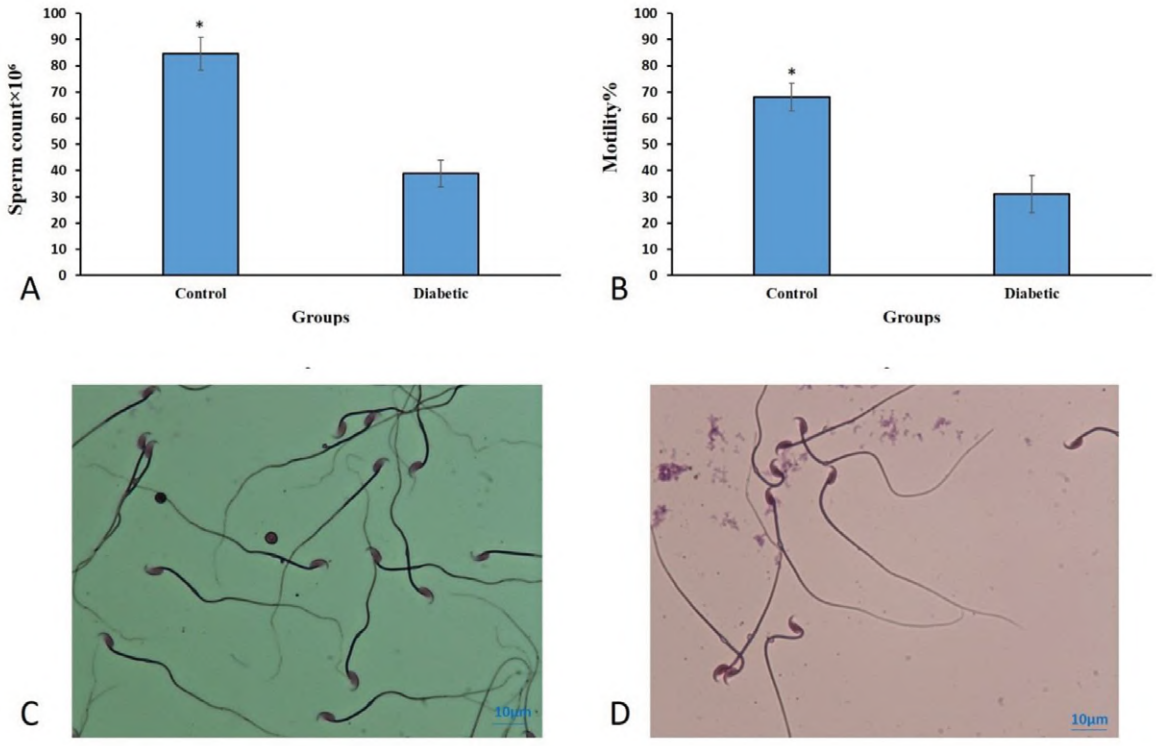

Fig. 2.- Total sperm count and sperm motility in the control and diabetic groups are shown (**A** and **B**). The significant difference between control groups in comparison to the diabetic groups is indicated. *p < 0.05. Diff quick staining of sperms. (**C**) Control group and (**D**) Diabetic group.

studies showed that diabetes could cause a reduction in testosterone levels in the serum and testes tissues in male mice by changing the function of Sertoli cells and affecting the leydig cells (Kanter et al., 2013). The dysfunction of leydig cells causes oxidative stress and increases free radicals, which could be detrimental to male fertility (Shrilatha, 2007). Moreover, diabetes can affect several sperm-related parameters of male fertility such as erection, semen concentration, semen volume, sperm count, sperm motility and testosterone levels; however, the relationship between standard sperm-related parameters and diabetes was not clear (Ficher et al., 1984; Hassan et al., 1993). It has been shown that diabetes is associated with the reduction of semen volume and the vitality and motility of spermatozoa. Also, spermatozoa of diabetic mice had less chromatin condensation and lower DNA integrity (Arikawe et al., 2006; Ricci et al., 2009).

The motility of sperms is associated with the mid-piece, which contains mitochondria for ATP synthesis which is therefore responsible for human fertility (Lüpold et al., 2009; Hargreave and Elton, 1983). Moreover, sperm viability is related to sperm morphometry, which was confirmed by observing that spermatozoa with a small head, width, area, and perimeter died after freezing and thawing (Marco-Jiménez et al., 2006). There are few studies conducted on the morphometric measurements of sperms (Jeyendran et al., 1986). One study on American soldiers analyzed the relationship between sperm length and fertility impairment (DeStefano et al., 1989; Boyle et al., 1992). The relationship between the dimensions of the sperm head with fertility after human intra uterine in semination (IUI) and intra cytoplasmic sperm injection (ICSI) has also been studied (Soler et al., 2005). Although the WHO recommends the evaluation of sperm morphometry, little attention has been paid to this parameter and its benefit in predicting fertility.

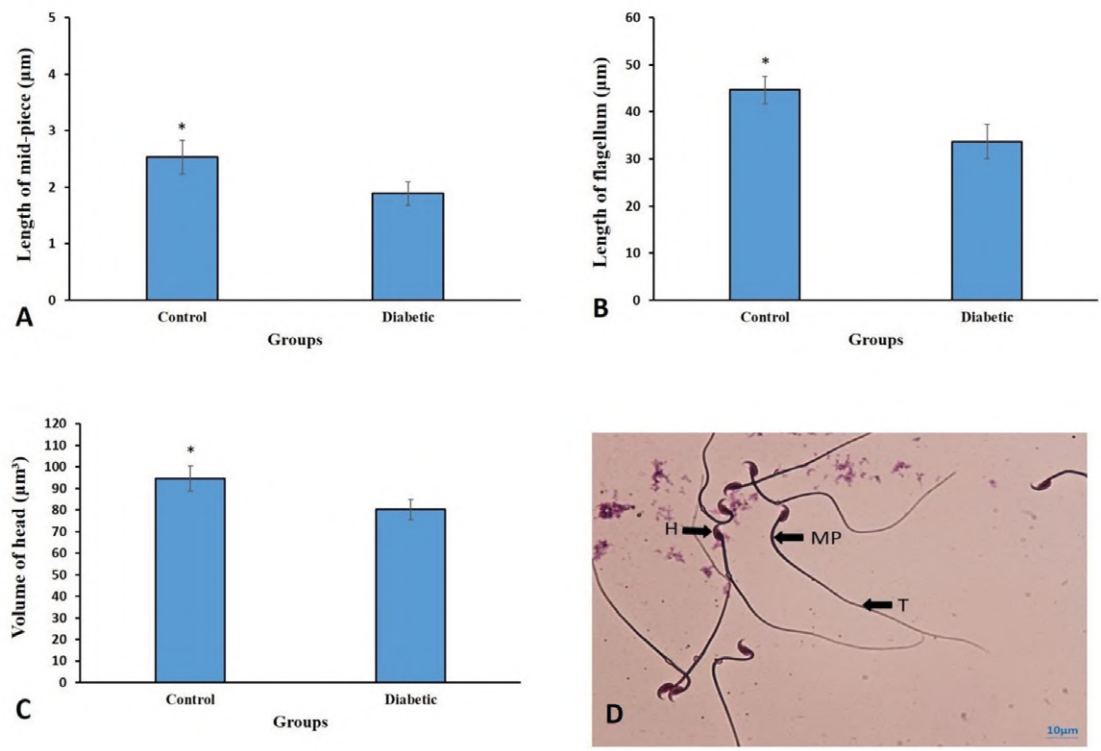

Fig. 3.- The sperms' mid-piece (**A**) and flagellum (**B**) length in the different groups are shown. The significant difference between control groups in comparison to the diabetic groups is indicated. *p < 0.05. The sperms' head volume (**C**) in the different groups are shown. The significant difference between control groups in comparison to the diabetic groups is indicated. *p < 0.05. (D) Diff quick staining of sperms, sperm head (H), sperms mid-piece (MP), sperm tail (T).

In recent research projects, stereological methods are growingly used in order to evaluate various morphometric parameters of three-dimensional objects (Rønn et al., 2000).

As stereological techniques have scientific advantages over quantitative results, this study utilized stereological methods for estimating sperm structure. Design-based stereology can enable invaluable three-dimensional (3D) information and quantitative data regarding the structural changes in sperm morphology such as sperm volume and sperm mid-piece and flagellum length that cannot be obtained using any other physiological, biochemical, or molecular techniques (Mühlfeld et al., 2010). The mentioned methods could not only be used in sperm analysis, but also in quantitative investigations of sperm parameters in various different studies. This study uses design-based stereological methods in order to obtain scientifically reliable estimates of the sperm head volume and sperm flagellum length in the control and diabetic mice. Our data indicated that the reduction of the sperm head volume and sperm flagellum length in diabetic mice in comparison with the control groups. These data support that the changes head volume and sperm flagellum length may related to the sperm fertility potential in diabetic mice.

ACKNOWLEDGEMENTS

The work was carried out at the Infertility and Reproductive Health Research Center, Shahid Beheshti University of Medical Sciences, Tehran, Iran (Registration No. 1395.440).

REFERENCES

ARIKAW A, DARAMOLA A, ODOFIN A, OBIKA L (2006) Alloxan-induced and insulin- resistant diabetes mellitus affect semen parameters and impair spermatogenesis in male rats. *Afr J Reprod Health,* 10: 106-113.

BOYLE CA, KHOURY MJ, KATZ DF, ANNEST JL, KRESNOW M-J, DESTEFANO F, SCHRADER SM (1992) The relation of computer-based measures of sperm morphology and motility to male infertility. *Epidemiology,* 3: 239-246.

DE PAZ P, MATA-CAMPUZANO M, TIZADO EJ, ÁLVAREZ M, ÁLVAREZ-RODRÍGUEZ M, HERRAEZ P, ANEL L (2011) The relationship between ram sperm head morphometry and fertility depends on the procedures of acquisition and analysis used. *Theriogenology,* 76: 1313-1325.

DESTEFANO F, ANNEST JL, KRESNOW M-J, SCHRADER SM, KATZ DF (1989) Semen characteristics of Vietnam veterans. *Reprod Toxicol,* 3: 165-173.

FICHER M, ZUCKERMAN M, FISHKIN RE, GOLDMAN A, NEEB M, FINK PJ, COHEN SN, JACOBS JA, WEISBERG M (1984) Do endocrines play an etiological role in diabetic and nondiabetic sexual dysfunctions? *J Androl,* 5: 8-16.

GHANBARI F, SHIRAVI A, MOGHADDAM HK, MOLZEMI S (2012) Effect of berberine hydrochlorid on testicular damage in streptozotocin-induced diabetic rats. *Knowledge and health*, 7: 129-135.

GUNELI E, TUGYAN K, OZTURK H, GUMUSTEKIN M, CILAKER S, UYSAL N (2008) Effect of melatonin on testicular damage in streptozotocin-induced diabetes rats. *Eur Surg Res,* 40: 354-360.

HARGREAVE T, ELTON R (1983) Is conventional sperm analysis of any use? *BJU Int,* 55: 774-779.

HASSAN AA, HASSOUNA MM, TAKETO T, GAGNON C, ELHILALI MM (1993) The effect of diabetes on sexual behavior and reproductive tract function in male rats. *J Urol,* 149: 148-154.

JEYENDRAN R, SCHRADER S, VAN DER VEN H, BURG J, PEREZ-PELAEZ M, AL-HASANI S, ZANEVELD L (1986) Association of the in-vitro fertilizing capacity of human spermatozoa with sperm morphology as assessed by three classification systems. *Human Reprod,* 1: 305-308.

KANTER M, AKTAS C, ERBOGA M (2013) Curcumin attenuates testicular damage, apoptotic germ cell death, and oxidative stress in streptozotocin-induced diabetic rats. *Mol Nutr Food Res,* 57: 1578-1585.

KARLSSON LM, CRUZ-ORIVE L (1997) Estimation of mean particle size from single sections. *J Microsc,* 186: 121-132.

KUSTER C, SINGER R, ALTHOUSE G (2004) Determining sample size for the morphological assessment of sperm. *Theriogenology,* 61: 691-703.

LUPOLD S, CALHIM S, IMMLER S, BIRKHEAD TR (2009) Sperm morphology and sperm velocity in passerine birds. *Proc Royal Soc London B: Biol Sci,* 276: 1175-1181.

MARCO-JIMENEZ F, VIUDES-DE-CASTRO M, BALASCH S, MOCE E, SILVESTRE M, GOMEZ E, VICENTE J (2006) Morphometric changes in goat sperm heads induced by cryopreservation. *Cryobiology,* 52: 295-304.

MAROTO-MORALES A, RAMÓN M, GARCIA-ALVAREZ O, SOLER A, ESTESO M, MARTÍNEZ-PASTOR F, PEREZ-GUZMÁN M, GARDE J (2010) Characterization of ram (Ovis aries) sperm head morphometry using the Sperm-Class Analyzer. *Theriogenology,* 73**,** 437-448.

MOSHER WD (1988) Fecundity and infertility in the United States. *Am J Public Health,* 78: 181-182.

MOSSMAN JA, PEARSON JT, MOORE HD, PACEY AA (2012) Variation in mean human sperm length is linked with semen characteristics. *Human Reprod,* 28: 22-32.

MUHLFELD C, NYENGAARD JR, MAYHEW TM (2010) A review of state-of-the-art stereology for better quantitative 3D morphology in cardiac research. *Cardiovasc Pathol,* 19: 65-82.

NAVARRO-CASADO L, JUNCOS-TOBARRA M, CHAFER-RUDILLA M, ONZOÑO LÍ, BLAZQUEZ-CABRERA J, MIRALLES-GARCIA J (2010) Effect of experimental diabetes and STZ on male fertility capacity. Study in rats. *J Androl,* 31: 584-592.

NING G, HONG J, BI Y, GU W, ZHANG Y, ZHANG Z, HUANG Y, WANG W, LI X (2009) Progress in diabetes research in China. *J Diabetes,* 1: 163-172.

NOORAFSHAN A, KARBALAY-DOUST S (2010) A simple method for unbiased estimating of ejaculated sperm tail length in subjects with normal and abnormal sperm motility. *Micron,* 41: 96-99.

PANAHI S, ABDOLLAHIFAR M-A, ALIAGHAEI A, NAZARIAN H, PAKTINAT S, ABDI S, FARAHANI RM (2017) Application of stereological methods for unbiased estimation of sperm morphology in the mice induced by busulfan. *Anat Cell Biol,* 50: 301-305.

RICCI G, CATIZONE A, ESPOSITO R, PISANTI F, VIETRI M, GALDIERI M (2009) Diabetic rat testes: morphological and functional alterations. *Andrologia,* 41: 361-368.

RØNN LC, RALETS I, HARTZ BP, BECH M, BEREZIN A, BEREZIN V, MØLLER A, BOCK E (2000) A simple procedure for quantification of neurite outgrowth based on stereological principles. *J Neurosci Meth,* 100: 25-32.

SCARANO W, MESSIAS A, OLIVA S, KLINEFELTER G, KEMPINAS W (2006) Sexual behaviour, sperm quantity and quality after short-term streptozotocin-induced hyperglycaemia in rats. *Int J Androl,* 29: 482-488.

SEED J, CHAPIN RE, CLEGG ED, DOSTAL LA, FOOTE RH, HURTT ME, KLINEFELTER GR, MAKRIS SL, PERREAULT SD, SCHRADER S (1996) Methods for assessing sperm motility, morphology, and counts in the rat, rabbit, and dog: a consensus report. *Reprod Toxicol,* 10: 237-244.

SHRILATHA B (2007) Early oxidative stress in testis and epididymal sperm in streptozotocin-induced diabetic mice: its progression and genotoxic consequences. *Reprod Toxicol,* 23: 578-587.

SOLER C, GAßNER P, NIESCHLAG E, DE MONSERRAT J, GUTIERREZ R, SANCHO M, BUENDÍA P, ÁLVAREZ J, BEHRE H, COOPER T (2005) Use of the integrated semen analysis system (ISAS®) for morphometrics analysis and its role in assisted reproduction technologies. *Rev Int Androl,* 3: 112-119.

Ameliorative effect of capsaicin against cardiac dysfunction induced by high fat diet in adult male rat

Ayat M. Domouky, Walaa A. Rashad

Human Anatomy & Embryology Department, Faculty of Medicine, Zagazig University, Egypt

SUMMARY

Overconsumption of high fat diet is a leading cause for developing obesity, which is strongly related to cardiovascular diseases. To elucidate the cardiac dysfunction induced by the effect of high fat diet and to evaluate the potential ameliorative effect of capsaicin against this toxicity, 40 adult male rats were divided into four groups: High fat diet (HFD) group contained 10 rats that were fed on HFD for 8 weeks. High fat diet and capsaicin group (HFD+CAP) group contained 10 rats that were fed on HFD + CAP for 8 weeks besides control groups. The extent of cardiac toxicity was evaluated physiologically and biochemically in addition to homogenate and histological examination of cardiac tissue. High fat diet led to significant increase in body weight, heart weight and body mass index. Moreover, HFD group showed significant increase in heart rate, systolic blood pressure with decrease in EF%. Biochemical investigation revealed significant increase in serum glucose, insulin level with insulin resistance, besides increase in serum total cholesterol, triglycerides and free fatty acids. HFD heart homogenate revealed decrease in total energy charge and total antioxidant capacity. Furthermore, histological examination displayed alteration of the normal histological structure of the heart tissue, increase in collagen deposition and significant increase in the immunopositivity of the inflammatory marker COX-2 and the apoptotic marker caspase-3. These effects were partially alleviated by consumption of capsaicin parallel with high fat diet in (HFD+CAP) group. However, even if capsaicin could ameliorate the effects of high fat diet, it is better to avoid HFD, as it can induce cardiac dysfunction.

Key words: Capsaicin – High fat diet – Obesity – Cardiac dysfunction – Inflammation – Apoptosis

INTRODUCTION

Consumption of a high-energy diet boosts a positive energy state and induces development of overweight and obesity (Swinburn and Egger, 2002). Obesity remains a global public health problem related to health behaviours and health outcomes with increased prevalence globally (Arroyo-Johnson and Mincey, 2016). Obesity is strongly related to cardiovascular diseases such as coronary heart disease (CHD) and heart failure (HF) (Stanley et al., 2012). Oxidative stress characterizes a recognized feature of obesity and is concerned in both vascular dysfunction

Corresponding author:
Walaa Abdelhaliem Rashad. Faculty of Medicine, Zagazig University, Department of Human Anatomy & Embryology, 10217 Zagazig, Egypt. Phone: 00201033037730. E-mail: waabdelhalim@medicine.zu.edu.eg / dr_wa_anatomy@yahoo.com

Submitted: April 11, 2021. **Accepted:** June 23, 2021

and cardiac fibrosis (Aubin et al., 2008; Lu et al., 2008). Many studies displayed that obesity's experimental model developed hypertension, hypercholesterolemia, hyperinsulinemia, renin–angiotensin system activation, and increased renal oxidative stress (Carroll et al., 2006).

The adult heart gains most of its energy from the oxidation of fatty acids (FAs), of which there are high levels in patients who feed on a high-fat diet (HFD) (Lopaschuk et al., 2010; Rider et al., 2013). Even though FAs are the main energy source of the myocardium, long-term exposure to free FAs may lead to fat deposition in cardiomyocytes and around the heart (Ji et al., 2017; Hu and Zhang, 2017). The harmful consequence of prolonged exposure to extra fats in the circulation on the heart is a result of the accumulation of toxic metabolic derivatives, which can lead to myocyte dysfunction and death via beginning of certain signalling cascades (Ji et al., 2017; Hu and Zhang, 2017)**.** Echocardiography is an ultrasound-based imaging method that enables serial, in vivo structural and functional characterization of the heart. Transthoracic echocardiography (TTE) has been widely used as a first-line investigation for the diagnosis of numerous cardiac disorders, including cardiomyopathies, valvular abnormalities and congenital heart defects. The ventricular ejection fraction (EF), the ratio of the stroke volume over the end-diastolic volume expressed as a percentage, is frequently used to gain an overall assessment of ventricular systolic function in humans and in small animals (Wang et al., 2018).

On the other hand, the co-administration of a natural antioxidant would counteract the deleterious effect of a high-fat diet on endothelial-mediated relaxation and reactive fibrosis (Baur and Sinclair, 2006; Das and Maulik, 2006). In consequence, the effect of HFD to develop an obesity state can be prevented by several factors like capsaicin (8-methyl-N-vanillyl-6-nonenamide), which is a compound with spicy smell and is the main capsaicinoid in chili peppers. It has a molecular formula ($C_{18}H_{27}NO_3$). Capsaicin shows monoclinic rectangular flaky colourless crystals (Pi et al., 2017). Capsaicin has been widely used in clinical practice. In cardiovascular studies, capsaicin was found to prevent obesity, induce the apoptosis of cancer cells, lower blood pressure and reduce blood lipids (Wong and Gavva, 2009). Capsaicin may show an anti-inflammatory effect via regulating the expression of some pro-inflammatory cytokines (such as COX-2) (Hwang et al., 2009). According to Woods et al., administration of a high-fat diet is an experimental model reproduces many features of human obesity (Woods et al., 2003). Therefore, our study aimed to achieve a new vision to the cardiac dysfunction effect of high fat diet by investigation of the hemodynamic, histopathological and biochemical changes in heart tissue in adult male rats, and to evaluate the potential ameliorative effect of capsaicin against this toxicity.

MATERIALS AND METHODS

Animals

40 healthy adult male rats (6-8weeks) weighing 180-220 g were used in this study. Rats were obtained from the Animal House of the Faculty of Medicine, Zagazig University, Egypt. They were housed in a temperature- and light-controlled room (12 h light/dark cycles) with free access to food and water. All experiments were performed in accordance with relevant guidelines and regulations of the Institutional Animal Care and Use Committee, Zagazig University (ZU-IACUC committee), approval number *ZU-IACUC/3/F/85/2020.*

Diet preparations

The high fat diet consisted of 42% lipids, 36% carbohydrates, and 22% proteins (kcal), the normal diet (ND) consisted of 12.5% lipids, 63.2% carbohydrates, and 24.3% proteins (kcal). To assess the therapeutic benefit of Capsaicin (0.003% of CAP, which correspond to a 0.399 mg/kg body weight) was added directly to rat chow (Baskaran et al., 2019).

Experiment protocol

40 adult male rats were divided into four groups, each containing 10 rats: Control group, which subdivided into normal diet (ND) subgroup, which contained 10 rats that were fed on normal diet (ND) for 8 weeks, and Capsaicin (CAP) subgroup,

which contained 10 rats that were fed on ND supplemented by Capsaicin for 8 weeks. High fat diet (HFD) group contained 10 rats that were fed on HFD for 8 weeks. High fat diet and capsaicin group (HFD+CAP) group contained 10 rats that were fed on HFD + CAP for 8 weeks. Female rats were excluded to avoid hormonal changes that might occur during the estrus cycles. The extent of cardiac toxicity was evaluated physiologically beside biochemical and histological examination of cardiac tissue samples from sacrificed rats.

Anthropometric measures

Measuring body weight: the animals were put in closed plastic containers and were weighed a day before the experiment and at the last day. The results were written in a record for each labeled rat (Brennan et al., 2009). Measuring rat length: nose-to-anus length was measured at the start and at the end of the experiment. An assistant was holding rats from the tail to lengthen the body, ensure the real nose-to-anus length of the animal and avoid false measures. A metal ruler graduated in centimeters was used by holding zero end at the anus and record the reading that reached the nose (Novelli et al., 2007). Calculating BMI index: body mass index (BMI) equals body weight (gm) / length^2 (cm^2), this index can be used as an indicator of obesity where the cutoff value of obesity BMI is more than 0.68 gm/cm^2 (Novelli et al., 2007).

Measurement of hemodynamic parameters

At the conclusion of the experiments, the heart rate, systolic blood pressure (SBP) was assessed by using the noninvasive tail-cuff method with a Narco BioSystems Electro-Sphygmomanometer. The average of two readings was recorded for each measurement.

Echocardiography

At week 8, rats were anaesthetized using 3% pentobarbital sodium (0.1 mL/100 mg) and their cardiac function and ventricular dimensions were evaluated by transthoracic echocardiography using a GE vivid E9 equipped with a 13-MHz phased-array transducer. All rats' hearts were recorded at the level of the papillary muscle in 2D and M-mode.

The parameters of left ventricular end diastolic diameter (LVEDD) and left ventricular end systolic diameter (LVESD) were measured. Functions were assessed by the following parameters: endocardial fractional shortening (FS), and ejection fraction (EF). left ventricular percent fractional shortening, (FS) was calculated from the M-mode using the following equation FS (%): [(LVIDD - LVISD)/LVIDD] X 100%. Left ventricular ejection fraction (EF%) was automatically calculated by the echocardiography machine according to the Teicholz formula (Platt et al., 2017). The parameters were determined for three cardiac cycles and averaged.

Biochemical study

Blood samples (about 8 ml/rat) were obtained at the end of the experimental period after overnight fasting and measurement of blood pressure (between 9:00-11:00 a.m.), blood samples were obtained from retroorbital venous plexus of each rat after ether inhalation (Sharma et al., 2014). The blood samples were allowed to clot at room temperature before centrifuging at 3000 rpm for 15 minutes. The serum was stored at -20° C.

Serum Biochemical analysis: Serum glucose level: by using glucose enzymatic (GOD-PAP)-liquizyme Kits (Biotechnology, Egypt). Serum insulin level: by using rat insulin enzyme-linked immunosorbent assay kit BioSource (Biotechnology, Egypt).

Calculation of homeostasis model assessment of insulin resistance (HOMA-IR): The following equation was used; [insulin (µU/mL) x glucose (mg/dl) /405] (Mari et al., 2005; Gutch et al., 2015). Healthy Range: 1.0 (0.5-1.4), Above 2.5 indicates insulin resistance.

Total cholesterol (TC), free fatty acids (FFA) and triglycerides (TG) were measured from serum according to colorimetric kits from Biovision (Egypt) and the manufacturers' protocol. Concisely, serum sample was matched with assay buffer and enzyme mixture, incubated in dark and measured at 570 nm utilizing a plate reader. Quantification was done from standard curve using the corresponding standards for cholesterol, TG, or FFA.

Cardiac dissection

After 8 weeks of feeding, the hearts were rapidly excised from the decapitated rats. The heart weight, and the ratio heart/body weight of each rat were measured.

Homogenate heart tissue analysis

Heart samples were homogenized in 50 mM phosphate buffer (pH 7.4) and sonicated over ice. The sonicated homogenates were centrifuged for 20 min at 3,200 × g at 5°C. A supernatant portion was dialyzed for 24 hours against two changes of cold 50 mM phosphate buffer.

Adenine nucleotide analysis: the supernatant of homogenized heart tissue was neutralized with an equal volume of 1M Na_2HPO_4 and centrifuged again at 10,000g and 4°C for 10 minutes. The supernatant was filtered through a 0.22 µm filter. Next, 50 µl aliquots were analysed using a high-performance liquid chromatography (HPLC) method with a Beckman C18 column (5 µm, 250 × 4.6mm). Analytes were isocratically eluted using 96% 0.05M KH2PO4 (pH 6.5) and 4% methanol for 30 minutes. Concentrations of adenosine triphosphate (ATP), adenosine diphosphate (ADP), and adenosine monophosphate (AMP) were determined at 254 nm using an external standard method for quantification. Total energy charge was defined as (ATP + ADP/2)/ (ATP + ADP + AMP) (Chen et al., 2018).

Total Antioxidant Capacity (TAC) was measured according to Cell Biolabs' OxiSelect™ Total Antioxidant Capacity (TAC) Assay Kit, based on the reduction of copper (II) to copper (I) by antioxidants such as uric acid. Upon reduction, the copper (I) ion further reacts with a coupling chromogenic reagent that produces a color with a maximum absorbance at 490 nm. The net absorbance values of antioxidants are compared with a known uric acid standard curve. Absorbance values are proportional to the sample's total reductive capacity. Results are expressed as "ng/mg".

Histological and morphometric examination

LV transverse sections of seven animals from each group were fixed in 10% buffered formalin and embedded in paraffin. Thick sections of 1 µm were cut from the tissue block and stained with haematoxylin and eosin, and with the collagen specific stain Masson's trichrome staining. Phosphate buffer (PBS), dissection set, 10% formal saline, alcohol, xylene and paraffin wax for preparation to light microscopic examination. H&E and Masson's trichrome stains were purchased from faculty of medicine, Zagazig University.

The myocyte cross-sectional area was determined for at least 100 myocytes per haematoxylin and eosin stained slide. The myocyte cross-sectional area measurements were obtained from digitized images (40× magnification lens) at Anatomy Department, Faculty of Medicine, Zagazig University. Myocyte cross-sectional area was measured using a digitizing pad, and the selected cells were cut transversely with the nucleus clearly identified in the centre of the myocyte. Area % collagen fibre was determined for the entire Masson's trichrome stained cardiac section were obtained from digitized images (40× magnification lens) at Anatomy Department, Faculty of Medicine, Zagazig University. The components of the cardiac tissue were identified according to color level as follows: green for collagen fibers; blue for myocytes; and white for interstitial space.

Immunohistochemical study for COX-2 and caspase-3 in the heart tissue

COX-2 antibodies, Caspase-3 antibodies, and Kits for enzymes assay were purchased from (Sigma-Aldrich chemical company, Germany and purchased from Sigma-Egypt). The immunohistochemical staining of for COX-2 was performed according to Pi et al. After deparaffinization and hydration, sections were incubated with 3% H_2O_2 for 5-10 min, followed by antigen retrieval in 0.01 M citric acid. After blocking in 5% BSA for 20 min, sections were treated with phospho-MAPK polyclonal antibody (1:1000) at 4°C overnight. Following incubation with HRP conjugated goat anti-rabbit IgG (1:1000) at 37°C for 20 min, visualization was performed with DAB, and counterstaining was performed with hematoxylin, followed by dehydration, transparentization and mounting. In blank control group, the primary antibody was replaced with

PBS. Positive cells had brown cytoplasm, intensity of Cox-2 immunoreactivity was measured and mounted using Canada balsam. Image analysis software (ImageJ 1.36b, http://rsbweb.nih.gov/ij) and expressed in percentage.

The immunohistochemical staining of for caspase-3 was performed according to (Bebars et al., 2017). 5 µm-thick sections were cut from the paraffin embedded blocks and stained by IHC technique according to data sheet (Cat. #RP-09605). The slides were incubated overnight at room temperature with a purified rabbit polyclonal antibody raised against caspase-3. It is received as 0.5 ml concentrated for use. The Envision method was used for detection of antibody binding. For negative control, the primary antibody was replaced by PBS. Finally, all sections were counter stained with Mayer's hematoxylin and examined by light microscopy. Positive cells had brown cytoplasm, intensity of caspase-3 immunoreactivity was measured and mounted using Canada balsam. Image analysis software (ImageJ 1.36b, http://rsbweb.nih.gov/ij) and expressed in percentage (Bressenot et al., 2009). Quantitative data were estimated in 5 different non-overlapped fields for the same slide of each animal, in each animal 5 slides were counted and a total number of 25 fields of each group were counted.

Statistical analysis

The collected data were statistically analyzed using SPSS program (Statistical Package for Social Science) version 18.0. Descriptive statistics were given as mean ± standard deviation (SD). One-way ANOVA were used to compare the mean values of more than two groups. Multiple comparisons were estimated by the least significant difference (LSD) test. A value of $p<0.05$ was accepted as statistically significant, a value of $p<0.001$ was accepted as highly statistically significant, and a value of $p>0.05$ was accepted as non-statistically significant. Spearman's rank correlation coefficient was used to analyze the association between serum hormonal and lipid levels against body mass index, and echocardiography (EF) against morphometric parameters.

RESULTS

Body and heart anthropometric measures analysis

Rats from the HFD group showed a highly significant increase in body weight compared with the rats from ND, CAP group. The mean of weight of the HFD group was 380±6 gm, while that of ND and CAP groups was 255±9 gm, 232±4 respectively. Consumption of capsaicin parallel with high fat diet in (HFD+CAP) group showed partial protection from weight gain, the average weight of the HFD+CAP group was 315±20 gm. In contrast to final body weight, the body length showed no significant difference between different study groups. Therefore, body mass index (BMI) showed a highly significant increase in the HFD group, the mean of BMI of the HFD group was 0.72±0.05 gm/cm^2, while that of ND, CAP, HFD+CAP groups were 0.48±0.03, 0.40±0.06 and 0.60±0.02 gm/cm^2 respectively (Table 1, Fig. 1 A, B, C).

Table 1. Anthropometric measures analysis in different study groups.

	Control group (n10)		HFD group (n10)	HFD+CAP group (n10)	P value
	ND subgroup (n10)	CAP subgroup (n10)			
Initial body weight (gm)	185±7	190±8	193±4	192±8	0.0653
Final body weight (BW) (gm)	255±9	232±4*	380±6*	315±20*, **	0.0000
Body length (BL) (cm)	23±3	24±5	23±4	23±3	0.9163
Body mass index (BMI) (gm/cm^2)	0.48±0.03	0.40±0.06*	0.72±0.05*	0.60±0.02*, **	0.0000
Heart weight (HW) (g)	1.2±0.04	1.3±0.06	2.6±0.16*	1.9±0.27*, **	0.0000
Heart wt./body wt. % (H/BW%)	0.53±0.03	0.56±0.04	0.68±0.22	0.6±0.14	0.0841

One-way ANOVA, and least significant difference (LSD) test, P > 0.05: no significant differences, P < 0.05: significant differences, P < 0.001: highly significant differences.
* significant vs ND subgroup; ** significant vs HFD group

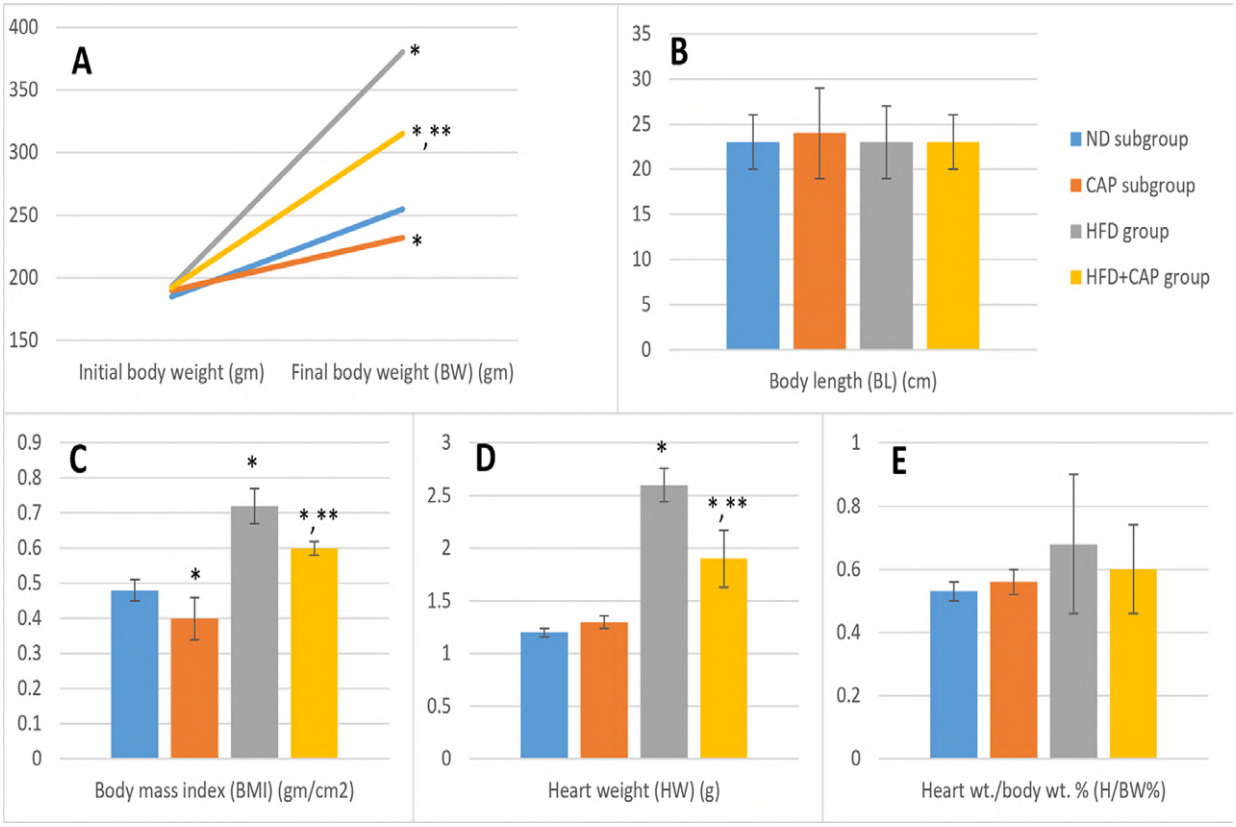

Fig. 1.- Anthropometric measures analysis in different study groups showed that rats from the HFD group showed a highly significant increase in body weight compared with the rats from ND, CAP group (**A**). In contrast to final body weight, the body length showed no significant difference between different study groups (**B**), therefore, body mass index (BMI) showed a highly significant increase in the HFD group (**C**). Moreover, Rats from the HFD group showed a highly significant increase in heart weight compared with the rats from ND, CAP group (**D**). In contrast to heart weight, the ratio between heart and body weights (H/BW%) showed no significant difference between different study groups (**E**).

Regarding heart measures, rats from the HFD group showed a highly significant increase in heart weight compared with the rats from ND, CAP group. The mean of heart weight of the HFD group was 2.6±0.16 gm, while that of ND and CAP groups was 1.2±0.04 gm, 1.3±0.06 respectively. Consumption of capsaicin led to partial protection, the average heart weight of the HFD+CAP group was 1.9±0.27 gm. In contrast to heart weight, the ratio between heart and body weights (H/BW%) showed no significant difference between different study groups (Table 1, Fig. 1 D, E).

Hemodynamic and Echocardiography parameters analysis

The rat fed with high fat diet exhibited significantly elevated heart rate, systolic blood pressure, LVESD, and significant reduction in EF% and FS% in comparison to both ND and CAP groups. These effects were alleviated by consumption of capsaicin parallel with high fat diet in (HFD+CAP) group (Table 2, Fig. 2).

Biochemical results analysis

Fasting serum glucose, insulin levels were significantly increased in HFD group as compared to ND and CAP groups. These effects were partially alleviated by consumption of capsaicin parallel with high fat diet in (HFD+CAP) group. With calculation of homeostasis model assessment of insulin resistance (HOMA-IR), the mean in rat on high fat diet was 3.8±0.4 while the mean in ND, CAP, HFD+CAP groups were 1.6±0.3, 1.5±0.3, 2.3±0.9 which indicate insulin resistance in HFD group (Table 3, Fig. 3 A, B, C).

The rat fed with high fat diet exhibited significantly elevated total cholesterol (TC), free fatty acids (FFA) and triglycerides (TG) in comparison to both ND and CAP groups. These effects were partially alleviated by consumption of

capsaicin parallel with high fat diet in (HFD+CAP) group (Table 3, Fig. 3 D, E, F).

Homogenate results analysis

Total energy charge was assessed by measurement of adenine nucleotide variants in the myocardia. The ATP and ADP concentrations in the myocardia of the HFD group were 2.23±0.36 and 2.17± 0.42 µg/ml, respectively, which were significantly lower than those of the other groups. On the contrary, the AMP concentration was significantly higher in the HFD group (1.54±0.27 µg/ml). Consequently, the HFD group had a significantly lower energy charge (0.57±0.15) vs 0.76±0.11, 0.81±0.15, 0.72±0.14 in ND, CAP,

Table 2. Hemodynamic and Echo parameters analysis in different study groups.

	Control group (n10)		HFD group (n10)	HFD+CAP group (n10)	P value
	ND subgroup (n10)	CAP subgroup (n10)			
Heart rate (beat/min.)	276±4	285±6**	312±6*	294±5*, **	0.0000
Systolic blood pressure (mmHG)	134±6	129±6**	181±4*	153±7*, **	0.0000
LVEDD	8.21±0.4	8.26±0.3	8.47±0.2	8.29±0.6	0.5079
LVESD	3.57±0.3	3.48±0.4**	4.04±0.5*	3.72±0.2	0.0090
EF%	71.5±3.4	68.3±2.6**	48.7±3.2*	68.5±4.2**	0.0000
FS %	36.84±2.1	35.46±3.7**	29.45±4.3*	32.65±3.5	0.0002

Left ventricular end diastolic diameter (LVEDD), left ventricular end systolic diameter (LVESD), ejection fraction (EF%), left ventricular percent fractional shortening (FS%).
One-way ANOVA, and least significant difference (LSD) test, $P > 0.05$: no significant differences, $P < 0.05$: significant differences, $P < 0.001$: highly significant differences.
* significant vs ND subgroup; ** significant vs HFD group

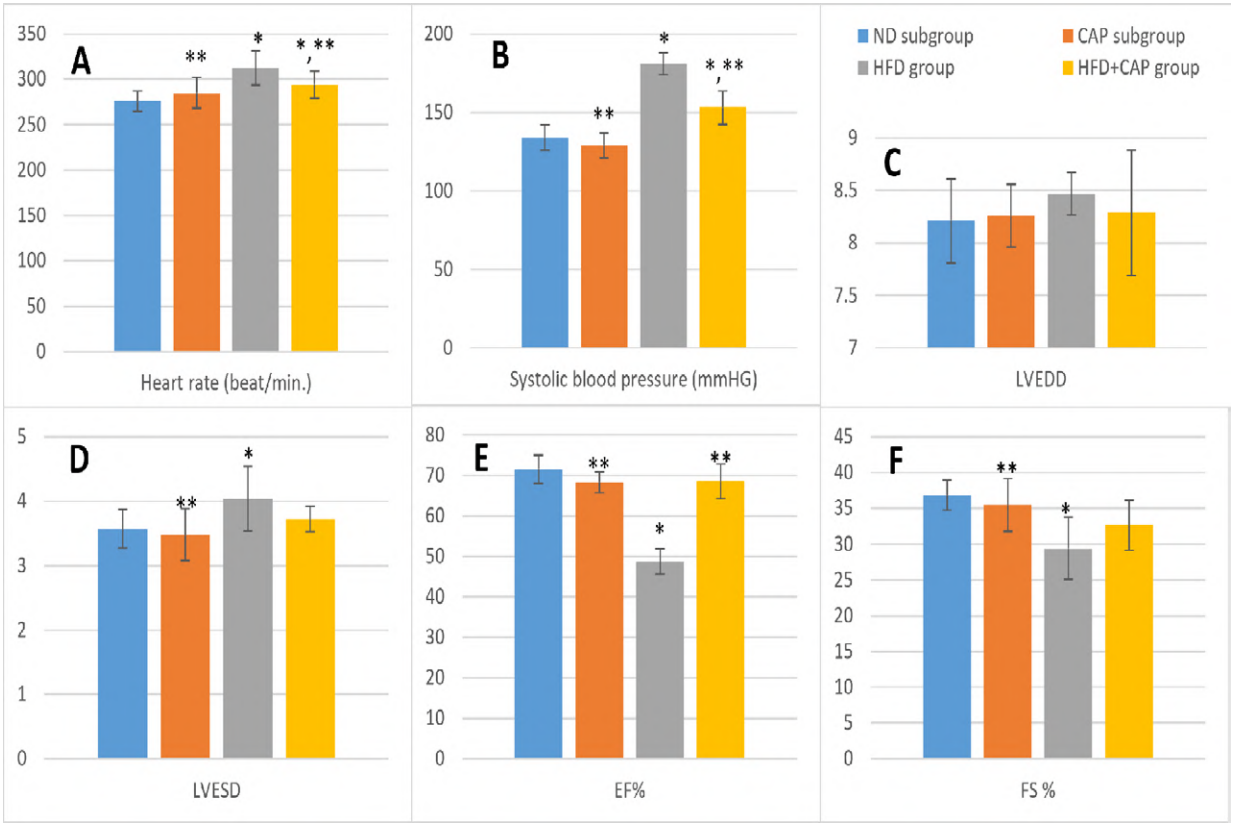

Fig. 2.- Hemodynamic and Echo parameters analysis in different study groups showed that rats fed high fat diet exhibited significantly elevated heart rate (**A**), systolic blood pressure (**B**), LVEDD (**C**), LVESD (**D**), and significantly reduction in EF% (**E**) and FS% (**F**) in comparison to both ND and CAP groups, these effects were alleviated by consumption of capsaicin parallel with high fat diet in (HFD+CAP) group.

HFD+CAP groups respectively (table 3, figure 3 G). Moreover, total antioxidant capacity was measured, the HFD group had an extremely significant lower antioxidant capacity (4.5±2.3) vs 15.7±2.2, 16.4±3.1, 12.4±2.7 in ND, CAP, HFD+CAP groups respectively (Table 3, Fig. 3H).

Table 3. Biochemical and homogenate results analysis in different study groups.

	Control group (n10)		HFD group (n10)	HFD+CAP group (n10)	P value
	ND subgroup (n10)	CAP subgroup (n10)			
Serum glucose level (mg/dl)	90±15	82±9**	150±23*	100±32**	0.0000
Serum insulin level (µU/ml)	7.2±0.8	7.6±1.2	10.4±0.5*	9.3±1.7	0.0000
HOMA-IR	1.6±0.3	1.5±0.3**	3.8±0.4*	2.3±0.9*, **	0.0000
Total cholesterol (TC) (mg/dl)	105±7	98±9**	182±12*	132±14*, **	0.0000
Free fatty acids (FFA) (µM/l)	0.34±0.11	0.29±0.08**	0.92±0.13*	0.45±0.23**	0.0000
Triglycerides (TG) (mg/dl)	64.6±2.14	54.5±1.75**	172±11.45*	112±13.45*, **	0.0000
ATP (µg/ml)	3.12 ± 0.37	2.98 ± 0.28	2.23 ± 0.36*	2.45 ± 0.36*, **	0.0000
ADP (µg/ml)	2.66 ± 0.22	2.56 ± 0.36	2.17 ± 0.42*	2.42 ± 0.15*, **	0.0000
AMP (µg/ml)	0.68 ± 0.21	0.62 ± 0.34	1.54 ± 0.27*	0.83 ± 0.23	0.0000
Total energy charge (µg/ml)	0.76 ± 0.11	0.81 ± 0.15**	0.57 ± 0.15*	0.72 ± 0.14	0.0030
Total Antioxidant Capacity (ng/mg)	15.7±2.2	16.4±3.1**	4.5±2.3*	12.4±2.7*, **	0.0000

One-way ANOVA, and least significant difference (LSD) test, $P > 0.05$: no significant differences, $P < 0.05$: significant differences, $P < 0.001$: highly significant differences.
* significant vs ND subgroup; ** significant vs HFD group

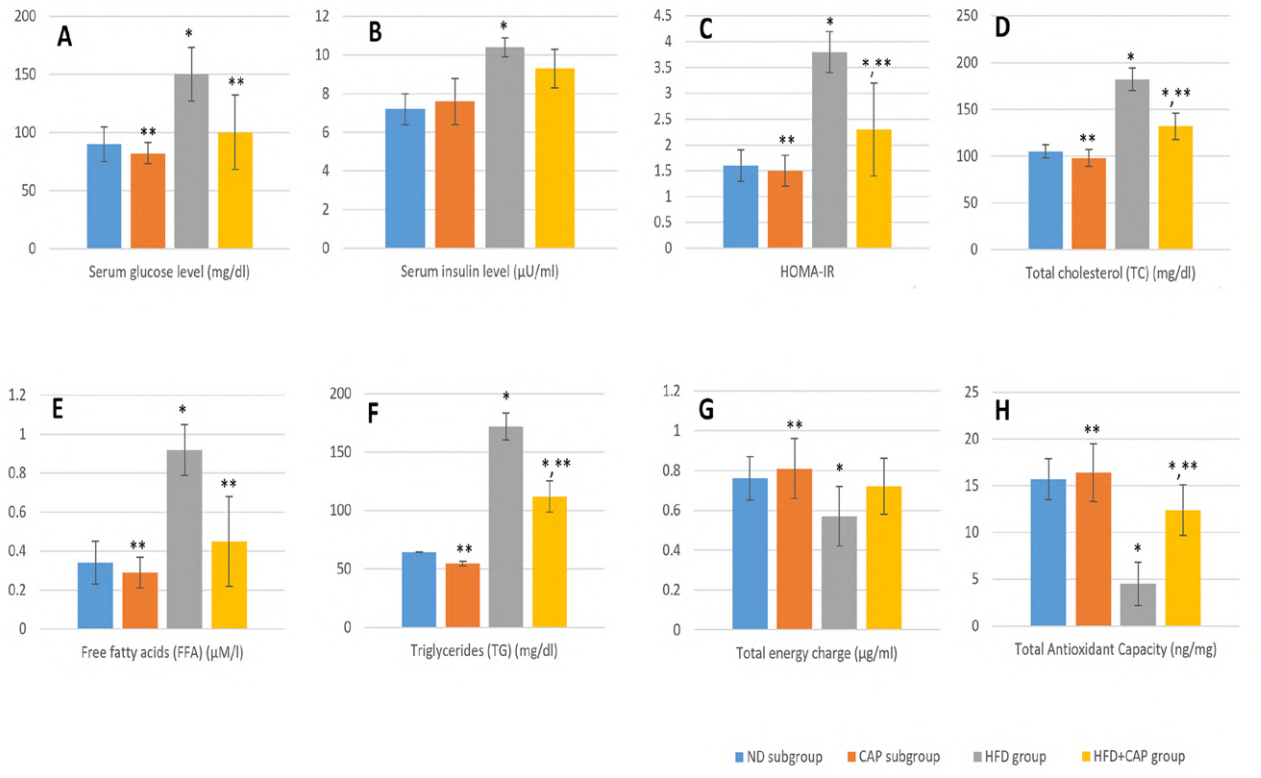

Fig. 3.- Biochemical and homogenate results analysis in different study groups showed that Fasting serum glucose (**A**), insulin levels (**B**) were significantly increased in HFD group as compared to ND and CAP groups. calculation of HOMA-IR (**C**) indicated insulin resistance in HFD group. Moreover, Rats from the HFD group exhibited significantly elevated total cholesterol (**D**), free fatty acids (**E**) and triglycerides (**F**). Total energy charge (**G**) and total antioxidant capacity (**H**) were significantly lower in HFD rats than those of the other groups.

Histological and morphometrical examination

Sections of the heart tissue in the ND group exhibited normal histological architecture of the myocardium as longitudinally striated, linearly arranged, branching and anastomosing muscle fibers (cardiac myofibers). They were joined together by intercalated discs and separated from each other by delicate layer of connective tissue. The cardiac muscle cells (cardiomyocytes) contained acidophilic cytoplasm with oval vesicular centrally located nuclei. (Fig. 4 A1, A2). In CAP group, the histological pattern of the heart tissue was similar to the ND group (Fig. 4 B1, B2). In the HFD group, alteration of the normal histological structure of the heart tissue was observed. Distorted cardiomyocytes with deeply stained pyknotic nuclei, vacuolated sarcoplasm, separation of the cardiac myofibers, inflammatory cellular infiltration, dilated congested blood vessels and extravasation of RBCs were observed (Fig. 4 C1, C2, E, F). In HFD+CAP group, improvement and restoration of the normal histological structure of the heart tissue was observed (Fig. 4 D1, D2). Myocyte cross-sectional area in the myocardia of the HFD group was 735±114 um^2, which were significantly more than those of ND, CAP, HFD+CAP groups (412±75, 398±123, 512±65 respectively) (Fig. 4G).

Masson's trichrome stained heart tissue sections showed normally distributed collagen fibers in between the cardiomyocytes were observed in ND and CAP groups (Fig. 5 A, B), but markedly increased bundles of collagen within the distorted cardiac tissue were observed in the HFD group (Fig. 5 C, D). Nearly normal appearance was observed in the HFD+CAP (Fig. 5E). Also, Area % collagen fiber was significantly increase in HFD group (25.7±8.3) in contrast to ND, CAP, HFD+CAP groups (16.5±3.4, 17.4±5.6, 21.2±7.4 respectively) (Fig. 5F).

Immunohistochemical staining reflected increase in the immunopositivity of the inflammatory marker COX-2 and the apoptotic marker caspase-3 in HFD group compared to other groups. These effects were partially alleviated by consumption of capsaicin parallel with high fat diet in (HFD+CAP) group, active cells appeared as brown stained in contrast to healthy cells that appeared blue with counter stain (Fig. 6).

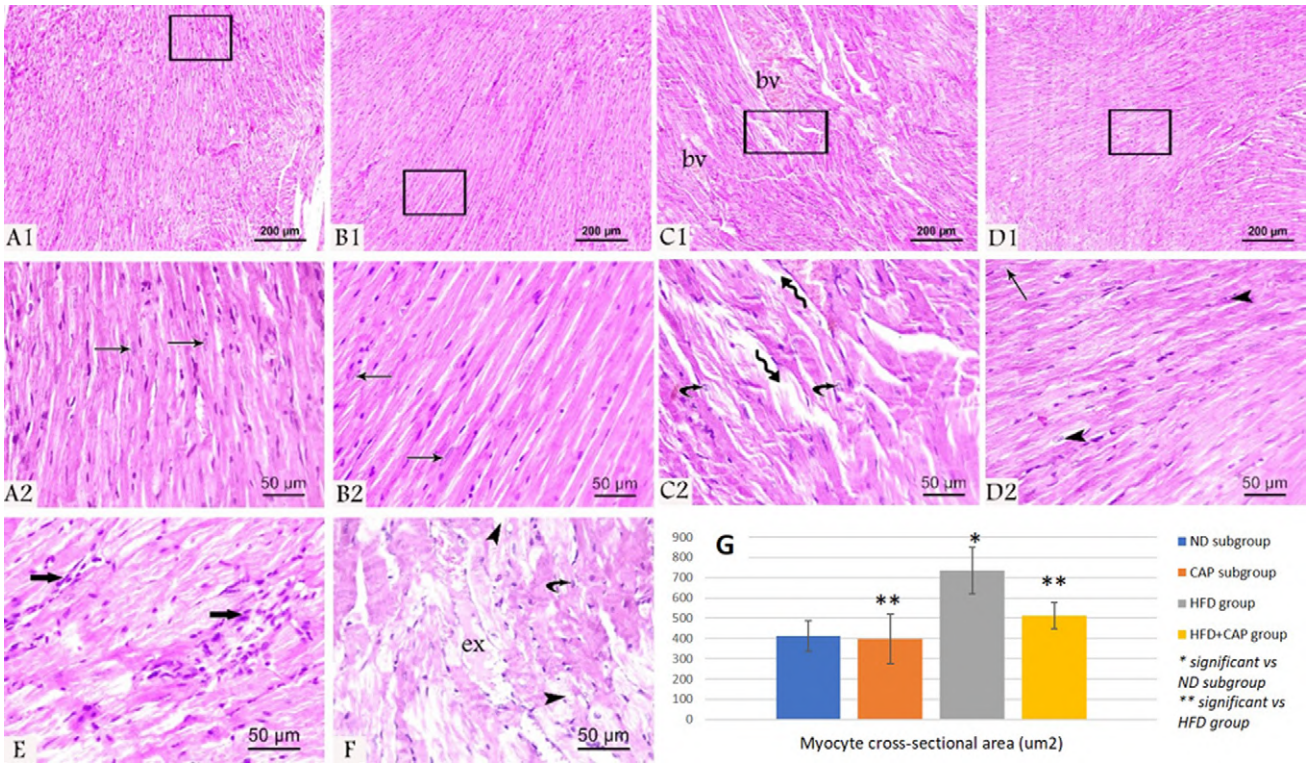

Fig. 4.- H&E-stained heart tissue sections from all the groups showing linearly arranged cardiac muscle fibers contained acidophilic cytoplasm with oval vesicular centrally located nuclei (arrow) in the ND (**A1, A2**) and CAP (**B1, B2**) groups. Notice the distorted cardiac muscle fibers, pyknotic nuclei (curved arrow), vacuolated sarcoplasm (arrowhead), inflammatory exudate (ex), dilated congested blood vessels (bv), inflammatory cellular infiltration (thick arrow) and separated cardiac muscle fibers (wavy arrow) in the HFD group (**C1, C2, E, F**). Restoration of the normal arrangement of the cardiac muscle fibers with oval vesicular centrally located nuclei (thin arrow) and some pyknotic nuclei (curved arrow) in the HFD + CAP group (**D1, D2**) are noticed. Morphometrical analysis showing increased myocyte cross sectional area in HFD group (**G**). Scale bars: A1, B1, C1 and D1 = 200 µm; A2, B2, C2, D2, E and F = 50 µm.

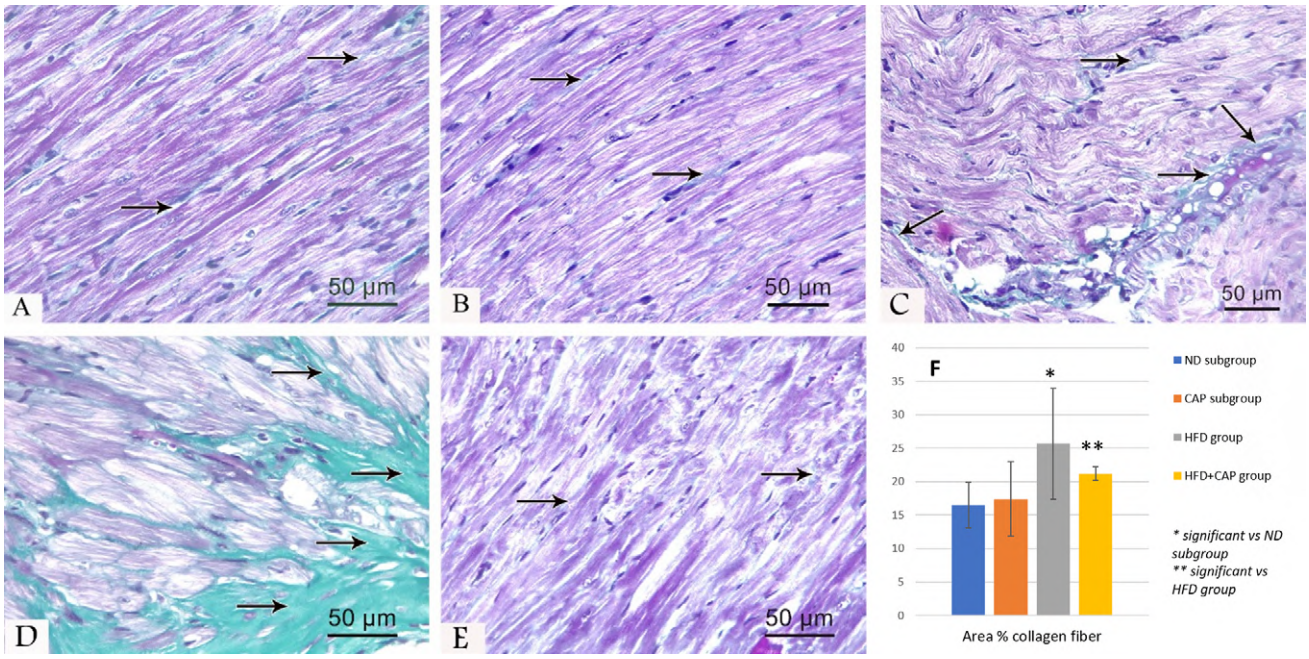

Fig. 5.- Masson's trichrome stained heart tissue sections from all the groups showing collagen fibers (arrow) which are normally distributed in the ND (**A**) and CAP (**B**) groups, markedly increased in the HFD group (**C, D**) and became normal in the HFD+CAP group (**E**). Morphometrical analysis showing significant increase of collagen fibers percentage in HFD group (**F**). Scale bars A-E = 50 µm.

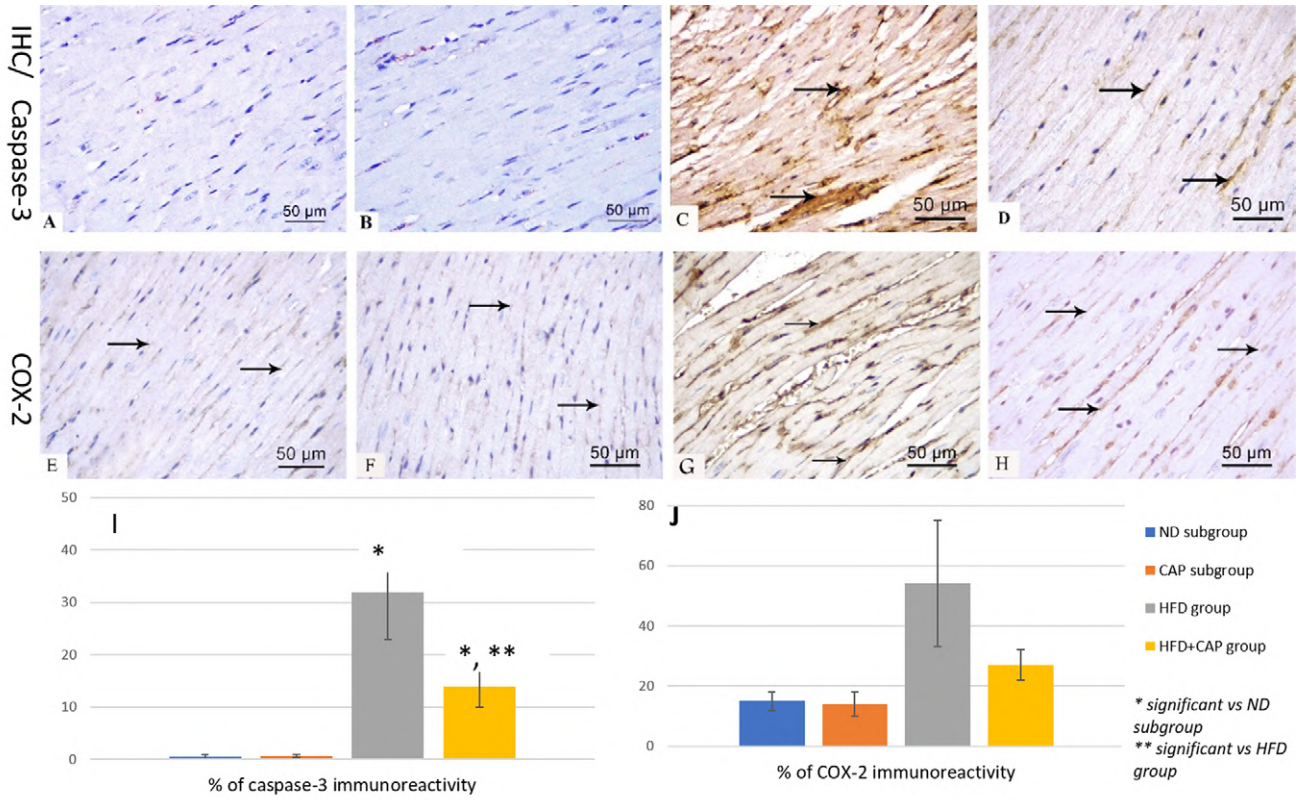

Fig. 6.- Caspase-3 (**A,B,C,D**) and COX2 (**E,F,G,H**) immuno-stained heart tissue sections from all the groups showing increased immunoreactivity (arrow) of both markers in HFD group (C,G) compared to other groups ND group (A,E), CAP group (B,F) and HFD+CAP group (D,H). Morphometrical analysis showing increased percentage of Caspase-3 (**I**) and COX2 (**J**) immunoreactivity in HFD group. Scale bars A-H = 50 µm.

Correlation between body mass index and other anthropometric and biochemical measures

Increase of body mass index in rats that were fed on HFD for 8 weeks was associated with significant positive correlation with heart weight (r=0.8303), heart wt. /body wt. % (r=0.5451), heart rate (r=0.8305) and systolic blood pressure (r=0.9406). Moreover, increase of body mass index in rats that were fed on HFD for 8 weeks was associated with significant positive correlation with serum biochemical parameters, serum glucose level (r=0.7568), serum glucose level (r=0.7568), serum insulin level (r=0.7093), total cholesterol (r=0.9066), free fatty acids (r=0.8268) and total triglyceride (r=0.9525) (Fig. 7).

Correlation between ejection fraction% and BMI and morphometric measures

Ejection fraction % as an indicator for left ventricular function showed a significant negative correlation with body mass index (r=-0.7697), heart rate (r=-0.8508), systolic blood pressure (r=-0.8721), myocyte cross sectional area (r=-0.8246), area % collagen fiber (r=-0.5271), % +ve COX2 cells (r=-0.7645) and % of apoptotic cells (r=0.7304). On the other hand, ejection fraction % showed a significant positive correlation with total energy charge (r=0.7016) and total antioxidant capacity (r=0.8938) (Fig. 8).

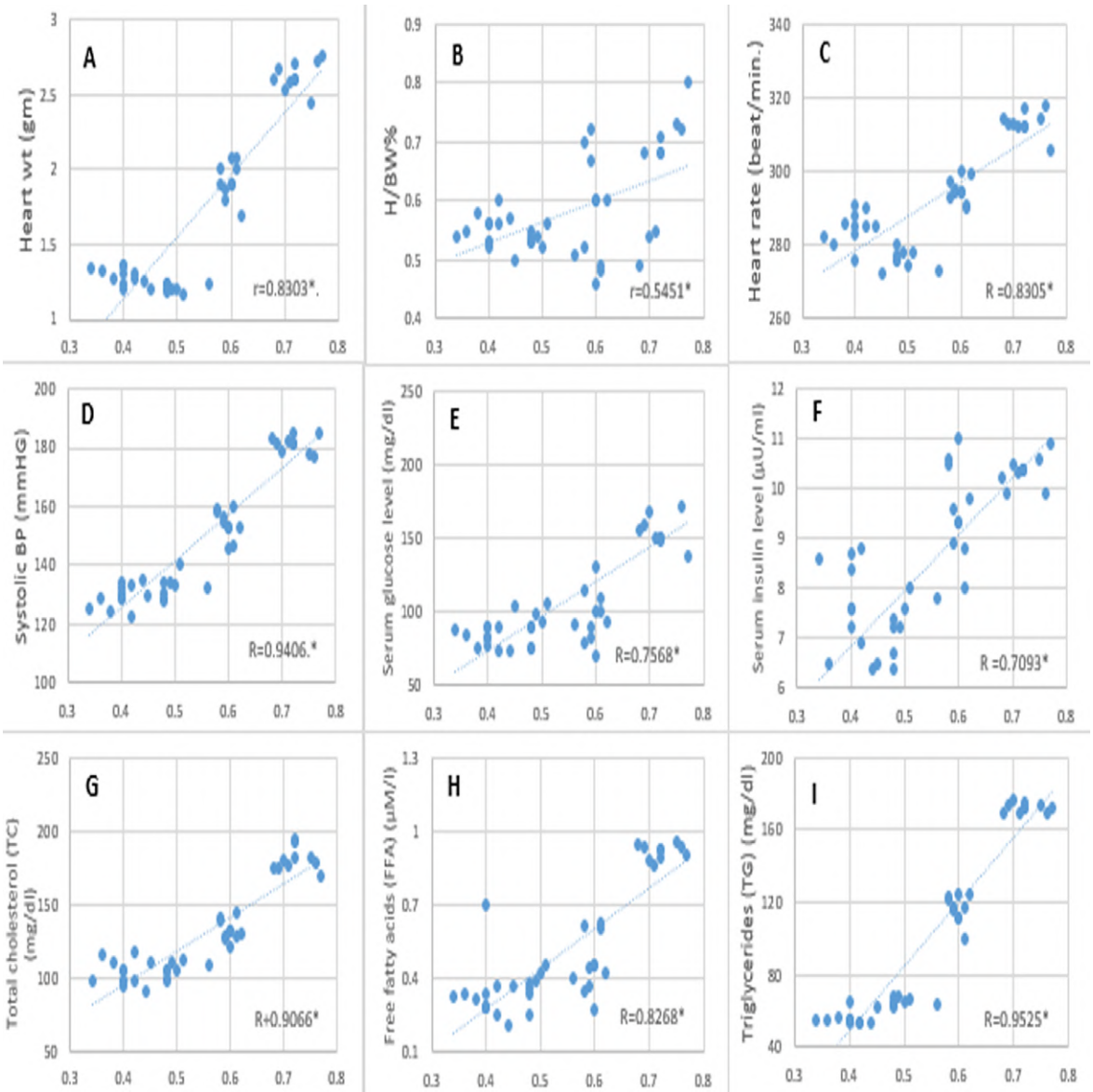

Fig. 7.- Correlation between body mass index and other anthropometric and biochemical measures, increase of body mass index in rats that were fed on HFD was associated with significant positive correlation with heart weight (**A**), heart wt. /body wt. % (**B**), heart rate (**C**) and systolic blood pressure (**D**). Moreover, increase of body mass index in rats that were fed on HFD was associated with significant positive correlation with serum biochemical parameters, serum glucose level (**E**), serum insulin level (**F**), total cholesterol (**G**), free fatty acids (**H**) and total triglyceride (**I**).

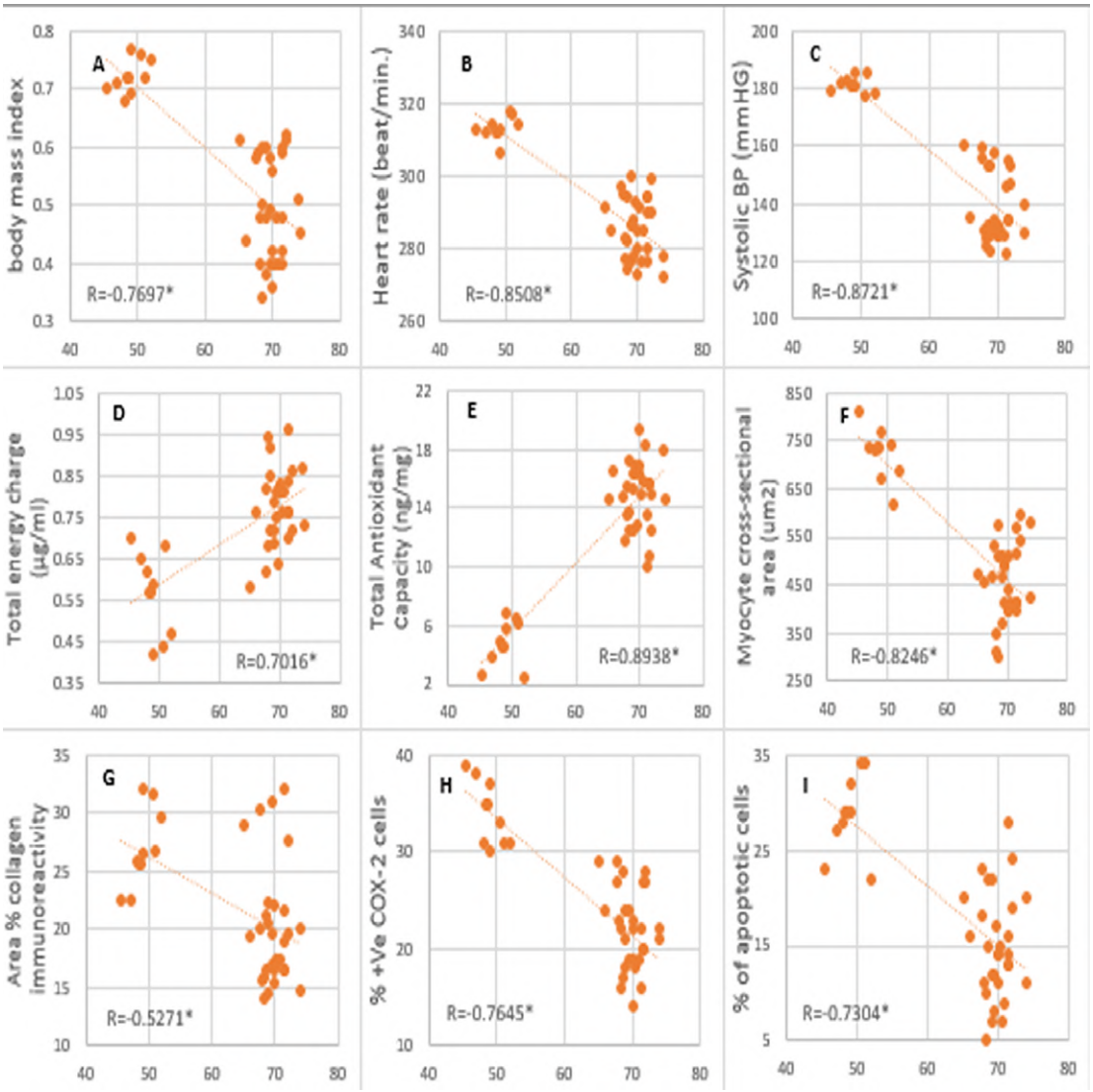

Fig. 8.- Correlation between ejection fraction% and BMI and morphometric measures showed a significant negative correlation with body mass index (**A**), heart rate (**B**), systolic blood pressure (**C**), myocyte cross sectional area (**F**), area % collagen fiber (**G**), % +ve COX2 cells (H) and % of apoptotic cells (**I**). On other hand Ejection fraction % showed a significant positive correlation with total energy charge (**D**) and total antioxidant capacity (**E**).

DISCUSSION

Obesity (Ob) has become one of the most prevalent metabolic diseases all over the world (Zhang et al., 2019). Ob is multifactorial in origin; overconsumption of high fat diet is a leading cause to develop obesity. Excess dietary fat increases both adipose and nonadipose tissue lipid content and, through lipotoxicity, leads to cell dysfunction and death, with or without the development of obesity (Hohos and Skaznik-Wikiel, 2017). Cardiovascular disorders are the critical causes of morbidity and mortality in association with Ob (Zhang et al., 2019). With worldwide overconsumption of high fat diet, it is mandatory to search about food additive which can make the balance and prevent cardiac dysfunction effect of HFD. So, it was aimed to achieve a new vision to the cardiac dysfunction induced by the effect of high fat diet through investigation of the hemodynamic, histopathological and biochemical changes in the heart of adult male rats, and to evaluate the potential ameliorative effect of capsaicin against this toxicity.

High fat diet used in the present study was sufficient to develop obesity in rats, Obese rats had an increase in body weight and heart weight, all these anthropometric parameters correlated directly with BMI, these results agreed with several studies (Carroll et al., 2006; Relling et al., 2006; Novelli et al., 2007; Bhandarkar et al., 2019; Mabrouki and Rjeibi, 2020) that induced obesity in rats through a hypercaloric diet. Further

hemodynamic analysis displayed significant increase in systolic heart rate and blood pressure as demonstrated by Wilde et al. (2000), Bhandari et al (2011), Bhandarkar et al. (2019), and Mabrouki and Rjeibi (2020): they reported significant increase in systolic, diastolic, mean arterial blood pressures and heart rate. Additional echocardiography examination to assess heart function in HFD rats revealed significant elevation of left ventricular end systolic diameter (LVESD), and significant reduction in left ventricular ejection fraction (EF%) and endocardial fractional shortening (FS%) in comparison to both ND and CAP groups. These results matched with Ge et al., (2012). Moreover, Li et al. (2018) observed enlarged LVESD, reduced EF and FS, but, in contrast with ours, this study, Li et al., observed also elevation of left ventricular end diastolic diameter (LVEDD).

Effect of HFD investigated biochemically and the results showed an elevation in fasting serum glucose, insulin levels in HFD group as compared to control groups. Calculation of homeostasis model assessment of insulin resistance (HOMA-IR), the mean in rat on high fat diet was 3.8±0.4, which indicates insulin resistance in HFD group. Similar biochemical results were reported by Mollica et al. (2017), Bhandarkar et al. (2019), Wang et al. (2021). Moreover, the rat fed with high fat diet exhibited significantly elevated total cholesterol, free fatty acids and triglycerides. All those biochemical parameters were in direct relation with body mass index, and this was corroborated by previous studied (De Leo et al., 2020; Mabrouki and Rjeibi, 2020; Wang et al., 2021).

Homogenate tissue analysis was done trying to understand the way by which HFD and obesity affect cardiac function, investigation of total energy charge showed that ATP and ADP concentrations in the myocardia of the HFD group were significantly lower than those of the other groups. On the contrary, the AMP concentration was significantly higher in the HFD group. Consequently, the HFD group had a significantly lower energy charge. These results suggested impaired mitochondrial dynamics, this was in accordance with Chen et al. (2018), who approved the effect of HFD in lowering total energy charge and impairment of mitochondrial dynamics.

This cardiac dysfunction has been described by many theories such as inflammation, LV fibrosis, collagen content alterations and increased oxidative stress (Sowers et al., 2011; Mollica et al., 2017). Many studies showed that oxidative stress and myocardial fibrosis are related to impairment of cardiac systolic function and insulin resistance (Whaley-Connell et al., 2007; Zhou et al., 2010; Begriche et al., 2013). So, our study investigated the total antioxidant capacity and the HFD group had an extremely significant lower antioxidant capacity, which is in accordance with (De Leo et al., 2020; Mabrouki and Rjeibi, 2020).

Further histological and morphometric examination of cardiac tissue observed that in HFD rats there were alteration of the normal histological structure of the heart tissue in form of increase myocyte cross-sectional area, distorted cardiomyocytes with deeply stained pyknotic nuclei, vacuolated sarcoplasm, separation of the cardiac myofibers, inflammatory cellular infiltration, dilated congested blood vessels and extravasation of RBCs, while Masson's trichrome stained heart tissue sections showed markedly increased bundles of collagen within the distorted cardiac tissue. Those histological results agreed with Sikder et al., (2018) and Bhandarkar et al., (2019), who interpreted the occurrence of cardiac fibrosis and the affection of cardiac performance by the excess deposition of collagen.

Immunohistochemical stained heart tissue sections in HFD rats reflected increase in the immunopositivity of the inflammatory marker COX-2 and the apoptotic marker caspase-3 in HFD group compared to other groups (Cole et al., 2011; Jørgensen et al., 2017), mentioned that COX2 was elevated with HFD with mitochondrial impairment and oxidative stress. Because inflammation is often associated by apoptotic events, the immunopositivity of caspase-3 was markedly increased in HFD group and this was in accordance with Fang et al. (2008) and Brugman (2016). Also settled with Li et al. (2018), who reported excessive apoptosis, deposition of collagen fibers and lipid droplets in cardiomyocytes.

Correlation between ejection fraction % as an indicator for left ventricular function and other findings showed a significant negative correlation with body mass index, heart rate, systolic blood pressure, myocyte cross sectional area, area % collagen fiber, % +ve COX2 cells and % of apoptotic cells. On the other hand, ejection fraction % showed a significant positive correlation with total energy charge and total antioxidant capacity. This was in agreement with Ge et al. (2012), who found negative affection of the cardiac function and reductions in EF and FS that were strongly negatively correlated with body weight and cardiac triglycerides content. They attributed these changes to impaired insulin resistance and increased oxidative stress that was also previously concluded by Manrique et al. (2013),; Pakdeechote et al. (2014), whose results convene with ours.

Cardiac dysfunction effects were partially alleviated by consumption of capsaicin parallel with high fat diet. Consequently, consumption of spicy foods as a food additive can make moderate balance and moderately prevent the harmful effect of HFD on heart. This conclusion is compatible with Almaghrabi et al., (2014), Sun et al. (2016) and Zheng et al. (2017), who conveyed that Capsaicin improves insulin resistance, decreases adipogenesis, regulates glucose homeostasis and ameliorates vascular dysfunction. Capsaicin guards against cardiometabolic diseases, such as obesity, hypertension, dyslipidemia in different target organs or tissues. Moreover Baskaran et al. (2019) suggested that CAP antagonizes HFD-induced metabolic stress and inflammation. Also, Kursunluoglu et al. (2018) investigated results in co-administration of capsaicin with cisplatin, and suggested that the antioxidant capacity of capsaicin alleviates the cardiotoxic effect of cisplatin. Gómez-Sierra et al. (2018) argue that capsaicin has analgesic, antimicrobial, anti-inflammatory, and antioxidant properties.

In summary, the high fat diet group showed significant increase in body weight, heart weight and body mass index. With hemodynamic and echocardiography investigation, HFD group showed significant increase in heart rate, systolic blood pressure with decrease in EF%, serum biochemical investigation revealed significant increase in serum glucose, insulin level with insulin resistance as well as increase in serum total cholesterol, triglyceride, free fatty acids. HFD heart homogenate showed decrease in total energy charge and total antioxidant capacity. Moreover, histological examination of heart tissue showed alteration of the normal histological structure of the heart tissue, marked increase of collagen bundles in the distorted cardiac tissue and significant increase in the immunopositivity of the inflammatory marker COX-2 and the apoptotic marker caspase-3 in HFD group compared to other groups. These effects were partially alleviated by consumption of capsaicin parallel with high fat diet. In brief, even though capsaicin could ameliorate effect of high fat diet, it is better to avoid HFD as it can induce cardiac dysfunction.

CONCLUSION

Even though capsaicin could ameliorate effect of high fat diet, it is better to avoid HFD as it can induce cardiac dysfunction.

AUTHOR CONTRIBUTIONS

All authors have been personally, equally, and actively involved in substantive work leading to the manuscript and will hold themselves cooperatively and personally accountable for its content.

ACKNOWLEDGEMENTS

Special thanks to the Anatomy Department, Faculty of Medicine, Zagazig University. Many thanks to Zagazig University Animal House Department and Scientific Medical Research Center.

REFERENCES

ALMAGHRABI SY, GERAGHTY DP, AHUJA KD, ADAMS MJ (2014) Vanilloid-like agents inhibit aggregation of human platelets. *Thromb Res,* 134: 412-417.

ARROYO-JOHNSON C, MINCEY KD (2016) Obesity Epidemiology Worldwide. *Gastroenterol Clin North Am,* 45: 571-579.

AUBIN MC, LAJOIE C, CLÉMENT R., GOSSELIN H, CALDERONE A, PERRAULT LP (2008) Female rats fed a high-fat diet were associated with vascular dysfunction and cardiac fibrosis in the absence of overt obesity and hyperlipidemia: therapeutic potential of resveratrol. *J Pharmacol Exp Ther,* 325: 961-968.

BASKARAN P, MARKERT L, BENNIS J, ZIMMERMAN L, FOX J, THYAGARAJAN B (2019) Assessment of pharmacology, safety, and metabolic activity of capsaicin feeding in mice. *Sci Rep*, 9: 8588.

BAUR JA, SINCLAIR DA (2006) Therapeutic potential of resveratrol: the in vivo evidence. *Nat Rev Drug Discov,* 5: 493-506.

BEBARS MM, AL-SHARAKY DR, GABER MA, AFIFY DR (2017) Immunohistochemical expression of caspase-3 in psoriasis. *J Clin Diagn Res,* 11: Ec01-ec05.

BEGRICHE K, MASSART J, ROBIN MA, BONNET F, FROMENTY B (2013) Mitochondrial adaptations and dysfunctions in nonalcoholic fatty liver disease. *Hepatology,* 58: 1497-1507.

BHANDARI U, KUMAR V, KHANNA N, PANDA BP (2011) The effect of high-fat diet-induced obesity on cardiovascular toxicity in Wistar albino rats. *Hum Exp Toxicol,* 30: 1313-1321.

BHANDARKAR NS, BROWN L, PANCHAL SK (2019) Chlorogenic acid attenuates high-carbohydrate, high-fat diet-induced cardiovascular, liver, and metabolic changes in rats. *Nutr Res,* 62: 78-88.

BRENNAN MP, SINUSAS AJ, HORVATH TL, COLLINS JG, HARDING MJ (2009) Correlation between body weight changes and postoperative pain in rats treated with meloxicam or buprenorphine. *Lab Anim (NY),* 38: 87-93.

BRESSENOT A, MARCHAL S, BEZDETNAYA L, GARRIER J, GUILLEMIN F, PLÉNAT F (2009) Assessment of apoptosis by immunohistochemistry to active caspase-3, active caspase-7, or cleaved PARP in monolayer cells and spheroid and subcutaneous xenografts of human carcinoma. *J Histochem Cytochem,* 57: 289-300.

BRUGMAN S (2016) The zebrafish as a model to study intestinal inflammation. *Dev Comp Immunol,* 64: 82-92.

CARROLL JF, ZENEBE WJ, STRANGE TB (2006) Cardiovascular function in a rat model of diet-induced obesity. *Hypertension,* 48: 65-72.

CHEN D, LI X, ZHANG L, ZHU M, GAO L (2018) A high-fat diet impairs mitochondrial biogenesis, mitochondrial dynamics, and the respiratory chain complex in rat myocardial tissues. *J Cell Biochem,* 119: 9602.

COLE MA, MURRAY AJ, COCHLIN LE, HEATHER LC, MCALEESE S, KNIGHT NS, SUTTON E, JAMIL AA, PARASSOL N, CLARKE K (2011) A high fat diet increases mitochondrial fatty acid oxidation and uncoupling to decrease efficiency in rat heart. *Basic Res Cardiol,* 106: 447-457.

DAS DK, MAULIK N (2006) Resveratrol in cardioprotection: a therapeutic promise of alternative medicine. *Mol Interv,* 6: 36-47.

DE LEO M, PIRAGINE E, PIRONE A, BRACA A, PISTELLI L, CALDERONE V, MIRAGLIOTTA V, TESTAI L (2020) Protective effects of bergamot (Citrus bergamia Risso & Poiteau) juice in rats fed with high-fat diet. *Planta Med,* 86: 180-189.

FANG CX, DONG F, THOMAS DP, MA H, HE L, REN J (2008) Hypertrophic cardiomyopathy in high-fat diet-induced obesity: role of suppression of forkhead transcription factor and atrophy gene transcription. *Am J Physiol Heart Circ Physiol,* 295: H1206-H1215.

GE F, HU C, HYODO E, ARAI K, ZHOU S, LOBDELL HT, WALEWSKI JL, HOMMA S, BERK PD (2012) Cardiomyocyte triglyceride accumulation and reduced ventricular function in mice with obesity reflect increased long chain fatty acid uptake and de novo fatty acid synthesis. *J Obes,* 2012: 205648.

GÓMEZ-SIERRA T, EUGENIO-PÉREZ D, SÁNCHEZ-CHINCHILLAS A, PEDRAZA-CHAVERRI J (2018) Role of food-derived antioxidants against cisplatin induced-nephrotoxicity. *Food Chem Toxicol,* 120: 230-242.

GUTCH M, KUMAR S, RAZI SM, GUPTA KK, GUPTA A (2015) Assessment of insulin sensitivity/resistance. *Indian J Endocrinol Metab,* 19: 160-164.

HOHOS NM, SKAZNIK-WIKIEL ME (2017) High-fat diet and female fertility. *Endocrinology,* 158: 2407-2419.

HU N, ZHANG Y (2017) TLR4 knockout attenuated high fat diet-induced cardiac dysfunction via NF-□B/JNK-dependent activation of autophagy. *Biochim Biophys Acta Mol Basis Dis,* 1863: 2001-2011.

HWANG JT, LEE YK, SHIN JI, PARK OJ (2009) Anti-inflammatory and anticarcinogenic effect of genistein alone or in combination with capsaicin in TPA-treated rat mammary glands or mammary cancer cell line. *Ann N Y Acad Sci,* 1171: 415-420.

JI R, AKASHI H, DROSATOS K, LIAO X, JIANG H, KENNEL PJ, BRUNJES DL, CASTILLERO E, ZHANG X, DENG LY, HOMMA S, GEORGE IJ, TAKAYAMA H, NAKA Y, GOLDBERG IJ, SCHULZE PC (2017) Increased de novo ceramide synthesis and accumulation in failing myocardium. *JCI Insight,* 2(9): e82922.

JØRGENSEN W, RUD KA, MORTENSEN OH, FRANDSEN L, GRUNNET N, QUISTORFF B (2017) Your mitochondria are what you eat: a high-fat or a high-sucrose diet eliminates metabolic flexibility in isolated mitochondria from rat skeletal muscle. *Physiol Rep,* 5(6): e13207.

KURSUNLUOGLU G, TASKIRAN D, KAYALI HA (2018) The investigation of the antitumor agent toxicity and capsaicin effect on the electron transport chain enzymes, catalase activities and lipid peroxidation levels in lung, heart and brain tissues of rats. *Molecules*, 23(12): 3267.

LI C, LI X, CHANG Y, ZHAO L, LIU B, WEI S, XU F, ZHANG Y, CHEN Y (2018) Aldehyde dehydrogenase-2 attenuates myocardial remodeling and contractile dysfunction induced by a high-fat diet. *Cell Physiol Biochem,* 48: 1843-1853.

LOPASCHUK GD, USSHER JR, FOLMES CD, JASWAL JS, STANLEY WC (2010) Myocardial fatty acid metabolism in health and disease. *Physiol Rev,* 90: 207-258.

LU Z, XU X, HU X, ZHU G, ZHANG Y, VAN DEEL ED, FRENCH JP, FASSETT JT, OURY TD, BACHE RJ, CHEN Y (2008) Extracellular superoxide dismutase deficiency exacerbates pressure overload-induced left ventricular hypertrophy and dysfunction. *Hypertension,* 51: 19-25.

MABROUKI L, RJEIBI I (2020) Cardiac ameliorative effect of moringa oleifera leaf extract in high-fat diet-induced obesity in rat model. *Biomed Res Int*, 2020: 6583603.

MANRIQUE C, DEMARCO VG, AROOR AR, MUGERFELD I, GARRO M, HABIBI J, HAYDEN MR, SOWERS JR (2013) Obesity and insulin resistance induce early development of diastolic dysfunction in young female mice fed a Western diet. *Endocrinology,* 154: 3632-3642.

MARI A, AHRÉN B, PACINI G (2005) Assessment of insulin secretion in relation to insulin resistance. *Curr Opin Clin Nutr Metab Care,* 8: 529-533.

MOLLICA MP, MATTACE RASO G, CAVALIERE G, TRINCHESE G, DE FILIPPO C, ACETO S, PRISCO M, PIROZZI C, DI GUIDA F, LAMA A, CRISPINO M, TRONINO D, DI VAIO P, BERNI CANANI R, CALIGNANO A, MELI R (2017) Butyrate regulates liver mitochondrial function, efficiency, and dynamics in insulin-resistant obese mice. *Diabetes,* 66: 1405-1418.

NOVELLI EL, DINIZ YS, GALHARDI CM, EBAID GM, RODRIGUES HG, MANI F, FERNANDES AA, CICOGNA AC, NOVELLI FILHO JL (2007) Anthropometrical parameters and markers of obesity in rats. *Lab Anim,* 41: 111-119.

PAKDEECHOTE P, BUNBUPHA S, KUKONGVIRIYAPAN U, PRACHANEY P, KHRISANAPANT W, KUKONGVIRIYAPAN V (2014) Asiatic acid alleviates hemodynamic and metabolic alterations via restoring eNOS/iNOS expression, oxidative stress, and inflammation in diet-induced metabolic syndrome rats. *Nutrients,* 6: 355-370.

PI R, WANG Y, CHEN P, XIE B, XU J, LI S (2017) Effects of capsaicin on the cholesterol lithogenesis in the gallbladder of C57BL/6 mice. *Int J Clin Exp Med,* 10: 2066-2075.

PLATT MJ, HUBER JS, BRUNT KR, SIMPSON JA (2017) Pulmonary flow as an improved method for determining cardiac output in mice after myocardial infarction. *J Am Soc Echocardiogr,* 30: 612-623.e1.

RELLING DP, ESBERG LB, FANG CX, JOHNSON WT, MURPHY EJ, CARLSON EC, SAARI JT, REN J (2006) High-fat diet-induced juvenile obesity leads to cardiomyocyte dysfunction and upregulation of Foxo3a transcription factor independent of lipotoxicity and apoptosis. *J Hypertens,* 24: 549-561.

RIDER OJ, COX P, TYLER D, CLARKE K, NEUBAUER S (2013) Myocardial substrate metabolism in obesity. *Int J Obes (Lond),* 37: 972-979.

SHARMA A, FISH BL, MOULDER JE, MEDHORA M, BAKER JE, MADER M, COHEN EP (2014) Safety and blood sample volume and quality of a refined retro-orbital bleeding technique in rats using a lateral approach. *Lab Anim (NY),* 43: 63-66.

SIKDER K, SHUKLA SK, PATEL N, SINGH H, RAFIQ K (2018) High fat diet upregulates fatty acid oxidation and ketogenesis via intervention of PPAR-γ. *Cell Physiol Biochem,* 48: 1317-1331.

SOWERS JR, WHALEY-CONNELL A, HAYDEN MR (2011) The role of overweight and obesity in the cardiorenal syndrome. *Cardiorenal Med,* 1: 5-12.

STANLEY WC, DABKOWSKI ER, RIBEIRO RF, JR, O'CONNELL KA (2012) Dietary fat and heart failure: moving from lipotoxicity to lipoprotection. *Circ Res,* 110: 764-776.

SUN F, XIONG S, ZHU Z (2016) Dietary capsaicin protects cardiometabolic organs from dysfunction. *Nutrients,* 8(5): 174.

SWINBURN B, EGGER G (2002) Preventive strategies against weight gain and obesity. *Obes Rev,* 3: 289-301.

WANG LW, KESTEVEN SH, HUTTNER IG, FENELEY MP, FATKIN D (2018) High-frequency echocardiography - transformative clinical and research applications in humans, mice, and zebrafish. *Circ J,* 82: 620-628.

WANG R, YOU YM, LIU X (2021) Effect of zanthoxylum alkylamides on lipid metabolism and its mechanism in rats fed with a high-fat diet. J Food Biochem. 45: e13548.

WHALEY-CONNELL A, GOVINDARAJAN G, HABIBI J, HAYDEN MR, COOPER SA, WEI Y, MA L, QAZI M, LINK D, KARUPARTHI PR, STUMP C, FERRARIO C, SOWERS JR (2007) Angiotensin II-mediated oxidative stress promotes myocardial tissue remodeling in the transgenic (mRen2) 27 Ren2 rat. *Am J Physiol Endocrinol Metab,* 293: E355-363.

WILDE DW, MASSEY KD, WALKER GK, VOLLMER A, GREKIN RJ (2000) High-fat diet elevates blood pressure and cerebrovascular muscle Ca(2+) current. *Hypertension,* 35: 832-837.

WONG GY, GAVVA NR (2009) Therapeutic potential of vanilloid receptor TRPV1 agonists and antagonists as analgesics: Recent advances and setbacks. *Brain Res Rev,* 60: 267-277.

WOODS SC, SEELEY RJ, RUSHING PA, D'ALESSIO D, TSO P (2003) A controlled high-fat diet induces an obese syndrome in rats. *J Nutr,* 133: 1081-1087.

ZHANG S, XU J, HE Z, XUE F, JIANG T, XU M (2019) Sodium selenate ameliorates cardiac injury developed from high-fat diet in mice through regulation of autophagy activity. *Sci Rep,* 9: 18752.

ZHENG J, ZHENG S, FENG Q, ZHANG Q, XIAO X (2017) Dietary capsaicin and its anti-obesity potency: from mechanism to clinical implications. *Biosci Rep,* 37(3): BSR20170286.

ZHOU X, MA L, HABIBI J, WHALEY-CONNELL A, HAYDEN MR, TILMON RD, BROWN AN, KIM JA, DEMARCO VG, SOWERS JR (2010) Nebivolol improves diastolic dysfunction and myocardial remodeling through reductions in oxidative stress in the Zucker obese rat. *Hypertension,* 55: 880-888.

Unusual case of supraspinatus tear

Michał Szlęzak[1,2], Aleksander Kwiatkowski[2,3], Robert Warnecki[4], Grzegorz Bajor[3]

[1] *Association of Neurophysiological-Orthopaedic Manipulative Physical Therapists, Poland*

[2] *Fizjosport Physiotherapy Center, Gliwice*

[3] *Department of Human Anatomy Medical University of Silesia, Katowice, Poland*

[4] *Private Orthodontic Medin, Opole*

SUMMARY

One of the most frequent causes of shoulder pain is the damage of the rotator cuff tendon. Its etiology is multifactorial and the symptoms often require prompt medical intervention. The glenohumeral joint is one of the largest and most complex joints in the human body, so it is very important to understand the many anatomical and pathological variations which may occur. One of such pathological variations is shoulder pain, which might be the result of an unusual rupture of the supraspinatus muscle. In this article we report a rare case of tearing of this muscle and creating of an additional attachment on the lesser tubercle. Moreover, the body produced a bursa that lines the inner layer of the shoulder skin. This work is needed by clinicians because it shows how, despite the massive damage to the muscle and the cartilage structures, the passive range of motion is maintained, and it also shows the role of the synovial bursa in the pathophysiology process. It is very important to learn more about anatomical and pathological variations in order to properly manage shoulder pain and dysfunctions.

Key words: Muscle tear – Supraspinatus – Rotator cuff – Tendon – Shoulder

INTRODUCTION

The complex structure of the glenohumeral joint endows the shoulder with the utmost mobility of any major joint in the human body. This characteristic is primarily due to a limited interface between the humerus and the scapula, requiring the presence of a large network of ligaments tendons, and other connective tissue elements to provide stability and allow for functional movement (Huegel et al., 2015). However, due to the complexity of the structures surrounding the shoulder joint, it is exposed to overload and frequent injuries such as tendinopathy and rotator cuff tears.

The glenohumeral joint is a multi-axis spherical free joint between the head of the humerus and the articular cavity of the scapula; it results in greater mobility of the arm at the cost of reduced stability.

Apart from the six basic movements, circumduction and movements in the horizontal plane are also possible. The shoulder blade moves along with the humerus in relation to each other according to a constant pattern: the scapulobrachial rhythm.

Although the humeral head is much larger than the glenoid cavity, their curvatures differ by as little as 1% (Mehta et al., 2003). Articular surface is enlarged by the labrum glenoidale, genus

Corresponding author:
Michał Szlęzak. Medical University of Silesia, Department of Anatomy, The School of Health Sciences in Katowice, Medyków 12, 40-742 Katowice, Poland. E-mail: michal@fizjosport.pl

Submitted: September 22, 2020. **Accepted:** February 1, 2021

fibrous cartilage, which widens the cavity and makes its concavity visible. The ligaments and the joint capsule are attached to the labrum.

The shape and concavity of the glenoid fossa may vary from person to person. On the outer side of the head of the humerus is the greater tubercle and on the inside the lesser tubercle. There is a bicipital groove between the above-mentioned tubercles (Bochenek et al., 1990).

Connection between the humerus and a scapula is formed by four muscles (supraspinatus, infraspinatus, teres minor and subscapularis); their insertions are very tightly connected with the inside of the joint capsule.

The muscles of the rotator cuff work as a whole and secure the head of the humerus in the articular cavity — they stabilize the shoulder joint in various positions, especially during abduction.

The supraspinatus is one of the four rotator cuff muscles of the shoulder and plays an important role in the dynamic upward stabilization of the humeral head within the glenoid fossa (Burke et al., 2002). It begins at the supraspinatus fossa on the supraspinatus fascia. The fibers converge to the side and end in a strong and short tendon on the greater tubercle of the humerus. The tendon also attaches to the joint capsule. The supraspinatus tendon is separated by a bursa subacromial from the coraco-acromial ligament, the shoulder process of the scapula and the brachial muscle.

Musculus supraspinatus is responsible for shoulder abduction, external rotation and tightening of the articular capsule. This muscle is not very variable individually (Bochenek et al., 1990).

Rotator cuff lesions (RCL) are one of the most common conditions affecting the shoulder — studies have found that16-40% of all shoulder complaints are linked with impingement related tendinopathies, which are often the precursor for rotator cuff tears (Neer et al., 2005). The aetiology of rotator cuff diseases is multifactorial, but the tendon supraspinatus is particularly prone to injuries (Benson et al., 2010), especially because of a sudden, violent fall, most often on a straightened upper limb. It can also be accompanied by damage to other soft structures, shoulder dislocation or even a collarbone or humerus fracture. Another reason may be a single, very heavy load on this muscle or repeated repetition of certain movements.

Rotator cuff lesions have considerable variability in location, tear pattern, functional impairment, and repairability.

Full thickness disruption of the lateral tendon stump is the most frequent type of RCL, comprising approximately 90.1% of all surgically treated lesions. Tendinous lesions most commonly involve the posterosuperior cuff. (Barth et al., 2006).

Full-thickness posterosuperior tears come in a variety of patterns. The most common categories include crescent tears, L- and reverse L-shaped tears, and U-shaped tears accounting respectively for 40%, 30% and 15% of posterosuperior rotator cuff lesions (Davidson et al., 2010). Recognition of these tear patterns is most useful for anatomical restoration during repair. Crescent tears have good medial to lateral mobility and are amenable to a double row repair. Longitudinal tears (L- and reverse L-shaped tears; U-shaped tears) have greater mobility in one plane and typically require margin convergence to achieve complete repair.

The Fosbury flop tear is a newly-described lesion, which occurs from a full-thickness tear that has flipped upon itself and adhered medially. Radiographically, this lesion showed a thicker-than-normal tendon stump on the bursal side of the retracted supraspinatus tendon in a superomedial orientation (Lädermann et al., 2015).

Furthermore, Ellman and Gartsman classification is increasingly used by orthopedists. The authors distinguish six types of muscle supraspinatus tears. In addition to the crescent, L-shaped and reverse, authors distinguish massive and trapezoidal tears. Moreover, partial tears may be intra-articular, intra-tendinous and bursal. The Ellman classification of partial tears is used in clinical practice (Cicak et al., 2015).

Disruption of the lateral tendon stump can be followed by adhesion under the acromion, the

coracoid process or the coraco-acromial arch (Romeo et al., 1998).

Studying the anatomical differences on the cadavers is essential for understanding and explaining related disorders in medical and surgical practice (Hegazy et al., 2019).

Some researchers note that supraspinatus injuries are not always typical. We have a division of tears according to the thickness of the tear, the type of tear (Crescent, Reverse, L-shaped, Trapezoidal and Massive tear), and whether a partial rupture can be intra-articular, intra-tendinous, or bursal (Cicak et al., 2015), therefore our goal is to show another, new type of supraspinatus tear.

CASE REPORT

During the investigation of the cadaver, of a 68-year-old man, preserved in 5% formalin solution, in the Department of Human Anatomy, at the Medical University of Silesia we found an unusual supraspinatus muscle tear. Tendon of the muscle was divided into two parts: anterior and posterior. The anterior part of the muscle was separated from the common tendon of the supraspinatus muscle, slipped off downwards anteriorly to the greater tubercle revealing the humerus head. Half of the fibers of the anterior part of this muscle found their attachment on the greater tubercle and the other half to the lesser tubercle. It follows that an additional supraspinatus attachment had developed on the lesser tubercle. The posterior part of the supraspinatus muscle also was slipped off but in posterior direction. The posterior part attached only to the greater tubercle.

During the examination, we did not find major changes of the remaining rotator cuff muscles and tendons. Moreover, no changes caused by the surgeries of the above-mentioned joint, chest and cervical spine were detected. On the opposite side of the body, we did not detect any pathological changes related to the tearing, rupture, damage and post-surgery condition of tendons and muscles of the rotator cuff.

Also, after many years using that pathological joint, the humerus head made a hole in the middle part of the deltoid muscle. Moreover, the body produced a bursa that lines the inner layer of the shoulder skin probably to protect from abrasion. The above-mentioned bursa was connected with the subacromial bursa, which was then fused with the skin.

Fig. 1.- Lateral view of the humeral joint. Anterior part of deltoid muscle (1), Posterior part of deltoid muscle (2), Humeral head (3), Tendon of supraspinatus muscle "posterior part" (4), Tendon of supraspinatus muscle "anterior part" (5).

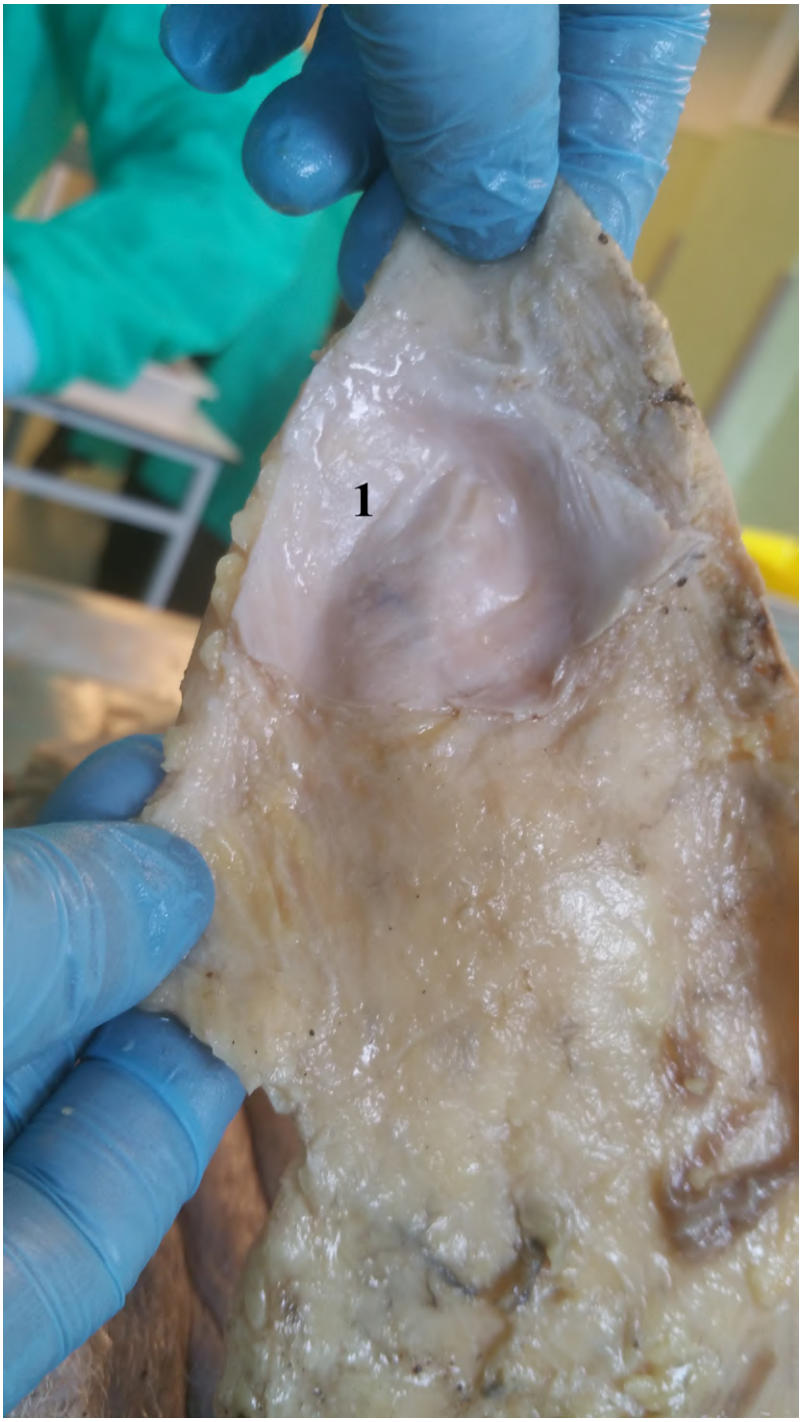

Fig. 2.- Inner layer of the skin. Bursa between the skin and humerus head (1).

Using the goniometer, we also examined the range of passive motion in the shoulder joints. Range of passive motion of the affected shoulder joint was significantly less than on the other, "healthy" side. Flexion of the affected joint was 35°, abduction 25° and in the second joint observed range of flexion 60°, abduction 45°. In addition, extensive damage to the cartilage of the humeral head was observed only on the right upper limb. No pathological or degenerative changes were observed in the acromioclavicular joint.

COMMENTS

Comparing the literature, a similar case took place in Kolts's cadaver research. In one of the rotator cuffs tears the author studied, the supraspinatus muscle tendon was divided into two parts: anterior and posterior, which also slipped off downwards to the greater tubercle revealing the humerus head. The posterior part of the supraspinatus muscle was attached to the major tubercle. The anterior part of the supraspinatus

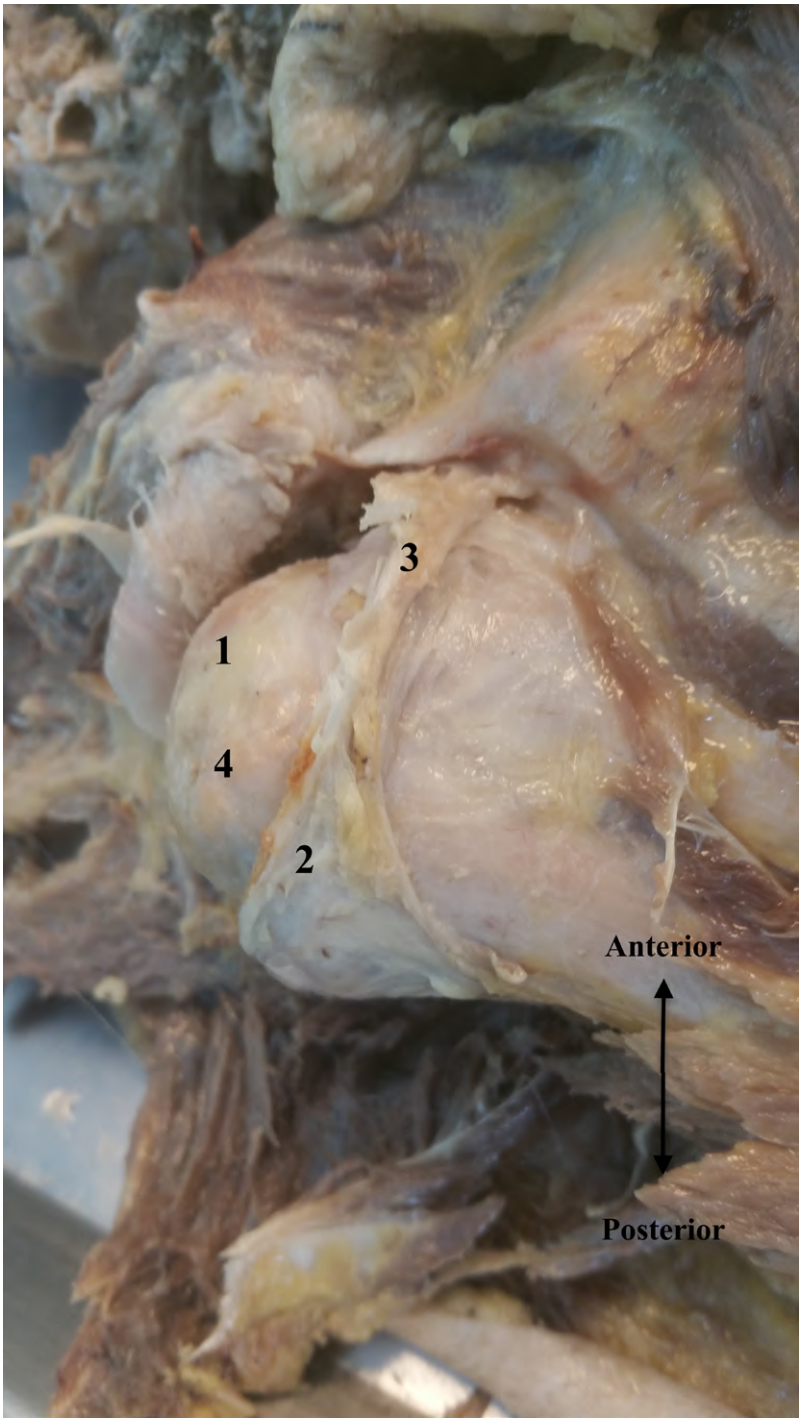

Fig. 3.- Lateral view of the humeral joint. Humerus head (1), Tendon of supraspinatus muscle "posterior part" (2), Tendon of supraspinatus muscle "anterior part", which runs perpendicular to the intertubercular groove (3), Greater tubercle of the humerus (4).

muscle was attached to the lesser tubercle and was named by the authors "accessory part". The authors claim that the fact of an accessory tendon might be of functional and clinical importance, because that tendon which has insertion on the lesser tubercle is weaker than the "common" tendon (Kolts et al., 1992).

In our case, an accessory tendon also can be distinguished, but the anterior tendon part attaches to the greater and lesser tubercles and the posterior part attaches only to the greater tubercle. Apart from the insertion to the greater and lesser tubercles, there is also a connection between two newly formed tendons that runs perpendicular to the intertubercular groove.

The mechanism development and insertion of an additional tendon can create new compensatory movement patterns and role for the glenohumeral joint, because ruptures occur in the part of the tendon that inserts on the greater tubercle. In

addition, in the fixing of the humerus head and abduction, the supraspinatus muscle can also act as an internal rotator.

The above lesion change does not have the characteristics that could suggest that it had occurred in the embryonic life, due to the fact that the edges of the lesion were scarred and accompanied by intense degenerative changes within the articular cartilage.

Research of the anatomical variations are clinically very important to reduce complications during surgeries, develop new methods of arthroscopic reconstruction of rotator cuff tears and reduce potential risk of injury during physiotherapy.

In addition, this study is important for imaging diagnosticians' analysis. Ultrasound examination completes the patient's clinical findings. It provides a high probability of finding a tendon tear and determining its size (Ziegler et al., 2004). Therefore, many clinicians are committed to this method of diagnosing rotator cuff tears. However, tendon echogenicity is not a fully reliable sign of a complete rupture of the cuff. MRI indicates a high level of reliability in diagnosing the rotator cuff tear. MRI allows free access to the location and indicates the size of the tear and the muscle condition. In contrast to the ultrasound, MRI shows the size of the tendon retraction and the condition of the muscle in relation to the fatty degeneration level (Cicak et al., 2015).

Our study is also interesting because it shows how passive range of motion is maintained despite massive muscle damage and massive damage to the cartilage structures. The change also shows the role of the synovial bursa in the pathophysiology process, as it separates the conflicting structures—in our case a lump larger than the skin.

ACKNOWLEDGEMENTS

The authors wish to thank the Medical University of Silesia in Katowice for sharing cadavers from a voluntary donation program for research.

REFERENCES

BARTH JR, BURKHART SS, DE BEER JF (2006) The bear-hug test: a new and sensitive test for diagnosing a subscapularis tear. *Arthroscopy,* 22: 1076-1084.

BENSON RT, MCDONNELL SM, KNOWLES HJ, REES JL CARR AJ, HULLEY PA (2010) Tendinopathy and tears of the rotator cuff are associated with hypoxia and apoptosis. *J Bone Joint Surg Br*, 92: 448-453.

BOCHENEK A, REICHER M (1990) Anatomia człowieka, pp 785-786.

BURKE WS, VANGSNESS CT, POWERS CM (2002) Strengthening the supraspinatus: A clinical and biomechanical review. *Clin Orthop Relat Res*, 402: 292-298.

CICAK N, KLOBUCAR H, NENAD M (2015) Rotator cuff injury. *Medicina Fluminensis*, 51(1): 7-17.

DAVIDSON J, BURKHART SS (2010) The geometric classification of rotator cuff tears: a system linking tear pattern to treatment and prognosis. *Arthroscopy*, 26: 417-424.

HEGAZY AA (2019) Human anatomy: an inlet of medicine and surgery. *IJHA*, 1(4): 1-1.

HUEGEL J, WILLIAMS A, SOKOLOWSKY J (2015) Rotator cuff biology and biomechanics: a review of normal and pathological conditions. Orthopaedic Research Laboratory, Department of Orthopaedic Surgery, University of Pennsylvania, Philadelphia, PA 19104, USA.

KOLTS I (1992) A note on the anatomy of the supraspinatus muscle. *Arch Orthop Trauma Surg*, 111: 247-249.

LÄDERMANN A, DENARD PJ, KOLO FC (2015) A new tear pattern of the rotator cuff and its treatment: Fosbury flop tears. *Int J Shoulder Surg*, 9: 9-12.

MEHTA S, GIMBEL JA, SOSLOWSKY LJ (2003) Etiologic and pathogenetic factors for rotator cuff tendinopathy. *Clin Sports Med*, 22: 791-812.

NEER CS 2nd (2005) Anterior acromioplasty for the chronic impingement syndrome in the shoulder. *J Bone Joint Surg Am*, 87(6): 1399-1399.

ROMEO AA, LOUTZENHEISER T, RHEE YG (1998) The humeroscapular motion interface. *Clin Orthop Relat Res*, 350: 120-127.

ZIEGLER, DEAN W (2004) The use of in-office, orthopaedist-performed ultrasound of the shoulder to evaluate and manage rotator cuff disorders. *J Shoulder Elbow Surg*, 13: 291-297.

Anomalous left superior pulmonary vein draining into the left brachiocephalic trunk: case report

Daniel G. Gonsalves, Guilherme R. Ventura, Renato Rissi

Department of Anatomy, University Center Padre Albino, 15809-144, Catanduva, São Paulo, Brazil

SUMMARY

Partial anomalous pulmonary venous connection characterizes a direct connection between the pulmonary veins and the right atrium or venous system. This condition is physiologically explained in the recirculation of oxygenated blood through pulmonary vasculature to the arterial system. Patients who have this condition exclusively are usually asymptomatic. During a routine human anatomy dissection, a vein which presented a variable path near the left lung hilum was observed. Following the dissection to observe its path, it was identified as the left upper pulmonary vein. However, its drainage was in the left brachiocephalic vein, which described a pattern of anatomical variation. In the present case, as there is only one abnormality present in the left upper pulmonary vein, it was suggested that the patient was asymptomatic, as the characteristic had only been observed post mortem by chance, with no correction performed. Raising awareness of this condition can help medical students around the world to diagnose it.

Key words: Case report – Anomalous vein – Anatomic variation – Pulmonary vein

INTRODUCTION

Partial Anomalous Pulmonary Venous Connection (PAPVC) is a congenital cardiac defect which characterizes a direct connection between the pulmonary veins and the right atrium or venous system (or its tributaries) (Sahay et al., 2012). If it affects all the pulmonary veins, it is called Total Anomalous Pulmonary Venous Connection (TAPVC) and it is classified according to Darling et al. (1957) as: supradiaphragmatic (supracardiac or type 1 and cardiac or type II) and infradiaphragmatic (or type III). In general, all the pulmonary veins with anomalous insertion are implanted in the same place in a person.

According to Spratt (2016), anomalous connections between the pulmonary and systemic venous system were first recognized by Winslow (1739), who collected 106 cases.

Partial anomalous connection of the right pulmonary veins is 10 times more frequent than that of the left pulmonary veins (Snellen et al., 1968), which is an asymmetrical occurrence caused by frequent drainage of some of the right pulmonary veins into the junctional area between the right atrium and the superior vena cava (SVC) in the presence of normal left pulmonary veins, and the complete absence of isolated left

Corresponding author:
Dr. Renato Rissi. Department of Anatomy, University Center Padre Albino, 13083-865, Catanduva, São Paulo, Brazil. Phone: 55-17-996036245. E-mail: renato_rissi@yahoo.com.br

Submitted: January 22, 2021. **Accepted:** March 29, 2021

pulmonary venous connection to the right atrium. The prevalence of pulmonary vein anomalies is 0.2% to 0.7% (Specht and Brown, 1953; Haramati et al., 2003).

Abnormal connection of solitary pulmonary veins was always affected to the most proximal venous structure among the four possible derived from the main embryonic channels (SVC and inferior vena cava on the right side and left SVC and coronary sinus on the left side). Common pulmonary veins from one lung also drained in accordance with this proximity rule, if this may also be taken to apply to the drainage of right pulmonary veins into the right atrium. The one exception was the drainage of all right pulmonary veins into the portal venous system (Snellen et al., 1968).

PAPVC is physiologically explained in the recirculation of oxygenated blood through pulmonary vasculature to the arterial system, which is called left-to-right shunting. In patients with only this condition (with no other cardiac alterations), its effects depend on the proportion of anomalous drainage compared to total pulmonary venous recurrence, but patients are usually asymptomatic. Its consequences depend on the following factors: number and size of the variant veins involved; pulmonary segments or lobes where the alteration is originated (difference in blood distribution for each lobe) (Ward and Mullins, 1998; Talner, 1998).

These unusual connections between the pulmonary veins and many other adversely inappropriate neighboring veins are explicable only by the very early embryonic bed to form the pulmonary veins leading to the left atrium, the primitive connections with stages in which the developing foregut, trachea, and lung buds are supplied by connections through the loose mesenchyme and communicate with the primitive cardinal veins in several places.

With the development of certain channels in this primitive vascular bed to form the pulmonary veins leading to the left atrium, the primitive connections with the cardinal veins usually disappear. The unusual development of one or more of them and its retention by the adult derivative of the particular part of the cardinal system involved are probably the ones that are most responsible for the occurrence of these unusual pulmonary connections (Keith et al., 1954; Steinberg and Finby, 1956).

It is our goal to increase the awareness of the anatomical and physiological repercussions of PAPVC, because it can help medical students to diagnose it in the future.

CASE REPORT

In a routine dissection for the improvement of anatomical parts, a cadaveric anatomical piece of the neck and the chest region, which belongs to the institution's collection, was analyzed. It was possible to deduce that it was a male, by the presence of facial hair (beard and moustache). Other than that, it had no identification of age, color and origin, and it was obtained by an anonymous body donation into the 20th century – at that time, the institution did not keep identification record of the bodies. The study was started under the protocol of the ethics committee, number 12923919.8.0000.5430.

The dissection of the mediastinum began in the large vessels and the cardiac base. Subsequently, it advanced to the lower mediastinal region and pleuropulmonary cavities, emphasizing the hilum and the left pulmonary pedicle.

After the performance, a vein presenting a variable path was observed near the left lung hilum and aroused interest. Following the dissection to observe its path, it was identified as the left superior pulmonary vein (LSPV). However, the LSPV was deviating from the normal path at the left pulmonary hilum, taking on a cranial trajectory, running on the mediastinal surface of the left upper lobe, entering the mediastinum, and then draining into the left brachiocephalic vein (Fig. 1). Despite this fact, the left brachiocephalic trunk followed its normal path, joining the contralateral one and leading to the right atrium.

Evaluating the piece still, in the hilum the left lower pulmonary vein, as well as the two right pulmonary veins, had normal path leading to the left atrium. The other large vessels, bronchi and limph nodes, were dissected and observed

without finding any anatomical variations that justified the presence of the reported variation.

COMMENTS

PAPVC is a rare congenital heart condition characterized either by failure of connection or drainage of pulmonary veins (Kottayil et al., 2011). It is a condition that has an estimated incidence of 0.7% in the population (Healey, 1952). Another important fact is that it was found in 0.4-0.7% of autopsies in patients with other congenital heart diseases (Said et al., 2011; Ashrafpoor et al., 2013), and that in a recent Computed Tomography (CT) study, involving 1825 CT exams, Partial Anomalous Pulmonary Venous Connection was seen in 0.2% of adults (Haramati et al., 2003).

It is also important to note that PAPVC incidence female-to-male ratio is 2 (Senocak et al., 1993), is twice as frequent in the right lung and occurs in 10% of patients who have effects on the atrial septum (Dilman et al., 2009). It is a normally asymptomatic abnormality and it can be easily diagnosed and corrected in the first years of life due to the easy access to imaging tests. If present, the symptoms include dyspnea, fatigue, palpitations, angina and/or peripheral edema (Edwin, 2010). The symptoms depend on the number of pulmonary veins involved and the extent of fluid overload due to the left to right shunt (Brody, 1942). Spratt (2016), in the Bergman's Comprehensive Encyclopedia of Human Anatomic Variation book, cited an intraoperative finding by Savu et al. (2010) that described similar characteristics of PAPVC found in this present study. The available correction for such cases is surgical, correcting the drainage of the anomalous vein to the left atrium (Elbardissi et al., 2008; Bobylev et al., 2013). However, treatment is only indicated for symptomatic patients such as hemodynamically significant left-to-right shunt, usually presenting with right ventricle overload and recurrent lung infections due to surgical treatment of other cardiac abnormalities,

Fig. 1.- Pattern of anatomical variation found in left superior pulmonary vein drainage (drains into the left brachiocephalic vein). Abbreviations and symbols: AV: azygos vein, SVC: superior vena cava; RBV: right brachiocephalic vein, LBV: left brachiocephalic vein, LJV: left jugular vein, LSV: left subclavian vein, LSPV: left superior pulmonary vein.

assessing risks and consequences (Ward and Mullins, 1998). In the present case, as there is only one abnormality present in the left upper pulmonary vein, it is suggested that the patient was asymptomatic in life, since the characteristic had only been observed post-mortem by chance, with no correction performed.

AUTHOR'S CONTRIBUTION

D.G. Gonsalves: Project development, data collection, data analysis and manuscript writing. G.R. Ventura: Project development, data collection, data analysis and manuscript writing. R. Rissi: Project development, data analysis and manuscript editing.

ACKNOWLEDGEMENTS

D.G. Gonsalves was recipient of fellowships from University Center Padre Albino (UNIFIPA, grants PESQMED2019674).

REFERENCES

ASHRAFPOOR G, AZARINE A, REDHEUIL A, COHEN S, RAISKY O, MOUSSEAUX E, ISERIN L (2013) Partial anomalous pulmonary venous return in adults with prior curative congenital heart surgery detected by cross-sectional imaging techniques. *Int J Cardiol,* 168(4): 109-110.

BOBYLEV D, BREYMANN T, BOETHIG D, ONO M (2013) Surgical repair of partial anomalous pulmonary venous connection shunting from left atrium to innominate vein. *J Cardiothorac Surg*, 8: 100.

BRODY H (1942) Drainage of the pulmonary veins into the right side of the heart. *Arch Pathol*, 33: 22l.

DARLING RC, ROTHNEY WB, CRAIG JM (1957) Total pulmonary venous drainage into theright side of the heart. Report of 17 autopsied cases not associated with other major cardiovascular anomalies. *Lab lnvest*, 6(1): 44-64.

DILLMAN JR, YARRAM SG, HERNANDEZ RJ (2009) Imaging of pulmonary venous developmental anomalies. *Am J Roentgenol*, 192(5): 1272-1285.

EDWIN F (2010) Left-sided partial anomalous pulmonary venous connection should diagnosis lead to surgery? *Interact Cardiovasc Thorac Surg*, 11: 847-848.

ELBARDISSI AW, DEARANI JA, SURI RM, DANIELSON GK (2008) Left-sided partial anomalous pulmonary venous connections. *Ann Thorac Surg*, 85: 1007-1014.

HARAMATI LB, MOCHE IE, RIVERA VT, PATEL PV, HEYNEMAN L, MCADAMS HP, ISSENBERG HJ, WHITE CS (2003) Computed tomography of partial anomalous pulmonary venous connection in adults. *J Comput Assist Tomogr*, 27: 743-749.

HEALEY JE JR (1952) An anatomic survey of anomalous pulmonary veins: their clinical significance. *J Thorac Surg*, 23(5): 433-444.

KEITH JD, ROWE RD, VLAD P, O'HANLEY JH (1954) Complete anomalous pulmonary venous drainage. *Am J Med*, 16: 23-38.

KOTTAYIL BP, DHARAN BS, MENON S, BIJULAL S, NEEMA PK, GOPALAKRISHNAN SK, JAYAKUMAR K (2011) Anomalous pulmonary venous connection to superior vena cava: Warden technique European. *Eur J Cardiothorac Surg*, 39(3): 388-391.

SAHAY S, KRASUSKI RA, TONELLI AR (2012) Partial anomalous pulmonary venous connection and pulmonary arterial hypertension. *Respirology*, 17(6): 957-963.

SAID SM, BURKHART HM, DEARANI JA, EIDEM B, STENSRUD P, PHILLIPS SD, SCHAFF HV (2011) Outcome of caval division techniques for partial anomalous pulmonary venous connections to the superior vena cava. *Ann Thorac Surg*, 92(3): 980-984.

SAVU C, PETREANU C, CADAR G, MATACHE R, GALIE N (2010) (cited by Spratt, 2016) Pulmonary vein anomaly in patient with pulmonary aspergillosis. *Chirurgia (Buchur)*, 105(2): 275-278.

SENOCAK F, OZME S, BILGIÇ A, OZKUTLU S, OZER S, SARAÇLAR M (1994) Partial anomalous pulmonary venous return. Evaluation of 51 cases. *Jap Heart J*, 35(1): 43-50.

SNELLEN HA, VAN INGEN HC, HOEFSMIT EC (1968) Patterns of anomalous pulmonary venous drainage. *Circulation*, 38: 45-63.

SPRATT JD (2016) Intrathoracic Veins. In: Tubbs RS, Shoja MM, Loukas M (eds). *Bergman's Comprehensive Encyclopedia of Human Anatomic Variation*. Hoboken: Wiley-Blackwell, pp 832-853.

SPECHT HD, BROWN AF (1953) Drainage of pulmonary veins into ductus venosus with other anomalies. *AMA Arch Intern Med*, 92: 148-151.

STEINBERG I, FINBY A (1956) Clinical and angiocardiographic features of congenital anomalies of the pulmonary circulation: A classification and review. *Angiology*, 7: 378-395.

TALNER NS (1998) The physiology of congenital heart disease. In: Garson A, Bricker TJ, Fisher DJ, Neish SR (eds). *The Science and Practice of Pediatric Cardiology*, 2nd ed. Williams and Wilkins, Baltimore, p 1107.

WARD KE, MULLINS CE (1998) Anomalous pulmonary venous connections, pulmonary veinstenosis, and atresia of the common pulmonary vein. In: Garson A, Bricker JT, Fisher DJ, Neish SR (eds). *The Science and Practice of Pediatric Cardiology*, 2nd ed. Williams and Wilkins, Baltimore, p 1431.

WINSLOW J (1739) (cited by Spratt, 2016) Exposition anatomique de la structure du corps humain. Amsterdam: Aux Depens de Compagnie. Mem Acad Roy Sci, 113.

Variant of the sinus node artery with an unusual origin and course. A unique postmortem visualization after corrosion casting technique

Christos Nerantzis

Consultant in cardiac disorders, Forensic Service of Athens, Greece

SUMMARY

The purpose of this study was to expand our knowledge about anatomical variations of the origin, course and end of the sinus node (SN) artery. Herein I describe a rare postmortem corrosion casting finding, which concerns a unique and previously unreported case where the SN artery had an abnormal origin and course to the SN area. Although the patient was asymptomatic, knowledge of this anatomical variation, its possible involvement with invasive or surgical procedures and its clinical consequences should be considered.

Key words: Heart – Coronary arteries – Sinus node artery – Sinus node area

INTRODUCTION

The origin and course of the sinus node (SN) artery in normal hearts have been well investigated (James, 1961; Mac Alpin, 1975; Nerantzis and Avgoustakis, 1980; Nerantzis et al., 1983). In most of the cases the SN artery originates from the proximal 2-3 cm of the right coronary artery and the proximal 1-2 cm of the left circumflex (LCx) artery, which is branch of the left coronary artery. The SN artery has no constant origin, but has a constant termination, which is used as a good guide to the location of the SN area. Congenital anomalies of origin and course of a SN artery with or without symptoms are of special interest for anatomists, interventional cardiologists and cardiac surgeons. I describe here an asymptomatic though unique and previously unreported case, in which the SN artery consists of the continuation of the posterolateral part of the left circumflex.

CASE REPORT

The case concerned an asymptomatic 26-year-old healthy female cadaver, victim of a car accident, without known cardiac history. The car accident was not her own fault (information from her relatives). The case is from a series of 60 human hearts (41 males and 19 females) in which the coronary vessels were studied by our corrosion casting technique (Nerantzis et al., 1978). Polyester material is injected into the coronary arteries during closure of the coronary sinus orifice in the right atrium with cotton wool. After this, I received tiny pieces of myocardium from different parts of both atria and from around the SN area to be examinant histologically for

Corresponding author:
Christos Nerantzis. Granitsa 2, Athens, Greece, TT=1141. E-mail: Theano9@otenet.gr

Submitted: February 15, 2021. **Accepted:** June 30, 2021

Not final proof's revision by the authors

ischemic heart changes. I took care to avoid cutting of vessels. Concentrated hydrochloric acid we used for corrosion of the muscles for 24 hours. In the reported case I found that the posteroanterior projection was most useful in identifying the origin and course of the SN artery until its end. The LCx coursing in the postero-lateral atrioventricular grove (AVG) until 5 cm before the crux gives branch (wide arrow) to the posterior surface of the left ventricle. Immediately after that, it leaves the AVG, moving upwards and to the right with a serpentine course (lower thinner arrow) for about 6 cm, meeting the posterior interatrial groove (IG). The artery continues its course in the upper IG (upper thinner arrow) for about 4 cm turn around the superior vena cava in a counterclockwise direction, giving blood to the SN area. During its course, it gives branches to the posterior and upper surface of the left atria (LA), right atria (RA) walls, in the interatrial septum and in the SN area. The SN artery, with its inter and intracoronary branches, forms a useful atria anastomotic net. I have not found histological changes around the SN area.

COMMENTS

Although this anomaly does not give rise to symptoms, it is essential for anatomists, as well as for cardiac surgeons and interventional cardiologists, so that they can be aware of this variation when supplying their surgical or intervention procedures. According to our previous classification (Nerantzis et al., 1983), the SN artery belonged to group B, since during its course perfuses a small part of LA, the interatrial septum and a large part of the RA. The distal origin of the SN artery is not necessary to provoke perfusion disturbance to the SN area, as supported by Verhaeghe and Hauwaert(1967), and James (1973), because I have not found histological changes in the myocardium of both

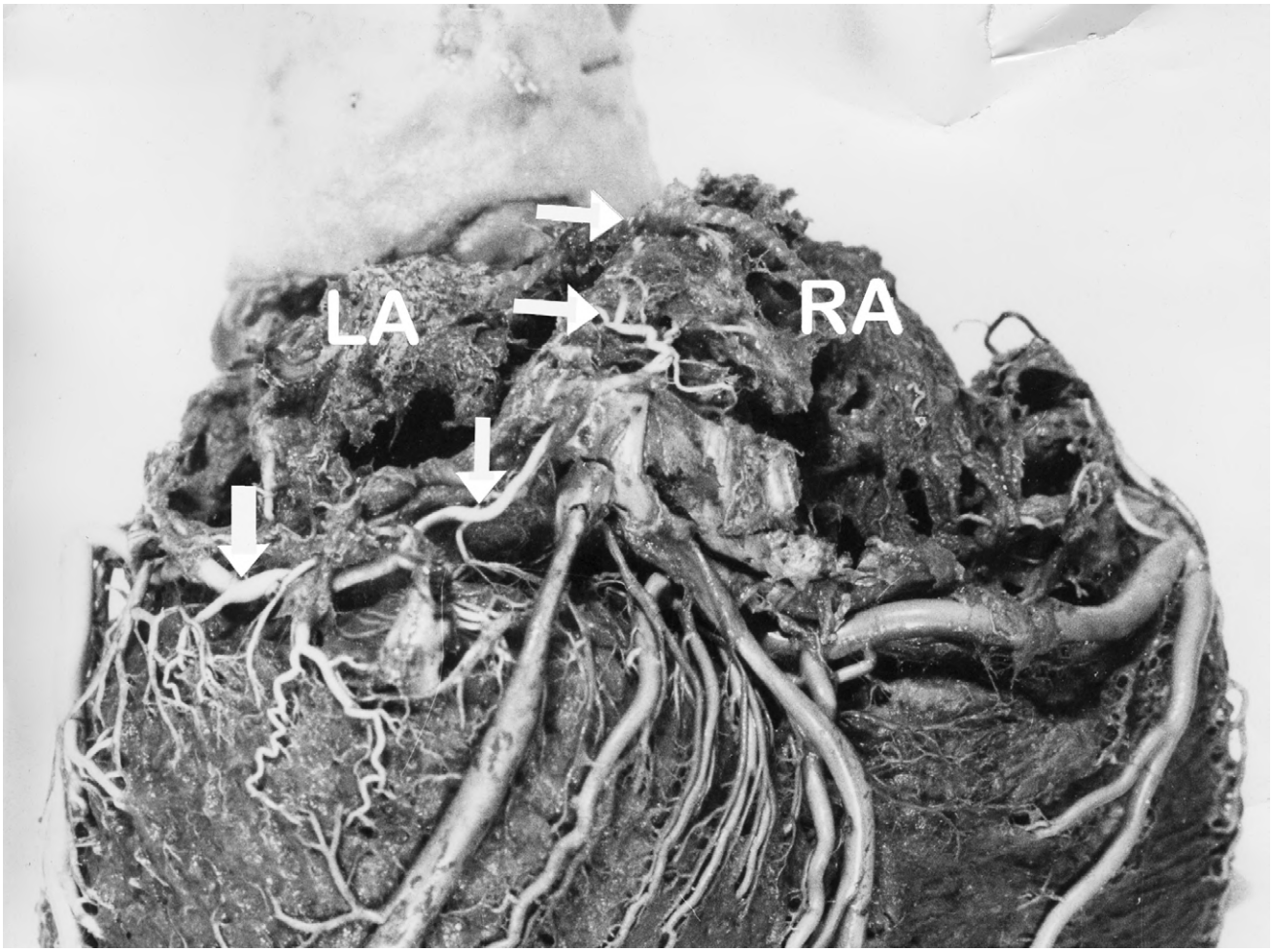

Fig. 1.- Slightly backward oblique posteroanterior view of corrosion casting of heart. It shows the origin of the sinus node artery from the left circumflex (wide arrow), and its course to the sinus node area (three narrow arrows).RA=right atrium, LA=left atrium.

atria and in the SN area. The SN artery appears to be disproportionally large in comparison with other atria arteries for two reasons, a) it receives a strong pulse to regulate its functioning (Verhaeghe et al., 1967) and b) it supplies with blood large part of atria myocardium, except the SN area (Nerantzis et al., 1983).

In conclusion, detailed anatomical knowledge of the blood supply to the SN is essential because of the wider implementation of cardiac surgery or interventional cardiology, in order to avoid damage of the SN artery during their medical procedures. I believe that such a complication could result in the destruction of the artery, damage of the collateral circulation, dysfunction of the atria myocardium and the onset of arrhythmias as mentioned and by Gaudino et al. (2003).

REFERENCES

GAUDINO M, NASSO G, MINATI A, SALICA A, LUCIANI N, MORELLI M, POSSATI G (2003) Early and late arrhythmias in patient in preoperative sinus rhythm submitted to mitral valve surgery through the superior septal approach. *Ann Thorac Surg*, 75: 1181-1184.

JAMES TN (1961) Anatomy of the coronary arteries. Paul B. Hoeber, New York, pp 12-37, 133-150.

JAMES TN (1973) The sinus node as a servomechanism. *Cir Res*, 32: 307-313.

Mc ALPIN WA (1975) Heart and coronary arteries. Springer, New York, pp 133-150, 163-209.

NERANTZIS CE, AVGOUSTAKIS D (1980) An S-shaped atrial artery supplying the sinus node area. An anatomical study. *Chest*, 78: 274-278.

NERANTZIS CE, ANTONAKIS EB, AVGOUSTAKIS DG (1978) A new corrosion casting technique. *Anat Rec*, 191: 321-325.

NERANTZIS CE, TOUTOUZAS P, AVGOUSTAKIS D (1983) The importance of the sinus node artery in the blood supply of the atrial myocardium. An anatomical study of 360 cases. *Acta Cardiol*, 38: 35-47.

VERHAEGHE L, VAN DER HAUWAERT L (1967) Arterial blood supply of the human sinus node. *Br Heart J*, 29: 801-806.

The management of scientific achievement in life sciences: a perspective from the complexity

Pablo Álvarez[1], Marta Reyes[2], Arturo Argüello[3]

[1] Foundation for the Biosanitary Research of Eastern Andalusia (FIBAO) and Granada Biohealth research institute (ibs.Granada), Granada, Spain

[2] Guest researcher, University of Granada, Spain

[3] Andalusian Public Progress and Health Foundation (FPS)

SUMMARY

In the area of biomedicine, there have been numerous scientific achievements that have resulted in a growing proliferation of therapeutic innovations, designed to improve life. The effectiveness of the transfer of scientific achievements is playing a vital role in health systems innovation. The expectations of quality of life due to the advances in the diagnosis and treatment of various pathologies have grown significantly. In this work, a review of trends and quantitative indicators has also been carried out by searching the databases of documents produced and published on scientific achievement in life sciences, analyzing the percentage of annual growth during the period 2010- 2021, showing that the increase in theoretical research and scientific innovation in health has increased exponentially and the interest of the scientific community in this area is clear, as evidenced by the predominance of the number of research articles. The number of articles of research has been 10,353 and 2,636 review articles. It is important to highlight that the percentage of document growth per year is very significant: in 2020 it was 14.28% while in 2010 it was 4.9%.

We analyze the conceptual framework of Innovation in biomedicine, which is based on scientific and technical advances and the panorama of intellectual property. This analysis allows life sciences researchers to expand the concept of innovation in this area, being useful for formulating health research policies capable of translating their scientific achievements, where possible, into health innovations and truly valuable for future advances in health.

Key words: Healthcare innovation – Innovation process – Scientific achievement

HISTORICAL REFERENCES AND A BRIEF DEFINITION OF INNOVATION IN HEALTH

In the last ten years, many works carried have been carried out in the field of characterization of the human talent of the bio-health sector, focusing

Corresponding author:
Pablo Álvarez. Biosanitary Research of Eastern Andalusia Foundation (FIBAO) and Granada BioHealth research institute (ibs.Granada), Avda de Madrid, 18014 Granada, Spain. Phone: 608376697. E-mail: palvarez@fibao.es

Submitted: April 27, 2021. **Accepted:** May 13, 2021

Not final proof's revision by the authors

lately on the analysis of key characteristics and problems of human talent in the field of life sciences. Primary and secondary information sources have been used with qualitative and quantitative methodology that identify the characteristics of scientific knowledge in the global context.

The current strategies of scientific knowledge are based on comprehensive actions that allow us to take advantage of innovation to address the fundamental scientific and social challenges of the third millennium. (Raymond et al., 2010; Kobylarek, 2019).

In the field of biomedicine, the different institutions are interested in promoting translational research in the biomedical research sector, and thereby promote innovation in health by improving the health of the population and the economy itself. The social utility of talent is the main driver of productivity and sustainable growth (Barile and Saviano, 2018). Governments and civil society itself have proposed a renewed focus on the social benefits of translational research. The preferred place for innovation, in the area of human health, is found in the context of new diagnostic and therapeutic molecules, as well as health technologies capable of being more efficient and effective.

Innovation is a concept that has emerged strongly in the health sector: it is defined as the potential that new scientific achievements present to be socially useful. In medicine, it appears as a fundamental challenge for the achievement of new therapeutic tools for the health sector and for the application of changes that add value to social problems (D'Alvano and Hidalgo, 2012). In the health sector, the impulse of innovation is being implemented, establishing lines of action aimed at promoting sustained innovation and oriented towards socially relevant objectives. This strategy implies the implementation of new ways of working and the adoption of new diagnostic and therapeutic tools (Bernardi and Exworthy, 2020).

The COVID-19 pandemic is being a clear example of the usefulness of innovations, derived from scientific achievements to solve health problems. The amount and speed of innovative therapeutic responses to the health crisis are being extraordinary. The COVID-19 genome was mapped with dizzying speed and diagnostic and treatment tests have been developed in record time; developments in clinical trials of therapies and vaccines are being more than remarkable (Saidi et al., 2020). The speed of these advances in the COVID-19 experience is demonstrative of the transformative effect of scientific and technological knowledge to achieve scientific and technological innovations necessary in a health crisis.

SCIENCE AND TECHNOLOGY, GENERAL TRENDS OF INNOVATION IN BIOMEDICINE

Innovation in this area is in the process of exponential change and development; consequently, academic and other institutions are considering new creative strategies involving ways to manage and retain talent. (Thayer et al., 2018)

The current dynamics of biomedical research management is allowing the explosion of promising new fields of research and technology, whose scientific achievements make it possible to translate into transversal improvements in medical care. Knowledge management (KM) is an emerging field of expertise (Haider et al., 2018). In different scientific areas, especially in Medicine, knowledge management (KM) constitutes an area of specialization with potential, which allows for translating scientific achievements into transversal improvements in health in a more effective and efficient way.

Different analyses are influencing the development models of KM. However, KM's progress is growing in arithmetic progression and not as much as it should. It is necessary that the different academic and business institutions assume a more proactive and visible role in the advancement of the KM, demonstrating that it is an area of emphasis, whose time has come.

Knowledge management increases the exchange of knowledge with social organizations and is based on an adequate transfer of knowledge to society and industry (McInerne, 2002; Argüello and Álvarez, 2021). In this implementation, the

effort is aimed at the social utility of the knowledge generated in public or private institutions. Therefore, its effective management must be based on the understanding of the dynamic nature of knowledge as a dynamic process.

Management of biotechnological innovation in industry has had a direct impact on the productivity of pharmaceutical R&D. Biomedical research groups develop new ways of working, fostering scientific-technical collaboration and exchange, prioritizing the diversity of applications of new information technologies, enabling the convergence of scientific achievements in areas such as medicine, biotechnology, biology, engineering, computing or nanotechnology (Carmen et al., 2018).

THE CYCLE OF INNOVATION IN BIOMEDICINE: PANORAMIC OF THE FUTURE

State-of-the-art information technologies make it easy for researchers to interconnect flexibly, enabling efficient research.

Innovation in biomedicine is based on scientific and technical advances which involves both public and private sectors, which requires specific financial investments (Uhl-Bien et al., 2007; Álvarez et al., 2014).

The development of its future is conditioned to the creation of incentives for the promotion of R & D, providing shared research infrastructure of the latest generation; fostering interdisciplinary research and the translation of scientific achievement to society, as well as updating the regulatory environment.

In biomedicine, many of the research groups that generate translational knowledge are distributed in universities, opis or industries, so the ability to retain, manage and exploit knowledge comes from various public and private research organizations (Bolisani and Bratianu, 2018).

Therefore, the social utility of scientific achievement and innovation in health requires an expert management of assets, as well as a specific organization, adequate financing and a pertinent vision of the future (Ahern et al., 2014).

In the life sciences, scientific achievements must be accessible. The openness of knowledge is essential for the performance of innovation; so in the case of the human genome, for the progress of personalized medicine, it is necessary to establish and regularize the databases of genetic research and the maintenance and use of biobanks.

For high quality research, databases are fundamental, as they facilitate broad access to biomedical data and materials.

In the field of intellectual property, currently, different governments are designing relevant actions capable of improving the social use of intellectual assets (Cardona, 2013).

Intellectual property and patents are one of the best strategic tools to generate and commercialize new drugs, utility models and strategic intangible assets in the health sector. These benefits affect health in general as well as the generation of wealth in particular.

The intellectual property area is working to generate greater efficiencies in the exploitation of intellectual property. Collaborative innovation is an example of theseuses as a means to optimize innovation, the translation of knowledge to promote R&D by promoting the commercialization of new drugs and utility models.

In order to detect current trends in the management of scientific achievement in life sciences, a scientific-metric analysis based on the scientific and technical literature has been carried out to quantitatively analyze the bibliometric contributions of this specific area.

The bibliometric scientometry tools allow the identification of the existing information on a specific topic. With the new web tools, it is possible to carry out complete searches that make it possible to carry out better bibliometric analyses of the scientific literature published in a specific field.

To carry out the main purpose of this work, which is to provide an updated vision of scientific achievement in life sciences as well as its future perspective, a bibliometric analysis has been carried out to detect the trend of the subject in the field of the scientific community.

We have made a schematic flow diagram of the bibliographic search and selection and analysis of the documents produced in the analyzed temporal space (Fig. 1).

The objective of the bibliometric analysis carried out has been to scientometrically analyze the documents published, quantitatively and qualitatively analyzing the production of scientific documents in Scientific Achievement in Life Sciences.

Subsequently, we focus on the results obtained from what has been published in Management of Scientific Achievement in Life Sciences using the ScienceDirect database in the 2010-2021 time-frame, both inclusive.

The choice of this database was made because ScienceDirect explores scientific and technical research in Engineering and Physical Sciences, Life Sciences, Health Sciences and Humanities and Social Sciences, including the number of publications, type of document, title of the journal and area in which the publication is included. This search engine allows researchers to access full-text documents and allows them to locate book citations, theses, reports, etc.

Subsequently, the publications were selected in accordance with the type of article (research, review, congress, book chapter and editorial) as well as the year of publication. As a next step, we develop guidelines for the analysis of the documents included in this study depending on the type of document, being classified as: Articles produced as research articles, review articles, short communications, and articles published in peer-reviewed journals.

On the other hand, the documents that include: Books in general. Included are books and encyclopedias, book chapters, editorials, and conference proceedings, editorials, practical guides, conferences, etc.

To analyze the quantitative evolution and show the qualitative mapping of trends, the number of articles published in journals with impact factor as indicators to measure the quality of scientific production was selected and analyzed, thus obtaining qualitative evidence from the published articles.

RESULTS AND COMMENTS

The scope of the research was carried out by collecting documents produced and selected from academic databases and using the keywords: Management of scientific achievement in Life Sciences.

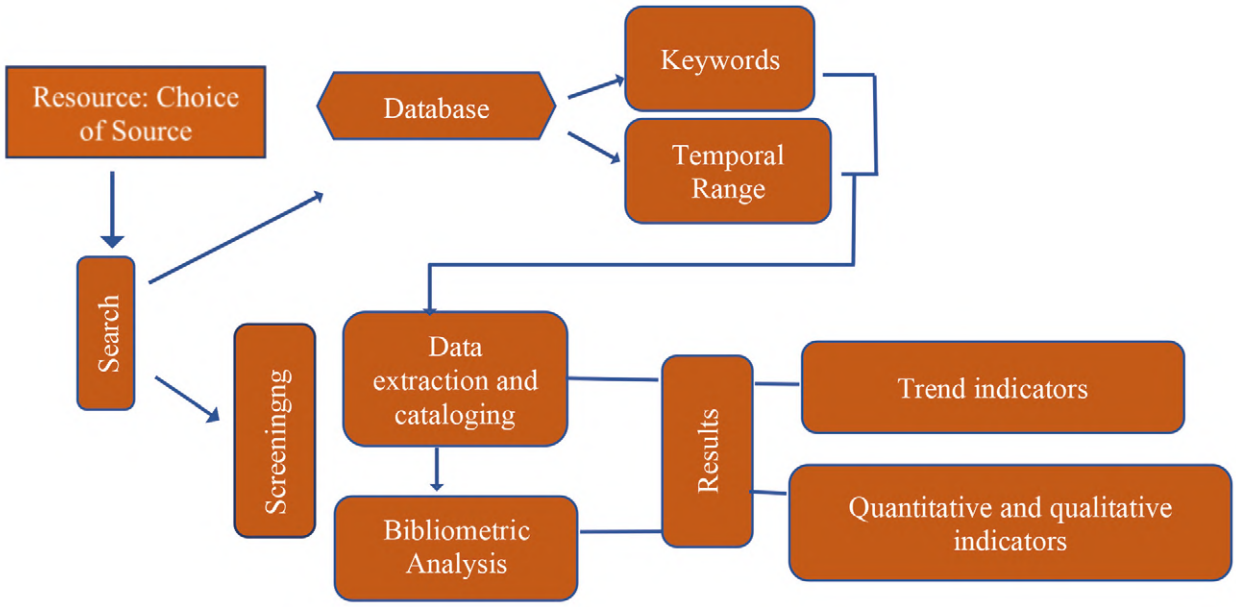

Fig. 1.- Diagram of the development of the work: Route of the bibliographic search and the respective selection of the analyzed documents.

We have used different search engines for free access to scientific and academic literature that allow us to locate references, full texts and the number of citations of an article.

To identify the largest number of documents produced, the academic databases used were: Search Engine, iSEEK Education, Springer Link, Google Scholar, RefSeek, World Wide Science and ScienceDirect.

The justification for using these search engines have been established: Springer link provides researchers with access to millions of scientific journal papers, books, series, protocols, and reference works.

iSEEK Education is a dedicated search engine that collates hundreds of thousands of authority resources from universities, governments and established non-commercial vendors. It provides smart search and a web-based personal library to help locate the most relevant results immediately, thereby saving time by finding information quickly.

RefSeek is a web search engine for students and researchers that aims to make academic information easily accessible. RefSeek searches over a billion documents, including web pages, books, encyclopedias, magazines, and newspapers. It offers students extensive coverage of topics without overloading the information of a general search engine, increasing the visibility of academic information and compelling ideas that are often lost in a tangle of sponsored links and business results.

WorldWideScience.org is a global science portal made up of national and international science portals and databases. WorldWideScience.org accelerates scientific discovery and progress by providing a comprehensive search of databases around the world.

Google Scholar is a search engine that allows us to locate academic documents such as articles, theses, books, patents, conference-related documents, and abstracts. It feeds on information from various sources: university publishers, professional colleges, preprint repositories, universities, and other academic organizations. It provides an easy way to search academic literature. One can search many disciplines and sources: articles, theses, books, abstracts and opinions from academic publishers, professional societies, online repositories, universities and other websites. Google Scholar helps us find relevant jobs within the world of academic research.

Dialnet is one of the largest databases of scientific content in Latin-American languages and has various documentary resources: journal articles, articles of collective works, books, conference proceedings, bibliographic reviews, doctoral theses

ScienceDirect is a website that provides access to a comprehensive medical and scientific search database, with more than 12 million content from 3,500 academic journals and 34,000 electronic books, allowing access to scientific and technical research in Engineering and Physical Sciences, Life Sciences, Health Sciences and Humanities and Social Sciences, including the number of publications, type of document, title of the journal and the scope in which the publication is made.

ANALYSIS OF DOCUMENTS PRODUCED

We have detected that the number of documents displayed by the different selected search engines is diverse.

The search engines that show the greatest similarity in the number of documents found have been Google Scholar with 37,600 documents, RefSeek with 32,800 and ScienceDirect. with 32093. Table 1 shows the number of documents in the analyzed databases.

Table 1. Number of documents in the analyzed databases.

Search engine	Nº Documents
iSEEK Education	56597
Springer Link	46843
Google Scholar	37600
RefSeek	32800
World Wide Science	1354
ScienceDirect.	32093

Subsequently we focus on the results obtained from what has been published in Management of Scientific Achievement in Life Sciences using the ScienceDirect database in the 2010-2021 time-frame, both inclusive,

The choice of this database was made because ScienceDirect explores scientific and technical research in Engineering and Physical Sciences, Life Sciences, Health Sciences and Humanities and Social Sciences, including the number of publications, type of document, title of the journal and area in which the publication is included. This search engine allows researchers to access full-text documents and allows them to locate book citations, theses, reports, etc.

Subsequently, the publications were selected on the basis of the type of article (research, review, congress, book chapter and editorial) as well as the year of publication.

As a next step, we develop guidelines for the analysis of the documents included in this study depending on the type of document, being classified as: Research articles produced as research articles, review articles, short communications, and articles published in peer-reviewed journals.

On the other hand, the documents that include: Books in general. Included are books and encyclopedias, book chapters, editorials, and conference proceedings, Editorials, practical guides, conferences, etc.

To analyze the quantitative evolution and show the qualitative mapping of trends, the number of articles published in journals with impact factor as indicators to measure the quality of scientific production was selected and analyzed, thus obtaining qualitative evidence from the published articles.

Trend review: quantitative indicators

Once the search in the indicated databases was completed, we obtained the documents produced and published. Fig. 2 shows the numerical values of the documents published by year and their evolution in the analyzed temporal space, and Fig. 3 shows the percentage of them according to the databases used.

We have also analyzed the percentage of annual growth (Fig. 4) and the Number of documents produced by year, annual percentage and inter-annual increase.

Analysis of documents produced depending on the year analyzed

In general, the growth in the number of documents published in the area of Scientific Achievement Management in Life Sciences is progressive throughout all the years analyzed.

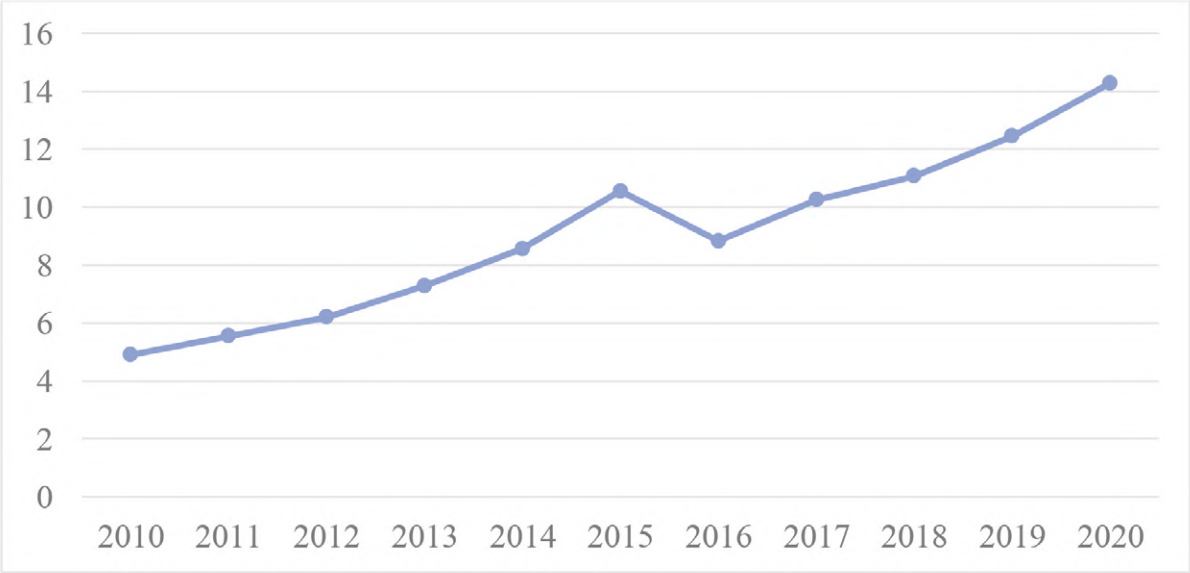

Fig. 2.- Number of of the documents published by year.

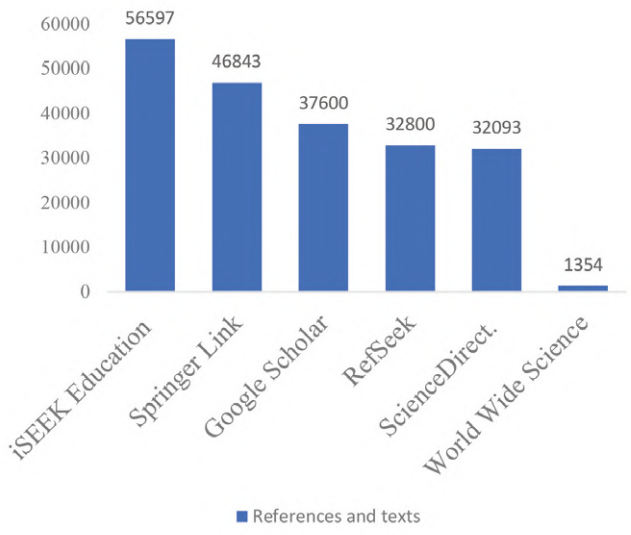

Fig. 3.- Total numerical values Documents according to the databases used.

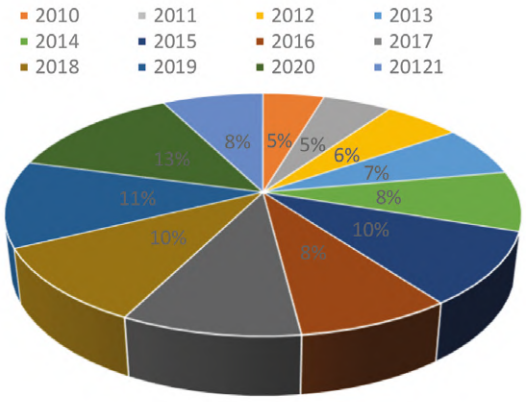

Fig. 4.- Percentage of annual growth of documents produced.

These results constitute a clear indicator of a quantitative trend, and is a demonstration of the growing and progressive interest of the scientific community in this topic. It is important to highlight that the percentage of document growth with respect to the total is very significant: in 2020 it was 14.28% while in 2010 it was 4.9% (Table 2).

It should be noted that the publications made in 2021 are not yet fully compiled by the different scientific search engines.

Qualitative data

Analysis of the distribution and evolution of publications according to the type of article:

a.- Articles published in journals with impact factor and peer evaluation.

b.- The rest of the research documents published on this matter without the criteria of "a" section.

Table 2. Analysis of documents produced depending on the year analyzed. Number of documents produced by year, annual percentage and interannual increase.

Year	Nº of documents	Percentage documents	Year-on-Year increase
2010	814	4,9 %	1,09
2011	914	5,55 %	1,13
2012	1021	6,2 %	1,11
2013	1198	7,28 %	1,17
2014	1410	8,57 %	1,18
2015	1736	10,55 %	1,23
2016	1453	8,83 %	0,84
2017	1687	10,25 %	1,16
2018	1822	11,07 %	1,08
2019	2049	12,45 %	1,06
2020	2350	14,28 %	1,15

The selected research articles were grouped by type of article: research articles and review articles. Fig. 5 shows the evident predominance of research articles published in journals with an impact factor.

Research articles are always the majority over documents in general, this preponderance being a constant in the selected period. In the years analyzed, the research articles produced are significantly higher in number with respect to the rest of the types of documents produced: they constitute 74% of the total (Fig. 5). These data demonstrate that in the scientific community there is a predominant interest in the research articles: the number of research articles has been 10,353 and the number of review articles is 2,636 (Fig. 6).

Therefore, these results represent a clear qualitative trend indicator, since the increase in research articles published in indexed journals,

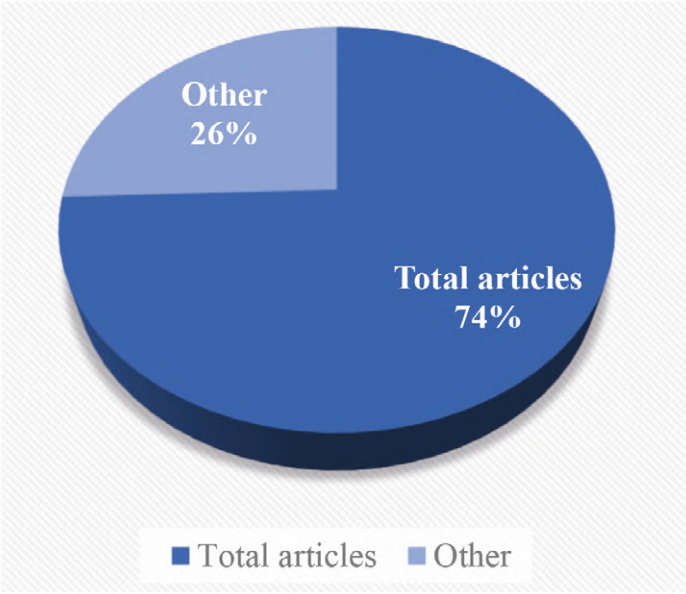

Fig. 5.- Percentage of total documents: research articles and others.

with an impact factor and with peer evaluation, constitutes a quality indicator, being a constant in the years analyzed.

The proportion of types of articles remains in a constant rhythm throughout the period analyzed.

THE MANAGEMENT OF INTELLECTUAL PROPERTY IN THE CURRENT CONTEXT

Patents in the concept of open innovation, different from the traditional technology transfer, need regulatory updates. In the area of life sciences, scientific and technological advances occur with an exponential progression (Armitage et al., 2011; Alvarez et al., 2019). Its scientific achievements are carried out with the participation of different areas of knowledge and its social transfer and innovation in health integrates multiple scientific and clinical achievements, which with the necessary interoperability, make an efficient use of the scientific achievement acquired.

For example, the technologies involved in diagnostic biomarkers and synthetic biology involve different multidisciplinary scientific achievements in different areas such as molecular biology, nanotechnology, BigData database, advanced computing, mathematical models, algorithms, utility models, biomarkers, etc.

The administrations must carry out the drafting of the pertinent legislation that regulates the promotion of the social utility of scientific achievements, especially those financed with public funds (Argüello et al., 2020). Currently in the universities, there has been a rapid growth of its regional economic development influence, and this has generated an increasingly complex network in the field of university technology transfer, which has resulted in the academy, the industry, the regional government and users of innovation based on knowledge constitute a functional unit, is the so-called fourth Helix (Miller et al., 2018; Blackler, 1993) The empowerment of the translation of scientific knowledge produced in the academic environment to the industry (Pahl-Wostl, 2007) is directly related to the increase in the development options of personalized medicine. The consideration of the patient individually enables the design for its treatment with precision, facilitated by the massive use of biomarkers in the initial decision-making.

NEW POLITICAL CHALLENGES BASED ON ADVANCES IN BIOMEDICINE

The management of organizations: a perspective from the complexity.

The rhythms of evolution and growth of the scientific achievements of the university and industrial institutions have demonstrated that there are many concepts that must be re-

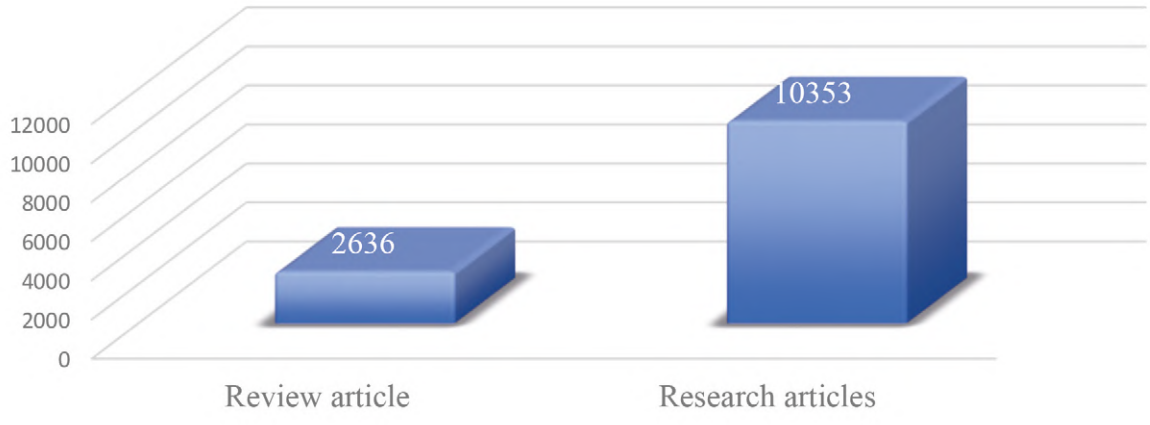

Fig. 6.- Number of research articles and review articles.

evaluated. The strategic plans and structures have a certain obsolescence, conditioning the appearance of new ones that are configured as a tendency for the new generations (Álvarez et al., 2014). In the field of Science and Technology, there have been profound transformations. New spaces of understanding appear with the target of the importance and social legitimacy of scientific achievement, Collings et al. (2018) incardinated this in the Global Ethics and Bioethics. Basically, current dynamics condition new forms of governance of R & D & I that adapt to new social and economic realities. We think that the organization of the management of scientific achievements is ordered as an integrating system in which social and industrial utility are highly interrelated. Technicians of scientific and technical transfer are the main instruments that organizations have in order to make translational research tangible: they generate and offer the social utility of knowledge, and they induce changes and transformations in the productive system.

REFERENCES

AHERN T, LEAVY B, BYRNE PJ (2014) Complex project management as complex problem solving: A distributed knowledge management perspective. *Int J Project Manag*, 32(8): 1371-1381.

ÁLVAREZ P, MARCHAL J, BOULAIZ H, CARRILLO E, VÉLEZ C, RODRÍGUEZ-SERRANO F, MELGUIZO C, PRADOS J, MADEDDU R, ARANEGA A (2012) 5-Fluorouracil derivatives: a patent review. *Expert Opin Ther Pat*, 22: 107-123.

ÁLVAREZ P, BOULAIZ H, VÉLEZ C, RODRÍGUEZ-SERRANO F, ORTIZ R, MELGUIZO C, PRADOS J (2014) Qualitative and quantitative analyses of anatomists' research: evaluation of multidisciplinarity and trends in scientific production. *Scientometrics*, 98(1): 447-456.

ÁLVAREZ P, REYES M, SÁNCHEZ-CANTALEJO J, ARGÜELLO A (2019) Analysis of factors associated with Grant for PCT national phase entries patent: a mathematical model. *Eur J Anat*, 23(5): 333-340.

ARMITAGE D, BERKES F, DALE A, KOCHO-SCHELLENBERG E, PATTON E (2011) Co-management and the co-production of knowledge: Learning to adapt in Canada's Arctic. *Global Environ Change*, 21(3): 995-1004.

ARGÜELLO A, SOLANA VH, JÜRGENS B, ARÁNEGA P (2020) Análisis de patentes y desarrollo territorial: Ejemplo en el ámbito Biosanitario. *J Econ Bus Intellig*, 2: 13-19.

ARGÜELLO A, ORUEZABAL RI, ÁLVAREZ P (2021) Las unidades de inteligencia competitiva y prospectiva como motor director de la innovación tecnológica en los sistemas sanitarios. *J Econ Bus Intellig*, 3(5): 43-49.

ARRIZABALAGA J (2021) The challenge of (re)emerging diseases, the limits of the biomedical response and the new paradigm of global health. *História, Ciências, Saúde- Manguinhos*, 28(1): 255-281.

BARILE S, SAVIANO M (2018) Complexity and sustainability in management: insights from a systems perspective. In: *Social dynamics in a systems perspective*. Springer, Cham, pp 39-63.

BERNARDI R, EXWORTHY M (2020) Clinical managers' identity at the crossroad of multiple institutional logics in its innovation: The case study of a health care organization in England. *Information Systems J*, 30(3): 566-595.

BLACKLER F (1993) Knowledge and the theory of organizations: Organizations as activity systems and the reframing of management. *J Manag Studies*, 30(6): 863-884.

BOLISANI E, BRATIANU C (2018) The emergence of knowledge management. In: *Emergent knowledge strategies*. Springer, Cham, pp 23-47.

CARDONA OD (2013) The need for rethinking the concepts of vulnerability and risk from a holistic perspective: a necessary review and criticism for effective risk management. In: *Mapping vulnerability*. Routledge, pp 56-70.

CARMEN E, WATT A, CARVALHO L, DICK J, FAZEY I, GARCÍA-BLANCO G, LIQUETE C (2018) Knowledge needs for the operationalization of the concept of ecosystem services. *Ecosystem Services*, 29: 441-451.

COLLINGS DG, WOOD GT, SZAMOSI LT (2018) Human resource management: A critical approach. Routledge, pp 1-23.

D'ALVANO L, HIDALGO A (2012) Innovation management techniques and development degree of innovation process in service organizations. *R&D Management*, 42(1): 60-70.

DOELLO K, ORTIZ R, ÁLVAREZ PJ, MELGUIZO C, CABEZA L, PRADOS J (2018) Latest in vitro and in vivo assay, clinical trials and patents in cancer treatment using curcumin: a literature review. *Nutr Canc*, 70(4): 569-578.

HAIDER LJ, HENTATI-SUNDBERG J, GIUSTI M, GOODNESS J, HAMANN M, MASTERSON VA, SINARE H (2018) The indisciplinary journey: early career prospects in sustainability science. *Sustainability Science*, 13(1): 191-204.

KOBYLAREK A (2019) Social responsibility of science. *J Educ Culture Soc*, 10(2): 5-11.

MCINERNEY C (2002) Knowledge management and dynamic nature of knowledge. *J Am Inform Sci Technol Soc*, 53(12):1009-1018.

MILLER K, MCADAM R, MCADAM M (2018) A systematic literature review of university technology transfer from a quadruple helix perspective: toward a research agenda. *R&D Management*, 48(1): 7-24.

PAHL-WOSTL C (2007) The implications of complexity for integrated resources management. *Environ Modeling Software*, 22(5): 561-569.

RAYMOND CM, FAZEY I, REED MS, STRINGER LC, ROBINSON GM, EVELY AC (2010) Integrating local and scientific knowledge for environmental management. *J Environ Manag*, 91(8): 1766-1777.

SAIDI T, THUNE TM, BUGGE M (2020) Making 'hidden innovation'visible? A case study of an innovation management system in health care. *Technol Analysis Strategic Manag*, 1-13.

THAYER AL, PETRUZZELLI A, MCCLURG CE (2018) Addressing the paradox of the team innovation process: A review and practical considerations. *Am Psychologist*, 73(4): 363.

UHL-BIEN M, MARION R, MCKELVEY B (2007) Complexity leadership theory: Shifting leadership from the industrial age to the knowledge era. *Leadership Quarterly*, 18(4): 298-318.

Considerations for the containment of COVID-19 in cadavers: ensuring the continuance of human dissection for the education of healthcare professionals

Beverley Kramer[1], Bernard Moxham[2] and Reubina Wadee[3]

[1] School of Anatomical Sciences , Faculty of Health Sciences, University of the Witwatersrand, Johannesburg South Africa
[2] Cardiff School of Biosciences, Cardiff University, Museum Avenue, Cardiff, CF10 3AX, United Kingdom
[3] Department of Anatomical Pathology, School of Pathology, Faculty of Health Sciences, University of the Witwatersrand, Johannesburg South Africa/ National Health Laboratory Service

SUMMARY

Human cadavers may present risks to staff and students in anatomy, particularly when new infectious diseases, such as COVID-19, arise. The processing of human tissues in relation to infectious diseases, particularly the fixatives used, was reviewed to try to formulate knowledge to safeguard staff and students working in anatomy laboratories. Advice from virologists indicates that the SARS-CoV-2 virus is unlikely to remain in cadavers that are adequately fixed, particularly if the cadavers are left undisturbed for a prolonged period. However, bodies that are known to be COVID-19-positive should not be accepted into donor programs. It is also recommended that staff and students who come into contact with cadavers should be vaccinated against the virus. In the light of these precautions, teachers and students can retain confidence in being able to continue their education using human cadaveric material.

Key words: COVID-19 – Body donation programs – Anatomy education – Dissection

COMMENTARY

The SARS-CoV-2 virus appeared in Wuhan, China in late 2019 and spread rapidly across the globe. By March 2020, the World Health Organisation (WHO) had designated the global health emergency as a pandemic owing to the virulence of the virus and the spread of infection. The pandemic has caused disruption of global economies and interference with the operation of organizations and institutions (Bianchi et al., 2020, Brassett et al., 2020), particularly health sciences institutions.

The coronavirus was named severe acute respiratory distress syndrome 2 (SARS-CoV-2) (Lai et al., 2020), with the disease being termed COVID-19 (Gosney et al., 2020). The virus is classified as a “risk group 3” human pathogen (PHA, 2020). Transmission of COVID-19 (SARS-CoV-2) is by droplets and fomites (WHO, 2020). While faeces in some instances have tested positive for SARS-CoV-2, faecal material does not appear to be infectious at this time (AST, 2020).

Corresponding author:
Professor B. Kramer. School of Anatomical Sciences, Faculty of Health Sciences, University of the Witwatersand, Johannesburg, South Africa. Phone: +27825545529. E-mail: Beverley.kramer@wits.ac.za

Submitted: March 12, 2021. **Accepted:** March 30, 2021

Although it was at first postulated that COVID-19 could not be spread through exposure to a COVID-19-positive dead body (WHO, 2020), evidence exists to the contrary (Sriwijitalai and Wiwanitkit, 2020). However, in a fast changing research field such as this, it has subsequently been reported from an in-depth analysis among pathologists that, if adequate personal protective equipment (PPE) is worn, there is little risk of transmission of COVID-19 at autopsy (Davis and Williamson, 2020). Postmortem swabs have detected the virus for up to 13 days after death (RCP, 2020a). Further data are required to authenticate the handling of COVID-positive bodies as current guidelines on safety provide differing evidence (Dijkhuizen et al., 2020; Yaacoub et al., 2020). It is of major importance that staff and students in anatomy laboratories are protected from possible infection by this, and other, viruses. The advent of a new virus such as SARS-CoV-2 presents challenges for anatomists in dealing with dissection and anatomy laboratory sessions, and finding the appropriate procedures to render the body "safe" for dissection is crucial.

Although the use of human cadaveric material for the teaching, learning and assessment of anatomy has over time been hotly debated (e.g Dyer and Thorndike, 2000; Gregory and Cole, 2002; McLachlan et al., 2004; Peterson and Regan de Bere, 2006; Papa and Veccarezza 2013; McMenamin et al., 2018; Memon 2018; Moxham and Pias, 2017), there is considerable evidence that anatomists, students and laypersons regard human dissection as necessary for the training of healthcare professionals (Patel and Moxham, 2006; Moxham and Plaisant 2007; Kerby et al., 2011; Moxham et al., 2016), not just for the acquisition of anatomical knowledge but also for the development of professional skills and attitudes (Lempp, 2005; Moxham and Moxham, 2007; Pearson and Hoagland 2010; Kerby et al., 2011; Palmer et al, 2021). However, with the advent of the COVID-19 pandemic, teaching has used a virtual platform, laboratory work has been prohibited and has led some anatomists to suggest that virtual cadavers will replace real cadavers (Singal et al., 2020; Iwanga et al., 2021; Nakloo et al., 2021). Recent evidence that the advent of the coronavirus has affected institutions and caused discontinuance of face-to-face teaching comes from the reports in 2020 of Bianchi et al., Evans et al., Longhurst et al., Pather et al., and Iwanaga et al. Although these measures have led to much ingenuity for teaching, the negative consequences relate to loss of staff-student face-to face teaching, loss of experiential and practical teaching and loss of acquisition of team and professional skills. In addition, high workloads are causing additional stress for staff. An overreliance on electronic methodologies in a computer-dominated age has become apparent at a time when patient-doctor relationships should be re-evaluated as patients might require a more personal relationship. In our view, blended learning, including the use of cadaver-based laboratory tuition alongside computer-assisted technologies, offers the best of all worlds for the education of the emergent healthcare professional. In consequence, it is crucial that the risks of using cadavers that might be infected by SARS-CoV-2 be evaluated.

Working in an anatomy laboratory has always had some challenges in relation to infectious diseases. Historically, as sterile techniques were not applied in the early days of dissection and bodies were not fixed, students and staff were often infected by the transfer of diseases from the cadaver (Kaufman, 2005; Shoja et al., 2013). As a result of the introduction of appropriate precautions, few deaths of anatomists and students are now known to occur (Shoja et al., 2013). A variety of pathogens may be present in an unembalmed dead body. For example, *Mycobacterium tuberculosis* is said to have been transmitted to an embalmer, possibly during the process of embalming a cadaver (Sterling et al., 2000). Pathogens which may be present include, *Mycobacterium tuberculosis,* HIV, hepatitis B and C, prions and corona viruses (Roth et al., 1992; De Craemer, 1994; Healing et al., 1995; Kappel et al., 1996; Catteneo et al., 1999).

Institutions around the world have fostered body donor programs (Garment et al., 2007; McHanwell et al., 2008; Cornwall and Stringer, 2009; Reiderer et al., 2012; Hutchinson et al., 2020) in order to safeguard dissection of the human body (Hildebrandt, 2010; Rokade and Gaikawad, 2012;

Cornwall, 2014; Kramer and Hutchinson, 2014). The advent of the novel coronavirus affected institutions and caused discontinuance of the acceptance of bodies for dissection into donor programs (see Brassett et al., 2020). At this stage, it is not known what long-term impact there will be on the quality of teaching and learning anatomy. However, it is important for anatomists who value human dissection for teaching (Böckers et al., 2010; Ghosh 2017; Moxham and Pias, 2017; Ross et al., 2020) that the supply of human bodies for this purpose is ensured and that dissection for staff and students remains safe.

The coronavirus is not the first disease that has challenged the handling of human cadavers. For example, it is estimated that as many as 65% of individuals involved in unsafe burial practices during the Ebola outbreak in West Africa became infected (Hoffman and Healing, 2019). It needs to be emphasized, therefore, that the appropriate precautions to protect those staff who transport, prepare and embalm bodies for anatomical dissection should be adhered to rigorously and must include PPE and processes as outlined in the guidelines provided by the International Federation of Associations of Anatomists (IFAA, 2020). In particular, invasive procedures and the generation of aerosols should be avoided (Finegan et al. 2020; RCP 2020b). While some institutions have re-opened their laboratories for student dissection (e.g., Ross et al., 2020; University of the Witwatersrand, Johannesburg), the question remaining uppermost in many anatomists' minds is the adequate preservation of bodies for dissection in the future, due to risks from novel infectious diseases.

While it is appreciated that each institution will have Standard Operating Procedures and legal requirements that will affect issues, and while thus far the risk of transmission from handling of COVID-19-positive bodies is considered to be low (ECDC 2020), it is nevertheless recommended that, in general, bodies which are known to be COVID-19-positive should not be accepted into donor programs. It is appreciated that this raises some ethical concerns. For example, should a body be found to be COVID-19-positive after being admitted for anatomical examination, who is then responsible for the body? In the case of bodies where the death certificate does not indicate whether COVID-19 was present at the time of death, it is recommended that testing should be undertaken. While testing (Ravi, 2020) or screening (AST, 2020) of bodies for coronavirus has been recommended prior to accepting bodies into a donor program, it is appreciated that the cost of testing all bodies may be prohibitive for some institutions in low resource settings and logistics could be complicated.

Even when testing is possible, as COVID-19 infection cannot be ruled out by a negative result on screening (Winichakoon et al., 2020), it is recommended that *all* bodies received in an anatomy department should be treated as if they were infectious, whether this be with a coronavirus infection or another infectious pathogen. There is an extensive array of inactivation procedures that have been suggested for enveloped viruses such as the coronavirus, but not all would be suitable for whole body fixation. The following inactivation methods have been proposed: Heat inactivation (Darnell et al., 2004), UV or gamma irradiation (Darnell et al., 2004; Kumar et al., 2015), phenol and guanodine isothiocyanate-based nucleic acid extraction agents (Darnell et al., 2004; Kumar et al., 2015) or fixatives such as formaldehyde, formalin, paraformaldehyde or glutaraldehyde (Darnell et al., 2004; Kumar et al., 2015; Bain et al., 2020) and ethanol (Shidham et al., 2020). Low alcohol concentrations in fixatives may not adequately inactivate the virus (Rossi et al., 2019; Gosney et al., 2020). Furthermore, those handling bodies in the early stages of donation should be be trained (Finegan et al., 2020) and equipped with effective PPE (see CDPC, 2019; Finegan et al., 2020).

Embalming to contain infectious agents

Currently, there is no evidence in the literature to show that the COVID-19 virus is inactivated in a preserved body specifically, although Shidham et al. (2020) state that viral infectivity is greatly reduced by formaldehyde and ethanol. While embalming of COVID-19-infected bodies is not recommended by the WHO (2020), embalming cannot be avoided in anatomy departments.

However, through the use of adequate embalming, the risk of spreading infections from the cadaver to staff and students can be minimized (Demiryurek et al., 2004**).** Anatomy departments generally use embalming fluids which contain fixatives and disinfectants and comprehensive reviews of human body preservation are available in the literature (Demiryurek et al., 2004; Brenner, 2014).

Formaldehyde appears to be the chemical of choice for embalming (Brenner, 2014) and is the most widely used fixative for cadaver preservation in the US (Coskey and Gest, 2015). However, many other preservatives are also used (Brenner, 2014). Formalin is made as an aqueous solution from formaldehyde (37%). It has excellent tuberculocide, bactericide and virucide properties which cause alkylation of groups of proteins and of some purine bases (Rutala, 1996). Its reaction with nucleic acids is important in attenuating viruses (Brenner, 2014). The use of formalin as a preservative has diminished in certain parts of the world, as formaldehyde above a certain level is known to compromise respiratory function (Akbar-Khanzadeh et al., 1994; Whitehead and Savoia 2008). While the adverse effects of formaldehyde in general have been widely reported (Khaliq & Tripathi, 2009; Ahmed, 2011; Raja & Sultana, 2012 ; Brenner, 2014; Sugata et al., 2016), formalin is still widely used as a preservative.

Both antiviral and antimycosal effects have been ascribed to alcohols dependent on the concentration and conditions (Brenner, 2014). Ethanol is known to denature proteins and dissolve lipids and is thus effective in controlling bacteria and fungi, but not against non-enveloped viruses (Demiryurek et al., 2002). It can be used alone or with other antimicrobial agents (Demiryurek et al., 2002).

The saturated salt solution method and Thiel's method of embalming, both having relatively low concentrations of formalin (0.75% and 0.6% respectively; Hayashi et al, 2016), have been shown to be bactericidal (Hayashi et al., 2016) and virucidal (Benkhadra et al. 2009).

Phenol, which is a disinfectant, will at high concentrations destroy the entire cell, but at lower concentrations and higher molecular weight is bacteriocidal (Prindle, 1983). Certain phenolic detergents have been shown to be bacteriostatic (Brenner, 2014), bactericidal, virucidal, and tuberculocidal (CDC, 2008).

The use of high concentrations of sodium hydroxide, together with autoclaving (which obviously cannot be applied in whole body fixation), have been suggested for prions, which are highly resistant to general methods of disinfection (Brown et al., 1982) and require unique methods of inactivation (Prindle, 1983). Although the use of formaldehyde may decrease infectivity of prions, the risk of transmission still remains (Sakudo, 2013).

While much is still to be learned about the appropriate disinfectants for COVID-19 specifically, Henwood (2020) has postulated that disinfectants such as 70% ethanol and 0.1% sodium hypochlorite utilized for other coronaviruses (e.g. SARS-CoV and MERS-CoV) should inactivate COVID-19 on surfaces and on skin.

Information about the fixation of COVID-19 in cultures and in histological tissues is limited. In culture, the MERS-CoV virus was inactivated when exposed to formaldehyde-based fixatives for 30 minutes or for 60 minutes in a methanol-acetone solution (Kumar et al., 2015). In the case of histological tissues, it has also been suggested that fixatives utilized for SARS-CoV and MERS-CoV should be adequate for COVID-19 (Henwood, 2020). The SARS-CoV virus is inactivated in tissue samples fixed in 10% neutral buffered formalin at room temperature for one day and by 70% ethanol (Darnell and Taylor, 2006). Temperature and time are important in the inactivation of SARS-CoV by formalin and glutaraldehyde (Darnell et al., 2004). At 25°C and 37°C respectively, the infectivity of the virus on day 1 of fixation by formalin was significantly decreased. However, by day 3 of fixation some virus still remained infectious (Darnel et al., 2004). SARS-CoV was inactivated by glutaraldehyde after an incubation of 1–2 days (Darnel et al., 2004). The immersion of tissue blocks ($2cm^3$) in 10% formalin or phosphate buffered saline containing 4% paraformaldehyde for a period of 24 hours inactivates SARS-

CoV-2 (Bain et al., 2020). Although ethanol and formalin fixation may render the virus inactive (Barbareschi 2020), it should be borne in mind that low alcohol concentrations may not inactivate the virus (Gosney et al., 2020, Rossi et al., 2020).

The length of time for the fixation of viruses in large samples of tissue such as a whole body is of prime importance for anatomists, as specific viruses are known to remain viable in cadavers for some time after fixation (e.g., *Mycobacterium tuberculosis* for up to 48 hours; Weed and Baggenstoss, 1951). Prolonged periods of fixation prior to using whole bodies is thus preferable. Extended periods of fixation are said to reduce the risk of infection (Vigliar et al., 2020). Thus, increasing the period of fixation in formalin has been recommended for tissue blocks (Rossi et al., 2020). Prolonged fixation is also important, as it is known that tissue permeability rates vary for large pieces of tissue (Bain et al., 2020). The period for which bodies for dissection should be fixed to mitigate against infectious diseases needs investigation, but it is suggested that fixed bodies should remain undisturbed for prolonged periods of time (e.g., three months) to allow for permeation of the fixative to all tissues of the body.

Concluding remarks

In order to mitigate the transfer of any infectious disease from cadavers to staff and students within anatomy departments, safety measures must be implemented. Knowledge of preservatives and the time taken to adequately "fix" these infectious agents is helpful for those managing a donor programme or anatomy laboratory. Formalin, although known to be hazardous, appears to be the fixative with properties that would mitigate tuberculocidal, bactericidal and currently known virucidal infections. Unfortunately, there is no/ little information in the literature with regards to the time needed for fixatives to permeate all regions of a whole body, and hence cause inactivation of any virus that may be present. Thus, bodies should remain undisturbed for as long as possible following preservation with an appropriate preservative/fixative in order to allow for permeation of the fixative to all parts of the body. The use of effective PPE for those staff handling the body during the early stages of processing is essential.

Staff and students could thus be be protected, while allowing body donor programs to continue and student training to ensue.

Those individuals, whether staff or students who come into contact with cadavers, should be vaccinated against hepatitis B and *M. tuberculosis.* It is also recommended that vaccination against COVID-19 be included in the vaccination protocol/ regime for all staff and students in anatomy departments.

ACKNOWLEDGEMENTS

The authors acknowledge the generosity of the donors who bequeath their bodies for the training of health science professionals. Dr Tanya Augustine is thanked for comments on the manuscript.

CONTRIBUTORS NOTE:

BEVERLEY KRAMER, B.Sc., B.Sc. Hons., Ph.D., is an Emeritus Professor. Her research interests are broad and include experimental embryology, growth, anatomical education and research management. She is President of the International Federation of Associations of Anatomists (IFAA).

BERNARD JOHN MOXHAM, B.Sc. B.D.S. Ph.D., is an Emeritus Professor of Anatomy. He is a craniofacial biologist who also publishes extensively on the teaching of the biomedical sciences. He is the Immediate Past President of the International Federation of Associations of Anatomists, and has been President of the European Federation for Experimental Morphology and of the Anatomical Society. He founded the Trans-European Pedagogic Anatomical Research Group.

REUBINA WADEE, MBBCh, FC Path (SA) Anat, DipRCPath, MMed, PhD, is a principal pathologist and senior lecturer at the National Health Laboratory Service and School of Pathology, Faculty of Health Sciences at the University of the Witwatersrand, Johannesburg, South Africa. She lectures in the field of anatomical pathology. Her research interests are in gynaecologic and molecular pathology.

REFERENCES

AHMED HO (2011) Preliminary study: formaldehyde exposure in laboratories of Sharjah University in UAE. *Ind J Occup Environ Med,* 15: 33.

AKBAR-KHANZADEH F, VAQUERANO MU, AKBAR-KHANZADEH M, BISESI MS (1994) Formaldehyde exposure, acute pulmonary response and exposure options in a gross anatomy laboratory. *Am J Ind Med,* 26: 61-75.

AST (2020) American Society of Transplantation. COVID-19 (Coronavirus): FAQs for Organ Donation and Transplantation. 11 March 2020 Ed. Mt. Laurel, NJ: American Society of Transplantation. 8 p. URL: https://www.myast.org/sites/default/files/ COVID 19%20FAQ %20 Tx%20Cen ters%202020.03.11_FINAL.pdf [accessed July 7, 2020]

BAIN W, LEE JS, WATSON AM, STITT-FISCHER MS (2020) Practical guidelines for collection, manipulation and inactivation of SARS-COV-2 and COVID-19 clinical specimens. *Current Protocols in Cytometry,* 93: e77 dio:10.1002/epcy.77

BARBERESCHI M, ASCOLI VC, BONOLDI E, CAVAZZA A, COLOMBARI R, COZZI I, DAINESE E, FACCHETI F, FADDA G, FERRARA G, FRAGETTA F, GRAZIANO P, MURE G, ROSSI ED, ROSSI G, NEGRI G, ZANNONI G, SAPINO A (2020) Biosafety in surgical pathology in the era of SARS-Cov2 pandemia. A statement of the Italian Society of Surgical Pathology and Cytology. *Pathologica,* Epub 2020 Apr 1 DOI: 10.32074/1591-951X-14-20.

BENKHANDRA M, FAUST A, LADOIRE S, TROST O, TROUILLOUD P, GIRARD C, ANDERHUBER F, FEIGL G (2009) Comparison of fresh and Thiel's embalmed cadavers according to the suitability for ultrasound-guided regional anesthesia of the cervical region. *Surg Radiol Anat,* 31: 531.

BIANCHI S, GATTO R, FABIANO L (2020) Effects of the SARS-COV-2 pandemic on medical education in Italy: Considerations and tips. Euromediterranean *Biomedl J,* 15(24): 100-101.

BÖCKERS A, JERGE-BRETZKE L, LAMP C, BRINCKMANN A, TRAUE HC, BÖCKERS TM (2010) The gross anatomy course: An analysis of its importance. *Anat Sci Educ,* 3: 3-11.

BRASSETT C, COSKER T, DAVIES DC, DOCKERY P, GILLINGWATER TH, LEE TC, MIILZ S, PARSON SH, QUONDAMATTEO F, WILKINSON T (2020) COVID-19 and anatomy: Stimulus and initial response. *J Anat,* 237: 393-403.

BRENNER E (2014) Human body preservation – old and new techniques. *J Anat,* 224: 316-344.

BROWN P, GIBBS CJ, AMYX HL, KINGSBURY DT, ROHWER RG, SULIMA MP, GAJDUSEK DC (1982) Chemical disinfection of Creutzfeldt-Jakob disease virus. *N Engl J Med,* 306: 1279-1282.

CATTANEO C, NUTTALL PA, MOLENDINI LO, PELLEGRINELLI M, GRANDI M, SOKOL RJ (1999) Prevalence of HIV and hepatitis C markers among a cadaver population in Milan. *J Clin Pathol,* 52: 267-270.

CDC (2008) Chemical Disinfectants. Guideline for Disinfection and Sterilization in Healthcare Facilities). https://www.cdc.gov/infectioncontrol/guidelines/disinfection/disinfection-methods/chemical.html (accessed 19 October, 2020)

CDCP (2019) Centers for Disease Control and Prevention. 2019a Infection Control Guidance for Healthcare Professionals about Coronavirus (COVID-19). https://www.cdc.gov/coronavirus/2019-ncoy/hcp/infection-control-recommendations.html (accessed 8 March, 2021)

CORNWALL J (2014) Annual variation of body donor registrations in New Zealand. *Eur J Ana*t, 18: 55-59.

CORNWALL J, STRINGER MD (2009) The wider importance of cadavers: educational and research diversity from a body bequest program. *Anat Sci Educ,* 2: 234-237.

COSKEY A, GEST T (2015) The effectiveness of various methods of formaldehyde neutralization. *Clin Anat*, 28(4): 449-454.

DARNELL ME, TAYLOR DR (2006) Evaluation of inactivation methods for severe acute respiratory syndrome coronavirus in noncellular blood products. *Transfusion,* 46: 1770-1777.

DARNELL ME, SUBBARAO K, FEINSTONE SM, TAYLOR DR (2004) Inactivation of the coronavirus that induces severe acute respiratory syndrome, SARS-CoV. *J Virol Meth,* 121(1): 85-91.

DAVIS GG, WILLIAMSON AK (2020) Risk of COVID-19 transmission during autopsy. *Arch Path Lab Med*, Doi 10.5858/arpa.2020-0345-LE

DE CRAEMER D (1994) Postmortem viability of human immunodeficiency virus-implications for the teaching of anatomy. *N Eng J Med,* 331: 1315.

DEMIYUREK D, BAYRAMOGLU A, USTACELEBI S (2002) Infective agents in fixed human cadavers: A brief review and suggested guidelines. *Anat Rec (New Anat)*, 269: 194-197.

DIJKHUIZEN LGM, GELDERMAN HT, DUIJST WLJM (2020) The safe handling of a corpse (suspected) with COVID-19. *J Foren Leg Med*, 73: 101999.

DYER GSM, THORNDIKE MEL (2000) Quidne mortui vivos docent? The evolving purpose of human dissection in medical education. *Acad Med*, 75: 969-979.

ECDC. European Centre for Disease Prevention and Control (2020) Considerations related to the safe handling of bodies of deceased persons with suspected or confirmed COVID-19. Stockholm. https://www.ecdc.europa.eu/sites/default/files/documents/COVID-19-safe-handling-of-bodies-or-persons-dying-from-COVID19.pdf

EVANS DJR, BAY BH, WILSON TD, SMITH CF, LACHMAN N, PAWLINA W (2020) Going virtual to support Anatomy Education: A STOPGAP in the midst of the Covid-19 pandemic. *Anat Sci Educ,* 13: 279-283.

FINEGAN O, FONSECA S, GUYOMARCH P, MORCILLOMENDEZ MD, RODRIGUEZ GONZALEZ J, TiIDBALL-BINZ M, WINTER KA (2020) ICRC Advisory group on the management of COVID-19 related fatalities, International Committee of the Red Cross (ICRC): General guidance for the management of the dead related to COVID-19, *Foren Sci Int*: Synergy, https://doi.org/10.1016/j.fsisyn.2020.03.007

GARMENT A, LEDERER S, ROGERS N, BOULT L (2007) Let the dead teach the living: The rise of body bequeathal in 20th-Century America. *Acad Med,* 80: 100-105.

GHOSH SK (2017) Cadaveric dissection as an educational tool anatomical sciences in the 21st Century. *Anat Sci Educ*, 10: 286-299.

GOSNEY JR, HOFMAN P, TRONCONE G, LOPEZ-RIOS (2020) Cellular pathology in the COVID-19 era: a European perspective on maintaining quality and safety. *J Clin Pathol*, Epub ahead of print: doi:10.1136/ J Clin Path-2020-206789 1-3.

GREGORY SR, COLE TR (2002) The changing role of dissection in medical education. *MSJAMA*, 287: 1180-1181.

HAYASHI S, NAITO M, KAWATA S, QU N, HATAYAMA N, HiIRA S, ITOH M (2016) History and future of human cadáver preservation for surgical training: from formalin to saturated salt solution method. *Anat Sci Educ*, 91: 1-7.

HEALING TD, HOFFMAN PN, YOUNG SEJ (1995) The infection hazards of human cadavers. *Commun Dis Rep CDR Rev,* 5: R61-R68.

HENWOOD AF (2020) Coronavirus disinfection in histopathology. Coronavirus disinfection in histopathology. *J Histotech* https://doi.org/10.1080/01478885.2020.1734718

HILDEBRANDT S (2010) Lessons to be learned from the history of anatomical teaching in the United States: The example of the University of Michigan. *Anat Sci Educ*, 3: 202-212.

HOFFMAN PN, HEALING TD (2018) ISID Guide to infection control in the healthcare setting: The infection hazards of human cadavers. *Mehtar S (Ch ed)*. https://isid.org/guide/infectionprevention/humancadavers/ (accessed 19th October, 2020)

HUTCHINSON EF, KRAMER B, BILLINGS BK, BRITS DM, PATHER N (2020) The law, ethics and body donation: a tale of two bequeathal programs. *Anat Sci Educ,* 13: 512-519.

IFAA (2020) IFAA best practice guidelines for body donation programmes during the novel Coronavirus pandemic. https://www.ifaa.net Accessed September1, 2020.

IWANAGA J, LOUKAS M, DUMONT AS, TUBBS RS (2021) A review of anatomy education during and after the COVID-19 pandemic: revisiting traditional and modern methods to achieve future innovation. *Clin Anat,* 34: 108-114.

KAPPEL TJ, REINARTZ JJ, SCHMID JL, HOLTER JJ, AZAR MM (1996) The viability of *Mycobacterium tuberculosis* in formalin fixed autopsy tissue: Review of literature and brief report. *Hum Pathol,* 27: 1361-1364.

KAUFMAN MH (2005) Dangerous dissections: the hazard from bodies supplied to Edinburgh anatomists, winter session, 1848-9. *J R Coll Phys Edinb*, 35(3): 268-274.

KERBY J, SHUKUR ZN, SHALHOUB J (2011) The relationships between learning outcomes and methods of teaching anatomy as perceived by medical students. *Clin Anat,* 24: 489-497.

KHALIQ F, TRIPATHI P (2009) Acute effects of formalin on pulmonary functions in gross anatomy laboratory. *Ind J Physiol Pharmacol,* 53: 93-96.

KRAMER B, HUTCHINSON EF (2014) Transformation of a cadaver population: analysis of a South African cadaver program, 1921-2013. *Anat Sci Educ,* 8: 445-451.

KUMAR M, MAZUR S, ORK BL, POSTNIKOVA E, HENSLEY LE, JAHRLING PB, JOHNSON R, HOLBROOK MR (2015) Inactivation and safety testing of Middle East Respiratory Syndrome Coronavirus. *J Virol Meth*, 223: 13-18.

LAI C-C, SHIH T-P, KO W-C, TANG H-J, HSUEH P-R (2020) Severe acute respiratory syndrome coronavirus 2 (SARS-CoV-2) and coronavirus disease-2019 (COVID-19): the epidemic and the challenges. *Int J Antimicrob Agents,* 55: 105924.

LONGHURST GJ, STONE DM, DULOHERY K, SCULLY D, CAMPBELL T, SMITH CF (2020) Strength, Weakness, Opportunity, Threat (SWOT) analysis of the adaptations to Anatomical Education in the United Kingdom and Republic of Ireland in response to the COViD-19 pandemic. *Anat Sci Educ*, 13: 301-311.

MCLACHLAN JC, BLIGH J, BRADLEY P, SEARLE J (2004) Teaching anatomy without cadavers. *Med Educ,* 38: 418-424.

MCMENAMIN PG, MCLACHLAN J, WILSON A, MCBRIDE JM, PICKERING J, EVANS DJR, WINKELMANN A (2018) Do we really need cadavers anymore to learn anatomy in undergraduate medicine? *Med Teach*, 40: 1020-1029.

MCHANWELL S, BRENNER E, CHIRCULESCU ARM, DRUKKER J, VAN MAMEREN H, MAZZOTTI G, PAIS D, PAULSEN F, PLAISANT O, CAILLAUD MM, LAFORET E, RIEDERER BM, SAÑUDO JR, BUENO-LÓPEZ JL, DOÑATE-OLIVER F, SPRUMONT P,TEOFILOVSKI-PARAPID G, MOXHAM BJ (2008) The legal and ethical framework governing Body Donation in Europe - A review of current practice and recommendations for good practice. *Eur J Anat*, 12(1): 1-24.

MEMON I (2018) Cadaver dissection is obsolete in medical training! A misinterpreted notion. *Med Princ Pract,* doi: 10.1159/000488320

MOXHAM BJ, MOXHAM SA (2007) The relationships between attitudes, course aims and teaching methods for the teaching of gross anatomy in the medical curriculum. *Eur J Anat,* 11: 19-30.

MOXHAM BJ, PLAISANT O (2007) Perception of medical students towards the clinical relevance of anatomy. *Clin Anat,* 20: 560-564.

MOXHAM BJ, HENNON H, LIGNIER B, PLAISANT O (2016) An assessment of the anatomical knowledge of laypersons and their attitudes towards the clinical importance of gross anatomy in medicine. *Ann Anat*, 208: 194-203.

MOXHAM BJ, PIAS D (2017) A critique of utilitarian and instrumentalist concepts for the teaching of gross anatomy to medical and dental students. Provoking debate. *Clin Anat*, 30: 912-921.

NAIDOO N, SATYAPAL KS, LAZARUS L (2021) Could COVID-19 trigger a rebirth in anatomy education? A glimpse of anatomists' responses to pandemics of the past and present. *SN Compr Clin Med,* 15: 1-6.

PAPA V, VACCAREZZA M (2013) Teaching Anatomy in the XXI Century: New aspects and pitfalls. *Scien World J*. http://dx.doi.org/10.1155/2013/310348 (accessed 8 March 2021)

PATEL KM, MOXHAM BJ (2006) Attitudes of professional anatomists to curricular change. *Clin Anat,* 19: 132-141.

PATHER N, BLYTH P, CHAPMAN JA, DAYAL MR, FLACK NAMS, FOGG QA, GREEN RA, HULME AK, JOHNSON IP, MEYER AJ, MORLEY JW, SHORTLAND PJ, ŠTRAKLJ G, ŠTRAKLJ M, VALTER K, WEBB AL, WOODLEY SJ, LAZARUS MD (2020) Forced disruption of Anatomy Education in Australia and New Zealand: an acute response to the COVID-19 pandemic. *Anat Sci Educ*, 13: 284-300.

PALMER EG, REDDY RK, LAUGHEY W (2021) Teaching professionalism to medical students using dissection-based anatomy education: a practical guide. *Med Sci Edu*, 31: 203-213.

PEARSON WG, HOAGLAND TM (2010) Measuring change in professionalism attitudes during the gross anatomy course. *Anat Sci Educ*, 3: 12-16.

PETERSEN A, REGAN DE BERE S (2006) Dissecting Medicine. In: Rosenfeld D, Faircloth CA (eds). *Medicalized Masculinities*. Temple University Press, Philadelphia, pp 112-131.

PRINDLE RP (1983) Phenolic Compounds. In: Block SS (ed). *Disinfection, sterilization and preservation*. 3rd edition. Lea and Fabiger, Philadelphia, pp 197-224.

PHA. Public Health Agency of Canada. ePATHogen - Risk Group Database (2020) Available: https://health.canada.ca/en/epathogen [Accessed September 11, 2020].

RAJA DS, SULTANA B (2012) Potential health hazards for students exposed to formaldehyde in the gross anatomy laboratory. *J Environ Health*, 74: 36-40.

RAVI KS (2020) Dead body management in times of Covid-19 and its potential impact on the availability of cadavers for Medical Education in India. *Anat Sci Educ*, 13: 313-314.

RCP. Royal College of Pathologists (2020a) Review of COVID-19-related post mortems submitted through the RCPath portal. Unique document reference number G229A. https://www.rcpath.org/uploads/assets/5f2ed8aa-b304-4859-baf7b396322d2eb4/G229A-RCPath-Review-of-COVID-19-post-mortems.pdf (accessed 20 October 2020)

RCP. Royal College of Pathologists (2020b) RCPath advice on the opening of fresh or unfixed histopathological specimens during infectious disease outbreaks. Unique document reference number: G209 https://www.rcpath.org/uploads/assets/4556f1b9-3a6d-4132-b7d0d7c22dfc0a5c/7b8a6470-ac7c-4fe1-876ae3b2f051a258/RCPath-advice-on-the-opening-of-unfixed-histopathological-specimens-during-infectious-disease-outbreaks.pdf

RIEDERER BM, BOLT S, BRENNER E, BUENO-LÓPEZ JL, CHIRCULESCU ARM, DAVIES DC, DE CARO R, GERRITS PO, MCHANWELL S, PAIS D, PAULSEN F, PLAISANT O, SENDEMIR E, STABILE I, MOXHAM BJ (2012) The legal and ethical framework governing body donation in Europe - 1st update on current practice. *Eur J Anat,* 16: 1-21.

ROKADE SA, GAIKAWAD AP (2012) Body donation in India: Social awareness, willingness, and associated factors. *Anat Sci Educ,* 5: 83-89.

ROSS CF, PESCITELLI MJ, SMITH HF, WILLIAMS JM (2020) Teaching anatomy with dissection in the time of COVID-19 is essential and possible. *Clin Anat*, 1-2 doi:10.1002/ca.23640

ROSSI ED, FADDA G, MULE A, ZANNONI GF, RINDI G (2020) Cytologic and histologic samples from patients infected by the novel coronavirus 2019 SARS-CoV-2: An Italian institutional experience focusing on biosafety procedures. *Cancer Cytopathol,* 128(5): 317-320.

ROTH D, FERNANDEZ JA, BABISCHKIN S, DE MATTOS A, BUCK BE, QUAN S, OLSON L, BURKE GW, NERY JR, ESQUANAZI V, SCHIFF ER, MILLER J (1992) Detection of hepatitis C virus infection among cadaver organ donors: Evidence for low transmission of dis- ease. *Ann Intern Med,* 117: 470-475.

RUTALA WA (1996) APIC guideline for selection and use of disinfectants. *Am J Infect Control,* 24: 313-342.

SAKUDO A (2013) Inactivation methods for prions. In: Sakudo A (ed). *Prions: Current Progress in Advanced Research* Chapter 7. Caister Academic Press. https://doi.org/10.21775/9781910190951.07

SHIDHAM VB, FRISCH NK, LAYFIELD LJ (2020) Severe acute respiratory syndrome coronavirus 2 (the cause of COVID 19) in different types of clinical specimens and implications for cytopathology specimen: An editorial review with recommendations. *Cytojournal*, 17: 7. doi: 10.25259/Cytojournal_24_2020

SHOJA MM, BENNINGER B, AGUTTER P, LOUKAS M, TUBBS RS (2013) A historical perspective: Infection from cadaveric dissection from the 18th to 20th Centuries. *Clin Anat,* 26: 154-160.

SINGAL A, BANSAL A, CHAUDHARY P (2020) Cadaverless anatomy: Darkness in the times of pandemic Covid-19. *Morphologie*, 104: 147-150.

SRIWIJITALAL W, WIWANITKIT V (2020) COVID-19 in forensic medicine unit personnel: observation from Thailand. *J Foren Leg Med,* 72: 101964.

STERLING TR, POPE DS, BISHAI WR, HARRINGTON S, GERSHON RR, CHAISSON RE (2000) Transmission of Mycobacterium tuberculosis from a cadaver to an embalmer. *New Eng J Med*, 342: 246-248.

SUGATA Y, MIYASO H, ODAKA Y, KOMIYAMA M, SAKAMOTO N, MORI C, MATSUNO Y (2016) Levels of formaldehyde vapor released from embalmed cadavers in each dissection stage. *Environ Sci Pollut Res*, 23: 16176-16182.

ViIGLIAR E, LACCARINO A, BRUZZESE D, MALAPELLE U, BELLEVICINE C, TRONCONE G (2020) *J Clin Pathol* (Published Online First: 20 April 2020).

WEED LA, BAGGENSTOSS AH (1951) The isolation of pathogens from embalmed human bodies. *Am J Clin Path*, 21(12): 1114-1120.

WHO (2020) World Health Organization. Infection Prevention and Control for the Safe Management of a Dead Body in the Context of COVID-19: Interim Guidance 24 March 2020. 1st Ed. Geneva, Switzerland: World Health Organization. https://apps.who.int/iris/bitstream/handle/10665/331538/WHO-COVID-19-lPC_DBMgmt-2020.1-eng.pdf

WHITEHEAD MC, SAVOIA MC (2008) Evaluation of methods to reduce formaldehyde levels of cadavers in the dissection laboratory. *Clin Anat*, 21: 75-81.

WINICHAKOON P, CHAIWARITH R, LIWSRISAKUN C, SALEE P, GOONNA A, LIMSUKON A, KAEWPOOOWAT Q (2020) Negative nasopharyngeal and oropharyngeal swab does not rule out COVID-19. *J Clin Microbiol,* 58: e00297-20.

YAACOUB S, SCHUNEMANN HJ, KHABSA J, EL-HARAKE A, KHAMIS AM, CHAMSEDDINE F, EL KHOURY R, SAAD Z, HNEINY L, GARCIA CC, MUTI-SCHÜNEMANN GEU, BOGNANI A, CHEN C, CHEN G, ZHANG Y, ZHAO H, HANNA PA, LOEB M, PIGGOTT T, REINAP M, RIZK N, STALTERI R, DUDA S - the COVID-19 Systematic Urgent Reviews Group Effort (SURGE) group (2020) Safe management of bodies of deceased persons with suspected or confirmed COVID-19: a rapid systematic review. *BMJ Global Health,* 5: e002650. doi:10.1136/ bmjgh-2020-002650.

European Journal of Anatomy